Establishing Neuronal Diversity: Regulation of Olfactory Receptor Neuron Specification and Axon Guidance in Drosophila

by

Scott Barish

Department of Biology
Duke University

Date:_____
Approved:

_____
Pelin C Volkan, Supervisor

_____
David McClay

_____
Hiroaki Matsunami

_____
Amy Bejsovec

_____
Debra Silver

Dissertation submitted in partial fulfillment of
the requirements for the degree of Doctor
of Philosophy in the Department of
Biology in the Graduate School
of Duke University

2017

ABSTRACT

Establishing Neuronal Identity: Regulation of olfactory receptor neuron specification

and axon guidance in Drosophila by

Scott Barish

Department of Biology
Duke University

Date:_____
Approved:

_____
Pelin C Volkan, Supervisor

_____
David McClay

_____
Hiroaki Matsunami

_____
Amy Bejsovec

_____
Debra Silver

An abstract of a dissertation submitted in partial
fulfillment of the requirements for the degree
of Doctor of Philosophy in the Department of
Chemistry in the Graduate School of
Duke University

2017

Copyright by
Scott Barish
2017

Abstract

The human brain contains over 80 billion neurons that make approximately 100 trillion specific connections. Each neuron must acquire a specific identity that includes its, gene expression, morphology, connectivity, and location. The basic logic and mechanisms that are used to coordinate this process on the immense scale of the brain remain largely unknown. We use the *Drosophila* olfactory system as model to understand nervous system development because of the powerful genetic tools and the workable level of neuronal diversity, which contains 50 classes of olfactory receptor neurons (ORNs). Each class of neurons is defined by the exclusive expression of typically a single olfactory receptor and connect to 50 class-specific glomeruli in the antennal lobe of the brain. Here we demonstrate that a cross regulatory network of transcription factors patterns the antennal disc, which contains ORN precursors and will develop into the antenna. These transcription factors create seven rings that are each labeled by a unique combination of genes, which generate distinct sets of ORN fates. Manipulation of this network changes the ORN fates that are produced in the adult, thereby demonstrating its necessity for generating neuronal diversity. We next show that the DIP/Dpr family of proteins, which are members of the Ig superfamily of genes and heterophilically interact, is required for axon sorting among classes of ORNs to create 50 class specific glomeruli. The members of this family are expressed in a

combinatorial code in ORNs at times that correlate to glomerular formation. Computational analysis of DIP/Dpr expression patterns groups ORN classes into clusters that mimics their relative glomerular positioning in the antennal lobe. Class-specific or combinatorial knock down of *DIP* and *dpr* genes causes localized axon sorting defects where effected class invade neighboring glomeruli based upon the similarity of the DIP/Dpr expression codes. Our results highlight two functionally conserved strategies for generating and wiring a diverse neural circuit: prepatterning of precursors through combinatorial transcription factor expression, and the generation of differential adhesion force between classes of axons through combinatorial interactions of cell surface molecules. Not only are these strategies conserved in mammals, many of the genes that govern these processes are conserved as well, with genes like *Bar*, *ap,* and *dac* all having mammalian orthologues, and DIPs and Dprs sharing homology with Kirrel proteins. These studies have advanced our knowledge of the underlying logic that governs how a diverse nervous system is generated and coordinately wired.

Contents

Abstract iv

List of Tables xii

List of Figures xiii

Acknowledgements xvi

1. Introduction 1

1.1 Mechanisms of olfactory receptor neuron specification in Drosophila 3

1.1.1 Structure of the Drosophila olfactory system 3

1.2 Regulation of olfactory receptor expression 5

1.2.1 Larval and pupal patterning factors 6

1.2.2 Control of Morphological Identity 8

1.2.3 Control of sensillar subtype 9

1.2.4 Notch Signaling 11

1.2.5 Epigenetic regulation of OR genes 13

1.2.6 Late transcription factors 15

1.2.7 Cis-regulatory elements 17

1.2.8 MicroRNA control of ORN circuit assembly 19

1.3 Axonal Targeting 20

1.3.1 Coordination of wiring among neurons within the same sensillum 22

1.3.2 ORN Axon Guidance 23

1.3.3 Intra-class attraction 25

1.3.4 Inter-class repulsion 26

1.3.5 ORN-PN Matching 27

1.4 Concluding Remarks 28

2. A Functionally Conserved Gene Regulatory Network Module Governing Olfactory Neuron Diversity 34

2.1 Summary 34

2.2 Results 36

2.2.1 A time-course RNAseq analysis reveals mis-regulation of developmentally critical genes in rn mutant 36

2.2.2 A common molecular network patterning the antennal and leg appendages 38

2.2.3 Expansion of Bar expression in rn mutants underlies changes in ORN diversity and expansion of a default fate 39

2.2.4 Rn directly binds upstream of BarH2 and bab2 gene regions in vivo 40

2.2.5 Partitioning of prepatterning domains 42

2.2.6 Sensilla subtype fates mapping onto the prepatterned domains 43

2.2.6.1 Ring 1 43

2.2.6.2 Rings 2, 3, 4, and 5 44

2.2.6.3 Ring 6 45

2.2.6.4 Ring 7 45

2.2.7 Functional involvement of PD genes in generating ORN diversity 46

2.2.8 Separation of different precursor fates within a ring by Bab concentration gradients 51

2.2.9 Functionally conserved molecular network in patterning gustatory receptor neuron fates 52

2.3 Discussion 53

2.3.1 A common strategy with simple logic steps for generating neuronal complexity 55

2.3.2 ORN precursor fate specification and OR expression 58

2.3.3 Deployment of the same network module in diversifying olfactory and gustatory neurons 59

2.3.4 Modular evolution of gene regulatory networks and neuronal diversity 60

2.4 Materials and Methods 83

2.4.1 Fly genetics 83

2.4.1.1 Genotypes for fly genetics: 84

2.4.2 RNA extraction and library preparation 86

2.4.3 RNAseq analysis 87

2.4.4 Immunohistochemistry 88

2.4.5 Real-time RT-PCR 88

2.4.6 Chromatin immunoprecipitation 91

2.4.7 Statistical analysis 94

3. Transcriptional profiling of olfactory system development identifies distal antenna as a regulator of subset of neuronal fates 95

3.1 Summary 95

3.2 Results 96

3.2.1 Stage specific analysis of developing olfactory system transcriptome 96

3.2.2 Temporal Dynamics of OR Expression 100

3.2.3 Temporal Dynamics of IR Expression 104

3.2.4 Transcription Factor Expression 104

3.2.4.1 Clustering Analysis 106

3.2.5 Confirmation of Expression of Bar, Ap, Bab, and Dan 108

3.2.6 Dan Functions to Regulate the Expression of a Subset of Olfactory Receptors 109

3.3 Discussion 111

3.4 Materials and Methods 125

3.4.1 Fly Genetics 125

3.4.1.1 Fly Genotypes 125

3.4.2 Immunohistochemistry 126

3.4.3 RNA-seq 126

3.4.4 Analysis of RNAseq data 127

3.4.5 Estimating the Probability That a Gene Is Expressed 127

3.4.6 PCA Analysis 128

3.4.7 Gene ontology analysis 128

3.4.8 RNA extraction 128

3.4.9 qRT-PCR 129

4. Combinations of DIPs and Dprs control olfactory receptor neuron axon sorting in Drosophila 130

4.1 Summary 130

4.2 Results 131

4.2.1 DIP and Dprs are expressed in late stages of ORN wiring 132

4.2.2 DIPs and Dprs are expressed in a combinatorial code in ORNs 133

4.2.3 Mathematical analysis based on DIP/Dpr profiles of ORNs mimic their relative glomerular positioning 135

4.2.4 Combinatorial and ORN-specific roles of DIPs and Dprs in class-specific sorting of ORN axons 137

4.2.5 Overexpression of DIP proteins causes local axon sorting defects 141

4.2.6 Overexpression of Dpr1 causes non-cell autonomous splitting of ORN axons of the same class 143

4.2.7 Dpr10 controls glomerular targeting 145

4.3 Discussion 149

4.3.1 Local Axon Sorting 150

4.3.2 Adhesive DIP-Dpr Interactions 152

4.3.3 Regulation of DIP/Dpr Expression 154

4.3.4 Convergent molecular logic for glomerular organization 155

4.4 Materials and Methods 174

4.4.1 Fly Genetics 174

4.4.1.1 Fly Genotypes 174

4.4.2 RNA-seq 180

4.4.3 Analysis of RNAseq data 181

4.4.4 Immunohistochemistry 181

4.4.5 Statistical analysis of ORN class specific DIP/Dpr profiles 182

5. Conclusions and Future Directions 184

5.1 Conclusions 184

5.2 Future Directions 186

5.2.1 Completion of combinatorial maps 186

5.2.1.1 Completing the PD-network 186

5.2.1.2 ORN CSM profiles 188

5.2.2 Molecular mechanisms of ORN specification 189

5.2.3 Connecting specification and wiring 191

5.2.4 Developmental expression and function of DIPs/Dprs 193

5.2.5 Role of olfactory receptors in controlling ORN wiring 194

5.2.6 Modeling ORN specification and wiring 196

Appendix A: Supporting Text for Chapter 2 198

Explanation for the model in Fig 13B: 198

Explanation for the model in Fig 14A: 200

Explanation for the model in Fig 15A: 201

Appendix B: Supplemental Tables for Chapter 3 204

References 352

Biography 370

List of Tables

Table 1: Summary of the expression analysis shown in Fig 11. 70

Table 2: qPCR primers for olfactory receptors. 89

Table 3: ChIP-qPCR primers. 93

Table 4: Transcripts with the top 50 scores for PC1 from PCA. 204

Table 5: Transcripts with the top 50 scores for PC2 from PCA. 206

Table 6: Significantly differentially expressed genes between 3L and p8 stages. 208

Table 7: Significantly differentially expressed genes between p8 and p40 stages. 227

Table 8: Significantly differentially expressed genes between p40 and Adult stages. 272

Table 9: Key GO Terms in Fig 26. 323

Table 10: Key GO Terms in Fig 27. 326

Table 11: Key GO Terms in Fig 28. 329

Table 12: Normalized $\log_2$ expression values of olfactory receptors used to create Figure 29. 333

Table 13: Notch State and Expression Status of ORs Across Development. 335

Table 14: Normalized $\log_2$ expression values of transcription factors used to create Figure 31. 337

Table 15: Normalized $\log_2$ expression values of commonly used housekeeping genes. 347

Table 16: Raw expression values for Figure 35A. 347

List of Figures

Figure 1: Structure of the Drosophila olfactory system. 30

Figure 2: Control of ORN identity by larval prepatterning factors. 31

Figure 3: Generation of a sensillum of from a single SOP through the use of Notch signaling. 32

Figure 4: Development of the Drosophila antennal lobe. 33

Figure 5: Heatmap of olfactory receptor expression in the control and rn mutant adult antennae by RNAseq 62

Figure 6: Summary of RNA-seq analysis 63

Figure 7: Rn controls the expression of BarH1/2 and bab1/2 in the antennal disc 64

Figure 8: Expression of PD network genes in the antennal disc. 65

Figure 9: Relationship between BarH1/2 and rn. 66

Figure 10: Intercalation of prepatterning genes inside and outside the central fold 68

Figure 11: Expression pattern of PD network components in ORNs. 69

Figure 12: Expression of GFP in the mid-pupal antennal lobe driven by Bar or bab1 GAL4. 71

Figure 13: Model depicting the PD network that determines the precursor identities of the rings and the ORN populations. 72

Figure 14: Effect of Bar overexpression on ORN populations. 73

Figure 15: Effect of apterous overexpression on ORN populations. 74

Figure 16: Expansion of Or47b in Bar overexpression. 75

Figure 17: Changes in sensilla identity in rn mutant as well as Bar and ap overexpression. 76

Figure 18: TF expression in Bar overexpression. 77

Figure 19: Changes in TF expression in Ap overexpression.. 78

Figure 20: Effect of loss of apterous or bar on OR expression. 79

Figure 21: Overexpression of constitutively active EGFR. 80

Figure 22: Effects of hypomorphic bab mutants on ORN populations. 81

Figure 23: Regulation of GRN patterns by the PD network. 82

Figure 24: Expression of Gr5a and Gr43a in rn mutant legs. 83

Figure 25: PCA analysis and MA plot comparisons of gene expression across all time points and pairwise comparisons respectively. 115

Figure 26: Pairwise GO plot analysis of differentially expressed genes between 3L and p8 stages. 116

Figure 27: Pairwise GO plot analysis of differentially expressed genes between p8 and p40 stages. 117

Figure 28: Pairwise GO plot analysis of differentially expressed genes between p40 and Adult stages. 118

Figure 29: OR/IR developmental expression profiles grouped based on sensilla pairings of ORNs. 119

Figure 30: Expression of OR reporters in developing pupal antennae. 120

Figure 31: Clustering analysis of ~400 transcription factors based on expression profiles. 121

Figure 32: Hierarchical clustering of the expression patterns of transcription factors known to regulate ORN specification. 122

Figure 33: Confirmation of RNA-seq with immunofluorescence and reporter expression. the same level in all cells. 123

Figure 34: Dan is required for the expression of a subset of ORs. 124

Figure 35: Transcriptional profiles of CSM genes in the developing Drosophila olfactory system. 157

Figure 36: ORN class specific expression patterns of DIP and dpr genes. 158

Figure 37: Expression of DIPs and Dprs in the olfactory system. 159

Figure 38: Expression of DIPs and Dprs in Projection Neurons. 160

Figure 39: Combinatorial expression of DIPs and Dprs in the Drosophila olfactory system. 161

Figure 40: Multidimensional scaling clusters ORN classes by DIP/Dpr expression pattern, which mimics glomerular clusters in the antennal lobe. 163

Figure 41: Single knockdown of DIPs/Dprs with pan-ORN driver does not disrupt ORN wiring. 164

Figure 42: Cell-autonomous knockdown of *DIP-η* in Or47b ORNs disrupts sorting of Or47b axons from Or88a glomerulus. 165

Figure 43: Pan-ORN knockdown of *DIP-η* and *DIP-δ* splits Or47b glomerulus. 166

Figure 44: Overexpression of *DIPs*/*dprs* causes localized axon sorting defects. 167

Figure 45: Summary and penetrance of DIP/Dpr overexpression phenotypes. 169

Figure 46: Dpr10 controls ORN wiring in the antennal lobe. 171

Figure 47: Summary and penetrance of *dpr10* mutant phenotypes. 173

Figure 48: Some DIPs and Dprs share homology with Kirrels. 174

Acknowledgements

I would like to thank my advisor Dr. Pelin Volkan for her mentorship over the last several years. Without Dr. Volkan's guidance and creating a welcoming lab environment I would not have been able to flourish and thrive. I would also like to thank Dr. Tristan Li and Sumie Okuwa, who are former members of the Volkan Lab, without whom I would not have been able to complete this work. Tristan in particular, was like a second mentor to me and helped push me to become a better scientist. I would like to thank the other members of the Volkan lab for their comments and advice. I would like to thank my committee who has provided valuable input on my work and encouraged me throughout my time here. I would like to that Tetsuya Kojima, Larry Zipursky, Leslie Vosshall, Richard Benton, Kai Zinn, Hugo Bellen and others for generously sharing reagents used here. I would like to thank Corbin Jones, a collaborator and mentor who made so much of my work possible. I would like to thank Nina Sherwood for her advice and fun conversations. I aspire to be the kind of mentor and teacher that you are. I would like to thank my friends and family both near and far, on campus and off. Without you I would not have survived this journey. You are my inspiration and foundation. I will be eternally grateful for your support and love. Last but not least, I would like to thank all of the campus workers who keep our lab clean and functioning. Nothing I have done would have been possible without the work you do.

1. Introduction

The nervous system is one of the most complex biological systems in the world. The human brain contains 88 billion neurons that make approximately 100 trillion coordinated and specific connections (1). Neurons differ in their morphology, connectivity, function and gene expression (2). Functioning of the nervous system underlies nearly every human behavior, from sensory perceptions such as touch, sight, and smell (3). The nervous system is also astonishingly plastic, allowing for experience to alter and mold neurological circuits that control behavior and drive adaptation and evolution (4–6). Mutations that disrupt neuronal development are associated with brain cancers and neuropsychiatric disorders (6,7).

The nervous system must use highly repeatable programs that drive a small number of precursor cells to divide and differentiate into specific neurons and coordinate the guidance of axons and dendrites to connect with their appropriate targets must occur in each individual in an iterative and step-wise manner (8–11). Investigation of nervous system development has therefore been a topic of interest for over a hundred years. Santiago Ramon y Cajal pioneered the first studies of the nervous system that revealed the incredible diversity of neuronal morphologies and how the nervous system changes over time (12). Through the years, we have grown to appreciate that the nervous system is far more complex than Ramon y Cajal could have imagined (1,2). While significant progress has been made in understanding how development of the

nervous system progresses, many of the fundamental mechanisms that drive specification of neuronal identity remain poorly understood.

Neuronal identity is a broad term that encompasses several characteristics: location, connectivity, morphology, and gene expression. Each of these characteristics is interconnected and interdependent, but here I focus on the selection of a class-specific olfactory receptor as a proxy for gene expression and the sorting of axons, a process critical for establishing proper connections. The studies described here use the Drosophila olfactory system as a model to understand the foundational processes that are broadly applicable to a wide range of species. I begin by reviewing the current knowledge of olfactory system development in Drosophila, pertaining to olfactory receptor neuron specification and expression of a single olfactory receptor in each neuron, and the guidance of olfactory receptor neuron axons to their class-specific targets. I next demonstrate that a conserved network of cross-regulatory transcription factors patterns in developing olfactory tissue restricts the potential of olfactory receptor neuron precursors. Then I demonstrate that a family of immunoglobulin domain-containing proteins are expressed in subsets of olfactory receptor neuron classes and are required for the sorting of axons into class-specific glomeruli in the antennal lobe of the brain. I conclude by discussing the meaning of these results and how they may apply to other systems and species.

The following chapter is adapted from *Barish and Volkan (2015). Mechanisms of olfactory receptor neuron specification in Drosophila. WIRE's Developmental Biology; 4(6):609-21. doi: 10.1002/wdev.197*.

1.1 Mechanisms of olfactory receptor neuron specification in Drosophila

Detection of a broad range of chemosensory signals is necessary for the survival of multicellular organisms. Chemical signals are the main facilitators of foraging, escape, and social behaviors. To increase detection coverage, animal sensory systems have evolved to create a large number of neurons with highly specific functions. The olfactory system, much like the nervous system as a whole, is astonishingly diverse (13–15). The mouse olfactory system has millions of neurons with over a thousand classes, whereas the more compact Drosophila genome has approximately 80 odorant receptor genes that give rise to 50 neuronal classes and 1,300 neurons in the adult (16). Understanding how neuronal diversity is generated remains one of the central questions in developmental neurobiology. Here we review the current knowledge on the development of the adult *Drosophila* olfactory system and the progress that has been made towards answering this central question.

1.1.1 Structure of the Drosophila olfactory system

Adult flies have two main olfactory appendages, the antennae and the maxillary palps. The surfaces of both structures are covered with hair-like structures called sensilla (13,17–19). Each sensillum houses 1-4 olfactory receptor neurons (ORNs, Figure 1A)

(13,17–19). Sensilla can be divided into three morphological classes, trichoids, ceoloconics, and basiconics. They can be further divided into subtypes based upon the invariable combinations of ORNs they house (Figure 1B) (18). Each sensillum is named by two letters and a number, representing the olfactory appendage, the morphological class and the subtype number, respectively. For example, the at4 sensilla are the 4th subtype of the antennal trichoid sensilla. ORNs in the basiconic and trichoid sensilla express olfactory receptor (*Or*) genes, whereas coeloconic ORNs express the ionotropic receptors (*Irs*) (16,20). There are also ORNs, such as the CO_2 sensory neurons on the antennae, which express genes that resemble gustatory receptors (*Gr*) more than *Or* genes (21–23). ORN cell bodies reside at the base of sensilla where they are surrounded by supporting cells (Figure 1C) (18). Each ORN extends its dendrites into the sensillar protrusion where it is exposed to the environment through the cuticular pores that enable diffusion of odorants into the sensilla (Figure 1C) (19). Axonal projections of ORNs from the antennae enter the antennal lobe in the brain via the antenna nerve, whereas projections from the maxillary palp ORNs enter via the labial nerve (18,24,25). In the antennal lobe, axonal terminals of each ORN class synapse with the dendrites of projection neurons (PNs) within class specific glomeruli (Figure 1D) (24–26). The antennal lobe is the first relay station of olfactory processing and projection neurons then send this information into higher brain structures, by projecting their axon terminals primarily into the mushroom body calyx and lateral horn (19). The Drosophila

olfactory system serves as an excellent model for general nervous system development with a few distinct advantages. First, because each neuron expresses a single receptor and connects to a single glomerulus it is possible to more carefully understand the relationship between neuronal identity and axonal connectivity. Second, the terminal fate of ORNs generated from each individual precursor can be clearly defined as they cluster within the same sensillum. Using the unique genetic toolkit available in Drosophila, it is possible to trace the fate of each precursor and interrogate the function of different proteins in assembling this diverse circuitry.

1.2 Regulation of olfactory receptor expression

One of the major questions in understanding the development of the Drosophila olfactory system is how olfactory receptor genes are regulated in different ORN classes, where each ORN class expresses a single receptor from the large number of possibilities in the genome. What are the intrinsic and extrinsic factors that instruct each ORN to express a particular receptor? In *Drosophila Or* expression at the periphery seems to be highly zonal and deterministic (19,27). The mammalian olfactory epithelium is also divided into several zones, each containing ORNs that express distinct sets of olfactory receptors (28). However in contrast to *Drosophila,* mammalian neurons within each zone seem to stochastically express a single allele of a single receptor (27). This system of selection certainly has its advantages for mammals, which can have over 1,000 *Or* genes and over a million ORNs. The amount of regulatory factors needed to deterministically

specify each fate in the mammalian system would be staggering, so some stochasticity likely eases the regulatory burden on the organism. In addition, the dynamics of neuron turnover in mammalian olfactory system also can benefit from a stochastic selection process as new neurons are integrated into existing circuits. Specifying the ~60 ORN classes from the ~80 *Or* genes that exist in Drosophila however, is much more manageable by comparison, while maintaining a highly diverse system. The determinism seen in the *Drosophila* olfactory system may make it a better model for general nervous system development, which is less likely to rely on stochastic mechanisms where precise fate decisions are required.

1.2.1 Larval and pupal patterning factors

The antenna and maxillary palps, like many other adult structures in the fly, both arise from an imaginal disc, specifically the eye-antennal disc (29,30). Imaginal discs are small epithelial sacs that are put aside during embryonic development that give rise to adult structures during pupal metamorphosis. Each disc is specified into its respective structure by the expression of homeotic genes (29). Homothorax is the primary homeotic factor that controls antennal fate, although it is also known to have other functions in the leg disc (31,32). The legs and antennae have long been thought of as analogous organs. Both appendages are segmented, ventral organs, unlike unsegmented, dorsal organs such as the wing. Further, gain of function mutations of the homeotic gene *antennapedia* converts the antennae into legs (33). This suggests that the antennae and the legs may

share a common developmental strategy for diversifying cell types, which is particularly interesting because the legs are gustatory organs that are covered by sensilla that house diverse sets of gustatory receptor neurons expressing *Gr* and *Ir* genes (30,34–36). Most imaginal discs, including the leg and antennal discs are patterned by the expression of several genes and signaling pathways. For example, *engrailed* (*en*) is expressed early in disc development in the posterior compartment of the discs and activates *hedgehog*, which then signals to the anterior compartment of the disc (Figure 2A) (30). Hedgehog then activates both Wingless (Wg) and Decapentaplegic (Dpp), which are expressed in wedge-like patterns on opposite sides of the disc (Figure 2A) (37). The reason that these wedge-like patterns form is that in the posterior compartment of the disc, the downstream signaling pathway of Hh is repressed by En, thereby restricting the activation of Wg and Dpp. Wg and Dpp then diffuse outward to form signaling gradients, which specify the ventral and dorsal fate respectively, thereby layering a new axis on top of the anterior-posterior compartments. At the center of the disc, where the expression of Wg and Dpp meet, the combination of these signaling pathways establish the proximal-distal axis of the antenna through activation of *vein*, an EGF receptor ligand, and *distal-less* (*dll*) (Figure 2A). Both are expressed in the center of the disc (37) and give rise to the more distal regions of the antenna, namely the entire third segment. EGFR signaling is critical for delineating the proximal-distal axis of the antenna, with

the highest amount of activity in the center of the disc (distal) and gradually decreasing towards the outermost region (proximal) (32,37).

1.2.2 Control of Morphological Identity

Several genes are expressed in larval and pupal antennal discs that lay down an initial patterning, which is necessary for proper antennal development. Three of the factors expressed at these stages, *lozenge* (*lz*), *amos*, and *atonal*, control the morphological identity of sensilla (Figure 2B, C) (38–41). Lz, a member of the AML-1/Runt transcription factor family, is the first of these factors to be expressed, beginning at the third instar larval stage and controls both basiconic and trichoid fates, most of which generate ORNs that express *Ors* (26, 29). Interestingly, it has been proposed that the trichoid and basiconic identities are controlled by the level of expression of *lz* (41). Hypomorphic mutations in *lz* lead to antennae that lack basiconic sensilla, whereas strong *lz* mutants lack both basiconic and trichoid sensilla, suggesting different thresholds for Lz function for determining basiconic and trichoid fates (41). These data have led to the idea that a subset of lz+ precursors express a high level of *lz* and become basiconics and another express a low level of *lz* and become trichoids (Figure 2B, C). Lz also is a positive regulator of *amos*, a bHLH transcription factor that controls morphological class identity (38). Like *lz*, *amos* is required for both basiconic and trichoid sensilla (38). *Lz* mutants lack *amos* expression and broad activation of *lz* correspondingly leads to broad expression of *amos* (38). As such, *amos* expression begins after *lz*, around the initiation of

puparium formation (0 hrs APF, after puparium formation) and peaks around 6-8 hrs APF (38). It is worth noting that basiconic sensilla have their own morphological subclasses, named large, thin, and small basiconics. While both *lz* and *amos* are required for all three types of basiconics, the factors that divide each subtype are not known. The development of coeloconic sensilla, which express primarily *Irs* as opposed to *Ors*, requires another bHLH transcription factor, *atonal*, which is highly related to *amos* (Figure 2B) (40). *Atonal* expression starts before *amos*, but generally overlaps with it in early pupal development as sensory organ precursors are being selected (40). Both Amos and Atonal function as proneural transcription factors and control precursor selection and identity, which underlie their role in specifying sensillar morphological identity (38,40).

1.2.3 Control of sensillar subtype

Diversification decisions regarding sensillar subtype identity are regulated by additional factors. For example, unlike the regulators of morphological divisions of sensilla (*lz*, *amos* and *atonal*), Rotund (Rn), Dachshund (Dac) and Engrailed (En) specify sensillar subtype identity (42). Dac specifies several sensilla subtypes within basiconic sensilla, whereas En regulates specification within a subset of each morphological class (43,44). Rn, similar to En, is also required to specify half of the subtypes within each morphological class (Figure 2B, C) (42). However, unlike *en* mutants, *rn* mutants convert certain sensilla subtypes to others within each morphological sensilla type. For example,

in trichoid sensilla both at1 and at3 precursors express *rn*, whereas precursors for at4 and at2 do not (42). In *rn* mutants, at1 and at3 sensilla are converted to at4 sensilla (42). In this model, Rn diversifies both at1 and at3 fates from the default at4. In other words, each trichoid sensilla type can be defined as Rn+ or Rn-. Lineage tracing experiments show that Rn+ precursors do in fact give rise to not only half of the subtypes within trichoids but also basiconics and coeloconics (Figure 2B, C), suggesting that it functions to specify several fates within each morphological class (42). Indeed, in *rn* mutants, rn+ sensilla and the ORNs housed in them are converted to one of the default rn- sensilla and ORN identities within all sensilla morphological types (Figure 2B, C) (42). These results suggest that Rn regulates the combinations of ORN identities that can be generated from a given multipotent precursor cell. It is intriguing that *rn* is expressed in the very early stages of olfactory system development and is turned off prior to the onset of receptor expression. In addition, Rn does not bind to *Or*/*Ir* promoters, thus how Rn regulates the ORN differentiation potential of precursors and sensilla identity is still not clear (42). Thus, it is likely that Rn regulates the olfactory receptor expression patterns indirectly via induction of transcription factors, which can either directly interact with *Or* promoters or modify chromatin around *Or* promoters.

1.2.4 Notch Signaling

Once the precursor potentials are determined by the early patterning factors described in the previous section, each multipotent precursor undergoes several rounds of asymmetric divisions to generate 1-4 terminally differentiated ORNs in the same sensillum (8). Each consecutive asymmetric division from a single multipotent precursor is associated with binary segregation of possible cell fates. Notch signaling is a common pathway that is utilized for such binary segregation, and also contributes to proper segregation of ORN fates within each sensillum through lateral inhibition (Figure 3) (8). The current model suggests the initial precursor, pI, undergoes an asymmetric division and generates two daughters, pIIa and pIIb (Figure 3) (8). pIIa, a Notch-on precursor, generates outer, supporting cells, whereas pIIb, a Notch-off precursor generates the ORNs of each sensillum (8). pI, pIIa, pIIb all express *senseless (sens)*, a marker of precursor identity (8). pIIa and pIIb then each undergo a second round of asymmetric division to create the transit amplifying (or intermediate precursor) cells pOa and pOb, pNa and pNb respectively (8). pO cells express *cut*, whereas pN cells continue to express *sens* (8). As the number of ORNs in different sensilla vary from 1-4 cells, this division pattern is thought to be complemented by mechanisms, such as cell death or adoption of glial fates, which determine the total number of ORNs per sensillum (45). And finally, ORN classes within a given sensillum can be classified as Notch-on or Notch-off based upon their requirement for Notch for their identity (8). For example, mutations in the

positive effector of Notch signaling, *mastermind (mam)*, leads to duplication of one ORN identity (Notch-off) at the expense of another (Notch-on) within a sensillum (8). In contrast, in mutants for *numb*, which encodes a protein that antagonizes Notch signaling, the Notch-on ORN is duplicated at the expense of the Notch-off (Figure 3) (8). Thus, Notch signaling governs binary fate segregation of specific combinations of ORN identities from each precursor divisions. Mutations in early patterning factors, like *rn* mutants, cause regions of the antenna to lose pools of ORNs housed in sensilla from *rn*-positive precursors and are rather covered by sensilla from *rn*-negative precursors, keeping the ORN pairing and fate segregation appropriate. These results suggest that precursor identity must be multipotent yet be restricted in its potential to give rise to a restricted set of ORNs. Once this potential is set by early patterning factors, Notch signaling acts on each precursor division in a context dependent manner to segregate binary fate decisions toward terminally differentiated ORNs. It is unclear however, what molecularly defines the restricted ORN potentials of different precursors. It is likely that the transcriptional and chromatin profile patterns in the fields of cells antennal disc cells during development are what define the precursor cell potentials.

1.2.5 Epigenetic regulation of OR genes

Because Notch signaling is used broadly in all sensilla, each precursor must then have a restricted differentiation potential or allowable combination of olfactory receptor genes that can be expressed by its daughters. Thus, the intermediate precursor cells must retain a cellular memory for Notch signaling to act on during each asymmetric division. It is plausible to imagine that the mechanisms governing these processes will likely include chromatin regulation.

Indeed, recent work has connected the mechanism of Notch signaling in ORN specification to the chromatin modifiers Hamlet (Ham, a homolog of Prdm16) and C-terminal binding protein (CtBP) (46). *Hamlet* is expressed in a subset of ORNs within each sensillum and is required for regulating *Or* expression (46). Ham functions as a repressor of Notch signaling and complexes with CtBP to reduce the amount of activating H3K4 methylation and increase the amount of repressive H3K27 methylation around Notch target genes (46). Further, the transcriptional co-repressor Atrophin (Atro) has been shown to regulate *Or* expression in Notch-on ORNs (47). Loss of Atro leads to the derepression of Notch-on ORs in other Notch-on ORNs, and likewise, overexpression of *atro* represses Notch-on *Ors* (47). Interestingly, *atro* overexpression leads to a reduction in the amount of H3 acetylation in ORNs and the loss of *Or* expression in *atro* overexpression can be rescued by the loss of the histone deacetylase *hdac3* (47). These data suggest that modulation of chromatin and epigenetic states are

critical for proper segregation of alternate ORN fates. As Notch signaling is used broadly across all sensilla types, it is not clear how Notch signaling during asymmetric divisions regulate *Or* expression among the ORNs to be generated from each precursor in a context independent manner. One attractive possibility is that the prepatterning factors discussed earlier modify each precursor to create a unique *Or* expression competency, on which Notch signaling can then act to generate individual ORNs.

Recent work has also connected regulation of the CO_2 receptors Gr21a and Gr63a expression to chromatin modifying proteins, specifically the MMB/dREAM complex (48). The MMB/dREAM complex is composed of several transcription factors and chromatin remodeling factors. Two members of the dREAM complex, Myb and Mip130, positively regulate Gr63a expression, whereas other members, Mip120 and E2F2, repress Gr63a expression in inappropriate ORNs (48). dREAM complex antagonizes H3K9 methylation to regulate *Or* expression in the appropriate olfactory appendages and ORNs (48). These data present a new layer of complexity to what is known about *Or* regulation that may lead to many new insights. However, a true interrogation of chromatin states at *Or* promoters at multiple developmental stages will be necessary to truly understand how epigenetic modifications contribute to *Or* regulation.

1.2.6 Late transcription factors

There are several transcription factors that are expressed in later stages of ORN development and regulate *Or* expression in postmitotic ORNs. This set of transcription factors are similar to the terminal selector genes proposed by Oliver Hobert, that function by directly binding to the promoters of *Or* genes, as the terminal differentiation genes (49). The more extensively studied of these factors is *acj6*, which is required for *Or* expression in a subset of ORN classes (50). Acj6 is a POU domain transcription factor that is expressed in adult maxillary palps and antennae (50). In *acj6* mutants the response profiles of a large number of ORNs are changed suggesting a change in ORN identity (51). Later research showed that expression of both antennal and palp *Or* genes are affected in *acj6* mutants (51,52). In addition to presence of Acj6 binding sites upstream of these *Or* genes, most of the work on the molecular function of Acj6 in *Or* regulation was carried out for palp *Or* genes (53). These studies identified 13 different *acj6* splice isoforms, each of which differentially regulates subsets of *Ors* in the maxillary palp (53). Expression of a single isoform of *acj6* leads to the rescue expression of a subset *Ors* regulated by Acj6 in an *acj6* mutant and individual isoforms can have both activation and repression functions (53). The molecular details of how each isoform of *acj6* functions are still unclear but it is possible that each isoform binds to unique binding motifs or complexes with a unique set of other proteins. *Pdm3* is also POU domain transcription factor, whose expression and function are similar to that of *acj6*

(54). Pdm3 has also primarily been investigated in the palps, where it is required for activation of *Or42a* (54). Although *pdm3* is expressed broadly in the antenna and maxillary palp, its function in each ORN class is not clear. In the context of *Or42a*, Pdm3 is known to work cooperatively with Acj6, suggesting they work in combination or possibly dimerize to regulate expression of their target *Or* genes (54).

Given the large number of *Or* genes, and the singular expression of an *Or* gene in each ORN, the most parsimonious model suggests that a combinatorial code of transcription factors controls expression of different receptors in *Drosophila*. Most recently, Jafari et al. identified combinatorial function for Acj6 and six novel transcription factors (*zf30c*, *sim*, *xbp1*, *fer1*, *E93* and *onecut*), that are required for proper *Or* expression in the antenna (52). Of these six proteins, Xbp1 and E93, function to both activate and restrict *Or* expression and all others serve solely as activators (52). These factors, as well as Acj6 and Pdm3, support the combinatorial regulation model of *Or* expression. However, there is evidence to suggest that these TFs alone cannot entirely explain how ORNs select a particular *Or* to express. For example, analysis of TF binding motifs shows that binding motifs for specific TFs are often present upstream of many *Or* genes, yet the expression of only a subset of OR genes are affected in the TF mutants (52). This might be due to combinatorial or competitive interactions at specific promoter elements, or the neuron-specific patterns of TF expression. This set of TFs also act only in late stages of pupal development around the onset of *Or* expression. The only exception

being *zf30c*, whose expression is required in both early and late stages of development (52). We anticipate that a thorough lineage map of TF expression patterns along with mutational analysis and the chromatin landscape in different ORNs and precursors will help reconcile these contradictions in the future.

1.2.7 Cis-regulatory elements

A critical step in ORN specification is the selection of the olfactory receptor. In Drosophila, artificial *Or* promoter reporter constructs are able to faithfully recapitulate *Or* expression, even when not inserted in the endogenous locus. This observation has led to the conclusion that all of the information required for regulation of *Or* expression is contained within *Or* promoters. These sites are thought to encode information regarding which olfactory appendage, sensilla type and subtype a given *Or* gene will be expressed in. The decision determining in which olfactory appendage a given *Or* gene will be expressed requires two motifs, Dyad1 and Oligo1 (14). Dyad 1 is required for expression of *Or71a*, *Or46a*, and *Or85e* in the maxillary palps (14). Conversely, Oligo1 is required to repress antennal expression of the same maxillary palp ORs (14). Other TFs that regulate OR expression in late stages, such as *acj6* and *pdm3*, also have known binding motifs upstream of OR genes that are required for proper expression of specific set of *Or* genes (55). Examination of the trichoid *Or* promoter structure of *Or47b*, *Or88a*, *Or65a*, and *Or67d* has identified both activator and repressor elements (56). *Or47b*, *Or88a* and *Or65a* are expressed in at4 sensilla, whereas at1 sensilla have a single ORN expressing *Or67d*.

Miller and Carlson identified a GCAATTA motif common to the *Or47b*, *Or88a*, *Or65a*, and *Or67d* promoters they examined (56). Even though this motif served both as an activator and a repressor depending on the position of the motif within the promoter, the TF interacting with this specific motif is still unknown (56). In addition, both *Or47b* and *Or67d* promoters contain repressor elements that restrict their expression to the trichoid sensilla zone on the antennae (56). Deletion of these elements leads to *Or47b* and *Or67d* expression in basiconic sensilla, both in antennae and maxillary palps (56). Interestingly, not only do *Or47b* and *Or67d* promoter deletion transgenes show ectopic expression in different subsets of basiconic sensilla, but *Or67d* expression was also detected in non-neuronal cells, suggesting that there are other factors repressing the expression of specific trichoid *Ors* within subsets of basiconic sensilla (56).

These data point to two prevailing theories of *Or* regulation: larval patterning and restriction of precursor cell potentials that determine the allowable combinations of *Or* genes to be expressed in a given sensillum, and a combinatorial code of terminal selector TFs that control *Or* expression during or after the asymmetric precursor divisions. Both mechanisms work in conjunction with each other to specify ORN fates. This model would also allow for more evolutionary flexibility as evolutionary processes can add or eliminate regulatory factors at different precursor decision points to alter *Or* expression or ORN diversity. What is currently missing is a clear link between these two theories. Unification of these two theories could also explain some of the inconsistencies

between sets of results. For example, why are there Acj6 binding motifs present upstream of *Ors* that Acj6 does not regulate? As discussed earlier, this can be due to either differences in the expression pattern of TFs or the differences in chromatin landscape around *Or* promoters in specific precursors set up by early prepatterning genes. It is plausible to think that the expression of the appropriate OR gene requires the presence of both the appropriate factor and the accessibility of the chromatin. So even though all ORs might have the binding site for a given transcription factor, their expression might not be affected by that transcription factor because of chromatin modifications that are a result of programs that pattern and restrict the differentiation potential of precursors in specific lineages. Understanding the mechanisms that underlie the patterning of precursors will likely be critical to establishing this link and pushing the field forward, as well as leading to key insights into the developmental strategies for generating cellular and neuronal diversity.

1.2.8 MicroRNA control of ORN circuit assembly

In addition to the layers of transcriptional regulation of ORN specification described above, the microRNA *miR-279* has also been implicated in the control of ORN specification, specifically as a regulator of the position of CO_2 sensory neurons (57). In wildtype flies, the CO_2 receptors, *Gr21a* and *Gr63a,* are co-expressed in the ab1 sensilla on the antenna and connect to the most ventral glomerulus in the antennal lobe. In *miR-279* mutants however, *Gr21a* and *Gr63a* expressing ORNs are found in the maxillary

palp and connect to a medial glomerulus (57). The expression pattern and connectivity of these ectopic neurons resembles that of a hybrid between mosquitoes which are attracted to CO_2 and *Drosophila*, which normally avoid CO_2 (57). Further work has demonstrated that *miR-279* functions in the development of maxillary palp olfactory sensilla precursors. *miR-279* is expressed in sensory organ precursors in the maxillary palps and *miR-279* mutants have an extra neuron that is generated within particular palp sensilla (57,58). This is likely due to derepression of *miR-279* targets that function in the developmental program of the sensillum, which eventually determines the number of neurons. In the presence of *miR-279* these factors are downregulated in *Drosophila* leading to the elimination of CO_2 ORNs from the maxillary palps (57,58). The transcription factor Prospero may be a key regulator of this pathway, as it has been shown to activate *miR-279* (58). This work has revealed a new level of post-transcriptional regulation of the development of the *Drosophila* olfactory system, highlighting the complicated nature of generating such a diverse system.

1.3 Axonal Targeting

Not only must ORNs choose a receptor to express in a stereotyped manner, they must also connect to their class-specific glomeruli in the antennal lobe. ORN axons in the antenna form three major bundles that fasciculate to form the antennal nerve (59). Axons from the antennal nerve enter the antennal lobe beginning around 18-20 hrs APF, and once in the brain the antennal nerve defasciculates into a ventromedial and a

dorsolateral pathway (Figure 4) (59). ORN axons then cross the midline via the dorsal commissure and connect to the appropriate glomerulus in both contralateral and ipsilateral antennal lobes (25,26). Maxillary palp ORN axons enter the antennal lobe via labial nerve around 30 hours APF and are guided to their glomerular target regions through interactions with antennal ORN axons that are already within the lobe (Figure 4) (25,60,61). The rest of pupal development of the antennal lobe is devoted to refining and segregating the glomeruli, which are easily identifiable by size, position and structure. In order to achieve the class-specific connectivity of 50 different ORN classes to non-overlapping glomeruli, ORN axons of the same type must converge onto the same glomerulus and synapse with the proper PNs as well as repel axons of all other classes (Figure 4). One simple solution to this problem is the use of olfactory receptors as instructive cues to govern glomerular targeting in order to compartmentalize connectivity in such a diverse system. Indeed, this strategy has been adopted in mammalian olfactory system (62–64). In mammals, *Or* genes encode G-protein coupled receptors, and differences in agonist independent signaling from each OR leads to differences in the levels and combinations of cell surface molecules, which signal to sort out ORN axons as they innervate the olfactory bulb (63,64). Despite the organizational similarities of olfactory system in mammals and *Drosophila*, *Drosophila* ORNs do not require receptor function for glomerular targeting. This suggests that in *Drosophila* programs for regulation of *Or* expression and glomerular connectivity are distinct, but

must be coupled during ORN development. Indeed some of the early patterning factors, such as Hedgehog, also pattern the axonal projections and glomerular connectivity of ORNs (65). In addition, the molecular mechanisms that regulate *Or* expression, such as Notch signaling, and the transcription factors Acj6 and Pdm3, also play a significant role in controlling glomerular targeting (8,54,66). For example disrupting Notch signaling not only leads to conversion of sensory fates but also glomerular targeting (8). Both Acj6 and Pdm3 function to control targeting for different subsets of ORNs, with their loss producing ectopic glomeruli as well as glomeruli with diffuse boundaries (54,66). Because both Acj6 and Pdm3 are transcription factors, it is likely that they regulate expression of cell surface proteins and/or guidance molecules that control wiring identity. It is thought that combinations of cell surface and guidance molecules expressed by ORN classes ensure proper connectivity in stepwise fashion that includes ORN axon trajectory selection, inter- and intra-glomerular interactions that establish glomerular boundaries, and ORN-PN matching that ensures ORN wiring specificity.

1.3.1 Coordination of wiring among neurons within the same sensillum

As discussed earlier, cell bodies of ORNs are clustered within individual sensilla, which develop through asymmetric divisions of a single precursor cell. As ORN axons from the same sensilla enter the antennal lobe they take separate trajectories, along either dorsolateral or ventromedial bundles. Despite the well-known role of Notch signaling on binary segregation of ORN fate decisions regarding olfactory receptor

expression and targeting programs, until recently the molecular mechanisms working downstream of Notch to specifically regulate axonal trajectory selection were unclear. Recent work has connected Semaphorin-2b (Sema-2b) and Plexin-B (PlexB) signaling to proper bundle segregation during this process (67). Sema-2b is member of a family of secreted molecule, which signals through PlexB receptors. *sema-2b* is expressed in ORNs whose axons project along the ventromedial bundle and *sema-2b* mutants lose the binary bundle separation and exclusively project through the dorsolateral bundle (67). This evidence suggests that Sema-2b attracts and consolidates ORN axons into the ventromedial bundle. Notch-Delta signaling, in addition to controlling olfactory receptor expression among the ORNs, also segregates Sema-2b expression within ORNs in the same sensillum (67). Notch signaling negatively regulates Sema-2b expression, where Notch-off neurons are positive for *sema-2b* expression, suggesting Notch signaling negatively regulates *sema-2b* (67). Perturbations to Notch signaling lead to inappropriate expression of *sema-2b* accounting for the glomerular targeting defects observed in *mam* mutants. This is consistent with the observation that glomeruli targeted by Notch-on and Notch-off ORNs are segregated within subsections of the antennal lobe.

1.3.2 ORN Axon Guidance

Once in the antennal lobes, ORNs must navigate to specific regions to ultimately connect to their appropriate PN partners. General axon guidance molecules such as Dscam and Robo receptors were both shown to be required for this process (68,69). Both

Dscam and Robo receptors signal through the SH2/SH3 adaptor protein Dreadlocks (Dock) and the serine/threonine kinase Pak, which suggests that the action of these two molecules is coordinated (68,69). Drosophila has three Robo receptors (Robo, Robo2, Robo3), all of which are expressed in the olfactory system (69). *robo* is broadly expressed across the majority of ORN axons, whereas expression of *robo2* and *robo3* are more restricted (69). *robo2* is enriched in and near the commissure, and *robo2* mutants are unable to properly cross the midline and form ectopic glomeruli near the commissure (69). *robo3* is expressed primarily in axons that follow the ventromedial trajectory, and loss of *robo3* in these axons causes mistargeting and the formation of ectopic glomeruli, although some axons are still able to find the correct glomerulus (69). Suppression of Robo function leads to broad defects in glomerular structure, likely because many axons follow incorrect trajectories and choose incorrect targets leading to indistinct glomeruli (69). Similar to Robos, Dscam is also required for proper glomerular targeting. Dscam is a repulsive cell surface molecule and a member of the IgG superfamily (70). Dscam shows extraordinary molecular diversity through generation of approximately 38,000 alternative splice isoforms (70). Work on *dscam* in other contexts has suggested that stochastic alternative splicing within neurons leads to neuron-specific expression of a subset of *dscam* isoforms, which show isoform-specific homophilic binding (70). In the olfactory system, loss of *dscam* is associated with ectopic glomerular targeting and defects in both ipsilateral and contralateral ORN projections (68). These data suggest

that Dscam is critical for proper targeting and guidance of ORN axons, however this function of Dscam is diversity independent (68). Dscam diversity, on the other hand, is required for the proper class-specific convergence of ORN axons within glomeruli (70) Even though *dscam* null mutants show ectopic glomerular targeting, they can still converge to form proper glomerular structures (68). In contrast, in flies that express only a single *dscam* isoform, ORN axons also show mistargeting defects and are unable to converge into distinct glomeruli (70). It is possible that the diversity independent function of Dscam regulates the initial axon guidance to specific regions within the antennal lobe, whereas Dscam diversity is required for class-specific sorting and convergence into glomerular structures (68,69).

1.3.3 Intra-class attraction

One of the critical steps in ORN connectivity is the class-specific convergence and arborization of ORN axon terminals within a single glomerulus. This requires recognition among the ORN axons of the same class to confine them to the same glomerulus. As discussed above Dscam diversity is required for proper glomerular convergence, as diversity-compromised mutant ORN axons arrive at the antennal lobe yet are unable to converge and establish glomerular boundaries. This likely occurs due to repulsion of ORN axons of the same class in single *dscam* isoform mutants. In addition to Dscam, N-cadherin (Ncad), which belongs to the calcium-dependent cell adhesion molecule family, also contributes to the glomerular convergence (71,72). In the olfactory

system, *ncad* mutant ORN axons correctly target distinct regions within the antennal lobe, but they are not able to properly condense into protoglomeruli during mid pupal development leading to defects in the adult glomerular formation (71). These data suggest that Ncad is required for intra-class attraction during class-specific convergence of ORNs into a single glomerulus. It is not entirely clear whether Ncad also mediates interactions between ORNs or between ORNs and PNs. *ncad* is also broadly expressed across most ORN classes and as such ORN axons must have a way to distinguish and repel different classes.

1.3.4 Inter-class repulsion

Establishing 50 non-overlapping glomeruli for class-specific connections of 50 ORN classes requires inter-class repulsion, which ensures that axon terminals from different ORN classes do not intermingle. Semaphorin-1a (Sema-1a) has been shown to be largely responsible for repulsion between classes of ORN axons. Unlike Sema-2b, Sema-1a is a transmembrane protein that acts through the Plexin-A receptor. *sema-1a* is required for segregating different ORNs into distinct glomeruli (73). Mutants for *sema-1a* show an intermingling of different ORN classes (73). Mutant axons are able to follow the correct trajectories into and through the antennal lobe, but then fail to properly sort into the correct glomeruli, and instead stay intermingled (73). Unlike *ncad*, clonal analysis of *sema-1a* mutants demonstrate that it acts non-cell autonomously, which suggests that its primary role is to repel axons of different classes. This repulsive function is critical for

the formation of distinct glomerular boundaries (73). *sema-1a* is broadly expressed in most ORNs and different classes express *sema-1a* at different levels, but it is not clear how differential expression levels of *sema-1a* lead to glomerular segregation (73). However, Sema-1a signaling acts at short ranges in the olfactory system, which could explain how it can be broadly expressed but lead to fine tuning of glomerular boundaries.

1.3.5 ORN-PN Matching

The final step in establishment of ORN circuits is proper class-specific matching of ORNs with appropriate PNs for synaptic connectivity. It is plausible to imagine that cell surface molecules regulating ORN guidance will ultimately regulate ORN-PN matching. For example, in addition to its function in ORN connectivity, Dscam and Ncad have also been shown to affect PN targeting (74). Loss of *dscam* in PNs inhibits proper arborization of PN dendrites within glomeruli leading to dendritic clumping, consistent with its self-avoidance function identified in other dendritic structures (74). Overexpression of *dscam* in PNs, on the other hand, leads to more diffuse dendritic structures as well as positional shifts (74). Interestingly, the positional shift of PN dendrites also causes ORN axons to shift while maintaining ORN-PN matching (74). This suggests that ORN axons recognize the appropriate PN dendrites, likely through other transmembrane interactions. Indeed, gradients of Sema-2a and Sema-2b expressed by PNs are required to position both PN dendrites and incoming ORN axons to specific

zones within the antennal lobe (61,66). Ncad also contributes to ORN-PN matching. *ncad* mutant axons of both ORNs and PNs ultimately retract, unable to arborize within the glomerulus, and instead remain on the surface of the neuropil (71). The Luo group has also shown that the synaptic partner matching between ORN axons and PN dendrites requires the cell surface molecules, tenuerins (75). Teneurin-m (Ten-m) and Teneurin-a (Ten-a) are homophilic attraction proteins, expressed in matching pairs of ORNs and PNs (75). However, the partially overlapping expression of both *ten-m* and *ten-a* suggests that additional cell surface molecules working in combination should be specifying synaptic matching for 50 different ORN-PN to establish the proper connectivity of the olfactory circuits in the antennal lobes. Indeed, more recently Toll receptors, especially Toll-6 and Toll-7 were also shown to contribute to ORN-PN matching (76). Toll receptors are involved in embryonic patterning and innate immunity, however, their role in connectivity in the olfactory circuit seems to be independent of Toll pathways involved in these processes. Toll receptors encode transmembrane proteins with leucine rich repeats (LRR) involved in heterophilic protein-protein interactions. These results suggest both homophilic and heterophilic interactions govern synaptic partner selection between ORNs and PNs.

1.4 Concluding Remarks

Despite the considerable work that has been done to elucidate mechanisms controlling ORN specification and diversity, much of the molecular details coordinating

regulation of OR expression and wiring decisions to establish ORN circuits remains unknown. First, what molecular mechanisms link expression of specific olfactory receptor and wiring identity? While it is clear from the overall structure of the olfactory system that both decisions must be coordinated, receptor function is not required for proper targeting. As of yet only *notch, acj6* and *pdm3* have been shown to control both processes, but the molecular mechanisms utilized by these proteins at distinct developmental decision points remain largely unknown. Second, how do ORNs and their precursors determine which OR to express? While evidence exists for models of prepatterning of precursors as well as a combinatorial code of terminal selector TF expression, no clear link has yet been established between these two theories. It is likely that stepwise restrictions on distinct fate programs through combinations of transcription factors and cell surface molecules diversify sensory and wiring identities as ORNs are generated from precursors. Future work focusing on identification of these pathways and understanding their molecular and cellular details will allow us to understand mechanisms of neuronal diversity in the nervous system and will likely be broadly applicable in other systems.

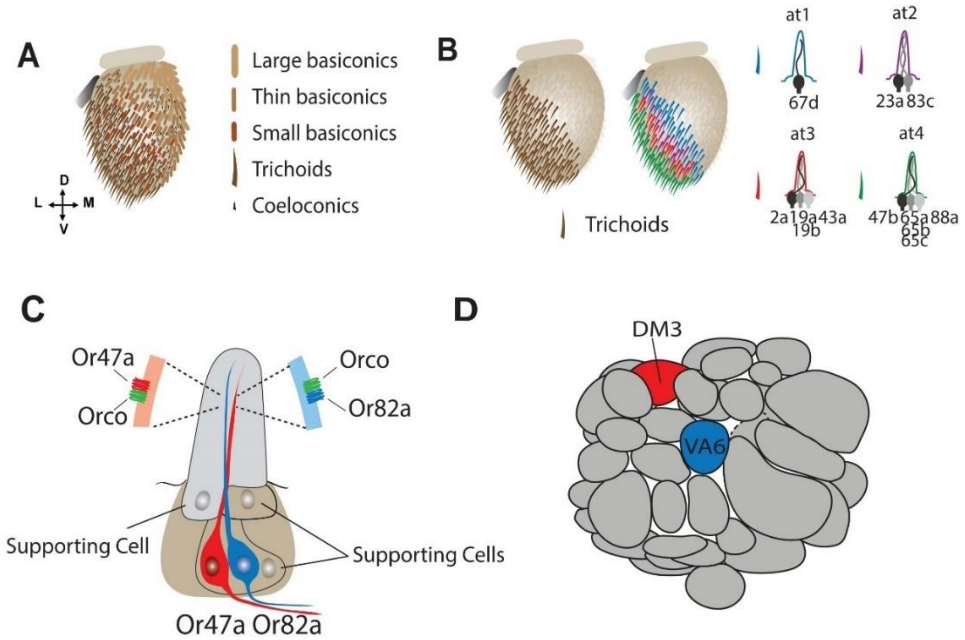

Figure 1: Structure of the *Drosophila* olfactory system. A) The antenna is covered by sensory hairs called sensilla that can be divided into three classes based upon their morphology, basiconics, trichoids and coeloconics. B) Within morphological classes, sensilla can be divided into subtypes defined by the combination of ORNs they house. There are four classes of trichoid sensilla, at1-4. Each houses a unique set of ORNs. C) An example a of a basiconic sensillum. ORNs project their dendrites into sensillum and express their receptors on the surface of their dendrites where the receptors dimerize with the olfactory co-receptor, Orco, and are exposed to the environment. D) The antennal lobe of the fly brain is divided into class-specific glomeruli, where ORN axons synapse with PN dendrites. Each glomerulus is distinguished by its size position and shape. The glomeruli corresponding to ORNs from C are highlighted.

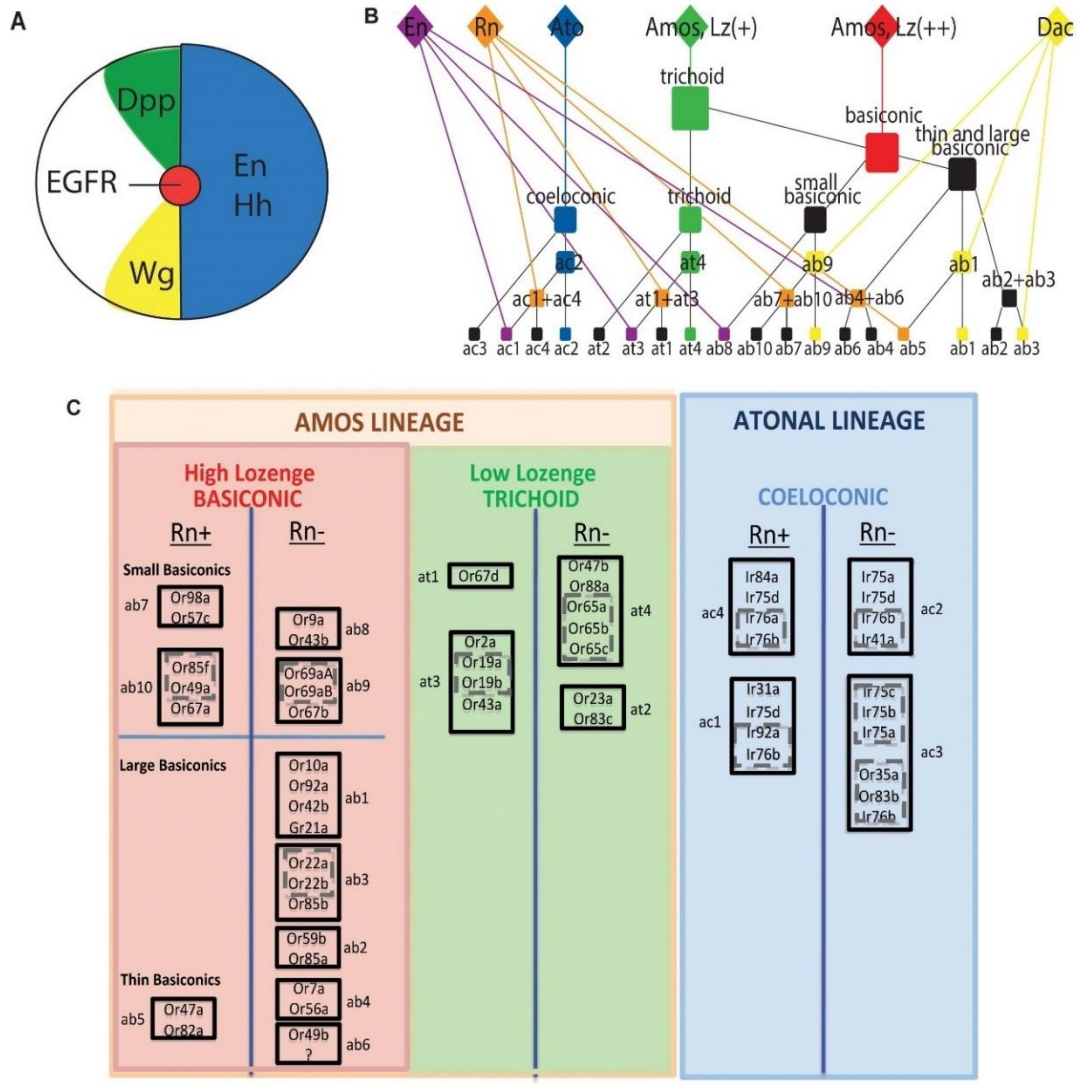

Figure 2: Control of ORN identity by larval prepatterning factors. A) Schematic of morphogen signaling in the antennal disc. *en* and *hh* are expressed in the posterior compartment of the disc and Hh diffuses and signals to the anterior compartment. Wg and Dpp signaling are activated by Hh and establish the dorso-ventral axis. In the center of the disc, where Wg and Dpp signaling events meet, EGFR is activated to establish the proximal-distal axis. B) Decision tree of SOP identity based upon combinatorial expression of prepatterning factors. Each SOP expresses a combination of prepatterning factors that control its fate in a nested and hierarchical fashion. The expression of any given factor modifies the fate of a given SOP based upon the previous or concurrent expression of other prepatterning factors. C) Expression of *lz*, *amos*, and *atonal* define sensillar morphological classes. *atonal* expressing precursors develop into coeloconic sensilla. *amos* expression is required for both basiconic and

trichoid sensilla. The level of *lz* expression then divides out the two classes, with basiconics and thichoids expressing high and low *lz* respectively. *rm* expression creates two populations of precursors within each morphological class, thereby increasing the number of possible sensilla fates by a factor of 2.

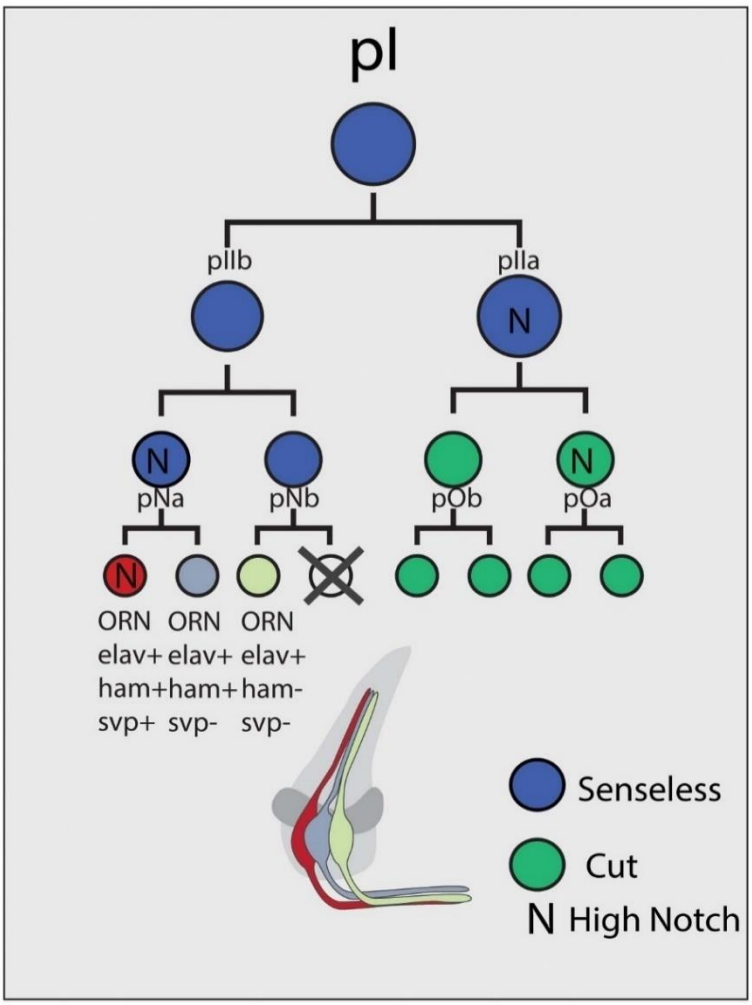

Figure 3: Generation of a sensillum from a single SOP through the use of Notch signaling. The initial SOP, pI, divides to create two daughter cell pIIa and pIIb, which will generate supporting cells and ORNs respectively. pIIb is Notch-off and laterally inhibits pIIa from adopting a neural precursor fate through Notch signaling. pIIa and pIIb undergo two more rounds of division each before generating terminally differentiated cells. Blue cells express *sens*, green cells express *cut*, and N represents a

Notch-On state. Each ORN within a sensillum can also be defined by the combinatorial expression of *elav*, *ham*, and *seven-up* (*svp*).

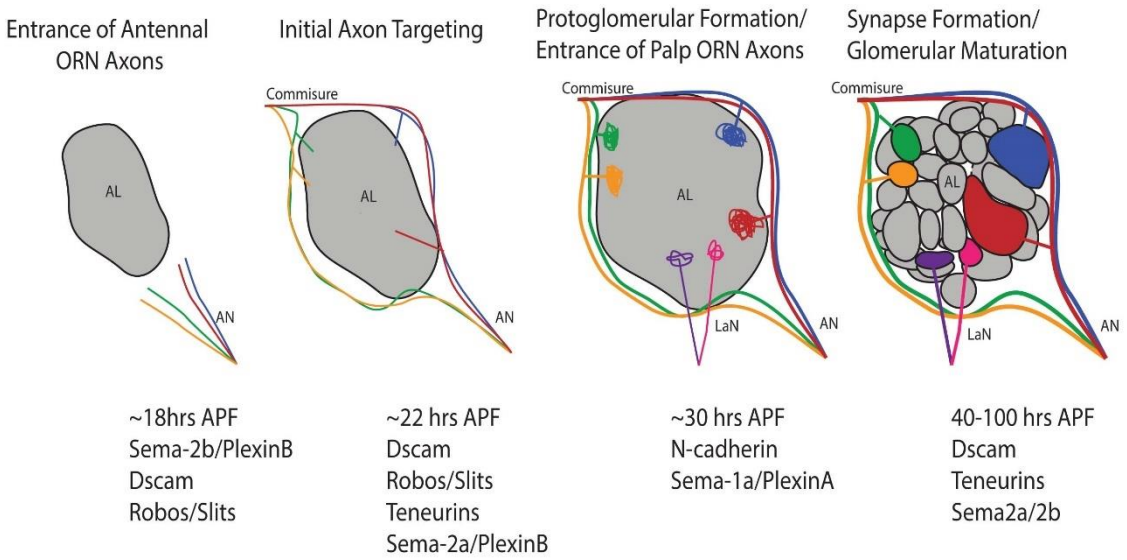

Figure 4: Development of the Drosophila antennal lobe. ORN axons enter the antennal lobe around 18 hrs APF via the antennal nerve, guided by Dscam and Robos, and defasciculate into two major bundles based upon Sema-2b/PlexinB signaling. Around 22 hrs APF ORN axons begin to target their respective glomeruli controlled by Dscam, Robos teneurins, and Sema-2b, and cross the midline at the commissure to reach the contralateral antennal lobe. Around 30 hrs APF maxillary palp ORN axons enter the antennal lobe and protoglomerular formation begins, under the control of Ncad and Sema-1a. From 40 hrs APF on, glomeruli segregate and form distinct boundaries and ORN axons synapse with their PN dendrites, under the guidance of Dscam, teneurins and Sema2a/2b.

2. A Functionally Conserved Gene Regulatory Network Module Governing Olfactory Neuron Diversity

This chapter is modified from the previously published work *Li and Barish et al. (2016). A Functionally Conserved Gene Regulatory Network Module Governing Olfactory Neuron Diversity. PLoS Genetics. 12(1):e1005780. doi: 10.1371/journal.pgen.1005780.*

2.1 Summary

Background

Sensory neuron diversity is required for organisms to decipher complex environmental cues. In *Drosophila*, the olfactory environment is detected by 50 different olfactory receptor neuron (ORN) classes that are clustered in combinations within distinct sensilla subtypes. Each sensilla subtype houses stereotypically clustered 1–4 ORN identities that arise through asymmetric divisions from a single multipotent sensory organ precursor (SOP). How each class of SOPs acquires a unique differentiation potential that accounts for ORN diversity is unknown. Previously, we reported a critical component of SOP diversification program, Rotund (Rn), increases ORN diversity by generating novel developmental trajectories from existing precursors within each independent sensilla type lineages.

The surfaces of these olfactory organs are covered by multiporous sensory hairs, called “sensilla”. Each antenna and maxillary palp contains about 410 and 60 sensilla, respectively, that house clusters of 1-4 ORNs [8,9]. Each ORN typically expresses a

single receptor gene from a repertoire of 80 genes, creating a total of 50 adult ORN classes that are clustered into stereotypical combinations within 22 individual sensilla subtypes [11].

Results

Here, we show that Rn, along with BarH1/H2 (Bar), Bric-à-brac (Bab), Apterous (Ap) and Dachshund (Dac), constitutes a transcription factor (TF) network that patterns the developing olfactory tissue. This network was previously shown to pattern the segmentation of the leg, which suggests that this network is functionally conserved. In antennal imaginal discs, precursors with diverse ORN differentiation potentials are selected from concentric rings defined by unique combinations of these TFs along the proximodistal axis of the developing antennal disc. The combinatorial code that demarcates each precursor field is set up by cross-regulatory interactions among different factors within the network. Modifications of this network lead to predictable changes in the diversity of sensilla subtypes and ORN pools.

Conclusions

In light of our data, we propose a molecular map that defines each unique SOP fate. Our results highlight the importance of the early prepatterning gene regulatory network as a modulator of SOP and terminally differentiated ORN diversity. Finally, our model illustrates how conserved developmental strategies are used to generate neuronal diversity.

2.2 Results

2.2.1 A time-course RNAseq analysis reveals mis-regulation of developmentally critical genes in *rn* mutants

Previously, we demonstrated that the Krüppel-like transcription factor Rn cell-autonomously diversifies ORN classes by branching off novel sensilla subtype lineages from parallel default ones. In *rn* mutants, ORN diversity is reduced almost by half. Neurons from at4 sensilla in the trichoid zone, ac2 in the coeloconic zone, and ab1 and ab9 in the basiconic zone are all expanded at the expense of specific ORNs in *rn*-positive sensilla subtypes (42). To reveal the molecular mechanism by which Rn modulates ORN precursor identities, we compared transcript abundances from a time-course RNAseq analysis in wild type (w^{1118}), heterozygous and homozygous *rn* mutant flies (see Materials and Methods) at four temporal landmarks during antennal development. We surveyed the prepatterning (larval), SOP selection (8hr pupal), neurogenesis (40hr pupal) and terminally differentiated adult stages (38–42,77). For the adult stage, changes in OR expression in *rn* mutants were consistent with the overall trend described from our previous report (Figure 5), suggesting that our experiment effectively identifies genes whose expression is affected by *rn*.

To find key developmental genes likely acting downstream of Rn, we focused on the three early stages. As Rn is only expressed during larval and early pupal periods, we reasoned that the genes under direct Rn control would show differential expression in one or more of these early time points. A Venn diagram generated from the final lists for

all early stages reveals that some genes may be misregulated only in one particular stage, while others show misregulation—both up and down—across multiple stages (Figure 6A, B, also see Materials and Methods).

Although an in-depth analysis of all genes affected by Rn is beyond the scope of this analysis, several pieces of evidence suggest that genes important for development are misregulated in the *rn* mutant background. GO term analysis showed an excess of misregulated genes with potential functions in development, such as transcription factors and signaling molecules. In addition, functional clustering analysis using the online tool, DAVID (78,79), for each category in the Venn diagram, uncovered a functional group including homeodomain(-like) proteins BarH1/2 (B-H1/2, Bar or B) and Bric-à-brac1 (Bab1) as being modified in rn mutants. Interestingly, both B-H1/2 and Bab1 showed changes in transcription levels only during early developmental stages (Figure 7A). It is important to note that B-H1 and B-H2, as well as Bab1 and Bab2, are functionally redundant, and have extensively overlapping expression patterns (Figure 8B) (80,81). Because only bab1 but not bab2 was included in the initial functional clustering analysis, we re-examined the RNAseq datasets for bab2. We found that bab2 had an overall higher level of expression than bab1, and similar trend of misregulation exists for bab2 (Figure 7A). While the p values were still above the arbitrary cutoffs in several cases—likely due to the cellular heterogeneity of antennal disc samples used in transcriptome analysis—the interrelatedness of these genes and *rn* suggested that they

together might have an important role in ORN diversity. Thus, we focused on B-H1/2 and Bab1/2 in this study and explored their roles in ORN diversification further.

2.2.2 A common molecular network patterning the antennal and leg appendages

Rn was previously reported to function in a gene regulatory network together with B-H1/2, Dachshund (Dac), Apterous (Ap) and Bab1/2 to pattern the segmentation of the *Drosophila* leg disc in the proximodistal (PD) axis (82,83). In the leg, the temporally dynamic PD gene regulatory network, under the influence of morphogen gradients, defines a number of concentric domains on the leg disc via cross-regulation, which in turn determines individual segment identities in the leg. These data led us to hypothesize that the neuronal diversity phenotypes observed in *rn* mutants arise due to the changes of expression domains for the PD network components during antennal disc patterning. To test this hypothesis, we first systematically examined the spatial patterns of these factors in the developing antennae of wild type animals, and found that each factor is expressed in a concentric ring along the PD axis of the discs (Figure 7B). The gene expression patterns are remarkably similar between the legs and antennae, suggesting that these two organs share the same molecular tool kits that pattern their respective discs (84–87).

Rn was previously shown to be a positive regulator of Bab1/2 and a negative regulator of B-H1/2 in the developing leg disc (84,85). Given the evolutionary relationship between the leg and the antennae, we thought a similar regulatory network

may exist in the antennal disc (88). Indeed, the regulatory relationships of PD genes from the leg-patterning network can explain the misregulation of B-H1/2 and Bab1/2 in the antennal disc in our RNA-seq data. This idea was then confirmed by examining their *in vivo* expression patterns (Figure 7C-E, Figure 8A). B-H1 is normally expressed in the center of the disc, bounded by the central fold (Figure 7C). In *rn* mutants, B-H1 is expanded outside of the central cells into cells that are normally Rn-positive and B-H1/2-negative, but the expansion is confined within the distal boundary of Dac (Fig 1C). The ectopic cells that are labeled with B-H1 antibody in *rn* mutants are positive for the *rn* promoter reporter, suggesting that this *rn*-positive precursor domain may have switched fates as a result of the loss of Rn and the expansion of B-H1/2 (Figure 7C). On the other hand, Bab2 expression is significantly reduced in *rn* mutants (Figure 7D, E). Consistent with the RNAseq results, we did not detect obvious changes in *ap* expression in the third instar larval stage (Figure 8A, Figure 10E and F). Taken together, these results suggest that a common PD gene regulatory network module operates in parallel during leg and antennal disc development.

2.2.3 Expansion of Bar expression in *rn* mutants underlies changes in ORN diversity and expansion of a default fate

In *rn* mutant antennae, the number of ORNs in some *rn*-negative sensilla (e.g. Or47b ORNs in at4) are increased at the expense of ORNs in *rn*-positive sensilla (42), and this occurs in parallel to the expansion of *Bar* in the antennal disc. To test if the expansion of Bar leads to an increase in at4 ORNs in *rn* mutants, we analyzed *Bar/rn*

double mutants. Normally, approximately 60 Or47b ORNs are found in wild type and this number is increased to ~90 in *rn* mutants (42). We first generated eyFLP-induced MARCM clones, which induced small clones that are either wild type or *Bar* mutant in approximately 20% of all ORNs (Figure 9C, D). These analyses showed that the number of total Or47b ORNs in *Bar* mutant clones was not significantly different than that of the wild type clones. However, when generating similar *Bar* mutant antennal clones in *rn* mutant animals, we detected a statistically significant suppression of Or47b ORN expansion down to ~80 cells, using ANOVA and post-hoc Student's T-test (Fig 2A, B, $p>0.01$, Fcrit=3.25, df=39). We specifically detected a loss of Or47b ORNs from the ectopic antennal zone seen in *rn* mutants (Figure 9A). These data suggest that the expansion of Bar is causal for the increase of at4 ORN fates in *rn* mutants. As at4 sensilla are *rn* and *dac*-negative (42,43), they are likely developed from the Bar-positive inner circle of the disc (Figure 7B, also see below for genetic analyses and fate mapping). Consistently, at4 ORNs express the *Bar* promoter reporter (Figure 11, Table 1). Remarkably, Bar seems to be dispensable for the endogenous at4 fate (Figure 9C-D), presumably due to the robustness of this fate to genetic perturbations.

2.2.4 Rn directly binds upstream of *BarH2* and *bab2* gene regions in vivo

Next, we wanted to know if the genes in the network directly regulate each other. We focused on the function of Rn, as this may help explain the misregulation of *B-H1/2* and *bab1/2* in *rn* mutants. Previous *in vitro* assays have shown that Rn binds to a T-

rich motif (T13) in the LAE (leg and antennal enhancer) sequence upstream of *bab2* to activate its expression during leg and antennal development. However, *in vivo* evidence for Rn binding targets has been missing due to the lack of a high-quality antibody. We generated a fly line that carries an EGFP endogenous tag for Rn (Rn-EGFP), which was confirmed and validated for functionality (89). We then used EGFP antibodies to do chromatin immunoprecipitation (ChIP) followed by qPCR to test binding of Rn to *bab* or *Bar* regulatory elements in the antennal discs.

qPCR primers were designed in the first 2kb upstream of the transcription start site (TSS) in the *Bar* loci (Materials and Methods). A primer set covering the T13 motif in the *bab2* enhancer was used as a positive control, while the M1 motif region from Or82a promoter was used as a negative control (42,85). ChIP on antennal disc tissues was able to detect direct binding of Rn to the published *bab2* enhancer and the promoter region of *B-H2* using the Rn-EGFP line, and further confirms that Rn does not bind to OR promoters (Figure 9E). We noticed that the binding of Rn to the *bab2* promoter is more robust compared to *B-H2* sites, which might arise due to the differences in the genomic organization of these binding sites. Since both *B-H2* and *Or82a* contain T13-like motifs in their upstream regions, the binding of Rn seems to require some special chromatin environment and/or the facilitation of binding by other factors in addition to the presence of a T13 consensus sequence. While our analysis cannot distinguish whether Rn binds to a different motif in the *B-H2* promoter, these results suggest that the

concentric TF domains may be formed by cross-regulatory relationships, and that Rn regulates components of the network through directly binding to their promoters.

2.2.5 Partitioning of prepatterning domains

We noticed that the expression domains of several PD factors overlap in the third instar antennal disc, and therefore we wanted to dissect the spatial relationships between these factors more carefully. To simplify the descriptions, we use the central fold (CF) as a landmark, which is usually observed as an unstained dark circle in a superficial section of confocal images, to separate the disc into inner and outer regions (Figure 10B, Figure 8D). In the outer region, *dac*, *rn* and *bab* are expressed from more distal to more proximal areas in the disc (Figure 10B). Due to the substantial overlap in their expression patterns, these three factors divide the region into four concentric rings. We number the rings starting with the outermost one being R(1), and therefore R(1) to R(4) are assigned to this region because they express combinations of *dac*, *rn*, and *bab* (Figure 10A, B, Figure 8D). *bab* is expressed in a gradient, similar to its previously reported expression in the leg discs (90). Our results show that the highest level of Bab is found near the central fold, and its expression decreases toward both outermost and innermost areas of the disc (Figure 10B, Figure 8C).

Three more rings can be found inside the central fold. R(5) is the only ring that shows quadruple labeling by 4 factors examined (*rn*, *bab*, *ap*, and *Bar*) (Figure 10C, D). This ring also corresponds to the only region that expresses Rn inside of the central fold

(Figure 10C-F). Bar expression cannot be detected in the centermost region (Figure 10C-E). Taken together, the partial overlapping patterns of *dac*, *rn*, *bab1*/2, *B-H1/2* and *ap* expression demarcate seven concentric ring domains in the third instar antennal disc, and each ring is marked by a unique combination of prepatterning factors (Figure 10A, Figure 8D).

2.2.6 Sensilla subtype fates mapping onto the prepatterned domains

Next, we asked which precursor identities are generated from each of these seven domains. As all of the components within a sensillum arise from a single SOP, we wanted to know the sensilla subtype identities of SOPs from each concentric domain. To do this, we used promoter-driven reporter lines for each individual gene to label ORN axons. Because ORN sensory identities are closely linked with the glomerular identities in the brain, we can infer which ORN classes express the given factor from the glomerular labeling pattern in this analysis (Figure 11, Table 1, and Figure 12). *Bar*- and *bab*-GAL4s were analyzed at both adult and pupal stages, whereas *ap*-GAL4 was analyzed only at mid-pupal stages due to the lack of adult expression.

2.2.6.1 Ring 1

ab1, ab9, and ab3 are labeled by the *dac* reporter, but negative for *rn*, *Bar* and *ap* (Table 1), and it has been shown that Dac is required for the specification of these three sensilla subtypes (43). Therefore, we map ab1, ab9, and ab3 to R(1) (Figure 13A). However, they are also positive for *bab* based on reporter expression in ORNs (Table 1,

Figure 11). Because there is no ring that is positive for Bab and Dac expression but negative for Rn in the 3rd instar larval antennal disc based on antibody stainings (Figure 10A), we attribute this discrepancy to either an artifact of the *bab* reporter or late expression of Bab unrelated to precursor fate determination.

2.2.6.2 Rings 2, 3, 4, and 5

Next, we wanted to map sensilla to the middle 4 rings all of which are *rn*-positive. Because the only Rn-positive, Bab-negative and Dac-positive domain is R(2) (Fig 3A), we assigned this ring with the ab10 fate, which is the only sensilla subtype that meets the same criteria (Table 1, Figure 11, 13A). Likewise, ab7 and ai1 are the only two sensilla subtypes that are triple labeled by *rn*, *bab* and *dac* reporters, and are therefore mapped to R(3) (Table 1, Figure 13A). at1, at3, ab5 are labeled by *rn* and *bab* but not by any other reporters, we assigned them to R(4) (Table 1, Figure 13A). Finally, ac1 and ac4 are mapped to the quadruple positive R(5). Consistent with this mapping, these two sensilla are positive for *rn* and *bab*, and ac1 is labeled by the *ap* reporter, ac4 is labeled by the *Bar* reporter. Even though it seems neither of these two sensilla are labeled by all 4 factors simultaneously, the expression of these factors may be only required for precursor fate specification in a narrow window of the larval stage, and later restricted to specific lineages and daughter cells for downstream functions. Consistent with this explanation, *ap* expression is highly dynamic, and disappears in the adult stage. We also detected *dac* and *Bar* expression in IR75d ORNs in coeloconic sensilla, which is the only

ORN class that is found in more than one sensilla subtype (ac1, ac4, and ac2). We currently cannot distinguish whether this is due to a developmentally related event unique to this ORN class or is an artifact of the reporter expression.

2.2.6.3 Ring 6

R(6) is labeled by Bar, *ap,* and Bab in the antennal disc (Figure 10A, C-E). The only remaining sensillum that is unambiguously labeled by these three factors is at4. Consistent with the notion that these sensilla arise from R(6), at4 sensilla are expanded in *rn* mutants (42) and this expansion is dependent on the expansion of *Bar* expression in the disc during development (Figure 9A, B). The only other sensilla subtype that is left and also expanded in *rn* mutants is ac2, which is *bab*-, *Bar*-positive, and *ap*-, *rn*-negative. Given that ac2 behaves similarly to at4 from our genetic studies (see below) and previously published results (42), we deduced that the R(6) region generates precursors that give rise to ORNs in ac2, as well as at4 sensilla (Figure 13A). The reporter line we used for *ap* may not capture its expression in ac2 ORNs properly due to the complexity of its enhancer elements.

2.2.6.4 Ring 7

Finally, at2, ab2, ab4, ab6, ab8, and ac3 are *rn*-negative and unaffected in *rn* mutants (42). This would place them either in the center of the disc or on the periphery, based on whether they express *dac* (periphery) or *ap*/*bab* (center). Because all contain at least one ORN class that is positive for *ap* and/or *bab*, but they are all negative for *dac*, we

assigned them to R(7) in the center (Table 1, Figure 11, 13A). ab3 has been placed within R(1), because of the expression of *dac* and its requirement for the development of ab3 ORNs (Figure 13A). However, ab3 behaves similarly to the sensilla subtypes from the center R(7) in some genetic manipulations (see the following section). We are thus unable to fully resolve the origin of ab3 sensilla. It is possible that ab3 is determined by different sets of factors, one specified in R(7), and the other one specified in the outermost R(1).

These series of analyses provide us with a sensilla subtype fate map on the concentric domains of the larval antennal disc. Each ring is labeled by a unique set of PD transcription factors, corresponding to a specific subset of sensilla subtype fates (Figure 13A). We used this model to explain the majority of the phenotypes observed in *rn* mutants and other perturbations of the network components (Figure 13B, Appendix A).

2.2.7 Functional involvement of PD genes in generating ORN diversity

Our model makes predictions as to how manipulations of the patterning network would lead to changes in ORN diversity. As previously reported, *rn* mutation effectively halves the amount of ORN diversity in the antenna (42) (Figure 7E-G, Figure 9A-D). We constructed a scheme to depict the spatial relationships of the PD transcription factors in *rn* mutants (Figure 13B). In this model, the TF combinations in rn-positive domains, namely R(2) to R(5), are altered due to the changes to the expression of Bar, Bab and Rn. As a result, R(1) would be expanded into R(2) and the proximal portion of R(3).

Similarly, R(6) would be expanded into R(4) and R(5) in *rn* mutants (Figure 13B, Appendix A).

Because we observed an expansion of Bar in *rn* mutants and this expansion is required for their ORN phenotypes, we wanted to test the effects of ectopic *Bar* expression in the *rn* expression domain on ORN populations. Ap was previously shown to protect Bar from being repressed by Rn during leg development (84), and as expected, *ap* overexpression resulted in the ectopic expression of Bar protein outside of its normal boundaries in the antennal disc (Figure 15B, C). Therefore, either overexpressing Bar directly or indirectly by overexpressing *ap* should at least partially recapitulate the adult ORN phenotypes in *rn* mutants. We analyzed OR expression as readouts of ORN classes using quantitative RT-PCR (qRT-PCR) for a panel of 20 olfactory receptor genes representing each of the antennal sensilla subtypes in these genetic backgrounds. We confirmed that this assay provides a reliable readout of ORN fates, by showing that the predicted OR expression profiles in *rn* mutants were readily reproduced (Figure 13C) (42).

As predicted, when *Bar* or *ap* was overexpressed, the changes in the expression of the majority of ORs trended towards changes observed in *rn* mutants (Figure 14D, 15D). One exception was Or47b in at4 that was downregulated in *Bar* overexpression lines. We have already shown, however, that the expansion of *Bar* expression accounts for the increase of at4 sensilla in *rn* mutants. To reconcile this discrepancy, we re-examined the

expression of *Or47b* using a reporter line in *Bar* overexpressing flies. Although we observed an overall decrease in the number of Or47b neurons consistent with the qPCR result, the domain of expression was expanded to the medial region similar to the manner observed in *rn* mutants (Figure 16). In agreement with the expansion of at4 sensilla, glomerular sizes appeared larger for all at4 ORNs (Or47b, Or88a, and Or65a) compared to wild type (Figure 17A, B and D), a similar phenomenon observed in *rn* mutants. (Figure 17A, C) (42). In contrast, the target glomeruli are lost for ab5 ORNs, which show dramatic reduction based on OR expression in qRT-PCR (Figure 14D, 15D, 17A-D Fig). We further validated the expression of a subset of ORs in the antenna using reporter lines, we could recapitulate the same changes in OR expression uncovered by the qPCR analysis (Fig 17E-M). Of particular note is that ORs in the same sensillum (ab10: Or49a, ab7: Or67c) changed in a similar manner to their partner OR genes (ab10: Or67a, ab7: Or98a) (Figure 14D, 15D, 17E-M). These results suggest that manipulating the PD gene network causes switches of SOP fates and ORN populations.

During our examination of Bar-overexpressing larval antennal discs, we found that the central fold (CF) disappeared (Figure 14B, C, 18). In contrast, *ap* and *bab* expression patterns were unaffected (Figure 18). Similarly, *dac* showed normal

expression, despite the reported function of Bar to repress *dac* in the distal area, which suggests that the repression may be time-sensitive and/or context-dependent (80,86).

Next, we examined the effects of *ap* overexpression on the expression patterns of the network genes in the antennal disc. Similar to *rn* mutants, an expanded Bar zone is bounded by the distal limit of *dac* in this background (Figure 15B, C). However, unlike in *rn* mutants, *Bar* does not fully extend to the boundary, and hence, these proximal cells in R(4) are positive for *rn* but negative for *dac* and *Bar* (Figure 19D). They also express *bab* and *ap*, making them a separate subpopulation within R(4). In addition, we saw a loss of *rn* expression in R(5), leaving the domains within the central fold devoid of Rn expression (Figure 19A-C). The simplest interpretation of these data is that increased levels of *ap* repress *rn* expression in a context-dependent manner. Moreover, we found that *dac* expression is decreased in R(2) and R(3) that also express Rn (Figure 15B, C), suggesting that *rn* promoter-mediated *ap* expression represses *dac* in this overlapping domain. Because Dac represses *bab* (91), the reduction in *dac* expression should theoretically cause an increase in Bab expression, although we cannot detect any obvious changes for Bab. This may be due to its overall low concentration in this region by repression from other factors (91).

Based on these analyses, we drew similar illustrations for precursor domains in the *ap* and *Bar* overexpression backgrounds (Figure 14A, 15B, Appendix A). They reveal different patterns of gene expression for a number of rings compared to the *rn* mutants,

which may account for their differences in adult ORN classes as shown by the qPCR results (Figure 14D, 15D). We conclude that the PD genes function in combinations to diversify precursor and ORN fates.

We next examined the requirement of Bar in producing the four fates that arise from the *Bar*-positive region (Figure 13A). To do this, we created *Bar* mutant clones that delete both *BarH1* and *BarH2*. However, our analysis did not reveal any significant changes in adult OR expression (Figure 20A, Figure 9C, D). The most likely explanation for this observation is that Ap and Bar may have partially redundant functions for some sensilla subtypes, such as at4 and ac2 in R(6). Consistent with this, transheterozygous *ap* mutant alleles using $ap^{md544GAL4}$ and the *nap1* deficiency did not affect ORNs from at4 and ac2 precursors, either. In fact, only three sensilla subtypes (ab4, ab6, and ac1) from R(7) and R(5) showed modest decreases in OR expression in *ap* mutants (Figure 13A, 20B). These results suggest that the developmental refinement of SOP fates in the three inner rings are robust, which makes their dependence on factors like Bar and Ap limited.

It has been shown in the leg that this network of PD genes functions under the control of an EGF signaling gradient, which is highest at the center of the disc and decreases outward (92). There, EGFR signaling represses *rn* and activates *Bar* expression (82,92). We next tested the hypothesis whether perturbations in EGFR signaling can cause modifications to ORN fates. To do this, we expressed a constitutively active EGFR (92) using rn^{89GAL4} and performed qRT-PCR on ORs (Figure 21A). As expected, these

experiments showed that ectopic activation of EGFR function is associated with an expansion of Bar and reduction of Rn expression in the antennal disc (Figure 21B, C). In addition, the ORN classes originated from R(1), R(2), R(3), and R(5) precursor domains were affected in the adult. These results suggest that EGFR signaling may indirectly regulate ORN diversity by modulating the PD gene network.

2.2.8 Separation of different precursor fates within a ring by Bab concentration gradients

Bab is partially activated by Rn, and it is significantly downregulated in *rn* mutants (Figure 7F, G). It is plausible to think that Bab functions downstream of Rn to specify *rn*-positive precursor fates. If this is the case, we should see reduced expression of the receptors from the eight *rn*-positive sensilla subtypes in a *bab* mutant. To our surprise, only two of the eight receptors tested showed reductions, and another two were even increased in the bab^{PR72} hypomorphic allele (Figure 22B).

We noticed a range of changes for sensilla subtypes from the same ring (Figure 22B). For example, among sensilla specified in R(7), ab2 and ab6 are reduced, whereas at2 is increased in the *bab* mutant. The simplest interpretation is that different levels of Bab are required to distinguish these fates in the same ring. When the overall level of Bab is decreased, some sensilla requiring higher Bab may be converted to the ones that require lower Bab. Similarly, only ac1 from R(5) is reduced, and one explanation is that the lowered Bab expression is still above the threshold for specifying ac4, but not for ac1. Alternatively, ac1 (requiring higher Bab) may be converted to ac4 (requiring lower Bab),

and compensates for the loss of the endogenous ac4, which may die due to the loss of Bab. The same reasoning can be applied to ai1 versus ab7 from R(3). For R(4), we saw increases in at1 and ab5, and a trend towards downregulation for at3 in the mutant, albeit the latter was not significant (Fig 8B). We then counted the number of Or19b neurons housed in at3 sensilla, and found that it is significantly reduced (Figure 22C, D). This discrepancy in the qPCR result may be due to the random fluctuation of gene expression levels, especially when the changes in the numbers of cells are small. This result suggests that similar conversions may occur in R(4) among the three fates when Bab is reduced. In contrast, the *bab*-positive at4 and ac2 from R(6) appear to be normal in this hypomorphic allele. This could either be because these two sensilla are specified with wider ranges of Bab levels or some other factors are needed to differentiate the two fates. Taken together, these data suggest that Bab could be an essential factor to distinguish alternate SOP fates within a ring using its concentration gradient.

2.2.9 Functionally conserved molecular network in patterning gustatory receptor neuron fates

The distal portions of both the legs and antennae are chemosensory organs covered by sensilla. The legs, being part of the gustatory system, display neuronal and molecular diversity that is characterized by a huge variety of gustatory receptors expressed on the legs. Unlike ORNs, individual gustatory receptor neurons (GRNs) express multiple receptors, and a given GRN class can be found in different sensilla within different GRN clusters (36).

Because the legs and antennae use the same molecular network to pattern these chemosensory appendages, we asked if a similar genetic program operates to pattern the adult GRN fates. We tested this hypothesis in *rn* mutants as Rn is thought to be required for the development of tarsal segment 3 (ta3), and this segment is lost in *rn* mutants (93). However, we do not have a reporter line that uniquely labels ta3.

On the other hand, *Gr5a* and *Gr61a* are expressed in the mid and hind legs, where they are restricted to the GRNs in ta4 and ta5. In both cases, we could reproducibly detect an extra neuron in the mid or hind legs in *rn* mutants (Figure 23 and 24). To confirm this result, we used a reporter to label the bitter receptor Gr58c, which is expressed by a partner neuron in the same sensilla. We observed ectopic Gr58c neurons in *rn* mutants (Figure 23). In contrast, the *Gr43a*-expressing neurons, which coexpress *Gr61a* but are housed in another sensillum appeared be unchanged in the mutant (Figure 24). These results suggest that the sensilla, 5b and 4s, that house the *Gr5a*/*Gr61*-expressing sugar neurons and the *Gr58c*-expressing bitter neuron are expanded towards the proximal segment of the legs in *rn* mutants (Figure 23). Taken together, we speculate that the same molecular network is used in parallel to diversify chemosensory neurons in the antennae and legs.

2.3 Discussion

How neuronal diversity in the brain is generated from a limited genomic toolkit remains largely unknown. In the *Drosophila* olfactory system, selective expression of

typically a single olfactory receptor gene from a repertoire of approximately 80 possible genes generates 50 different classes of ORNs. ORN classes are found in invariable clusters of 1-4 neurons in individual sensilla, which can be classified into types based on their morphology and subtypes based on the specific combination of ORN classes they house (18,19,24). Here, we show that a functionally conserved cross-regulatory transcription factor (TF) network module patterns the ORN precursor field along the proximodistal axis prior to neurogenesis. The interactions between different components of the TF network module partition the precursor field into concentric domains in response to an EGF signaling gradient. These domains represent clusters of epithelial cells with distinct differentiation potentials, which are defined by unique combinations of TFs that ultimately drive specialization of these cells into sensilla subtype lineage-specific SOPs. Genetic manipulations of the network alter this combinatorial code and lead to predictable shifts between sensilla subtypes and neuronal identities. Our results suggest that this early TF network plays a major role during neuronal diversification by prepatterning the antennal disc, thereby restricting the identities of cells in the precursor field.

Although our model of sensilla fate mapping can explain the majority of sensilla subtype specification and consequent ORN diversity, it is likely incomplete. For example, some distinct sensilla subtypes within a ring are specified by the same set of factors suggesting that additional/unknown genes must be contributing to the

differentiation process. One possibility is that factors that establish the dorsal/ventral (D/V) axis or anterior/posterior axis, such as *engrailed* and other prepatterning genes such as *lozenge,* can be superimposed onto the presented network and used in this process. These factors might function to regulate the expression of proneural genes, *atonal* and *amos,* adding an additional spatio-temporal aspect to regulate the selection of SOPs from prepatterned fields, as in the case of *amos* being regulated by *lozenge* (38,39,41,94). Further work should address the contribution of these axis determination events to ORN diversification. The current study mainly focused on the final phase of the prepatterning stage, and hence the functional relevance of the temporal aspect of the TF network deserves further investigation.

2.3.1 A common strategy with simple logic steps for generating neuronal complexity

We propose a conserved stepwise strategy to explain the overall ORN diversity. First, the prepatterning phase generates distinct pools of epithelial cells with unique differentiation potentials. This is followed by sensory organ precursor selection by proneural genes. Finally, these precursors undergo neurogenic divisions that allocate alternate fates into daughter cells through Notch signaling and terminal selector transcription factors. One salient aspect of this cellular diversification strategy is its modularity. Each step is driven by context-independent rules, yet produces vastly different neuronal outcomes across systems in a developmentally context-dependent manner. For example, Rn is used to generate distinct precursor differentiation potentials

in both the antennal and leg discs to increase the complexity of the patterned precursor fields, which give rise to ORNs and GRNs, respectively. Similarly, Notch is reiteratively used during SOP divisions to generate each sensillum. Its function of segregating binary cell fates is context-independent, although the exact fates being segregated are quite different for each sensillum (8). Therefore, this stepwise mechanism simplifies the overall difficulty of creating neuronal diversity all at once by logically deconstructing similar differentiation processes into single-purpose steps with shared control elements. Even though our findings are in the PNS, there are similar examples of stepwise patterning and diversification in the fly CNS. For example, different neuroblast lineages in the *Drosophila* embryonic CNS are first specified by spatially restricted factors within specific positions of an orthogonal grid in the embryo (95). Anterior-posterior axis specification is controlled by Hox-segment polarity genes, which determine the overall fate, just as in the PNS (leg vs. antenna). Dorsoventral patterning is controlled by cross-regulatory transcription factors, which are turned on in response to different concentrations of morphogens such as Hedgehog and Dpp. Similar to olfactory SOPs, patterning of the neuroepithelium is followed by the expression of proneural genes and selection of neuroblasts, which undergo asymmetric divisions and neurogenesis. The division patterns and factors that are asymmetrically segregated into each daughter cell are remarkably similar regardless of the neuroblast lineages to which they belong (95,96).

There are also parallels between our findings in the fly olfactory system and the more complex vertebrate olfactory system. Even though stochastic selection has been proposed as a mechanism for the expression of specific OR genes by different ORNs, the restriction of mammalian OR expression into distinct zones suggests that a deterministic mechanism may also be at play (14). Consistent with this hypothesis, some OR classes that are restricted to specific domains in the mammalian olfactory epithelium were shown to contain known TF binding sites (97,98). Interestingly, some TFs, such as the mammalian orthologue of Apterous, Lhx2, have evolutionarily conserved developmental functions in olfactory neurons (99). We are curious to see if any of the mechanisms used in diversifying fly ORNs are also used in the mammalian system during the step of OR zonal separation. We suspect that some of the mechanisms used in diversifying fly ORNs may also be used in the mammalian system during the step of OR zonal separation.

Examples of similar neuronal diversification cascades utilizing gene regulatory networks under morphogen gradient control are also seen in the vertebrate CNS and PNS. In the classic example of spinal cord neuron diversification, morphogen gradients (BMP/Shh) along the D/V axis of the neural tube activate different sets of transcription factors in the precursors to set up a number of domains prior to neurogenesis, thereby diversifying both progenitor and sensory neuronal subtypes they generate (100,101). Recently, the radial glia that give rise to neurons of the cortex were also found to be

heterogeneous (102). Such combinatorial TF network modules confer positional and temporal information to each neural stem cell in order to create a diverse progenitor population in the mammalian cerebral cortex (102). Segmental patterning of these neural stem cells contributes to neuronal and glial diversity (103). Similarly, cortical projection neuron fates can be switched among lineages when the corresponding gene network is modified, changing the zonal partitioning of the neocortex (104). These results, in light of our findings, point to a common strategy composed of modular and simple commands functioning in a nested manner to increase neuronal diversity in multiple developmental contexts.

2.3.2 ORN precursor fate specification and OR expression

We associate terminal differentiation of ORNs with the specific selection of an OR gene for expression. At least in flies, it is possible that OR expression and ORN diversity are regulated by a set of "terminal selector genes," similar to those proposed by Oliver Hobert (49). Here a TF, or combination of TFs, directly regulates the expression of genes required for terminal differentiation and function (49). So far, a list of postmitotic TFs have been shown to directly regulate OR expression by associating with OR promoters (47,52–54,105). However, the loss of these TFs only affects the expression of specific subsets of OR genes, and yet most OR genes have binding sites for these factors. The functional specificity of each TF and their expression patterns in ORN classes have not been well defined. It is possible that chromatin states around OR

promoters in different ORN classes govern how these TFs function within each class. Epigenetic modulations of chromatin status have been shown to play an important role in numerous developmental processes, including the development of the olfactory system (46,48,106–108). The prepatterning TFs could recruit epigenetic modifying factors to change the open and closed states of the chromatin around genes critical for different fates. These modifications can be inherited during cell divisions, and affect the genomic accessibility of later factors. Regardless of the exact mechanisms in between, it is likely that the expression/function of terminal selector genes are regulated, at least in part, by the developmental context established by the prepatterning network that we have described. Establishing a clear link between the early patterning networks and the late terminal selector TF network will be critical to resolving these paradoxical results.

2.3.3 Deployment of the same network module in diversifying olfactory and gustatory neurons

This patterning network is remarkable in its functional and structural similarity in driving neuronal diversity in two related chemosensory organs, the antennae (olfactory) and the legs (gustatory). At the top of the hierarchy of the cascade, Hox genes determine the overall neuronal identities within the discs during embryogenesis. Olfactory lineages, for instance, are determined by the gene *homothorax* in the antennal disc, whereas *homothorax* is inhibited by Antennapedia in the leg discs conferring gustatory identities (30). Strikingly, regardless of the particular Hox gene, the PD gene network module seems to perform similar diversification commands in both

chemosensory systems. It will be interesting to ask how different sets of identity genes are regulated in different tissues on the molecular level, and how the cellular memory is passed down through the cascade.

2.3.4 Modular evolution of gene regulatory networks and neuronal diversity

Understanding the diversification process from homogeneous fields of precursors to diverse, terminally differentiated neuronal populations will provide key insights into how cascades of master regulatory transcription factor networks can generate and modify the cellular complexity seen in multicellular organisms. Understanding this diversification process can also help us understand the origins of this complexity. At an evolutionary scale, clear analogy exists between ORN precursor diversification process and the segment diversification during early embryogenesis along the myriapods-insect lineage (109). The addition or elimination of TFs governing either process might reflect, or likely instruct the generation of new fates. Based on a modern version of "the law of development" postulated almost two centuries ago (110), the history of the acquisition of increased complexity of a tissue and the concommitant genetic changes giving rise to that complexity is recapitulated by the temporal role and order of the genes that give rise to that complexity. Under this assumption, a primordial state in antennal development might be the expression domains of Bar and Dac in the antennal disc. Rn was then added to this network later in development and evolution. This would explain the dramatic decreases in ORN diversity and the expansion of

specific ORN populations in default sensilla subtypes in *rn* mutants as well as *Bar/ap* overexpression. Indeed, the onset of *rn* expression is later in third instar discs compared to *dac/Bar/ap* (84), and Rn seems to be unique to Arthropods, especially insects. Thus, it is plausible that Rn is a newer addition to the network. Conceivably, Rn evolved to generate novel olfactory neurons in order to help the ancestral Arthropods exploit novel olfactory niches.

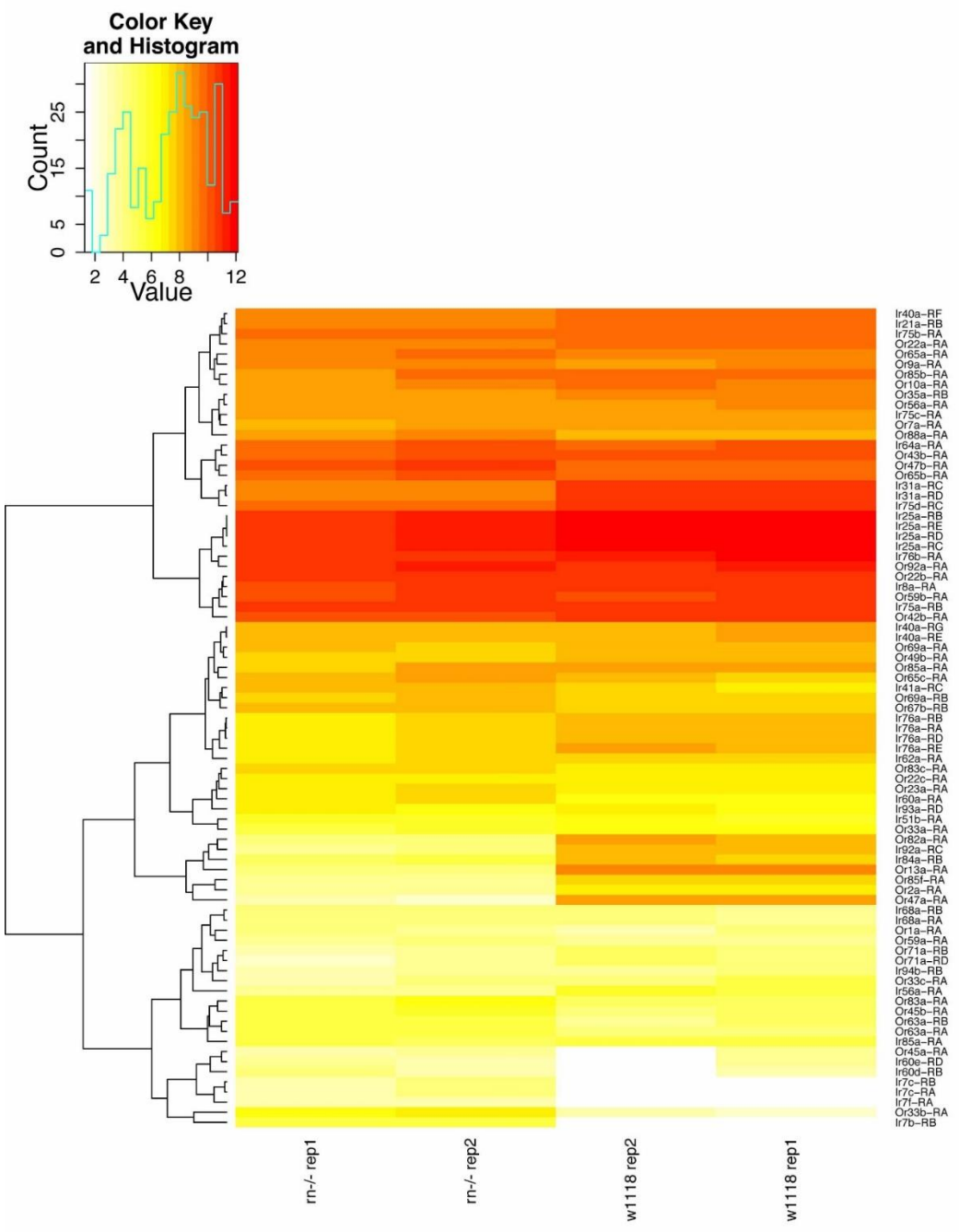

Figure 5: Heatmap of olfactory receptor expression in the control and *rn* mutant adult antennae by RNAseq. Normalized expression of all olfactory receptors in the adult stage by DESeq2 is shown. Sequencing results of two biological replicates of paired-end reads per genotype is used as the input. Each transcription variant is treated individually.

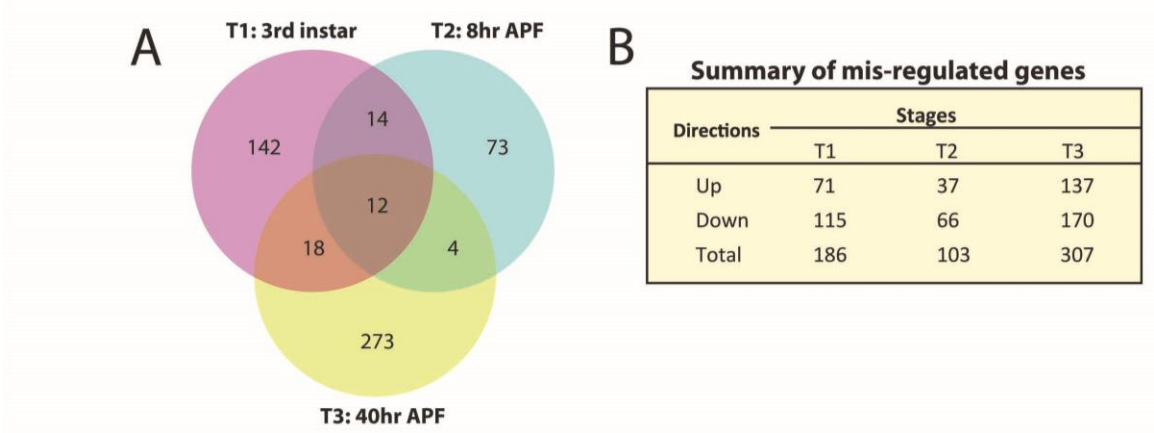

Directions	Stages		
	T1	T2	T3
Up	71	37	137
Down	115	66	170
Total	186	103	307

Figure 6: Summary of RNA-seq analysis. (A) Venn diagram showing the numbers of genes misregulated in *rn* mutants in the three early stages T1 (3rd instar larval), T2 (8hr APF), and T3 (40hr APF). (B) Summary of misregulated genes based on the directions.

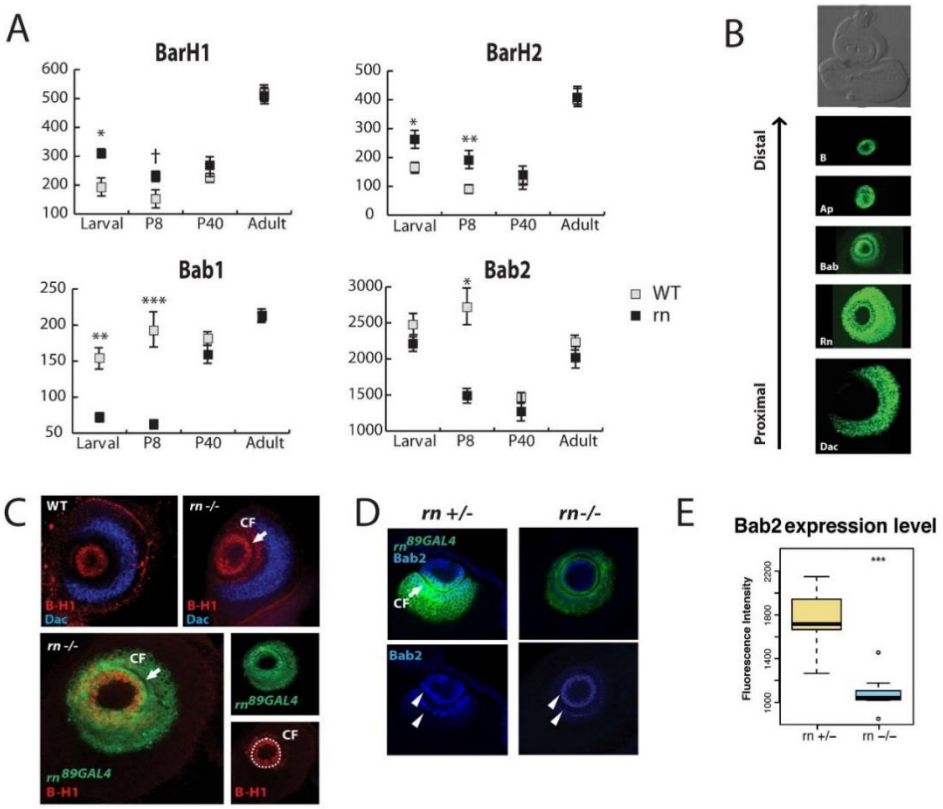

Figure 7: Rn controls the expression of *BarH1*/2 and *bab1*/2 in the antennal disc. (A) Expression levels of B-H1/2 and Bab1/2 between the control and mutants in different stages. Normalized expression data by DESeq2 was used. † p<0.1 * p<0.05 ** p<0.01 *** p<0.001. (B) Expression patterns of PD genes in the third instar larval antennal disc. They are expressed in concentric rings along proximodistal axis. Anti-B-H1 (T. Kojima), anti-Bab2 (F. Laski), anti-Dac were used to visualize Bar, Bab and Dac. ap^{rK568} (stained with anti-β-gal) and CRISPR tagged Rn-EGFP (89) were used to visualize Ap and Rn. Images were taken from different animals. (C) Confirmation of RNAseq results on Bar expression. Antibodies to B-H1 (red) were used. Expansion of B-H1 outside CF (arrow) is apparent in *rn* mutants. The expansion of Bar is restricted within the distal boundary of Dac (blue). In the expanded zone outside the central fold, Bar expression overlaps with Rn expression (lower panel). (D) Bab2 antibody staining (blue) shows concentration gradients in wild type. In these composite images, two circles (arrow heads) on the ridges of the central fold show the highest concentrations, but the high level of expression is continuous along the central fold (see S2C Fig). Bab2 level is weaker in *rn* mutants, although the overall pattern is unchanged. The rn^{89GAL4} reporter labels cells that have active *rn* promoter (green). CF, central fold (arrow). (E) Quantification of Bab2 levels in (F). n=10, *** p<0.001

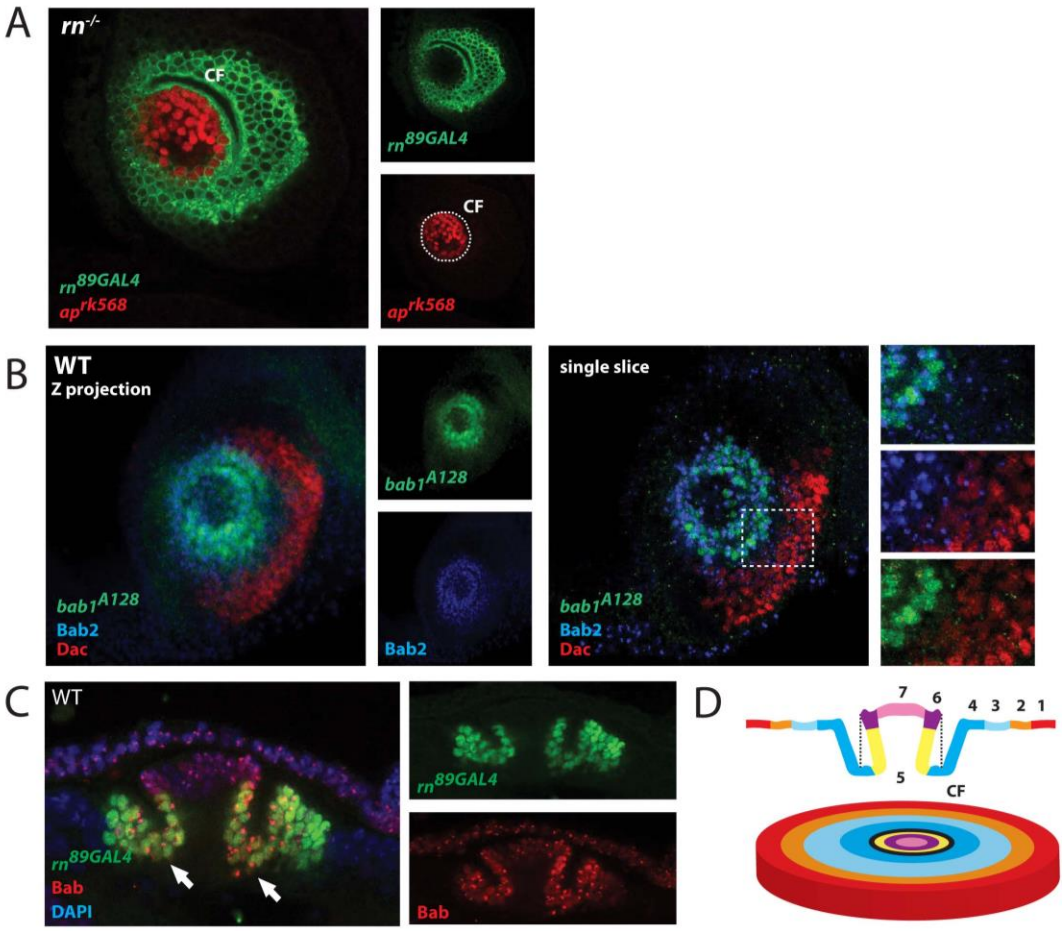

Figure 8: (A) *ap* expression (red) visualized by the enhancer trap line *ap*^{rK568} remains inside the central fold (compared to Fig 10E and F). CF, central fold (dashed line). (B) Confocal images of the third instar larval antennal disc. Bab1 expression is visualized by staining the enhancer trap line *bab1*^{A128} with β-gal antibody. Bab2 is stained with its antibody (F. Laski). These two genes are partially redundant and overlapping in expression. Both genes show gradient expression and are confined within the boundary set by Dac (red). A single slice of the confocal image shows the boundary between Bab and Dac. Boxed area is shown on the right. Weak Bab2 slightly overlaps with Dac, while the overlapping between *bab1*^{A128} and Dac is not obvious, presumably due to the level of expression below the detectable range. (C) A side view of the antennal disc highlighting the central fold. Both Rn (green) and Bab (red) are present continuously throughout the central fold. White arrows point to the central fold. (D) Cartoon schematic showing the rings of the antennal disc as viewed from the side.

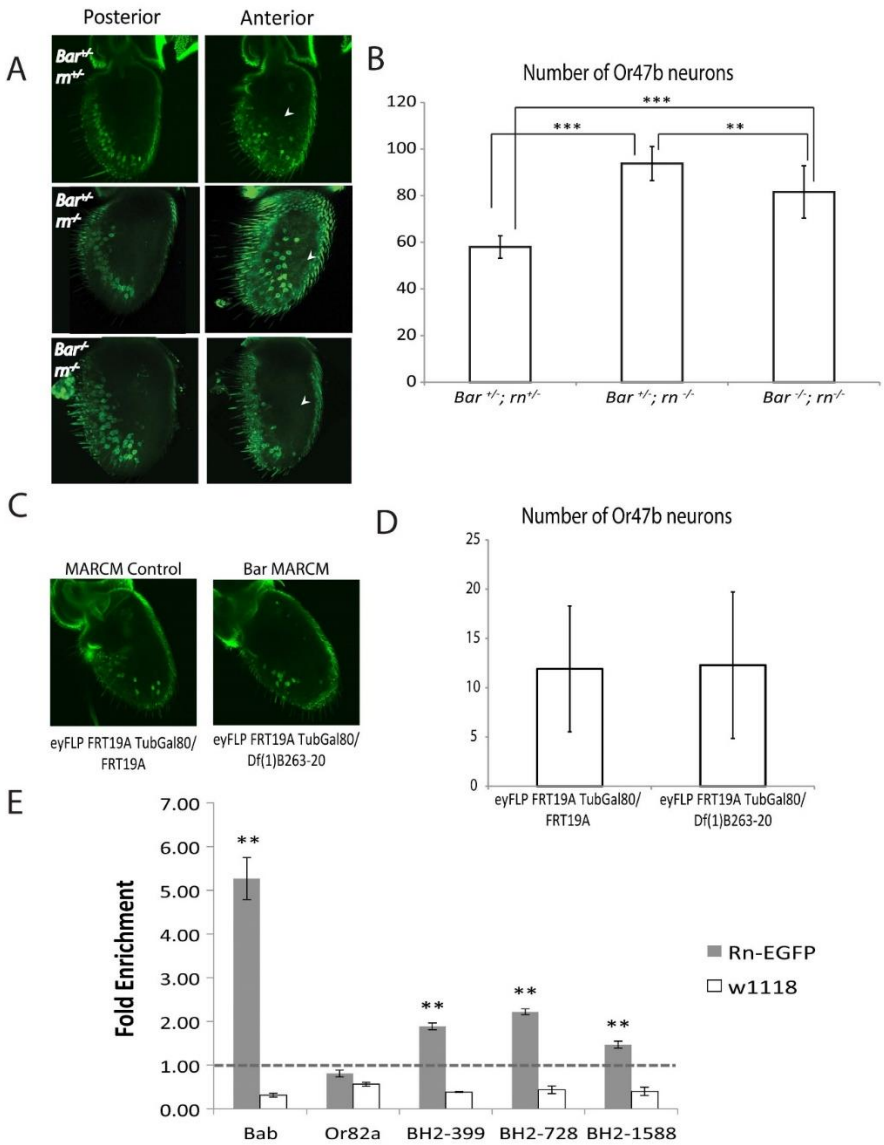

Figure 9: Relationship between *BarH1/2* and *rn*. (A) Expression of Or47b from at4 sensilla as detected by *Or47b:mCD8-GFP* reporter in control, *rn* single mutant and *rn/Bar* double mutant flies. Or47b expression is expanded into an anterior zone (right panel, arrowhead) in the *rn*-/- antenna. When mutant clones for *BarH1/2* have been introduced in the *rn*-/- background, the expansion of Or47b expression in the anterior zone is no longer obvious (arrowhead). (B) Quantification of the numbers of Or47b expressing neurons from (A). There is a significant decrease in the number of Or47b neurons in *Bar/rn* double mutants as compared to *rn* single mutants. n=15. **p<0.01, ***p<0.001. (C) Or47b neurons in wildtype and *Bar* MARCM clones. Or47b neurons were labeled using *Or47bGAL4* to drive *UAS-mCD8GFP*. Clones were generated using

***ey-FLP FRT19A TubGAL80*. (D) There was no detectable difference between the numbers of Or47b neurons in wildtype and mutant clones. Quantification showed that the average number of cells observed was approximately one fifth of the total number of Or47b neurons (B), suggesting that MARCM occurred in a small portion of the antennal disc. (E) ChIP-qPCR using anti-EGFP antibodies to pull down endogenous Rn-EGFP from third instar antennal discs and test the binding of Rn to *Bar/bab* regulatory regions. T13 enhancer sequence upstream of *bab2*, which was previously reported to bind to Rn in vitro, showed enrichment for Rn-EGFP in the ChIP assay. Primers spanning different regions of *BarH2* upstream of its TSS (*BarH2-399, BarH2-728*, and *BarH2-1588*) also showed binding of Rn-EGFP. *Or82a*, which is expressed in ORNs that develop from *rn*-positive ORNs did not show binding as previously reported** (42). ****p<0.01.**

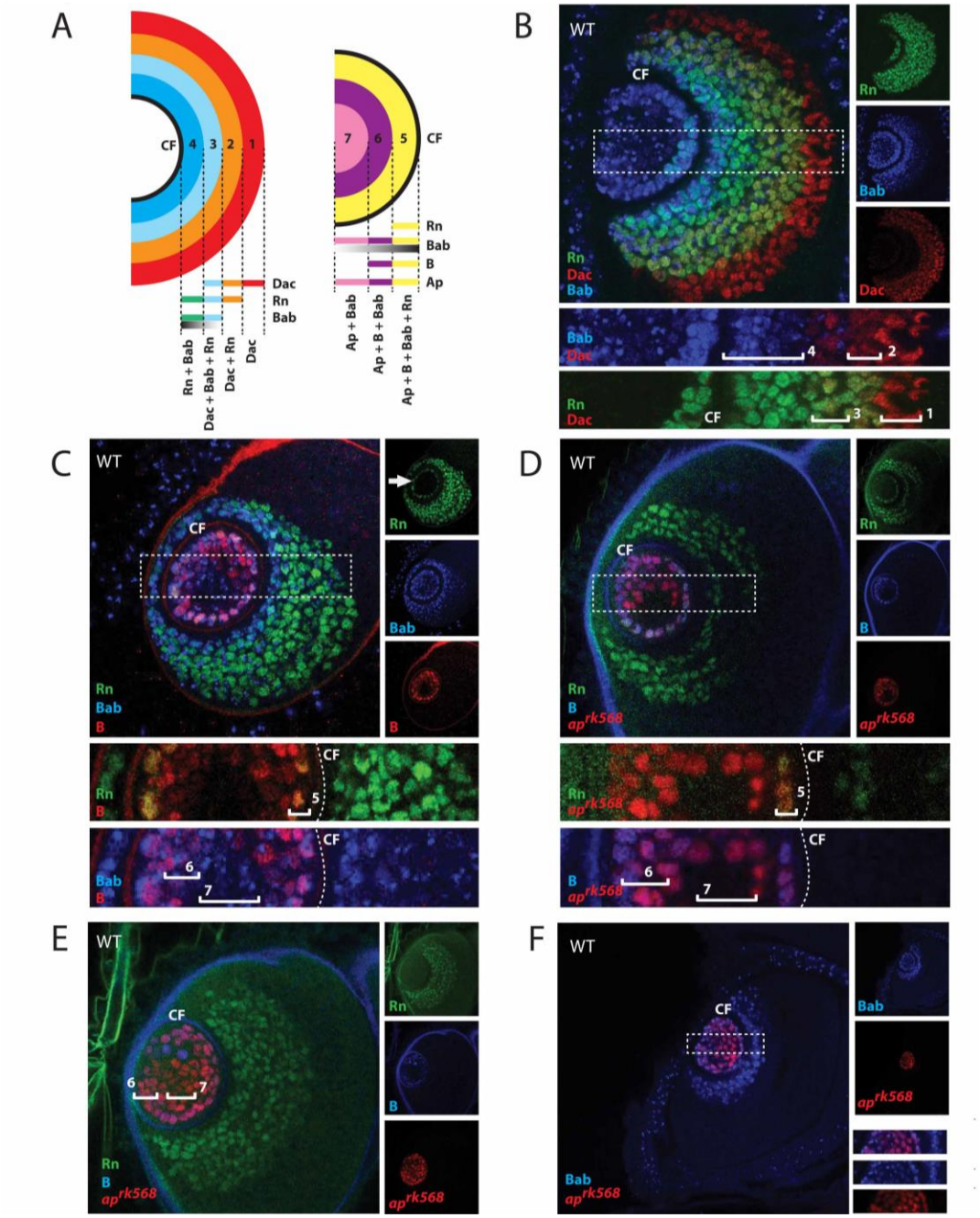

Figure 10: Intercalation of prepatterning genes inside and outside the central fold. (A) A schematic model showing 7 concentric domains in the antennal disc determined by unique combinations of transcription factors. Four rings are placed outside the central fold (CF), and three are inside. (B-F) Expression analysis of Rn, Bab and Dac (B); Rn, Bab, and Bar (C); Rn, Bar and *ap* (D and E); Bab and *ap* (F) demarcate 7 different rings in the antennal discs based on combinations of these factors as well as Bab

concentration gradient. Middle confocal sections were shown for (B-D), and superficial sections were shown for (E) and (F). Bab expression is highest near the central fold and decreases towards outermost and innermost regions. Bab was labeled with anti-Bab2. Rn was labeled with tagged EGFP in Rn-EGFP. Dac was labeled with a monoclonal anti-Dac antibody. Bar was labeled with anti-B-H1. *ap* was labeled with anti-β-gal in *ap*^{rK568}. Individual channels are shown on the right of each image. Boxed areas are shown below in higher magnification. Rn expression is seen as a circle (arrow) inside the central fold in the middle sections (C). Central fold is denoted by a dashed line. Each ring is numbered and marked by a bracket.

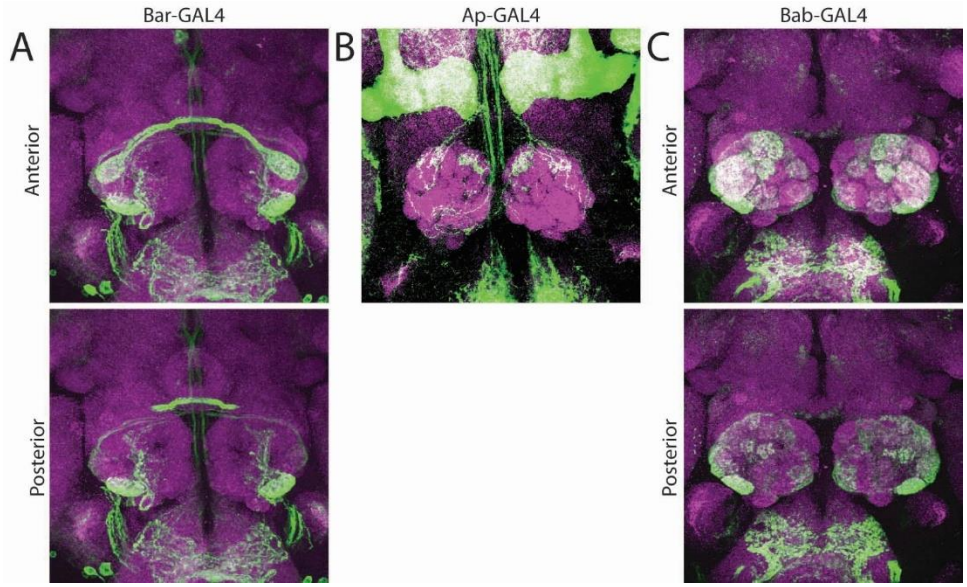

Figure 11: Expression pattern of PD network components in ORNs. Antennal lobe innervation of ORNs expressing GFP driven by (A) *Bar*^{NP4099}, (B) *ap*^{md544}, and (C) *bab1*$^{Pgal4\text{-}2}$. For *bab* and *Bar* expression, analysis was done on adults. For *ap*, 50-75 hour APF pupal brains were examined. Top rows show anterior confocal slices and the bottom rows show the posterior slices.

Table 1: Summary of the expression analysis shown in Fig 11. Pupal brains (50-75 hr APF) were used to examine *ap*-positive ORN identities by *ap*^{md544}-driven GFP. Adult brains were used for analyzing the *bab* (by *bab1*$^{Pgal4-2}$-driven GFP) and *Bar* (by *NP4099*-driven GFP) data. Weak expression is indicated by "+/-". *rn* and *dac* expression data are taken from published results (42,43)**.**

Sensilla	OR	Glomerulus	Pre-patterning Factors				
			Ap (developing brain)	Bar (adult)	Bab (adult)	Rn (Li *et al.*)	Dac (Song *et al.*)
at1	Or67d	DA1			+/-	+	
at2	Or23a	DA3	+		+		
	Or83c	DC3			+		
at3	Or2a	DA4m			+	+	
	Or19a/b	DC1			+	+	
	Or43a	DA4l			+	+	
at4	Or47b	VA1v			+		
	Or88a	VA1d	+	+	+		
	Or65a/b/c	DL3	+				
ab1	Gr21a	V					
	Or92a	VA2					+
	Or10a/Gr10a	DL1			+		+
	Or42b	DM1					+
ab2	Or59b	DM4	+				
	Or85a	DM5					
ab3	Or22a/b	DM2					+
	Or85b	VM5d			+		
ab4	Or7a	DL5	+				
	Or56a/Or33a	DA2			+		
ab5	Or47a	DM3				+	
	Or82a	VA6			+	+	
ab6	Or49b	VA5			+		
ab7	Or67c	VC4			+/-	+	+
	Or98a	VM5v			+/-	+	
ab8	Or9a	VM3					
	Or43b	VM2	+				
ab9	Or67b	VA3			+		+
	Or69aA/B	D			+		+
ab10	Or49a/Or85f	DL4				+	
	Or67a	DM6				+	+
ac1	IR31a	VL2p	+		+	+	
	IR92a/IR76b	VM1			+	+	
	IR75d	VL1		+	+	+	+
	?	VM6			+	+	
ac2	IR75a	DP1l			+		
	IR41a/IR76b	VC3m/VC5?			+		
	IR75d	VL1		+	+		+
ac3	IR75a/b/c	DL2d/DL2v?			+		
	Or35a/IR76b	VC3l					
ac4	IR84a	VL2a		+	+	+	
	IR76a/IR76b	VM4				+	
	IR75d	VL1		+	+	+	+
ai1	Or13a	DC2				+	+
	Or46aB?	VA7m			+	+	+

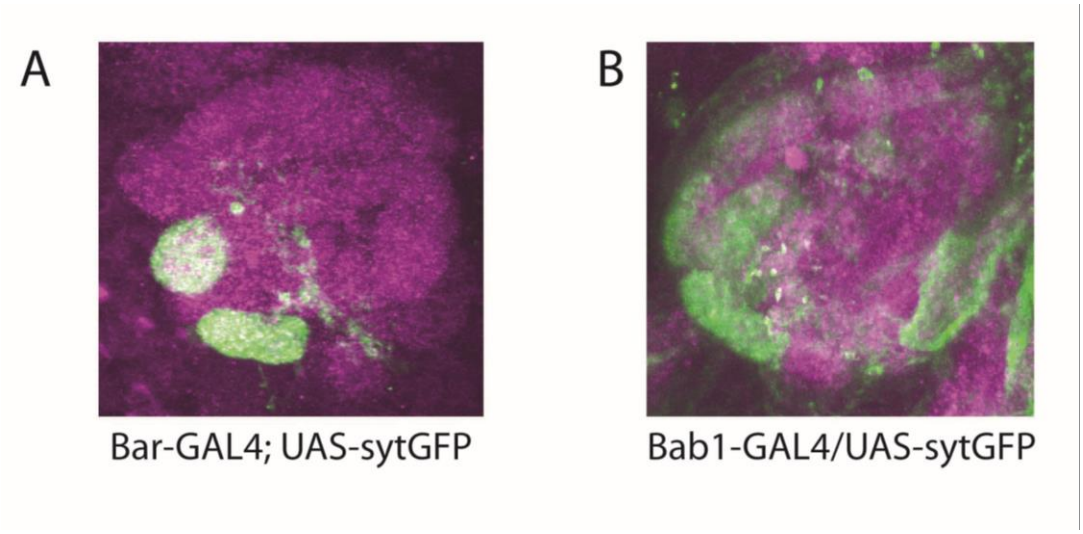

Figure 12: Expression of GFP in the mid-pupal antennal lobe driven by *Bar* or *bab1* GAL4. (A) A confocal Z-projection showing neuropil (magenta) and *Bar*-GAL4 UAS-sytGFP (green). (B) As in (A) but with *bab1*-GAL4. Both images were taken from approximately 50 hr APF pupal brains.

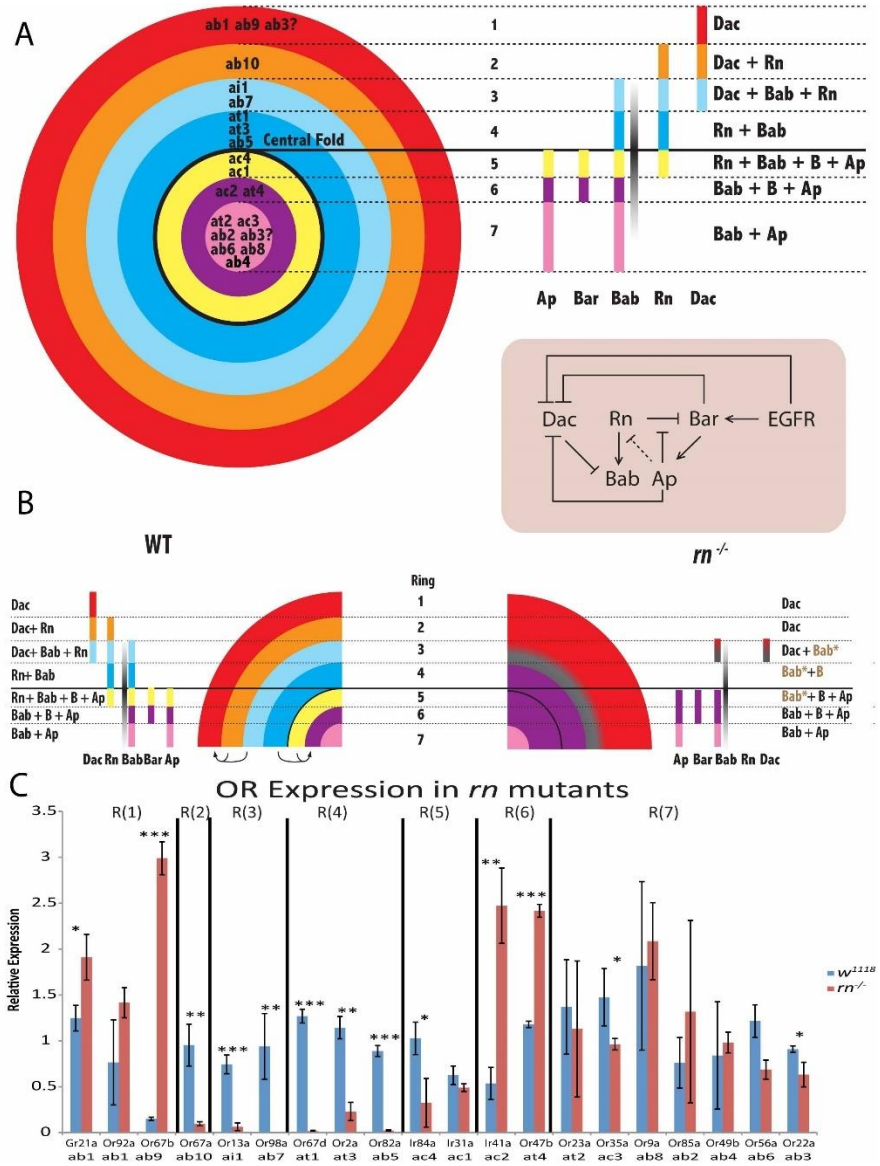

Figure 13: Model depicting the PD network that determines the precursor identities of the rings and the ORN populations. (A) Wild type antennal disc showing the 7 rings corresponding to subsets of sensilla subtype fates created by the combinatorial expression of the PD network components, as well as the Bab gradient. The cross-regulatory network that operates within the antennal disc is shown below. The origin of ab3 (with a question mark) is unclear. (B) Scheme showing the changes to the overlapping domains within the antennal disc in *rn* mutants. R(6) and R(1) are expanded at the expense of R(2-5). See Appendix A for explanations. (C) qRT-PCR of OR genes as a readout of ORN populations in antennal samples from *rn* mutant flies.

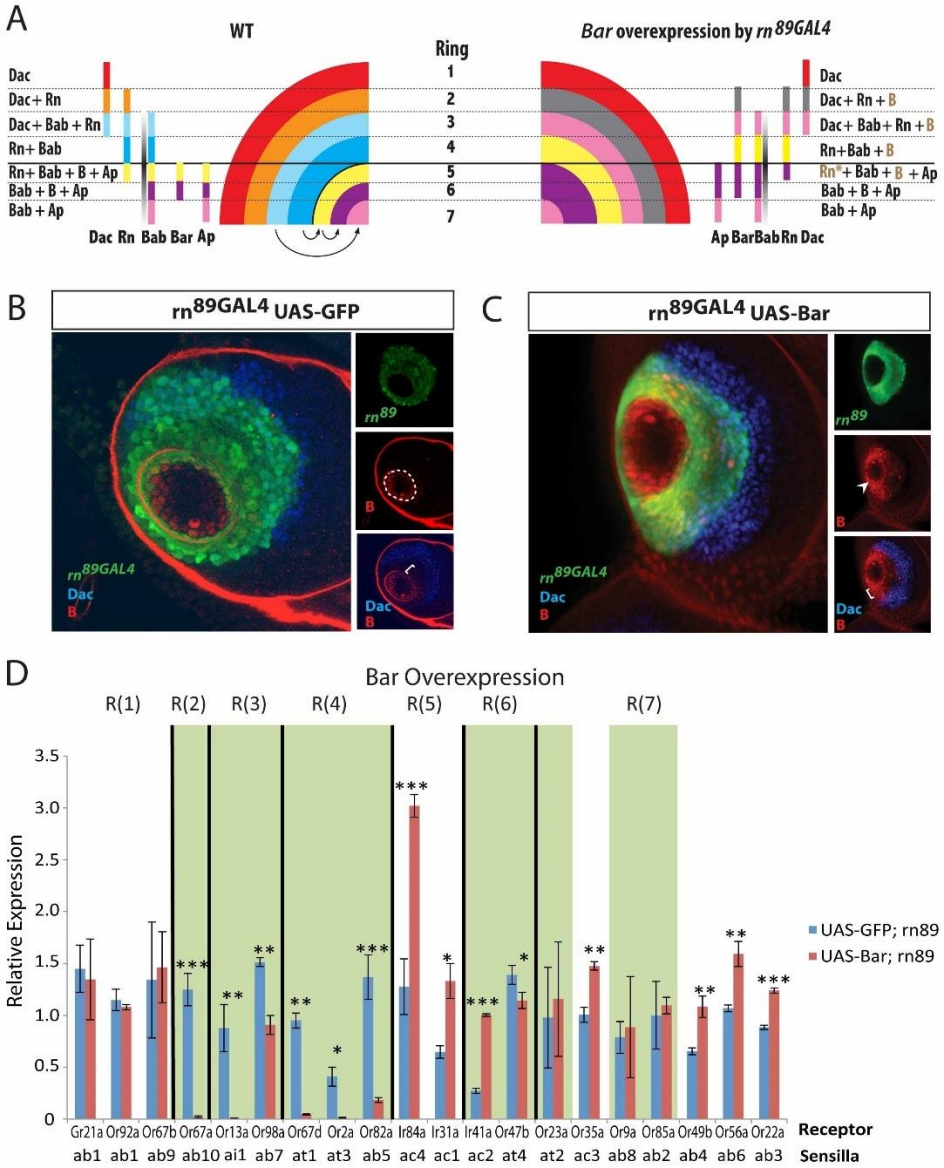

Figure 14: Effect of *Bar* overexpression on ORN populations. (A) Model depicting the changes to the combinatorial code in *rn*^{89GAL4} UAS-BarH1 flies. The fate conversions among the rings are represented by arrows. See Appendix B for explanations. (B) and (C) *Rn*^{89GAL4} UAS-GFP (green), Bar (red), and Dachshund (blue) staining on antennal discs from control (B) and *rn*^{89GAL4} UAS-BarH1^{M13} flies (C) shows expansion of Bar up to the Dachshund expression boundary (bracket). Central fold is missing in the overexpressing line (arrowhead). (D) qRT-PCR of OR genes as a readout of ORN populations in antennal samples from *rn*^{89GAL4} UAS-BarH1^{M13} flies. The receptors that show the same phenotype as in *rn* mutants are blocked in green shade.

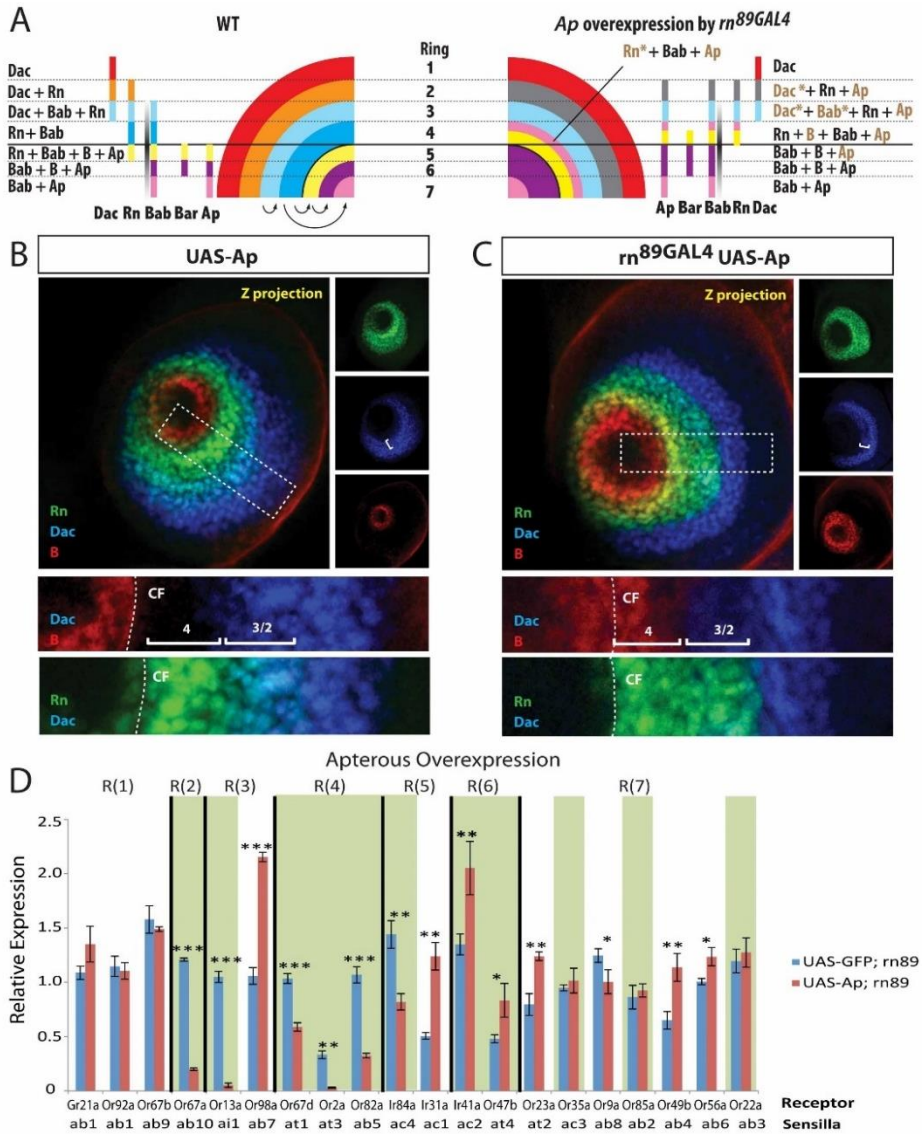

Figure 15: Effect of *apterous* overexpression on ORN populations. (A) Model depicting the changes to the combinatorial code in *rn*^{89GAL4} UAS-ap flies. (B) and (C) Rn-EGFP (green), Bar (red), and Dachshund (blue) staining on antennal discs from wild type (B) and *rn*^{89GAL4} UAS-ap flies (C) shows expansion of Bar to R(4) and decreased Dachshund staining in R(2/3) (brackets). Individual channels are shown on the right. Boxed areas are shown below at a higher magnification. (D) qRT-PCR of OR genes as a readout of ORN populations in antennal samples from *rn*^{89GAL4} UAS-ap flies. The receptors that show the same phenotype as in *rn* mutants are blocked in green shade.

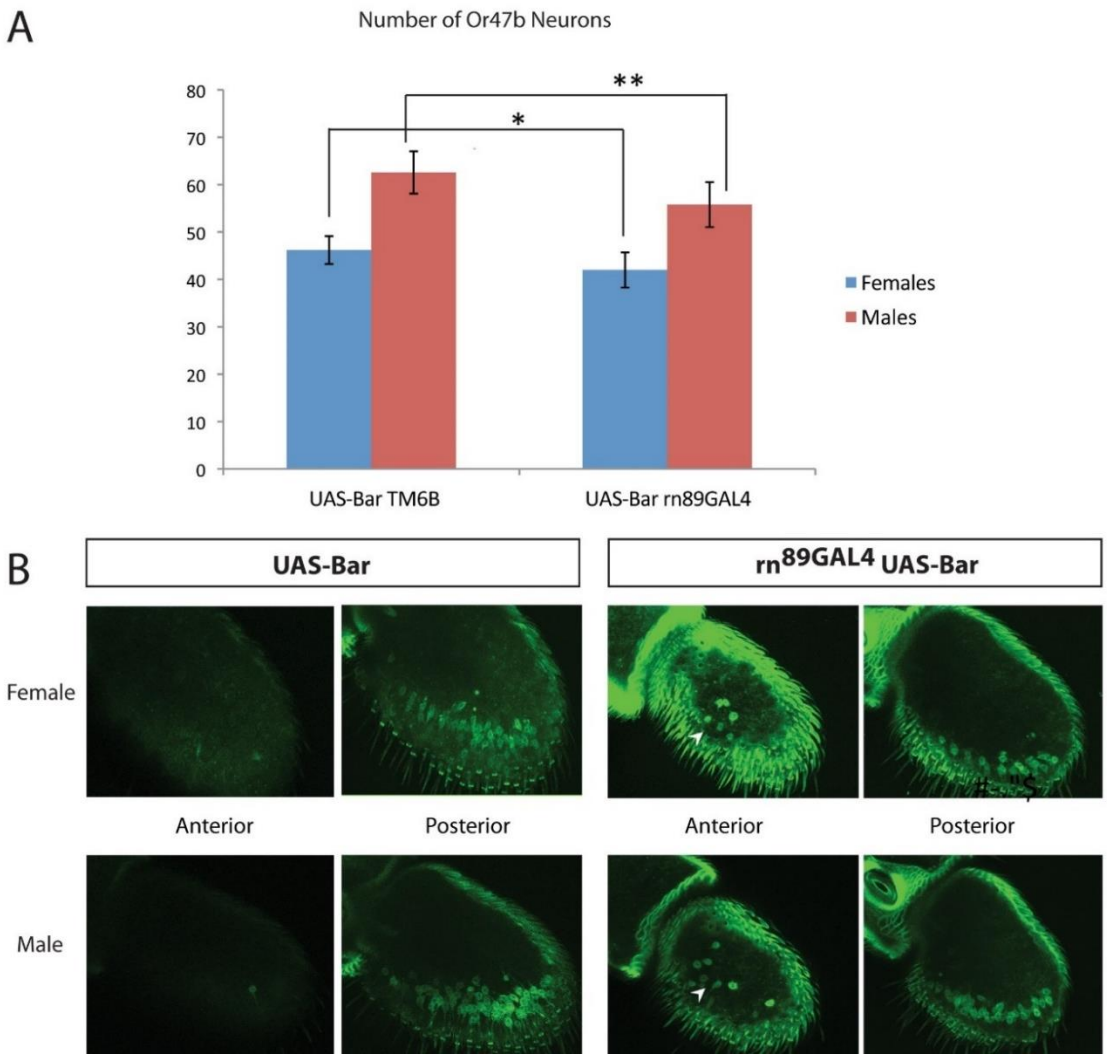

Figure 16: Expansion of Or47b in *Bar* overexpression. (A) Quantification of cell counts of Or47b neurons in (B). Flies that overexpress *BarH1* with the *rn*^{89Gal4} driver show significant reductions in the numbers of Or47b neurons in both females (blue) and males (red). * $p < 0.05$, ** $p < 0.01$. (B) Antennal images of Or47b neurons in *BarH1* overexpressing flies. Although the number of Or47b neurons is reduced, we detect ectopic neurons (arrowheads) in the anterior portion of the antenna, consistent with the phenotype seen in *rn* mutants.

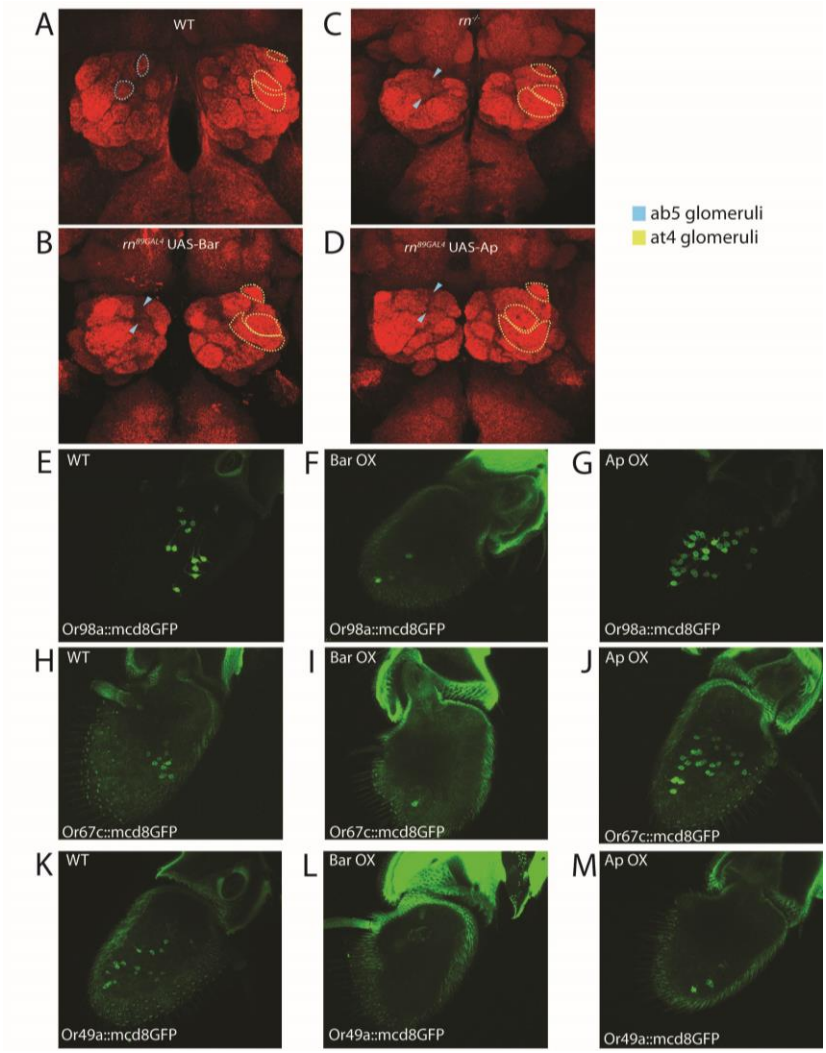

Figure 17: Changes in sensilla identity in *rn* mutant as well as *Bar* and *ap* overexpression. (A-D) Glomerular targets of ab5 ORNs (blue dashed lines) and at4 ORNs (yellow dashed lines are shown in wild type (A), *rn* mutants (B), BarH1, and Ap overexpression (C and D, respectively). The glomerular targets of at ORNs are expanded in all cases and the targets of ab5 ORNs are lost in all cases. (E-M) Analysis of OR expression in adult antennae also corroborates qPCR data (Fig 14D, 15D). ab7 sensilla (Or98a and Or67c) are downregulated in BarH1 overexpression (F) and (I) but are upregulated in Ap overexpression (G) and (J) compared to (E) and (H). Or49a, which pairs with Or67a in ab10 sensilla, is downregulated in both Bar and Ap overexpression (K-M).

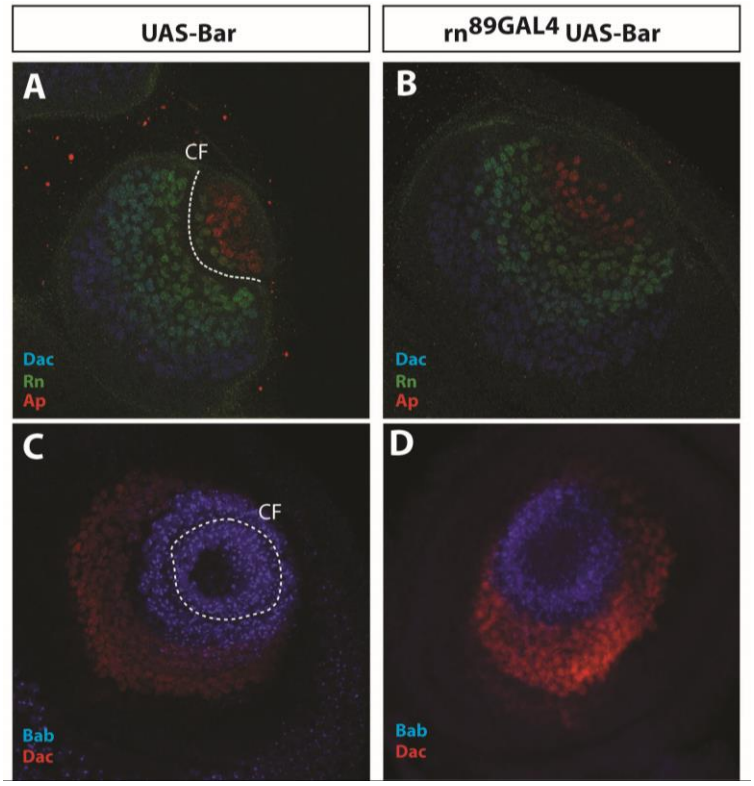

Figure 18: TF expression in *Bar* overexpression. (A) and (B) Single slices of 3rd instar larval discs showing the expression patterns of *rn, ap* and *dac* in control and *Bar* overexpressing lines. The central fold is highlighted as a dashed line and is absent in *Bar* overexpressing larvae. No change was detected in *rn* or *ap* staining. (C) and (D) Z-stacks of antennal discs stained for Bab and Dac in wildtype and *Bar* overexpressing discs. Beyond the loss of the central fold, no change in *bab* expression was detected.

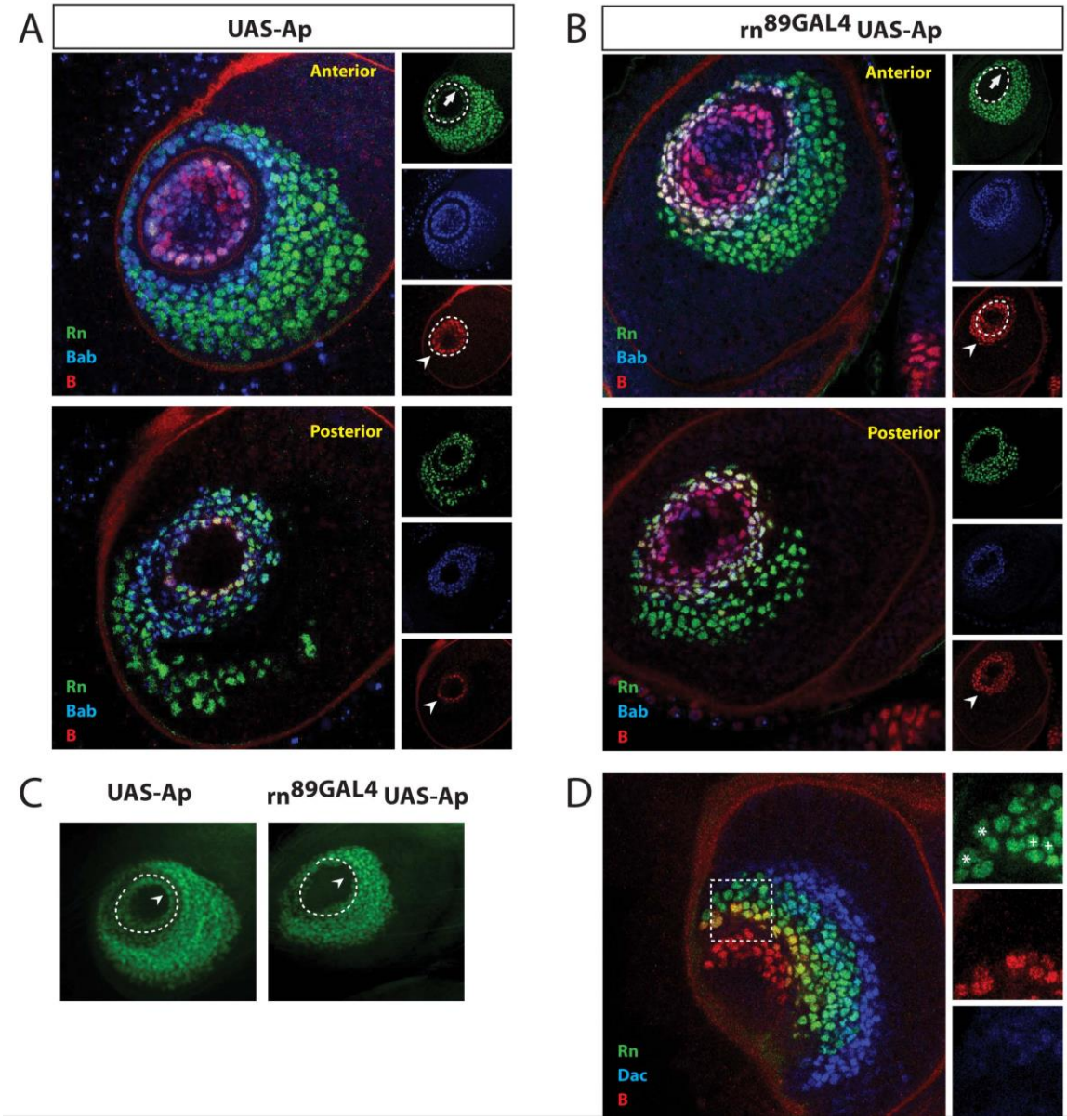

Figure 19: Changes in TF expression in *ap* overexpression. (A) and (B) Single slices of 3rd instar larval discs showing the expression patterns of *rn, bab* and *Bar* in control and Ap overexpressing lines. *Bar* is expanded outside of the central fold (arrowheads) in larvae that overexpress *ap*. No change was detected in Bab staining. *rn* expression is lost in R(5) inside of the central fold (arrows). (C) Loss of Rn (arrowheads) inside of the central fold (dashed line) in *ap* overexpressing larvae. (D) Single slice of the confocal image shown in Fig 15C. Limit of *Bar* expansion is defined by *dac* expression. *rn*-positive, *dac*-negative cells that do not express (asterisks) or express low levels of Bar (crosses) can be seen in the enlarged area (boxed).

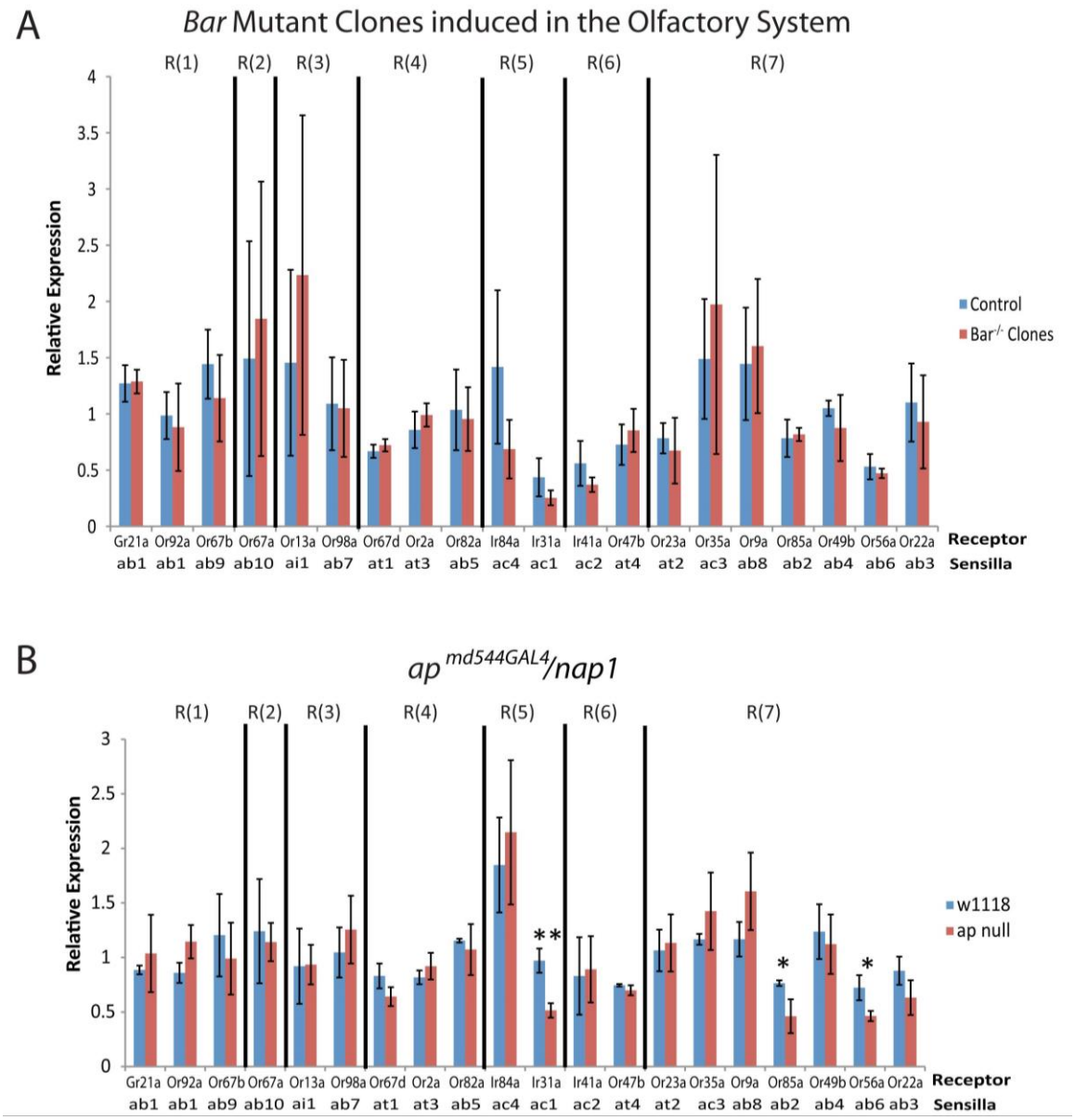

Figure 20: Effect of loss of *apterous* or *Bar* on OR expression. (A) Quantitative RT-PCR analysis for ORs in control (*ey*-FLP FRT19A/FM6) and *bar* mutant clones (*ey*-FLP FRT19A/D(f)1 Bar FRT19A). No significant changes were detected for all ORs tested. (B) Quantitative RT-PCR analysis of w^{1118} and *ap* mutants ($nap1/ap^{md544Gal4}$). The expression of *IR31a* (ac1), *Or85a* (ab2), and *Or56a* (ab6) were significantly reduced in *ap* mutants. All three ORN classes were also shown to be positive for *ap* expression (Table 1, Fig 5A). * $p < 0.05$, ** $p < 0.01$.

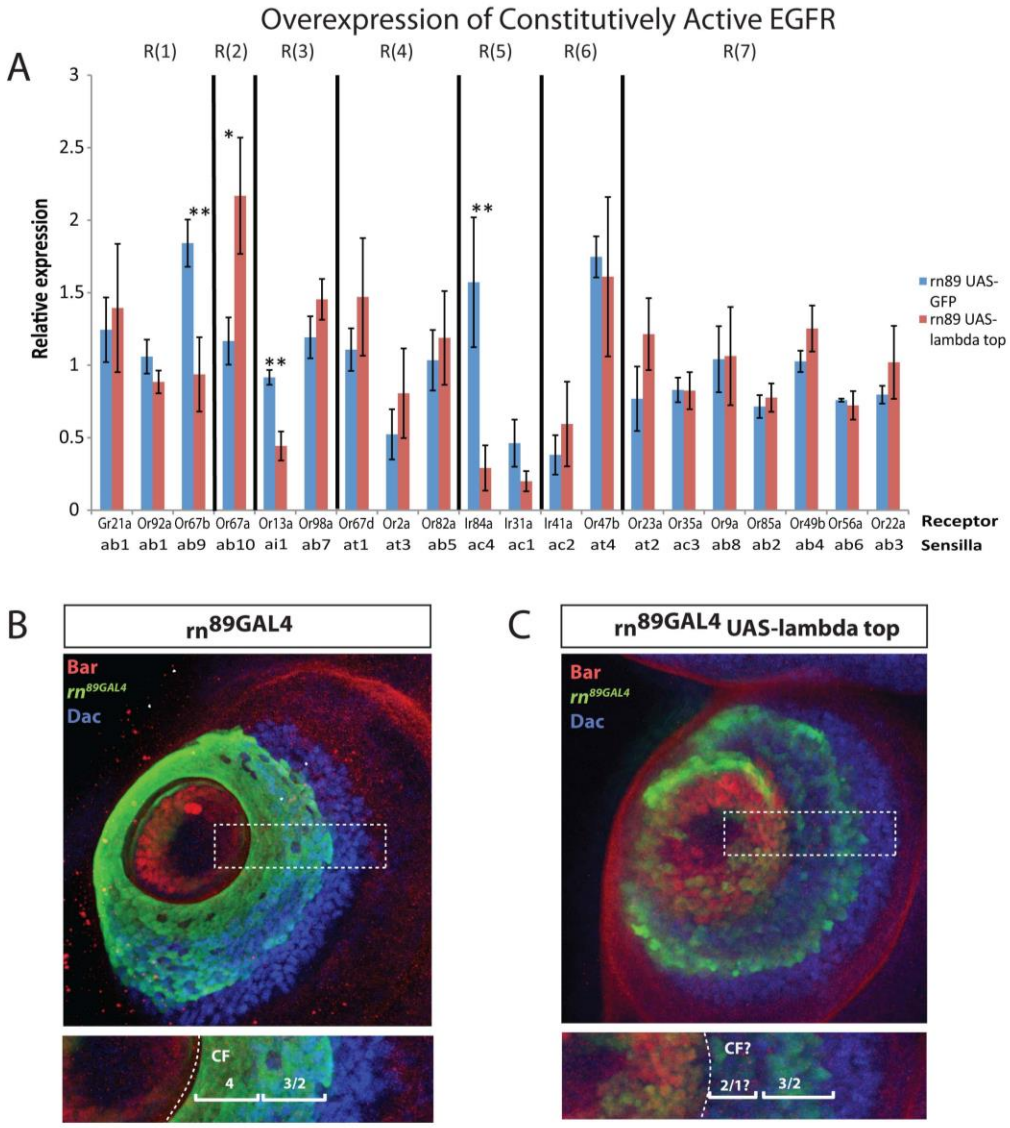

Figure 21: Overexpression of constitutively active EGFR. (A) Quantitative RT-PCR analysis of OR genes in UAS-GFP; *rn*^{89Gal4} and UAS-lambda top 4.4/ *rn*^{89Gal4} flies. *Or67b* (ab9), *Or13a* (ai1), and *IR84a* (ac4) were downregulated and *Or67a* (ab10) was upregulated in EGFR overexpressing flies (* $p < 0.05$, ** $p < 0.01$). (B) Staining on the control UAS-GFP; *rn*^{89Gal4} third instar larval discs for Bar (red), *rn*^{89} (green) and Dac (blue). The central fold (dashed line) and R(2)-(4) are highlighted. (C) Staining as in (B) in flies overexpressing EGFR. Bar-positive region had expanded and the location of the central fold had changed. Bar and Dac domains became adjacent to each other. There is also significant repression of *rn* expression, consistent with previous reports of the function of EGFR signaling.

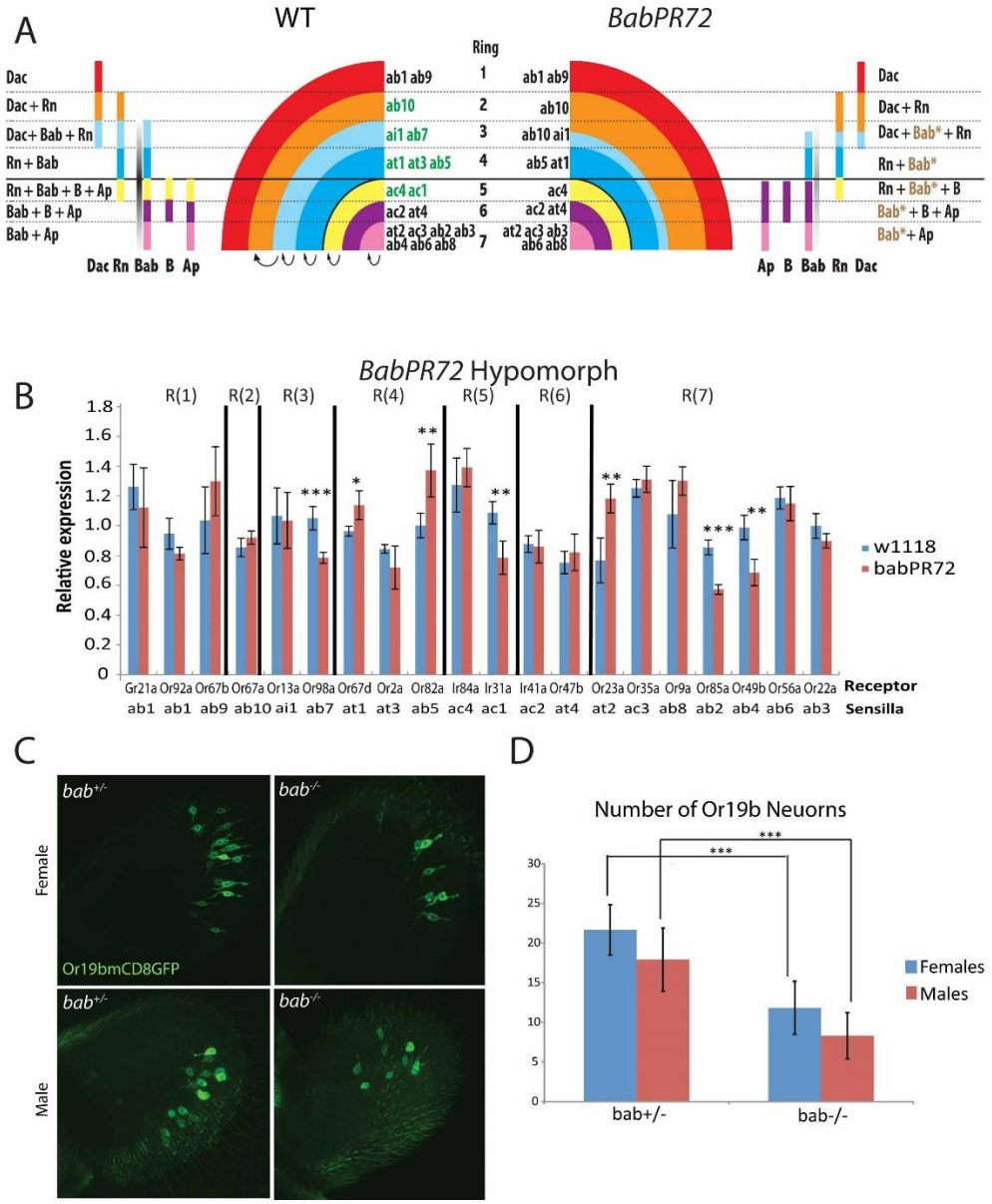

Figure 22: Effects of hypomorphic *bab* mutants on ORN populations. (A) Model depicting the changes to the combinatorial code in bab^{PR72} homozygous flies. The fate conversions among the rings and ORN pools are represented by arrows. (B) qRT-PCR of OR genes as a readout of ORN populations in antennal samples from bab^{PR72} homozygous flies. * $p<0.05$, ** $p<0.01$, *** $p<0.001$. (C) Antennal images of Or19b (at2) expression in control (left) and bab^{PR72} mutant (right) flies. The top panel is females and the bottom panel is males. (D) Quantification of the number of Or19b neurons from (C). Both males and females show a significant reduction in the number of neurons. *** $p < 0.001$.

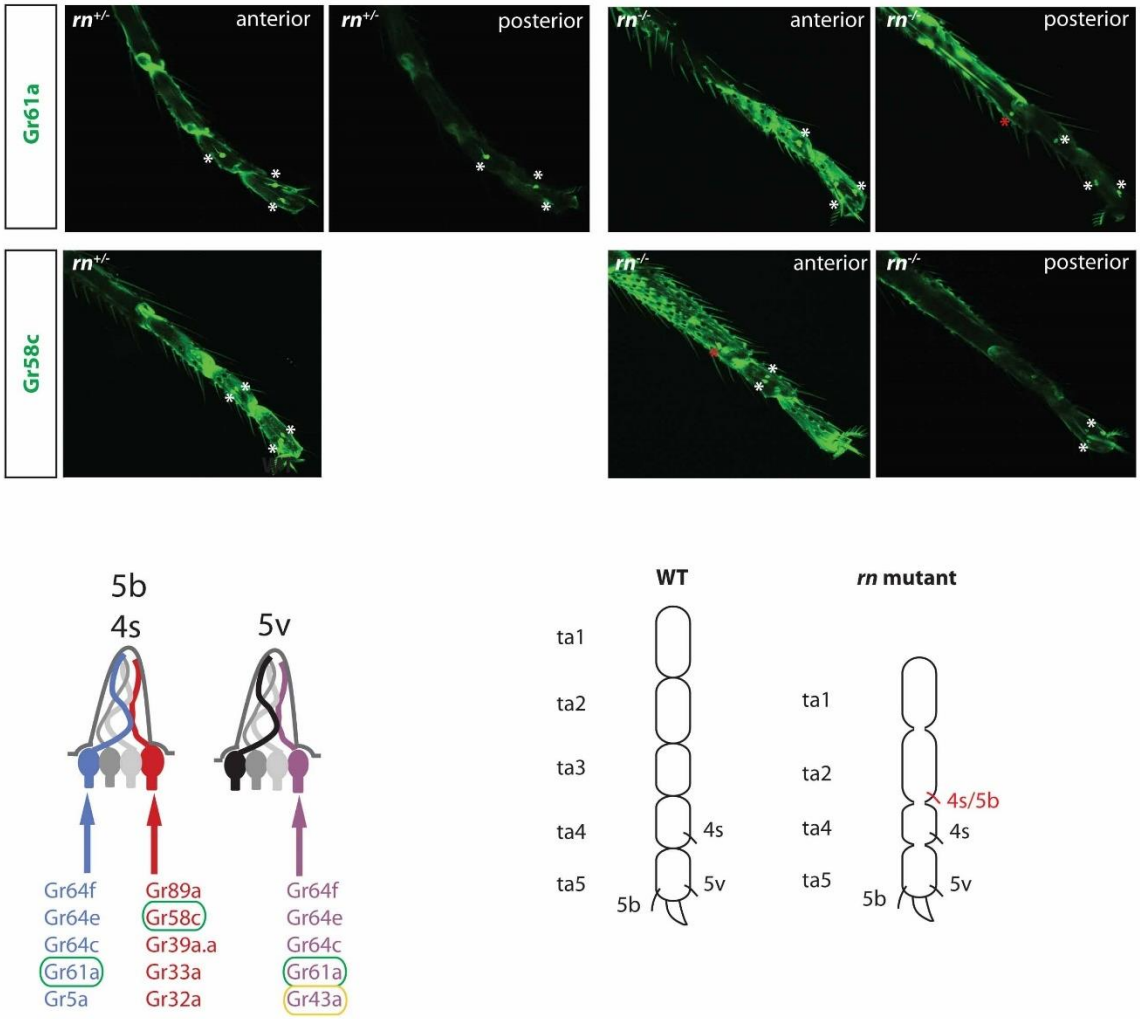

Figure 23: Regulation of GRN patterns by the PD network. GRN and ORN specification may be regulated by the same molecular network. In *rn* mutant, tarsal segment (ta3) is missing, and other segments are fused. Ectopic expression of Gr61a and Gr58c can be seen in the distal region of the second tarsal segment, suggesting a duplication of 4s/5b sensilla. Neurons labeled by the red asterisk in the pictures are the ectopic neuron only seen in the mutant. Different sections of confocal images are shown when neurons are not on the same focal plane. All legs are either from the mid or from the hind leg. Cartoon illustrating the *rn* phenotype in GRNs is shown below. The ectopic sensillum is labeled in red. The scheme for GRN classes and the receptors expressed in the 5b/4s and 5v sensilla are modified from (36)**. The GR that distinguishes 5b from 5v is circled in yellow (Fig 24). Receptors that are analyzed in the figure are circled in green. In the wild type, there is a pair of sensilla for each sensilla type, although only one for each pair is drawn.**

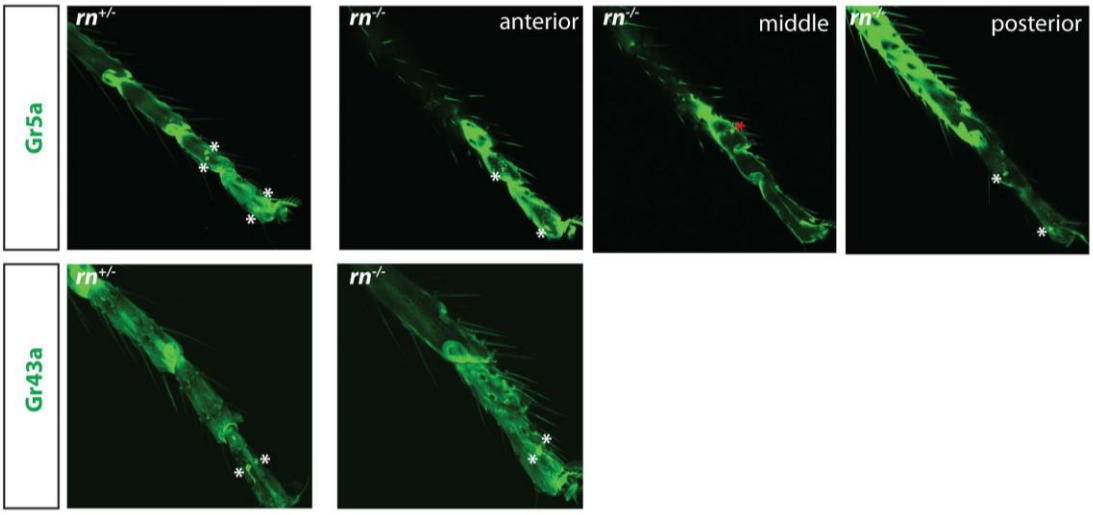

Figure 24: Expression of Gr5a and Gr43a in *rn* mutant legs. (Top) The sweet sensing Gr5a neuron (co-expressing Gr61a) is expanded in *rn* mutants. Control flies have four Gr5a neurons (left, white asterisks) in the 4th and 5th tarsal segments. In *rn* mutants an ectopic neuron is present (right, red asterisk). (Bottom) The bitter sensing Gr43a neurons are unchanged in *rn* mutants, suggesting the expansion of Gr61 (Fig 23) comes from 5b/4s instead of 5v sensilla.

2.4 Materials and Methods

2.4.1 Fly genetics

bab^{A128}, *Df(3L)bab*^{PR72}, were from Frank Laski. *Df(1)*$^{B263\text{-}20}$ *FRT19A, UAS-BarH1*^{M13} were from Tetsuya Kojima. UAS-Egfr.λtop4.4 was from Amanda Simcox. rn^{tot}, rn^{tod} was previously described (42). *OR-CD8 GFP, OR-GAL4, IR-GAL4, GR-GAL4* lines were from Leslie Vosshall, Barry Dickson, Richard Benton and John Carlson, respectively (18,24). Or67d^{GAL4} knock-in stock was a published line showing faithful expression of Or67d (111). *rn*^{89}, *bab1*$^{Agal4\text{-}5}$ (#6802), *bab1*$^{Pgal4\text{-}2}$ (#6803), *ap*^{md544}, *ap*^{rK568}, *UAS-ap, Df(2R)nap1, tubP-GAL80 ey-FLP FRT19A, FRT19A, UAS-CD8 GFP, UAS-Syt GFP, UAS-FLP* were all from

Bloomington Stock Center. NP4099 (*Bar*^{GAL4}) was from Drosophila Genetic Resource Center.

2.4.1.1 Genotypes for fly genetics:

Figure 7C. w^{1118}. *ap*^{rk568}. *Rn-EGFP*

Figure 7D and E. *rn*$^{+/-}$*: UAS-CD8 GFP/+; rn*^{89GAL4}*/TM6b. rn*$^{-/-}$*: UAS-CD8 GFP/+; rn*^{89GAL4}*/rn*^{tod}

Figure 8A. *ap*^{rK568}*/UAS-CD8 GFP; rn*^{89GAL4}*/rn*^{tod}

Figure 8B. *bab1*^{A128}*/+*

Figure 8C. *Rn-EGFP*

Figure 9A. *Bar*$^{+/-}$ *rn*$^{+/-}$*: eyFLP FRT19A Tub*^{GAL80}*/+; Or47b::mCD8-GFP/+; rn*^{tot}*/+. Bar*$^{+/-}$ *rn*$^{-/-}$ *: eyFLP FRT19A Tub*^{GAL80}*/+; Or47b::mCD8-GFP/+; rn*^{tot}*/FRT rn*^{tot}*. Bar*$^{-/-}$ *rn*$^{-/-}$*: eyFLP FRT19A Tub*^{GAL80}*/ Df(1)*$^{B263-20}$ *FRT19A; Or47b::mCD8-GFP/+; rn*^{tot}*/FRT rn*^{tot}

Figure 9C. Control: eyFLP FRT19A Tub^{GAL80}*/FRT19A; Or47b GAL4 UAS-GFP/+. Bar MARCM: eyFLP FRT19A Tub*^{GAL80}*/ Df(1)*$^{B263-20}$ *FRT19A; Or47b GAL4 UAS-GFP/+*

Figure 9E. *w*^{1118}*. Rn-EGFP*

Figure 10B, C. *Rn-EGFP.*

Figure 10D, E. *ap*^{rK568}*/+, Rn-EGFP*

Figure 10F. *ap*^{rK568}*/+*

Figure 11A-C and Figure 12A, B. *NP4099 Bar*^{GAL4}*; UAS-CD8GFP. ap*^{md544}*; UAS-CD8 GFP. bab1*$^{Pgal4-2}$*/UAS-CD8 GFP. NP4099 Bar*^{GAL4}*; UAS-Syt GFP. bab1*$^{Pgal4-2}$*/UAS-Syt GFP.*

Figure 13C. w^{1118}*. rn*^{tot}*/FRT rn*^{tot}

Figure 14B. *UAS-CD8GFP/+; rn^{89GAL4}/TM6B*

Figure 14C. *UAS-CD8GFP/+; rn^{89GAL4}/UAS-BarH1^{M13}*

Figure 14D. *UAS-CD8GFP/+; rn^{89GAL4}/TM6b. UAS-CD8GFP/+; rn^{89GAL4}/UAS-BarH1^{M13}*

Figure 16. *Or47b::mCD8GFP/+; rn^{89GAL4}/TM6b: Or47b::mCD8GFP/+; rn^{89GAL4}/UAS-BarH1^{M13}*

Figure 17C. *rn^{89GAL4}/rn^{tod}.*

Figure 17E-M. *OR::mCD8GFP. OR::mCD8GFP; rn^{89GAL4}/UAS-BarH1^{M13}. OR::mCD8GFP; rn^{89GAL4}/UAS-Ap*

Figure 18A. *Rn-EGFP UAS-BarH1^{M13}/TM6B*

Figure 18B. *Rn-EGFP UAS-BarH1^{M13}/rn^{89GAL4}*

Figure 18C. *UAS-BarH1^{M13}/TM6B*

Figure 18D. *UAS-BarH1^{M13}/rn^{89GAL4}*

Figure 15B and Figure 19A, C. *UAS-Ap/+; Rn-EGFP/TM6B*

Figure 15C and Figure 19B-D. *UAS-Ap/+; Rn-EGFP/rn^{89GAL4}*

Figure 15D. *UAS-CD8GFP/+; rn^{89GAL4}/TM6b. UAS-CD8GFP/+; rn^{89GAL4}/UAS-Ap*

Figure 20A. *eyFLP FRT19A Tub^{GAL80}/FM6. eyFLP FRT19A Tub^{GAL80}/ Df(1)$^{B263-20}$ FRT19A*

Figure 20B. *w^{1118}. Df(2R)nap1/ ap^{md544}*

Figure 21B. *w^{1118}: bab^{PR72}*

Figure 21C. *Or19b::mCD8GFP/+; bab^{PR72}/TM6b: Or19b::mCD8GFP/+; bab^{PR72}*

Figure 22. *UAS-CD8GFP/+; rn^{89GAL4}/TM6b. UAS-CD8GFP/+; rn^{89GAL4}/UAS-Egfr.λtop4.4*

Figure 23 and Figure 24. $rn^{+/-}$: *GR-GAL4/UAS-CD8 GFP; rn^{tot}/TM6b*. $rn^{-/-}$: *GR-GAL4/UAS-CD8 GFP; rn^{tot}/FRT rn^{tot}*.

2.4.2 RNA extraction and library preparation

For the RNAseq analysis, wandering third instar larval antennal discs (~70 for each genotype), 8hr APF pupal antennae (~50 for each genotype), 40hr APF pupal antennae (~50 for each genotype), and adult antennae (150 males and 150 females) from w^{1118}, rn^{tot}/*TM6b*, and rn^{tot}/rn^{tot} flies were dissected. RNA was extracted with RNeasy kit (Qiagen) following manufacturer's instructions, and was treated with on-column DNase digestion (Qiagen). We extracted RNA only from the antennal portion of the larval eye-antennal discs in order to remove contamination by transcripts from the developing eye. All samples were diluted to 20ng/ul in 55ul volume with H_2O, out of which 3.5ul was used for quality control using Bioanalyzer (Duke Microarray Core Facility). The concentrations were measured again with Qubit 2.0 (Life Technologies), and 700ng RNA was diluted to 50ul total volume with H_2O for each sample. RNA sequencing libraries were prepared with TruSeq Stranded mRNA Sample Prep Kit (Illumina) following the manufacturer's instructions. For the RNA fragmentation step, 94°C, 2min was used with the intention to obtain a median size ~185bp. PCR amplification was done with 15 cycles. A total of 24 multiplexed libraries (barcoded) were accessed for quality and mixed altogether before separating to two identical pooled libraries, which are subject to cluster

generation followed by Illumina 50bp paired-end sequencing by UNC High-Throughput Sequencing Facility (HTSF).

2.4.3 RNAseq analysis

Drosophila melanogaster transcriptome (r5.57) was downloaded from flybase and bwa indexed was created with bwa-0.7.8. Each sequencing file was aligned to the transcriptome, and .sam files for each sample were generated by putting two alignments from both reads together. At least over 80% of the total reads were able to align to the reference. After that, count tables were made for each sample with a customized python script, and further consolidated into a matrix containing transcript ID and read counts from all genotypes for each stage with a Ruby script. These matrices were used as inputs for differential expression analysis using a customized DESeq2 R script.

For each stage, we first filtered out ORs/IRs/GRs from the RNAseq datasets, and excluded the genes with low expression levels in all three genotypes (normalized count < 20). We then narrowed the analysis down to genes that show the same trend of differential expression when comparing homozygous vs. w^{1118} and homozygous vs. heterozygous datasets. Because the heterozygous background may have some dominant effects due to the presence of the balancer chromosome and the heterozygous flies do not show any OR phenotypes (42), saving genes that pass both comparisons would help remove irrelevant genes modified by the balancer chromosome and meanwhile enhance the discovery confidence. Because of these stringent filtering steps, we could maximize

our gene lists with a more relaxed cutoff (unadjusted $p < 0.1$) for the gene ontology (GO) and functional clustering analyses.

2.4.4 Immunohistochemistry

Samples were fixed with 4% paraformaldehyde, washed with phosphate buffer with 0.2% Triton X-100, and staining as previously described (57). Primary antibodies were used in the following dilutions: rabbit α-GFP 1:1000 (Invitrogen), chicken α-GFP 1:700 (Aves Labs), rat α-Ncad 1:20 (Developmental Studies Hybridoma Bank), mouse α-Bruchpilot 1:20 (Developmental Studies Hybridoma Bank), mouse α-CD2 1:1000 (Serotec), mouse α-Dac 2-3 1:20 (Developmental Studies Hybridoma Bank), rabbit α-β galactosidase 1:800 (Invitrogen), mouse α-β galactosidase 1:800 (Promega), rat α-Bab2 1:1500 (Frank Laski), rabbit α-Bar-H1 1:100 (Tetsuya Kojima). The following secondary antibodies were used: Alexa 488 goat α-rabbit 1:1000, Alexa 488 goat α-chicken 1:1000, goat α-mouse-Cy3 1:100, goat α-rat-Cy3 1:200, goat α-rabbit-Cy3 1:200, Alexa 568 goat α-mouse IgG highly cross-adsorbed 1:300, Alexa 647 goat α-rat 1:200, Alexa 633 goat α-mouse 1:200, Alexa 647 goat α-mouse 1:200. Confocal images were taken by an Olympus Fluoview FV1000 or Zeiss LSM 510 (Light Microscopy Core Facility).

2.4.5 Real-time RT-PCR

Antennae from approximately 50 flies were dissected for each genotype and at least three biological replicates were analyzed for each genotype. RNA was extracted with an RNeasy kit (Qiagen), treated with on-column DNase digestion (Qiagen), and

then reverse transcribed into cDNA using the SuperScript First-Strand Synthesis System for RT-PCR (Invitrogen). qPCR was performed using the FastStart Universal SYBR Green Master Mix (Roche) or the FastStart Essential DNA Green Master Mix using standard protocol. Expression for each gene was analyzed in triplicate. Ct values were used to calculate dilution factors for each gene based upon standard curves created for each gene. Dilution factors were then normalized to the average factor of all ORs tested.

Table 2: qPCR primers for olfactory receptors.

Primer Name	Sequence	Amplification efficiency
Or67d-qPCR-F	GCATCAGCTGTATACTAGAATGCTT	1.004581
Or67d-qPCR-R	GGGCCAGGCTTTCATAAAGAT	
Or23a-qPCR-F	ACTGTACCTGATCTCCGAGC	1.022281
Or23a-qPCR-R	GTCACATCGAGTAATCTATACAGCG	
Or2a-qPCR-F	CCTTCTACGATTGCAACTGGAT	1.05291
Or2a-qPCR-R	AACCTCATGACCTGCTCGAAG	
Or47b-qPCR-F	CAAATCTCAGCCTTCTGCGG	1.012215
Or47b-qPCR-R	GATACTGGCACAGCAAACTCA	
Gr21a-qPCR-F	CCAACATGTACGGCATGTACT	0.9796537
Gr21a-qPCR-R	ACAGACCCACCTCCTTGTAG	
Or92a-qPCR-F	TGATATCTTCAAGCTCTCGGATTG	0.9533596

OR92A-QPCR-R	TAGGCGGTCTTATAGAGGCG	
OR85A-QPCR-F	GAGCGACGATACAGAACCAC	0.9776528
OR85A-QPCR-R	AAGCGAACTTGGCCATCTTTAT	
OR22A-QPCR-F	CCGATCGTCGCTACAAATCC	1.034769
OR22A-QPCR-R	ATGCCAGCTTCACCATAGCC	
OR56A-QPCR-F	TTGACAGTTGGCGTTCCAAG	0.9354389
OR56A-QPCR-R	AAGCAAGGCTCAGTTCATCG	
OR82A-QPCR-F	CTCCAATTGGCATCTGGCTT	0.943322
OR82A-QPCR-R	GTTCGACAGATCCCAACGAAA	
OR49B-QPCR-F	ACAAGGTGGGAAAGTTGATGG	1.008808
OR49B-QPCR-R	AATGGCAGGACTCTTTCGCT	
OR98A-QPCR-F	ATTCAAGCCGCAGTTACAAGT	0.956284
OR98A-QPCR-R	TGCCAGCTTAGCCACCTTAAT	
OR9A-QPCR-F	GAGACCAACTGGACCGACTT	0.9326372
OR9A-QPCR-R	GAACAATCGTCGAGAAGGTGG	
OR67B-QPCR-F	AGATCGTTTGCATGCCTGTT	1.068821
OR67B-QPCR-R	GCCGGGTAAGTCAAGGTCAT	
OR67A-QPCR-F	ATTCAAGCCCATAACGCACC	1.045276
OR67A-QPCR-R	TCATCAGATCAGTGAGTCGAAGT	
IR31A-QPCR-F	CGAGATCTGTGATCTGCGTG	0.9775197

IR31A-QPCR-R	CCTGGGCATTACACATAGCTG	
IR41A-QPCR-F	CCAAATTGATTCATCTGCCGC	1.020108
IR41A-QPCR-R	ACCACGAGTACATAGCTCCAA	
OR35A-QPCR-F	CGACTTGGCCTTTACTACGGA	0.9652927
OR35A-QPCR-R	AGGGCTTGCTGTTCATCTCA	
IR84A-QPCR-F	CAGTTGGTCAGGTGTGATGG	0.9322729
IR84A-QPCR-R	AAAGTGGATGTTCTGGGTGTG	
OR13A-QPCR-F	CAATCGTTCACGCCAACAAC	0.9915544
OR13A-QPCR-R	ATCGAGGTACTTAGAATGGCCG	
ACT5C-QPCR-F	GGCGCAGAGCAAGCGTGGTA	1.029591
ACT5C-QPCR-R	GGGTGCCACACGCAGCTCAT	
GAPDH2-QPCR-F	CGTTCATGCCACCACCGCTA	1.053987
GAPDH2-QPCR-R	CCACGTCCATCACGCCACAA	

2.4.6 Chromatin immunoprecipitation

This procedure is modified based on a published protocol (112). For each genotype, approximately 800 eye-antennal discs were dissected. The samples were cross-linked with 1% formaldehyde in dissection buffer for 10min at room temperature. To quench cross-linking, glycine was added to 125mM final concentration, and the samples were incubated for 5min. The discs were homogenized and sonicated in a

Bioruptor machine for 13min (high frequency; 30 sec ON/30 sec OFF). The chromatin was pre-cleared with pre-washed Dynabeads Protein G (Life Technologies) for 1hr at 4˚C on a nutator. The pre-cleared chromatin was split into 2 tubes (1ml/tube), and another 20ul (2%) was saved as input and stored at -20˚C. 5ug Anti-GFP antibody (Ab290) or an equal amount of normal rabbit IgG were added to either tube, followed by overnight incubation at 4˚C. Beads were added to both tubes, and the samples were incubated for 2 hours at 4˚C on a nutator. Beads was briefly rinsed with wash buffer I (50mM K-HEPES, pH7.8, 140mM NaCl, 1mM EDTA, 1mM EGTA, 1% Triton X-100, 0.1% Na-deoxycholate, 0.1% SDS), and washed 1X with wash buffer I, 1X with wash buffer II (the same as buffer I, except that NaCl is 500mM), 1X with wash buffer III (250mM LiCl, 0.5% Igepal CA-630, 0.5% Na-deoxycholate, 1XTE), 2X with the TE buffer, at 4˚C, 5min/each wash. The chromatin was eluted 2X with pre-warmed elution buffer (1% SDS, 100mM $NaHCO_3$). For each elution, beads were incubated in 100ul solution for 10min at 65˚C, with gentle vortexing every 2-3 min. To reverse cross-link, 5M NaCl was added to each tube, followed by overnight incubation at 65˚C. The ChIP-ed DNA was treated with RNase and proteinase K, and extracted by PCR purification columns (Qiagen). The purified DNA was tested for enrichment of DNA fragments by qPCR. For each target gene, up to 150bp amplicons were selected every ~300bp in the first 2kb region upstream of the coding region. To test direct binding of Rn to the published 13bp T13 motif within the Bab2 LAE (leg and antennal enhancer) *in vivo*, a primer pair covering this region was

designed for ChIP-qPCR analysis (85). This result, provided being positive, would serve as a positive control. To confirm that Rn does not bind to the M1 motif upstream of *rn*-positive OR promoters, primer sets covering the motif from Or49a and Or82a promoters were designed and used in ChIP-qPCR analysis. This experiment can also be used as a negative control.

Table 3: ChIP-qPCR primers.

Primer Name	Sequence
Bab2_ChIP_T13_F	TATTTGCGTGGAGCCTTC
Bab2_ChIP_T13_R	TAACGATTGCCGCGATTT
Or82a_ChIP_M1_F	CACAGTACATACAGCCATACAG
Or82a_ChIP_M1_R	CGCTTCCTTCTGCTTGTT
B2_ChIP_399_F	CCCTCAAAGATAACGAACACG
B2_ChIP_399_R	CGAACTACAACCGCACAAA
B2_ChIP_728_F	TGAGTTTCAAGCTGCCATAA
B2_ChIP_728_R	TTGTACAGGAATGACAGAACAT
B2_ChIP_1588_F	CATGGTTTATTCAGAGGCAATAC
B2_ChIP_1588_R	CCAAGCATTTACGACCTGA

Note: B1 and B2 stand for Bar-H1 and Bar-H2, respectively. T13 and M1 are the motif names (42,85). The numbers correspond to the lengths between transcription start sites and the beginning of the amplicons.

2.4.7 Statistical analysis

Statistical analysis of Bab2 expression levels, qPCR results, and neuron counts was by unpaired, two-tailed Student's t test. For all tests, * $p < 0.1$, ** $p < 0.01$, *** $p < 0.001$. Single factor ANOVA was used to analyze the number of Or47b neurons. Post-hoc, unpaired, two-tailed Student's t tests were calculated after ANOVA.

3. Transcriptional profiling of olfactory system development identifies *distal antenna* as a regulator of subset of neuronal fates

This chapter is modified from the previously published work *Barish et al. (2017). Transcriptional profiling of olfactory system development identifies distal antenna as a regulator of subset of neuronal fates. Scientific Reports; 7:40873. doi: 10.1038/srep40873.*

3.1 Summary

Background

Drosophila uses 50 different olfactory receptor neuron (ORN) classes that are clustered within distinct sensilla subtypes to decipher their chemical environment. Each sensilla subtype houses 1-4 ORN identities that arise through asymmetric divisions of a single sensory organ precursor (SOP). Despite a number of mutational studies investigating the regulation of ORN development, a majority of the transcriptional programs that lead to the different ORN classes in the developing olfactory system are unknown.

Results

Here we use transcriptional profiling across the time series of antennal development to identify novel transcriptional programs governing the differentiation of ORNs. We surveyed four critical developmental stages of the olfactory system: 3rd instar larval (prepatterning), 8 hours after puparium formation (APF, SOP selection), 40 hrs APF (neurogenesis), and adult antennae. We focused on the expression profiles of

olfactory receptor genes and transcription factors—the two main classes of genes that regulate the sensory identity of ORNs.

Conclusions

We identify distinct clusters of genes that have overlapping temporal expression profiles suggesting they have a key role during olfactory system development. We show that the expression of the transcription factor *distal antenna* (*dan*) is highly similar to other prepatterning factors and is required for the expression of a subset of ORs.

3.2 Results

3.2.1 Stage specific analysis of developing olfactory system transcriptome

To analyze the transcriptional dynamics of olfactory system development in *Drosophila melanogaster*, mRNA was sequenced from developing antennal discs and antennae at four different stages (3L, p8, p40, adult). For every time point, we generated two biological replicates, each comprised of RNA pooled from >50 *w1118* flies (113). We first performed principal component analysis (PCA) to assess the sources of variation of transcripts across RNA datasets from 4 developmental stages (Fig 25A). Variation detected in the first two principal components (PC1 and PC2) showed high level of similarity between 3L and p8, both of which significantly differed in global transcription from p40 and adult antennae (Fig 25A). As expected, the biological replicates for each stage were most similar to each other, segregating away from the transcriptional profiles of other stages (Fig 25A). The first principal component segregates the samples based on

developmental time, such that, the right side of the graph corresponds to earliest developmental stages and the left is the more differentiated states (Fig 25A). The second principal component clusters the first three time—3L, p8, and p40--points close together while adult antennae are highly segregated by this principle component (Fig 25A). In other words, each developmental time appeared to have a unique transcriptional profile that clusters away from other stages, especially the adult stage. Given their temporal proximity, it is striking that the p40 and adult antennal transcriptional profiles appeared most distant from each other according to the second principal component (Fig 25A). We next analyzed which transcripts contribute to PC1 and PC2. Of the >29,000 transcripts that were analyzed only 17 had a correlation coefficient >0.1 for PC1 (Table 4). Three of these transcripts were annotated as having metabolic functions, three as odorant binding proteins (Obps), one as involved in lateral inhibition and 10 had no known function. 21 transcripts had correlation coefficients >0.1 for PC2 (Table 5), and of these 10 were involved in cuticle/chitin development, 8 had no known function and one each were involved in wing disc morphogenesis, lateral inhibition, and metabolism. These results are consistent with the observation that PC2 segregates adult antennae from the other three developmental stages and suggests that the primary transcriptional changes in the antenna that drive late stages of development control the development of the cuticle and adult structures. Given that almost half of the genes identified have no known function suggests that many of the key players in this process remain uncharacterized.

We next analyzed which genes were differentially expressed between each time point, which are represented in MA plots (Fig 25B-D). Genes that show significant differential expression in each comparison are represented by red dot ($p<10^{-6}$, Table 6-8). This analysis confirmed results from PC analysis: 3L and p8 appeared more similar and segregate from p40 and adult (Fig 25B-D, Table 6-8). These results underscore that the transcriptional profile of the developing olfactory tissue is dynamic across developmental time and that each stage has a characteristic transcriptional profile. Yet the antenna is a highly complex tissue, and defining the specific cell types undergoing these transcriptional changes requires detailed transcriptome analysis of sorted cell populations.

Analysis of both PCA clustering and MA plots comparing 3L-p8, p8-p40, and p40-adult sequences showed that transcriptional changes occurring in later stage transitions are much more dramatic as compared to earlier stages (Fig 25A-D). To identify the genes driving transcriptional differences between each time point, we determined enriched functional gene groups among the genes that vary across time points using Gene Ontology (GO) plot package in R (Fig 26-28). For each comparison, we performed two analyses: using the 500 genes either with the largest fold change or with the lowest p-values (Fig 26-28). The genes with the largest fold change between 3L and p8 are enriched for functions in chitin and cuticle development, and the extracellular matrix (Fig 26A-B, Table 9). Similar enrichment for structural components

of chitin, cuticle development, and the extracellular matrix are also detected for the 500 genes with lowest p-values, in addition to genes involved in developmental processes, transcription factor activity and neuronal fate commitment (Fig 26C-D, Table 9). Between p8 and p40 genes were significantly enriched for changes in the development of the cuticle and chitin synthesis (Fig 27A-B, Table 10). We also observed that there was enrichment among the genes with the lowest p-values, for cell cycle processes (Fig 27C-D, Table 10), which is consistent previous observations that all neurons of the antenna are generated by 40hrs APF (43). Finally, between p40 and Adult transcriptomes differentially expressed genes were enriched for odorant binding and sensory perception (Fig 28, Table 11) consistent with the upregulation of OR genes. Metabolic processes were also enriched for genes with the largest fold change between these time points (Fig 28A-B, Table 11). Interestingly, we also detected enrichment in both groups of genes for plasma membrane structure and function. We observe that processes such as cell cycle regulation, transcription factor activity, and neuronal fate commitment are enriched in the lowest p-value groups but not the largest fold change. This suggests that the largest transcriptional changes occur for genes regulating the development of antennal structure, while other developmental processes are make smaller though significant changes. Overall, these results suggest that earlier stages of antennal development are dedicated for cellular and structural development of the antennal

tissue, and the later stages, especially adult stages, are enriched in genes responsible for functional and sensory properties of the antenna.

3.2.2 Temporal Dynamics of OR Expression

Because it has been previously shown that the onset of olfactory receptor expression begins around 40 hrs APF (114), we were curious to see which, if any, ORs are expressed at this stage. We were able to detect OR transcripts at this stage, but they were expressed at much lower levels as compared to the adult stage (~2 orders of magnitude lower, Fig 29). Because the expression of ORs at p40 was so low, we wanted to determine if the expression in our RNA-seq data was biologically relevant. We first compared OR expression levels at p40 to the expression of gustatory receptors (GRs). Gustatory receptors primarily function in taste sensation and are expressed predominantly in the labial palps and legs (36,115,116). With the exception of the four olfactory GRs (Gr21a, Gr63a, Gr28b, and Gr10a) (24), GRs are not known to be expressed in the olfactory system, and should therefore not be expressed above background levels in the antenna (117). The structure of GRs and their expression in gustatory neurons, is relatively similar to ORs in the olfactory organs, except that multiple GRs can be expressed in the same neuron. Most reporters of GR expression show exclusion from the antennae (36,115,116,118). Using a negative binomial model (Methods), we calculated confidence intervals for each of the 62 antennal ORs to determine if they were above background expression levels. Nearly half (21; 17 ORs and 4 IRs) of the ORs in the

olfactory system were expressed at p40 (Fig 29, Table 12, 13, $p>0.05$). Typically, one receptor per sensilla subtype was expressed at p40 (Fig 29, Table 12, 13) with a few exceptions. For instance, ab1 expresses two receptors at p40 and is the only sensilla subtype to house four ORNs, as well as express GRs (Fig 29, Table 12, 13). In contrast, ab5 and ab8 sensilla also expressed two receptors at p40 and only house two ORN classes. Why specific subsets of the ORs are expressed early in each sensillum remains unknown, but may represent the sequence of developmental and cell-cell communication events as ORNs in the same sensillum pick specific olfactory receptors from limited possibilities.

We next wanted to confirm that we could detect expression of ORs at p40 with expression of OR reporters. Well-established OR-GAL4 drivers have been shown to be faithful reporters of OR transcription (18). Therefore, detecting expression of OR reporters at p40 should provide confirmation of the transcriptome results. For example, in our transcriptome data, among the at4 sensilla OR genes, Or47b is the first to be expressed, followed by the expression of Or65a and Or88a, which are not detected until the adult stage (Fig 29, Table 12, 13). We confirmed the temporal dynamics of ORs 47b and 88a using OR reporters in the antenna (Fig 30). The Or47b reporter is expressed at 40 hrs APF, but only in a few neurons (Fig 30A, C), corresponding to the low transcript levels of Or47b at this stage (Fig 29). Our results are also consistent with previous reports that show that OR transcript expression level correlates with the number of

neurons expressing a given receptor (113). The early OR expression is also unlikely to be a by-product of the larval olfactory system as the larval olfactory system is not housed in the antennal disc (18,119,120) and none of the ORs expressed early are OR genes previously shown to be expressed in the larval olfactory system (18,119,120). Or88a expression however is not detected until ~80 hrs APF, by which point Or47b expression has reached the adult level (Fig 30B, D). ORN fates within each sensilla subtype are defined by whether or not they require Notch for their development (Notch ON or Notch OFF) as they are generated from asymmetric divisions of sensory organ precursors (8,46). We therefore wanted to know whether the ORs that are expressed early shared a common Notch state (i.e. Notch-On of Notch-Off) (8), which might suggest that they are regulated by the same set of Notch dependent transcription factors. We did not observe any correlation however, among the Notch states of the olfactory receptors expressed at p40, based on previous genetic descriptions (Table 13). In fact, 9 of the ORs expressed at p40 are Notch-On fates and 8 are Notch-Off. So, while there is a slight bias for Notch-On fates, there does not appear to be a clear correlation between Notch state and expression of an OR gene at p40. Based on these criteria, our data also showed that a subset of ORs are expressed at uniformly low levels across the first three stages of development and then sharply increased in the adult. We found that Or19a/b (co-expressed in the same ORN) and Or43b, housed in at3 and ab8 sensilla respectively

were expressed throughout development, although at much lower levels than in the adult (Fig 29, Table 12).

Our results suggest that there is a temporal sequence to the onset of OR gene expression within a given sensillum, with some OR genes activated early, and others later. We speculate that the temporal sequence of OR expression among the ORNs in the same sensillum might arise as a result of inter-neuron communication that distributes limited OR gene possibilities individually to each neuron. It is possible that the sequence of OR expression is also tied to the molecular age of the receptor (121), with phylogenetically older receptors turning on first and newer ones later. This appears to hold true for both ab1 and at4 sensilla. For ab1 sensilla, Or92a is older than Or10a and is expressed at p40 (Figure 29, Table 12, 13), whereas we do not detect expression of Or10a until the adult stage (Figure 29, Table 12, 13). Or42b is older than either of these receptors (121) and is the first receptor to be expressed in ab1 sensilla (Figure 29, Table 12, 13). In at4 sensilla, Or47b is older than Or88a and turns on before Or88a (121) (Figure 29 and 30). Thus, given the dynamic nature of olfactory receptor sequence evolution, the temporal order of olfactory receptor expression within a sensillum might represent the processes that correlate with the evolutionary emergence of new receptors and their integration into new circuits as a novel class of ORN.

3.2.3 Temporal Dynamics of IR Expression

Four of the IRs were expressed at p40: Ir75a, Ir75b, Ir75c and Or35a (An OR expressed in coeloconic sensilla) (Fig 29). Ir75a is expressed in multiple sensilla and we, therefore, cannot determine which of the sensilla are expressing this receptor at p40. No Irs were expressed at all stages, but Ir75a was expressed at every stage except for 3L (Fig 29, Table 12, 13). As was the case for Or19a/b and Or43b, the expression of Ir75a was much lower at early developmental stages and sharply increased at the adult stage (Fig 29, Table 12). Each coeloconic sensilla subtype contains at least one receptor that is not expressed in the other sensilla subtype, whereas the others are shared across subtypes (20,122). Interestingly, we only observed expression of ac3 IRs (Or35a and Ir75b/c) at p40 (Fig 29, Table 12, 13). This suggests that the specification of ac3 sensilla occurs first, whereas other subtypes are specified at a later time than that of OR expressing sensilla.

3.2.4 Transcription Factor Expression

While it is well understood that transcription factors play a key role in specification of ORN identity at all stages of antennal development (38,40,42,52,113,123), the precise timing of the expression of these genes across development is not known. Given the combinatorial nature of ORN identity, it is plausible that combinations of transcription factors accumulate on promoters of genes regulating trajectory of a given ORN class in an additive manner, where newly added transcription factors build on, or complex with, existing transcription factors occupying and maintaining the memory of

cellular decisions. It is likely that the current set of transcription factors that regulate ORN specification is incomplete. Thus far, most studies have focused on the regulation of ORs in the basiconic and trichoid sensilla (52–54) and only a few have examined the regulation of ORs/IRs in coeloconic sensilla (40,42,113). Furthermore, these studies have primarily been conducted with biased approaches, focusing on only a few ORs at a time. Adopting unbiased approaches for determining which transcription factors may play a role in ORN specification is critical to advancing our understanding of the mechanisms of olfactory system development.

To identify transcription factors expressed during olfactory system development, we queried approximately 400 annotated transcription factors from Flybase and analyzed their expression profiles in our data set (Fig 31, Table 14). We observed three patterns of transcription factor expression: those that are expressed early, those that are expressed late, and those that are expressed throughout all stages (Fig 31, Table 14). These expression patterns are also generally predictive of the function of known transcription factors (Fig 32). Prepatterning factors and proneural genes, such as *rotund (rn*), *apterous (ap), lozenge (lz), amos,* and *atonal (ato)*, are expressed primarily at 3L and p8 but absent at the p40 and adult stages, consistent with previous reports (38,40,42,89) (Fig 32). Terminal selector transcription factors on the other hand, such as *acj6, fer1, onecut,* and *eip93F*, are highly expressed in p40 and adult antennae but largely absent from 3L and p8 antennal discs (Fig 32), consistent with their function as direct regulators of OR

expression (52). Other transcription factors from both the prepattering network and the terminal selectors (*Distal-less (Dll)*, *Bar-H1/2 (B-H1/2), dachshund (dac),bric-a-brac1/2 (bab1/2), xbp1* and *zf30c)* however, are expressed throughout development (Fig 27, Table 11) (43). It is unclear what function these genes have outside of their already well-defined roles in the development of the antennal disc (32,52,113,124).

3.2.4.1 Clustering Analysis

Because we observed a correlation among known transcription factors between their function and expression pattern, we reasoned that global analysis of the expression patterns of transcription factors could yield novel candidate genes that govern ORN identity. Hierarchical clustering analysis based on developmental expression profile uncovered groups of genes that likely have similar functions (Fig 32). Transcription factors were clustered based upon their average expression level and pattern across all stages. Clustering analysis revealed 11 clusters of transcription factor expression in the olfactory system (Fig 31, Table 15). The majority of known regulators of olfactory system development do not cluster together. Instead they segregate into separate groups, revealing more refined patterns of expression that may be predictive of function. Several clusters stood out because of their pattern and the genes that cluster within them. Cluster 3 contains genes that are primarily expressed early and their expression decreases or is absent at p40 and in the adult (Fig 4). This cluster contains *rn* and *ap* (Fig 31), both of which are critical prepatterning factors that regulate ORN identity (42,113).

This cluster also contains genes known to play a role in imaginal disc and antennal development, such as *twin of eyeless (toy)*, *teashirt (tsh), distal antenna (dan),* and *distal antenna related (danr)* (Fig 31) (125,126). It is possible that genes in this cluster play a role in prepatterning of the antennal disc and control ORN specification.

Cluster 5 contains three terminal selector genes *onecut, 48 related 1 (Fer1),* and *abnormal chemosensory jump 6 (acj6),* as well as *seven up (svp), prospero (pros),* and the glial marker *reversed polarity (repo)* (Fig 31), all of which function primarily in later stages of olfactory system development (52,127). These genes are all expressed lowly in larval antennal discs and their expression increases over time and are highly expressed in adult antennae (Fig 31, Table 14). Interestingly, *POU-domain protein 2* (*pdm2)* is present in this cluster, which may suggest that it functions as a terminal selector, particularly because other POU-domain transcription factors, *acj6* and *pdm3,* are known to regulate OR expression and connectivity (Fig 31) (54,123).

Thus far, two major proneural genes, *amos* and *atonal*, have been shown to regulate development of basiconic/trichoid and coeloconic sensilla, respectively (38–40). In agreement with their role in precursor selection, we found that both *ato* and *amos* expression peaks at p8 in our data (Fig 31, Table 14). Genes in cluster 8 are expressed almost exclusively at 3L and p8 (Fig 31). Most of the genes in this cluster are also known to function as proneural genes and in Notch-Delta signaling, such as *acheate (ac), scute (sc), asense (ase), senseless (sens), atonal (ato),* and *cousin of atonal (cato)* as well as some

enhancers of split (*E(spl))* (Fig 31, Table 15) (128–131). Of these genes, only *sens* and *ato* have been shown to function in the olfactory system (132). Investigating the effects of these genes on ORN and sensilla development will be critical in the future.

Interestingly, four *E(spl)s* were present in Cluster 8: *E(spl)-m6, m8, mdelta,* and *mgamma* (Fig 31). Three other *E(spl)* genes, *E(spl)-m7, m3* and *mbeta,* were detected in our data set but did not cluster in Cluster 8 (Fig 31). *E(spl)m3* and *mbeta* were present in Cluster 1 and were expressed at all developmental stages (Fig 31, Table 14). *E(spl)m7* was present in Cluster 3 and was expressed at 3L, p8, and p40, but its expression decreased in the adult. At early pupal stages, Notch mediates the selection of sensory organ precursors and the expression of proneural genes. During neurogenesis however, Notch signaling segregates binary cell fates during asymmetric divisions of sensory organ precursors to generate each sensillum (8,38,46). *Notch, Delta* and *Serrate* are all expressed throughout development in our analysis (Table 14). It is plausible to imagine that the expression of different *E(spl)* genes or different combinations underlie the different and context-dependent roles that Notch signaling plays during olfactory system development.

3.2.5 Confirmation of Expression of Bar, Ap, Bab, and Dan

We next confirmed expression of several transcription factors in the olfactory system using immunofluorescence and imaging of reporters. We have previously published that the transcription factors *BarH1/2 (B-H1/2)*, *apterous (ap),* and *bric-a-brac1/2*

(bab1/2) are expressed in the antennal disc and are critical regulators of ORN identity (113). In the RNA-seq data, we detected expression of *B-H1/2* and *bab1/2* at p40 and the adult (Fig 31, Table 14). *ap* expression however, is mostly absent at both of these stages in antennal transcriptomes (Fig 31, Table 14). Immunostaining for *B-H1/2* was detected broadly in the antenna and expression of the *Bar-H1-Gal4* was present in adult antennae, consistent with the transcription data (Fig 33A, B). Expression of *ap-Gal4* was present in a small number of ORNs at p40, but was entirely absent in adult antennae, as observed in the RNA-seq data (Fig 33C, D). We also detected weak expression of the *bab1-GAL4* in adult antennae, verifying our transcriptomic analysis (Fig 33E).

As mentioned above, we detect expression of *dan* mRNA at 3L and p8 in our RNA-seq data (Fig 31, Table 14) and we were able to confirm this and previous reports of expression with immunofluorescence in the antennal disc (Fig 33F). *dan* is expressed throughout the entire portion of the antennal disc that specifies the third segment of the antenna (Fig 33F). We also observe that *dan* expression is not uniform in all cells across the disc, and that some cells express high levels of *dan* and some barely have any fluorescent signal (Fig 33G).

3.2.6 Dan Functions to Regulate the Expression of a Subset of Olfactory Receptors

It has been previously reported that loss of *dan* function leads to the production of ectopic hairs on the 3rd segment of the antenna (126,133). In addition, overexpression of *dan* in the leg disc causes the claw to develop into an arista like structure (126).

Because *dan* was present in Cluster 3 and is expressed in a highly similar pattern to prepatterning factors like *rn* and *ap* (Fig 31), we were curious as to whether Dan may also regulate the development of ORNs as well as larger structures of the antenna. Using qPCR as published previously by our lab, we measured the expression of 20 OR genes representing at least one receptor that is expressed in each of the sensilla subtypes on the antenna in wildtype and *dan* mutant flies. We detected four ORs that were significantly down-regulated and three that were significantly up-regulated (Fig 34A). There does not appear to be any particular pattern of those ORs.

We were able to confirm our qPCR results by imaging of OR reporters in the antenna (Fig 34B-G). We observed a statistically significant decrease in the number of Or49b and Or98a ORNs in *dan* mutants (Fig 34B-G). It is plausible to think that different sensilla subtypes are specified by the expression of both *dan* and *danr*, but some subtypes are more sensitive to changes in *dan* expression. Correspondingly, we see some cells that express Dan at lower levels than other cells of the antennal disc (Fig 33G, white arrowheads). It would also be reasonable to think that a distinct subset of ORs would be misregulated in *danr* mutants. It has been previously published that down regulation of *dan* and *danr* via mutation of *ss* leads to an up-regulation of *Antennapedia (Antp)* (126), which could suggest that in *dan* mutants the antenna has undergone a partial conversion to a leg phenotype and therefore altered the expression of some OR genes.

3.3 Discussion

Here we report a detailed transcriptome analysis of the adult Drosophila olfactory system during development. Our analyses have revealed the temporal dynamics of all antennal olfactory receptor gene expression during ORN development. We also identified transcription factor programs in the developing olfactory system with stage specific functions corresponding to different processes in ORN development. And finally, we show that one of these transcription factors, *distal antenna*, is required for the development of a subset of ORN classes. Although this study is the first to analyze the transcriptome of the olfactory system across developmental stages, the antenna is a highly complex tissue and further cell type specific analyses will likely yield further insights into these processes.

ORNs in the same sensillum arise through asymmetric divisions of a single multipotent precursor cell, yet the timing for terminal differentiation of ORNs, as assayed by the onset of olfactory receptor expression, has not been identified. Our analysis showed that within each sensillum, there is a temporal order to the onset of expression among the olfactory receptor possibilities. That is, onset of olfactory expression occurs earliest in only one of the neurons, followed by other olfactory receptors expressed sequentially, suggesting cell to cell communication among ORNs that determines the temporal order of olfactory receptor expression. Indeed, perturbations in Notch signaling were shown to contribute to the selection of alternate

olfactory receptor expression by alternate ORNs in the same sensillum (8). Upon selection of a "default" olfactory receptor within each sensillum, Notch signaling can relay this information to neighboring ORNs to suppress expression of the "default" receptor and select another olfactory receptor transcriptionally available in the lineage. These modifications might require chromatin regulation, as mutations in *alhambra (alh),* a chromatin modulator, result in acquisition of the default olfactory receptor expression at the expense of alternate olfactory receptors without modifying the target site of ORN axons in the antennal lobe (114). There might be different spatial and temporal requirements of transcription factor and chromatin complexes for each sensilla lineage, as effects of *alh* mutants are restricted to only few sensilla (114). The expression patterns of both chromatin modulators and transcription factors in specific cell types remains an understudied area of olfactory system development.

The transcriptional profile of olfactory system development showed dynamic and complex trends in the expression of transcription factors that might function in specification of ORN fates. Three different trends for transcription factor dynamics were detected. Among these, a majority of prepatterning and proneural genes are expressed early and are turned off in later stages of ORN development. Transcripts for a small number of these transcription factors did persist till later stages. Transcription factors previously shown to directly regulate olfactory receptor expression in genetic studies, on the other hand, generally showed a trend towards expression in late developmental

stages, with only a few exceptions. Analysis of approximately 400 proteins with transcriptional regulatory roles revealed other factors that show similar temporal profiles to known factors. One of these factors is *distal antenna (dan),* which has been previously shown to be expressed in many developing neural tissues, including the antennal disc. In addition, it has been shown to regulate fate specification of neuronal pools from embryonic neuroblasts.

The majority of ORN classes were not affected by loss of *dan*, except for a few classes namely: Or49a, Or56a, Or98a and Or23a, which all showed changes in transcript levels in qRT-PCR from *dan* mutant antennae. Among these, the number of Or49b and Or98a ORNs were confirmed to be decreased by antennal reporter imaging, which underlies the decrease in their transcripts in *dan* mutant antennae. Most of the ORs that are affected by *dan* mutation developmentally arise from the center of the antennal disc except for Or98a (113). Other than this trend, there does not seem to be any clear pattern to which ORs are affected by loss of *dan*. Because of its broad expression pattern, we would have expected a wider array of ORs to have been affected and so it remains unclear why these particular ORs are more sensitive to changes in *dan* expression. It is plausible to imagine that expression of *dan* works together with the rest of the transcription factor networks patterning the antennal disc in a combinatorial code to determine different precursor potentials. Broad *dan* expression in the antennal disc is similar to the expression of *bab1* and *bab2,* which also belong to the combinatorial code

defining different zones on the antennal disc. Mutations in *bab1* and/or *bab2* also weakly affect only specific ORN fates(113). Of the ORs that were significantly down-regulated in *dan* mutants, none completely lost expression as has been reported in mutation of other genes that function in prepattering of the antennal disc (42,113). This is likely due to the possible redundant functions of *dan* and *danr* in the antennae (126,133). We would therefore predict to see more dramatic phenotypes and many more ORs affected in *dan-danr* double mutants. Previous work has shown that *dan* and *danr* are critical regulators of antennal identity (126,133). It is possible that they provide a link between the regulation of broad antennal development and the development of specific ORN identities. Understanding the interaction between *dan, danr* and the early prepatterning gene regulatory networks will provide key insights into the specification of different sensilla identities and ORN classes.

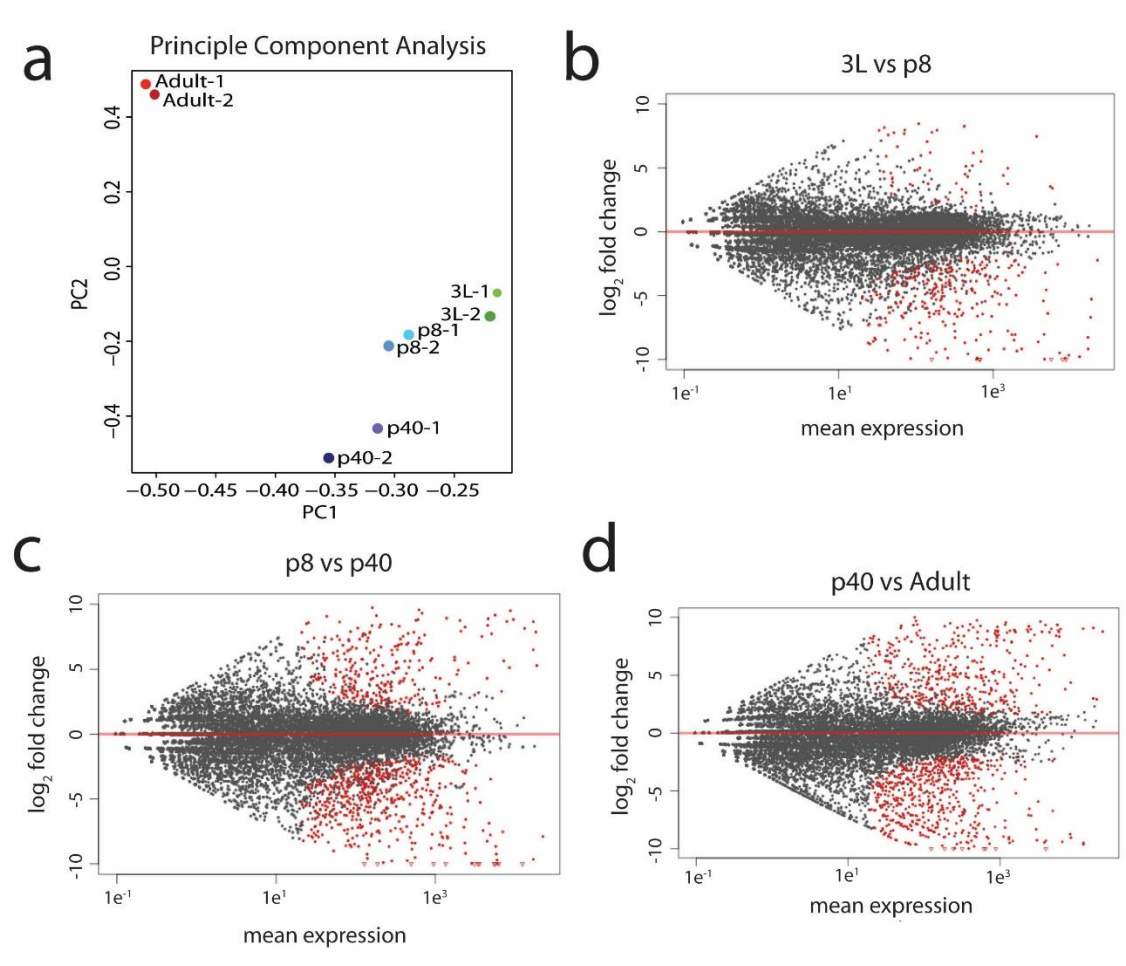

Figure 25: PCA analysis and MA plot comparisons of gene expression across all time points and pairwise comparisons respectively. (A) PCA analysis of all four transcriptional time points. The adult transcriptome appears the most divergent among the developmental time points, whereas the 3L and p8 timepoints show the highest similarity. (B-D) MA analysis showing differentially expressed genes between developmental stages ($p < 10^{-6}$), which are highlighted in red.

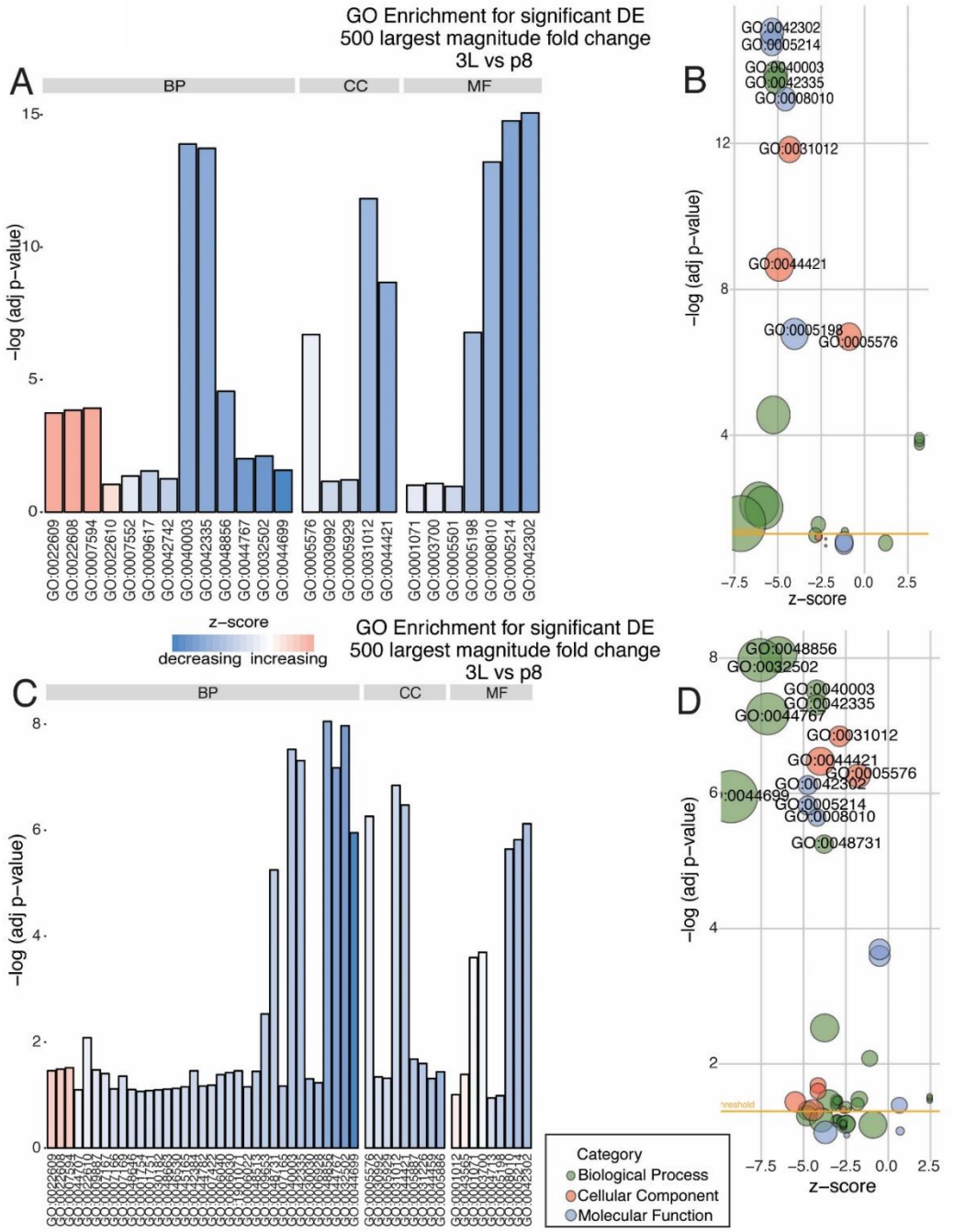

Figure 26: Pairwise GO plot analysis of differentially expressed genes between 3L and p8 stages. Bar graphs and bubble plots showing enrichment of GO terms for the 500 genes with the largest fold change (A, B) and the 500 genes with the smallest p-values (C, D). Key for GO term numbers is located in Table 9. Green = Biological Process, Red = Cellular Component, Blue = Molecular Function.

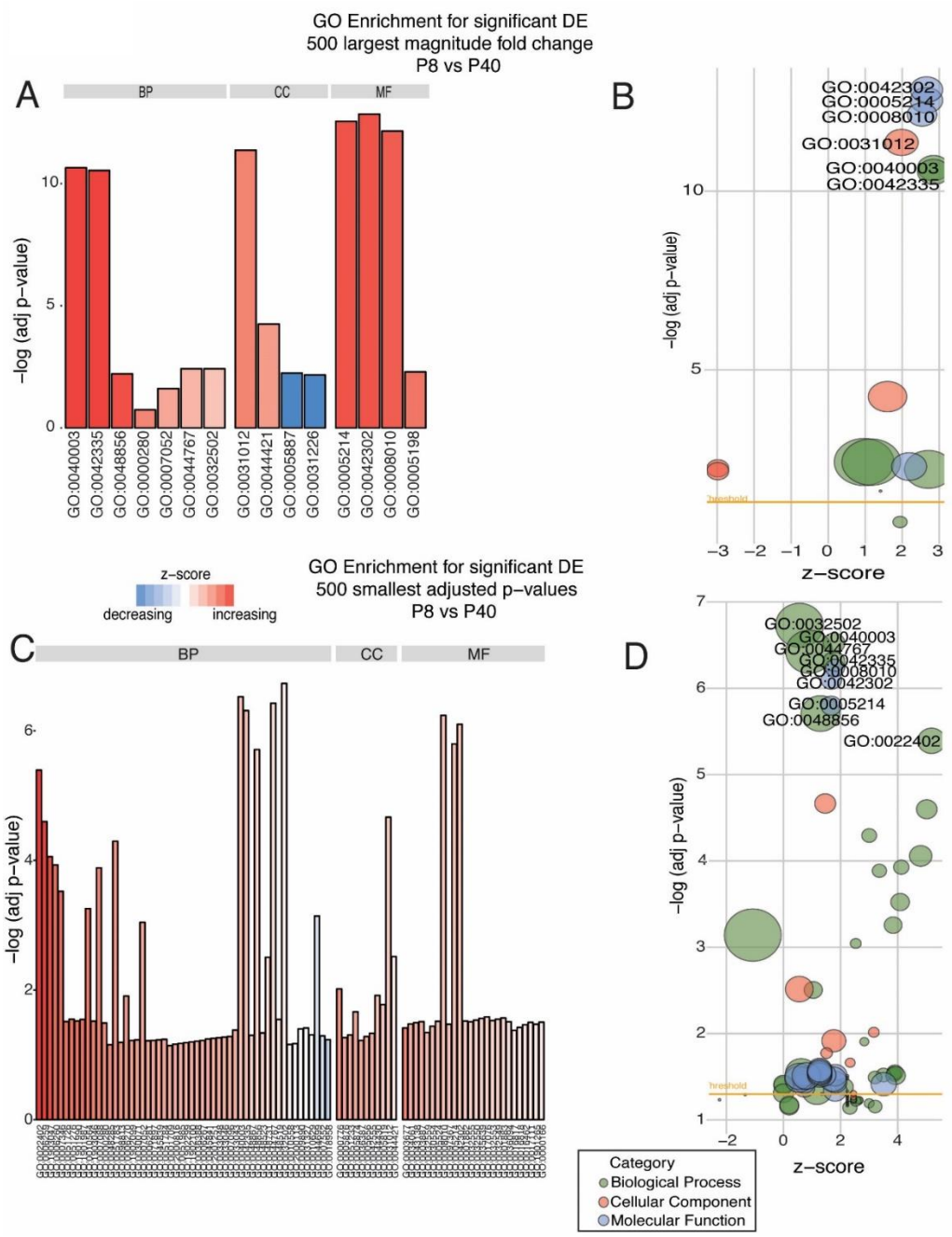

Figure 27: Pairwise GO plot analysis of differentially expressed genes between p8 and p40 stages. Bar graphs and bubble plots showing enrichment of GO terms for the 500 genes with the largest fold change (A, B) and the 500 genes with the smallest p-values (C, D). Key for GO term numbers is located in Table 10. Green = Biological Process, Red = Cellular Component, Blue = Molecular Function.

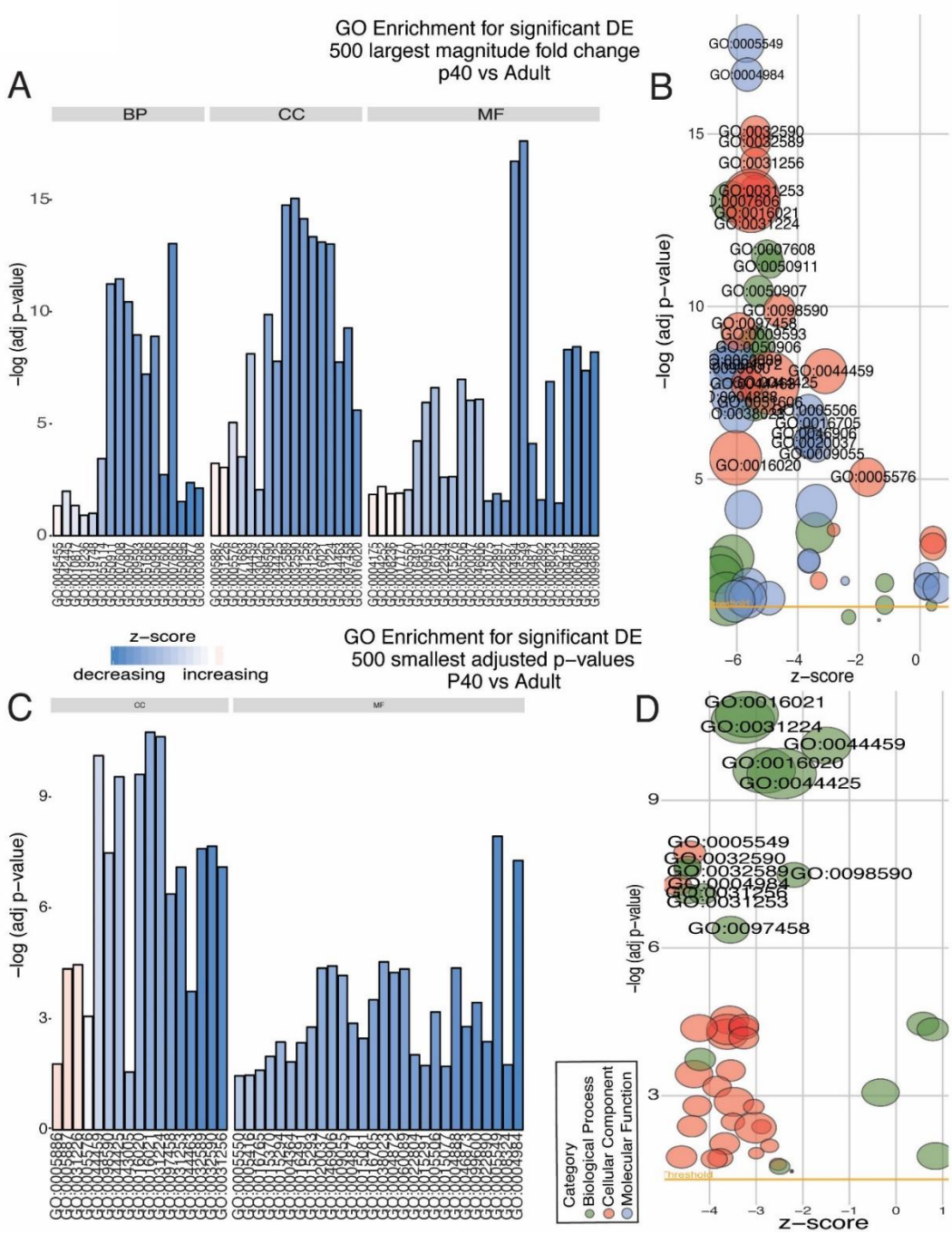

Figure 28: Pairwise GO plot analysis of differentially expressed genes between p40 and Adult stages. Bar graphs and bubble plots showing enrichment of GO terms for the 500 genes with the largest fold change (A, B) and the 500 genes with the smallest p-values (C, D). Key for GO term numbers is located in Table 11. Green = Biological Process, Red = Cellular Component, Blue = Molecular Function.

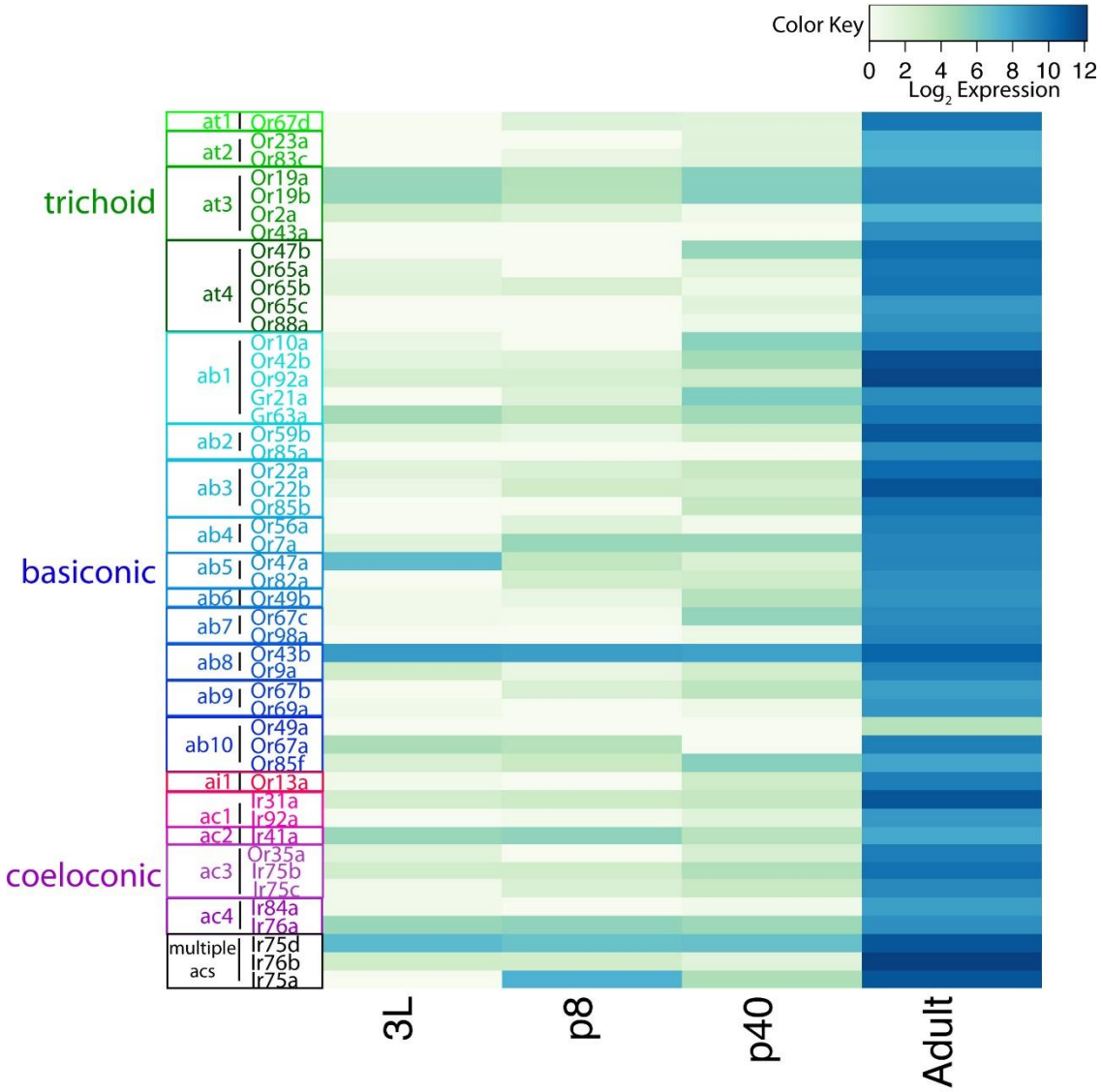

Figure 29: OR/IR developmental expression profiles grouped based on sensilla pairings of ORNs. Expression is graphed with normalized $\log_2$ expression values, where highly expressed genes are represented in dark blue and low expressed genes are represented with green or white.

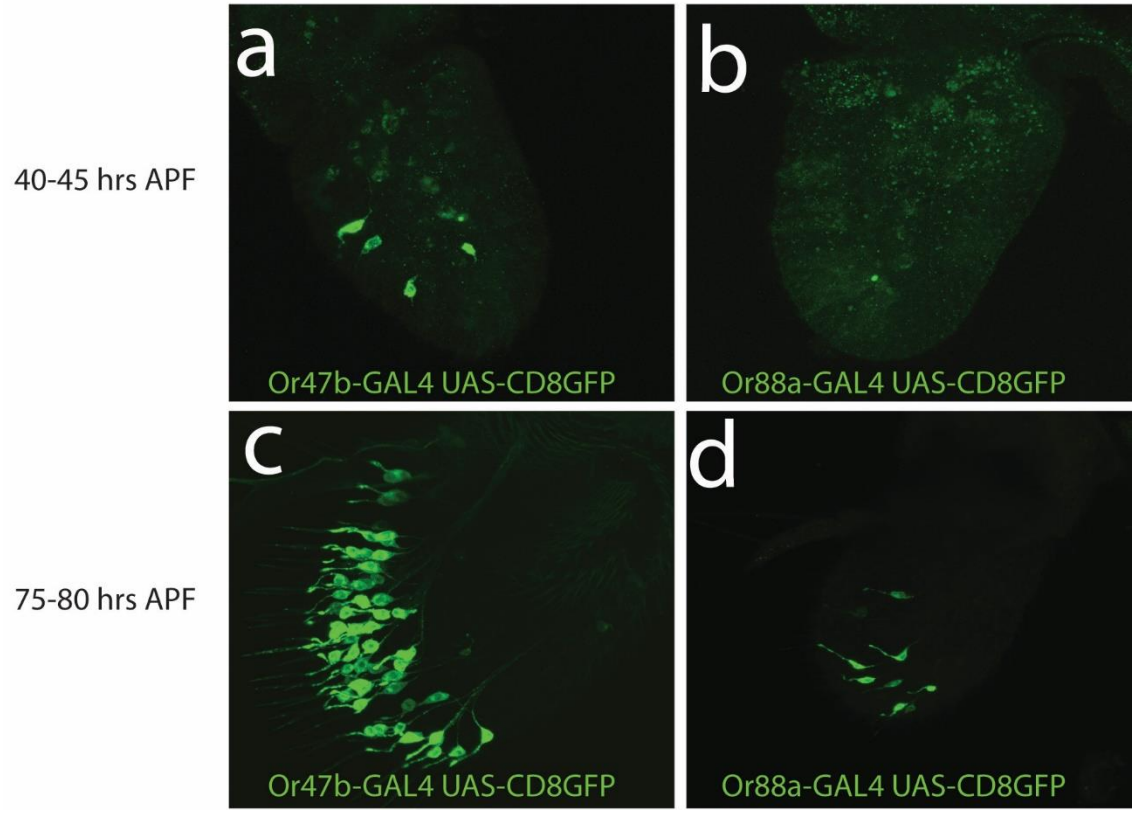

Figure 30: Expression of OR reporters in developing pupal antennae. A small number of neurons express OR47b (top left) at 40-45 hrs APF, whereas Or88a expression is not detected at this stage (top right). By 75-80 hrs APF Or47b expression appears fully developed (bottom left), while OR88a expression is present in only a few neurons (bottom right).

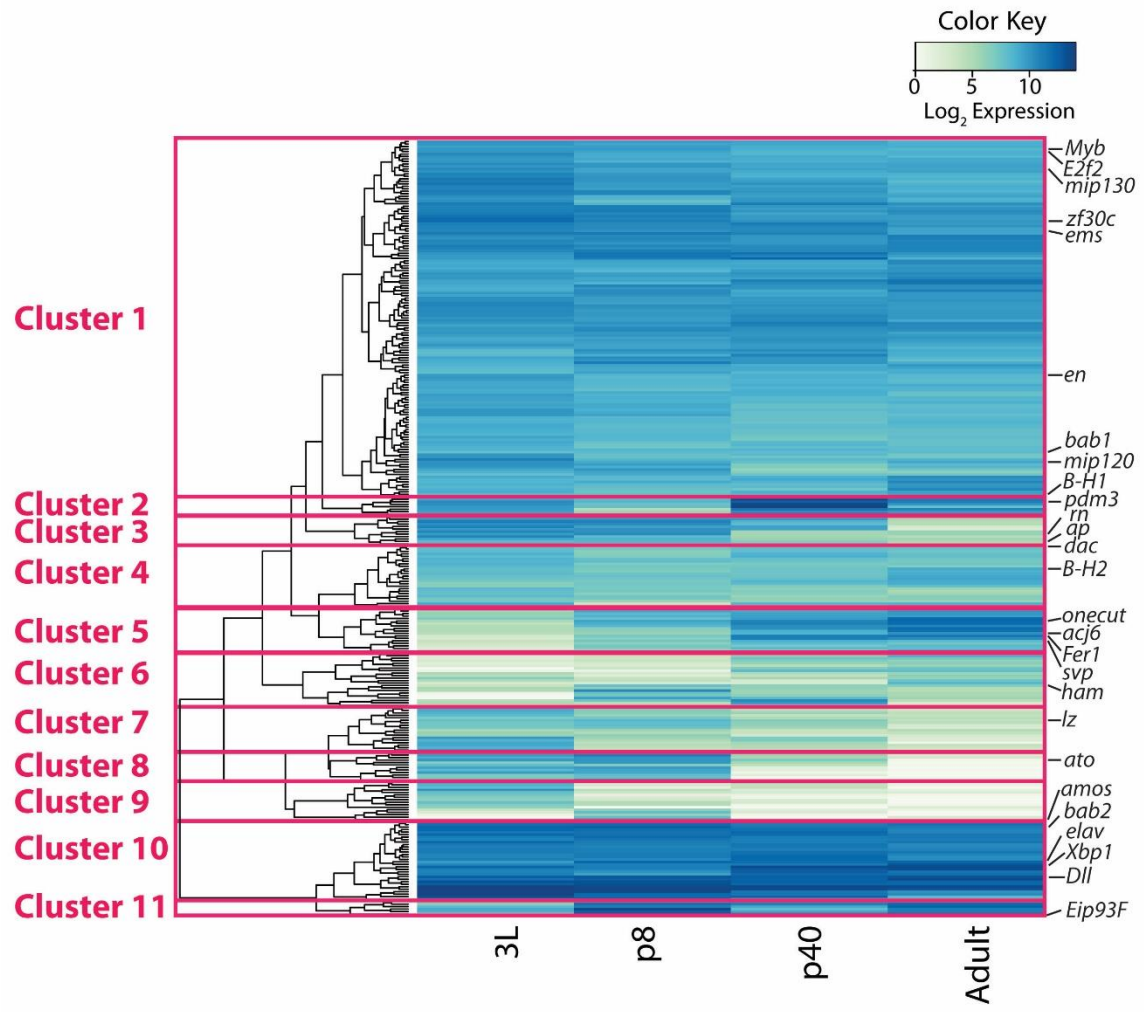

Figure 31: Clustering analysis of ~400 transcription factors based on expression profiles. 11 Clusters were identified based on similarity of expression profiles. Expression is graphed with normalized $\log_2$ expression values, where highly expressed genes are represented in dark blue and low expressed genes are represented with green or white.

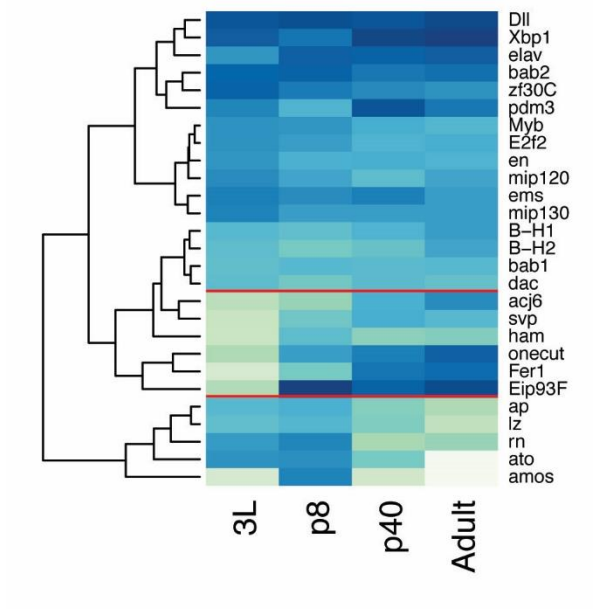

Figure 32: Hierarchical clustering of the expression patterns of transcription factors known to regulate ORN specification. Transcription factors in the olfactory system are expressed generally in accordance to their function. Prepatterning and pronueral factors cluster at the bottom of the heatmap, indicating high expression early in development and low expression later. Terminal selectors on the other hand cluster just above, corresponding to low expression early and high expression late in development. Genes that cluster at the top of the heat map are expressed highly throughout development and fall into both categories.

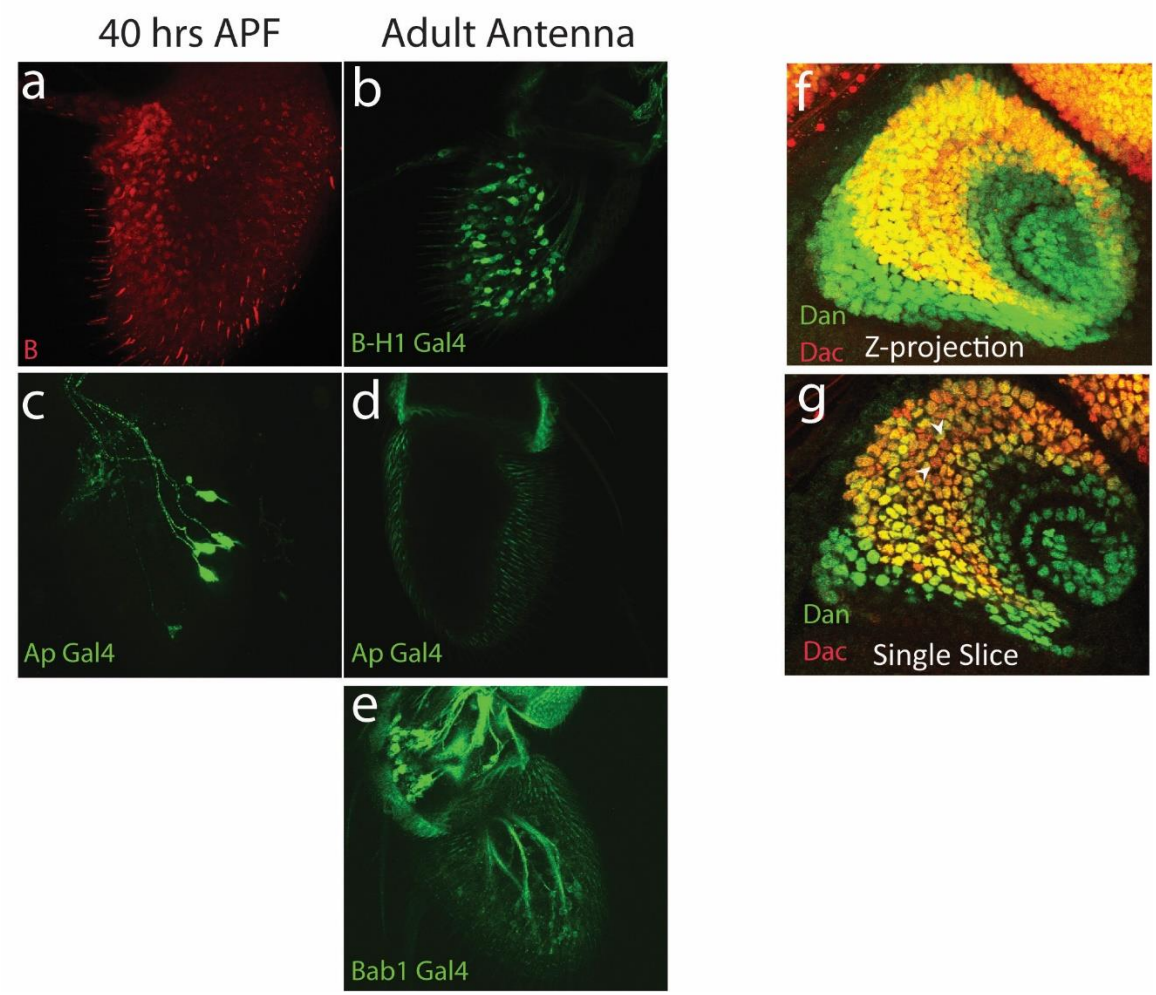

Figure 33: Confirmation of RNA-seq with immunofluorescence and reporter expression. (A-C) Expression of BarH-1 (A), Ap (B), and Bab1 (C) in p40 antennae (left) and adult antennae (right). (D, E) Expression of Distal antenna (Dan, green) in the antennal disc. Immunostaining for Dan show that it is broadly expressed throughout the antennal disc as has been previously reported. Single slices (E) also show that Dan is not expressed at the same level in all cells. White arrowheads highlight cells that show low Dan expression.

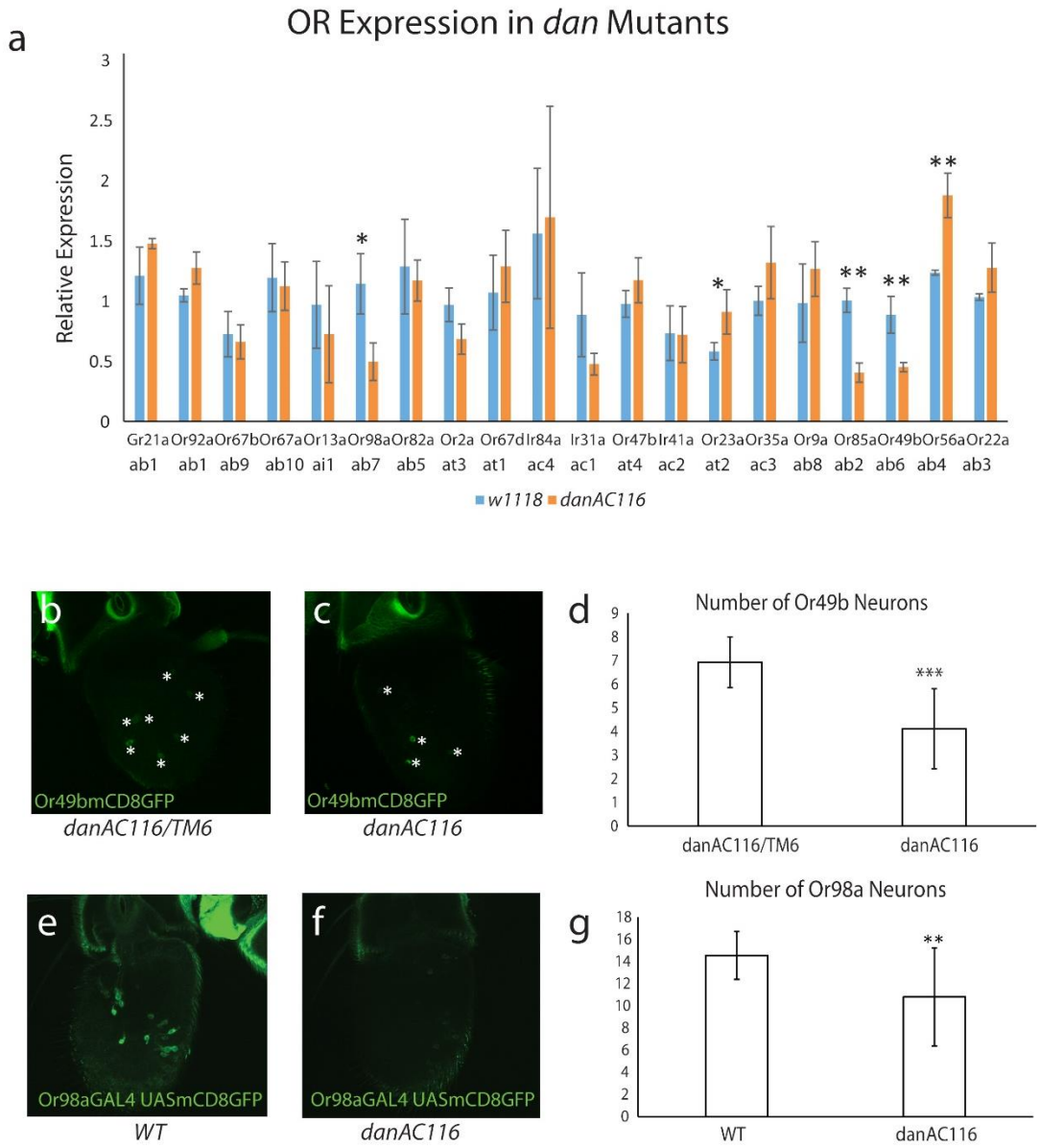

Figure 34: Dan is required for the expression of a subset of ORs. (A) qRT-PCR of OR genes as a readout of ORN populations in antennal samples from wildtype and *dan*^{AC116} mutant flies. Five receptors (Or98a, Or23a, Or49b, Or56a, and Or85a) showed a statistically significant misregulation in *dan* mutants. (B-G) Confirmation of qPCR results for Or49b and Or98a by antennal reporter imaging. An average of seven Or49b neurons were present in heterozygous antennae (B, D) and an average of four were present in mutant antennae (C, D). An average of 15 Or98a neurons were present in wildtype antennae (E, G) and an average of 10 neurons were present in *dan* mutant antennae (F, G). *p < 0.05 **p < 0.01 ***p < 0.001.

3.4 Materials and Methods

3.4.1 Fly Genetics

w1118 flies were used for RNA-seq analysis. OR CD8-GFPs and OR-GAL4s were gifts from Leslie Vosshall and Barry Dickson respectively. *bab1*$^{Pgal4\text{-}2}$ (#6803), *dan*^{AC116} UAS-CD8 GFP and *ap*^{md544} were acquired from Bloomington Stock Center. *NP4099* (*Bar*^{GAL4}) was from Drosophila Genetic Resource Center.

3.4.1.1 Fly Genotypes

Figure 30A, C. *Or47b-Gal4 UAS-CD8GFP*

Figure 30B, D. *Or88a-Gal4 UAS-CD8GFP*

Figure 33A. *w*^{1118}*, NP4099 (Bar*^{GAL4}*)/+; UAS-CD8GFP/+*

Figure 33B. *ap*$^{md544\ Gal4}$*/+; UAS-CD8GFP/+*

Figure 33C. *UAS-CD8GFP/+; bab1*$^{Pgal4\text{-}2}$*/+*

Figure 33D. *w*^{1118}

Figure 34A. *w*^{1118}*, dan*^{AC116}

Figure 34B. *Or49bmCD8GFP/+; dan*^{AC116}*/TM6B*

Figure 34C. *Or49bmCD8GFP/+; dan*^{AC116}

Figure 34D. *Or49bmCD8GFP/+; dan*^{AC116}*/TM6B, Or49bmCD8GFP/+; dan*^{AC116}

Figure 34E. *Or98a-Gal4 UASCD8GFP/+; dan*^{AC116}*/TM6B*

Figure 34F. *Or98a-Gal4 UASCD8GFP/+; dan*^{AC116}

Figure 34G. *Or98a-Gal4 UASCD8GFP/+; dan*^{AC116}*/TM6B, Or98a-Gal4 UASCD8GFP/+; dan*^{AC116}

3.4.2 Immunohistochemistry

Samples were fixed with 4% paraformaldehyde, washed with phosphate buffer with 0.2% Triton X-100, and staining as previously described. rabbit α-Bar-H1 (Tetsuya Kojima) or α-Dan (Minoree Kohwi) was used in a 1:100 and 1:500 concentration, respectively.

3.4.3 RNA-seq

RNAseq was performed as described before (113). Wandering third instar larval antennal discs (~70 for each genotype), 8hr APF pupal antennae (~50 for each genotype), 40hr APF pupal antennae (~50 for each genotype), and adult antennae (150 males and 150 females) from w^{1118} flies were dissected. We extracted RNA only from the antennal portion of the larval eye-antennal discs in order to remove contamination by transcripts from the developing eye. RNA sequencing libraries were prepared with TruSeq Stranded mRNA Sample Prep Kit (Illumina) following the manufacturer's instructions. For the RNA fragmentation step, 94°C, 2min was used with the intention to obtain a median size ~185bp. PCR amplification was done with 15 cycles. A total of 24 multiplexed libraries (barcoded) were accessed for quality and mixed altogether before separating to two identical pooled libraries, which are subject to cluster generation

followed by Illumina 50bp paired-end sequencing by UNC High-Throughput Sequencing Facility (HTSF), as described in Li and Barish et al 2016 (113).

3.4.4 Analysis of RNAseq data

Following Li et al (113). The *Drosophila melanogaster* transcriptome (r5.57) was downloaded from Flybase and bwa indexed was created with bwa-0.7.8. Each sequencing file was aligned to the transcriptome, and .sam files for each sample were generated by putting two alignments from both reads together. At least 80% of the total reads were able to align to the reference sequence. After that, count tables were made for each sample with a customized python script, and further consolidated into a matrix containing transcript ID and read counts from all genotypes for each stage with a Ruby script. These matrices were used as inputs for differential expression analysis using customized DESeq2 R script.

3.4.5 Estimating the Probability That a Gene Is Expressed

With *in situs* and similar tools it is straightforward to determine if a particular OR is expressed in adult. In the larval stages we need to use the RNAseq data to determine which genes are on or off. Negative binomial distributions are commonly used to model gene expression in RNAseq data. For each stage, we parameterized a negative binomial using the raw count data from non-antennal GR. These are expected to not be expressed and thus any "counts" associated with these genes should correspond to experimental noise. We then compared the observed levels of OR

expression to this distribution. *P*-values corresponding to the chance that the observed level of expression could have occurred by chance under this model were then calculated.

3.4.6 PCA Analysis

PCA was preformed using the normalized count tables described above and the princ comp function in R.

3.4.7 Gene ontology analysis

The data files of differential gene expression were processed & filtered with command line tools. Gene Ontology enRIchment anaLysis and visuaLizAtion (GOrilla) analysis (134) on differentially expressed genes (Fig S1). We entered the entire 34,946 reference sequences and 30169 of the genes from this list was recognized. 14,952 duplicate genes were removed (keeping the highest ranked instance of each gene) leaving a total of 15,217 genes. The GOrilla output was saved to a flat file with Excel, then processed with command line tools/a trivial regex Python script. he data was visualized with GOPlot (1.0.2) (135) and R (version 3.3.2). Results were compared topGO (136) and qualitatively similar.

3.4.8 RNA extraction

RNA extractions on *w1118* and dan^{AC116} flies were performed as described in Li and Barish *et al*., 2016 (113).

3.4.9 qRT-PCR

qRT-PCR from antennal RNA samples were performed for OR, GR, and IR genes in wild type and *dan* mutants. The primers used for OR and IR genes have been described in Li and Barish *et al*., 2016 (113).

4. Combinations of DIPs and Dprs control olfactory receptor neuron axon sorting in *Drosophila*

4.1 Summary

Background

The human brain contains over 80 billion neurons that make approximately 100 trillion connections. In *Drosophila*, 50 classes of olfactory receptor neurons (ORNs) connect to 50 class-specific glomeruli in the antennal lobe. Despite identification of cell surface molecules regulating axon guidance, how ORN axons sort to form 50 stereotypical glomeruli remains unclear.

Results

Here we show that the heterophilic binding proteins, DIPs/Dprs, are expressed in ORNs as glomeruli start to form. Each ORN class expresses a unique combination of DIPs/Dprs, with neurons of the same class expressing ligand-receptor pairs. Mathematical analysis of DIP/Dpr expression sorts clusters of ORN classes, which mimics their glomerular positioning in the antennal lobe, suggesting a role in ORN axon sorting. Perturbations of *DIP*/*dpr* gene function result in invasion of neighboring glomeruli.

Conclusions

Our results suggest that context-dependent adhesion through Dpr/DIP combinations sort ORN axons into different glomeruli. Mammalian orthologues of

DIPs/Dprs include Kirrel2/3, which sort mammalian ORN axons into separate glomeruli, suggesting convergent mechanisms of glomerular formation in mammals and flies.

4.2 Results

To identify candidate genes that may be involved in the establishment of 50 class specific glomeruli, we analyzed our previously reported antennal transcriptome data from four critical stages of development: 3rd instar larval antennal discs (3L), 8 hrs after puparium formation (APF) antennal discs (p8), 40 hrs APF antennae (p40) and adult antennae (Adult) (113,137). Axon guidance, glomerular sorting, and ORN-PN matching are inherently temporal processes that occur in a specific developmental order (Barish & Volkan 2015). We therefore mined this dataset to identify novel regulators of wiring specificity of ORNs, whose expression overlapped with the timing of glomerular formation. We queried approximately 250 Flybase annotated cell surface molecules (CSMs) and analyzed their developmental expression patterns using hierarchical clustering to group genes based upon their developmental expression patterns (Figure 35A, Table 17). We found 8 clusters of CSMs with distinct expression patterns (Figure 1A, B). Two broad patterns emerged from this analysis, genes that are expressed at constant levels throughout (Clusters 3, 5, 6, and 8, Figure 35A, B), such as *sema-1a/b* and *dscam1*, and genes that are weakly expressed early in development and increase in later stages (Cluster 1 and 2, Figure 35A, B), such as *robo3* (Table 16). Cluster 7 contained many genes that were highly expressed at the first three stages of development but

decreased at the adult stage, and Cluster 4 contained genes whose expression peaked at 40 hrs APF (p40). Known regulators of ORN wiring grouped into Clusters 7 and 8 as well as Cluster 1, meaning that they were expressed highly throughout development or lowly expressed early and increased their expression at the later stages (Figure 35A-C) consistent with their roles in ORN axon guidance, which begins very early in olfactory system development.

4.2.1 DIP and Dprs are expressed in late stages of ORN wiring

Even though most ORN axons arrive at the antennal lobe by 30 hours APF, the timing of OR gene expression and glomerular formation overlap and start around 40 hours APF (19,137). However, only a subset of ORs are expressed at 40 hrs APF, like Or47b (137). This suggests that the molecular and cellular events that sort ORN axons and connect them to appropriate PNs to form glomeruli occur at later pupal stages. We therefore hypothesized that genes that were highly expressed at the two later stages of development (p40 and Adult) but lowly expressed at the two early stages (3L and p8) were more likely to be involved in class-specific glomerular formation. Our analysis of CSM expression profiles showed that the majority of Dpr family of CSM proteins and their binding partner DIP proteins were expressed at p40 and in adult antennae, but showed low or no expression during earlier stages of antennal development (Figure 35D, E). These results pointed to a possible role for DIP/Dpr family members in glomerular formation.

4.2.2 DIPs and Dprs are expressed in a combinatorial code in ORNs

Dprs and their binding partners DIPs are members of the Ig superfamily of proteins and each contain 2-3 Ig extracellular domains (139). Members of the Ig superfamily of proteins, such as Dscam, and Kirrels, are well established to control axon guidance and sorting in other systems (70,140). DIPs and Dprs themselves have recently been shown to direct synaptic target matching in the *Drosophila* eye (139,141). In addition, the relatively large number of *dpr* and *DIP* genes (20 and 9 respectively) make them good candidates to contribute to a combinatorial code of CSMs that direct wiring specificity for each class of ORNs.

Although our RNA-seq data establish temporal patterns of *DIP* and *dpr* expression in the developing olfactory system, it does not inform us of the ORN class-specific expression of each *DIP* and *dpr* gene. To investigate which ORN classes express each *DIP* and *dpr*, we used MIMIC insertion-derived GAL4 lines to drive UAS-SynaptotagminGFP (sytGFP), which localizes to presynaptic terminals in the antennal lobes belonging to ORNs, and local interneurons, but not to PNs (139,141,142). Because it is known which ORN classes synapse at each glomerulus, we were able to map the expression of each *DIP* and *dpr* gene to a particular set of ORN classes, based on sytGFP expression in the antennal lobe (Figure 36, Figure 37A-L). These analyses showed that each ORN class has a unique *DIP* and *dpr* expression profile (Figure 39A). Some *DIPs* and *dprs* are expressed very broadly across ORN classes (*DIP-η*, Figure 36H), and others

are expressed in fewer ORN classes (*DIP-β, DIP-γ*, Figure 36E, F). These results suggest that the unique combination of DIPs and Dprs in each ORN class might direct ORN class specific glomerular formation.

Next, we analyzed expression of *DIPs* and *dprs* in the antenna to confirm the expression patterns we observed in the antennal lobe corresponded to expression in ORN cell bodies. To do this we used *DIP* and *dpr-GAL4*s to drive the expression of *UAS-CD8GFP* (Figure 37M-W). Consistent with our RNA-seq analysis, most of the genes we analyzed showed expression in ORNs consistent with glomerular expression patterns (Figure 37M-W). A small number of genes did not show expression in the antenna (Figure 37M-W), which suggests that they are instead expressed in local interneurons. We conclude that the majority of *DIPs* and *dprs* are robustly expressed in ORNs but a few are expressed in local interneurons.

Previous studies have shown that the expression of Dprs in photoreceptor cells and their interacting DIPs in the target lamina neurons contribute to synaptic partner matching in the *Drosophila* visual system. In order to ask whether DIPs/Dprs play a similar role in synaptic partner matching between ORNs and their target PNs we next analyzed the expression patterns of each *DIP* and *dpr* in PNs (Figure 38). We drove *UAS-DenMark-RFP* using *DIP* and *dpr-GAL4s*, which specifically labels postsynaptic dendrites (143), thereby labeling PNs in the antennal lobe. Similar to ORNs and in agreement with recent single cell RNAseq studies, some of the genes were

expressed in specific subsets of PNs (*DIP-η* and *DIP-γ,* Figure 38), while others were expressed much more broadly (*dpr10*, Figure 38) (144). Several however, were not expressed in PNs at all (*dpr12*, Figure 38). Unlike in previous reports, we did not observe any obvious pattern of DIPs and Dprs indicative of pre- and post-synaptic target matching between ORNs and their corresponding PNs. Taken together, our expression data suggest that DIP and Dprs may be involved in ORN-ORN axon interactions.

4.2.3 Mathematical analysis based on DIP/Dpr profiles of ORNs mimic their relative glomerular positioning

Analysis of DIP/Dpr patterns in each ORN class, showed that interacting DIP-Dpr pairs are expressed in the same ORN classes (Figure 39A-C). DIPs and Dprs heterophilically interact in a combinatorial code that has been previously described (Figure 39B) (141). We also found some ORN classes additionally express Dpr ligands without their DIP receptors, which might regulate interactions with DIP receptors on neighboring ORN axons during development (Figure 39A-C, see discussion). In order to determine which ORN classes are most similar based upon their DIP/Dpr gene signatures from the GAL4 expression patterns, we applied hierarchical biclustering to the data (Figure 39A). This analysis clustered specific classes of ORNs together (Figure 39A). For example, Or47b and Or88a ORNs clustered together and have some of the least complex DIP/Dpr profiles together compared to others, such as Or67d, that are more complex (Figure 39A).

Given our results, we predicted that the final regulation of axon sorting, glomerular formation and positioning would be dictated by the unique class-specific DIP/Dpr expression profile of each class of neurons. In order to test whether the unique class-specific DIP/Dpr relationships among ORN classes can describe their relative glomerular positions in the antennal lobe, we performed multidimensional scaling (MDS) on the expression pattern data set (Figure 40A). We used the expression of *DIP* and *dpr* genes in each ORN class as the input variables. The genes and gene combinations defining each ORN class were used to create a matrix of "distances" between ORN classes. We predicted that this statistical analysis would group similar combinations of DIP/Dpr profiles for each ORN class, and sort them to distinct coordinates with respect to one another. Once the MDS results were plotted, we used K-means clustering to determine clustered ORN classes, and color coded them based on this analysis on the MDS plot (Figure 40B). We next color coded antennal lobe glomeruli based upon the clusters derived from the k-means analysis (Figure 40C). Plotting ORN classes using this method revealed many clusters, such as Or23a, Or65abc, Or47a, Or69a, and Or49a ORN classes, which target neighboring glomeruli in the antennal lobe (Figure 40B, C). Interestingly, ORN classes that reside in the same sensillum or belong to the same morphological sensilla class did not cluster together (data not shown). Even though there are significant overlaps between the ORN clusters in the MDS plot and the positioning of glomeruli in the antennal lobes, they are not identical. Further refinement

will require analysis of the entire CSM profiles of ORN classes, their modes of interaction, and function. Regardless, our analysis highlights relative relationships among particular classes of ORNs based upon their *DIP*/*dpr* expression profiles, and supports the hypothesis that DIPs/Dprs regulate class-specific sorting of ORN axons into distinctly positioned glomeruli.

4.2.4 Combinatorial and ORN-specific roles of DIPs and Dprs in class-specific sorting of ORN axons

Based on the class-specific expression patterns of *DIPs* and *dprs*, we suspected that knocking down individual genes would cause disruptions to class-specific sorting of ORN axons and glomerular formation. To investigate whether DIPs and Dprs are required for the wiring of ORN axons we initially drove RNAi against a panel of DIPs and Dprs individually using the *peb-GAL4*, which is expressed in all ORNs, and analyzed Or47a, Or47b, and Gr21a axon terminals in the antennal lobe. These experiments did not reveal any significant changes in wiring patterns (Figure 41). We predicted that this is likely due to the combinatorial and redundant function of the DIP/Dpr proteins expressed in specific ORNs or their glomerular neighbors.

To simplify our analysis and better understand the combinatorial function of DIPs and Dprs we chose to focus our experiments on a group of five neighboring glomeruli, VA1v (Or47b), VA1d (Or88a), VL2a (Ir84a), DC3 (Or83c) and DC1 (Or19a/b). We initially focused on these neighboring glomeruli because DIPs and Dprs are membrane bound molecules with short range heterophilic and adhesive interactions

(139,141). Among these five classes, Or47b and Or88a ORNs have the least complex DIP/Dpr profiles that also clustered in the MDS plots, and only differ in a small number of Dprs (Figures 39C, 40B, C). Thus, we reasoned that sorting of these two glomeruli may be particularly sensitive to genetic manipulation. For example, Or47b ORNs are positive for *DIP-η*, *DIP-θ*, *dpr2*, *dpr3*, and *dpr12*, whereas Or88a ORNs express all of the same genes plus *dpr8* and *dpr10* (Figure 39A, C). Ir84a, Or83c, and Or19a/b ORNs are more similar to one another, yet have slightly more complex combinations compared to Or47b and Or88a: Ir84a ORNs express *DIP-η*, *DIP-θ*, *DIP-δ*, *dpr2*, *dpr8*, *dpr9*, *dpr10*, *dpr11*, and *dpr12*; Or83c neurons express *DIP-η*, *DIP-θ*, *DIP-β*, *DIP-γ*, *DIP-δ*, *DIP-ε*, *dpr2*, *dpr8*, *dpr9*, *dpr10*, *dpr11*, and *dpr12* and Or19a/b neurons express *DIP-η*, *DIP-θ*, *DIP-δ*, *dpr2*, *dpr5*, *dpr8*, *dpr9*, *dpr10*, *dpr11*, and *dpr12* (Figure 39A, C). This code differentiates each class of ORN axons from each other and provides candidate genes to manipulate singly or in combination to investigate the role of DIPs and Dprs in controlling ORN axon wiring.

We hypothesized that manipulating the DIP/Dpr code in these ORN classes would cause local wiring defects such as invasion of neighboring glomeruli within this cluster. To test this hypothesis, we drove RNAi against single or combinations of DIPs and Dprs either in all ORNs or in specific classes. Because *DIP-η* is expressed in all five of these glomeruli and we did not observe any defects when *DIP-η* was knocked down in all ORNs (Figure 41D), we began by knocking down *DIP-η* in Or47b neurons using

the *Or47b-GAL4*. In this scenario, of the five glomeruli on which we chose to focus, only Or47b neurons will lack DIP-η, while the four other classes will retain expression of *DIP-η*. We expected that manipulation of DIPs/Dprs in the Or47b ORNs should cause axons to invade the Or88a ORN target glomerulus VA1d because these two glomeruli clustered together in our MDS analysis (Figure 40B, C). We found that knockdown of *DIP-η* specifically disrupted the wiring of Or47b ORNs to its target VA1v glomerulus causing it to dramatically expand (Figure 42A, B). This phenotype was extremely penetrant, with 85% of individuals displaying expansion of the VA1v in one or both antennal lobes, (n=12) but wildtype individuals never displayed any invasions (n=10, Figure 42C). We observed that the expansion of the Or47b glomerulus was not random, and always appeared to overtake the VA1d glomerulus, which is the immediate, dorsal neighbor to the VA1v glomerulus (25). Double labeling of Or47b and Or88a axons revealed that Or47b axons indeed invade the VA1d glomerulus, but this does not disrupt the ability of Or88a axons to converge into a glomerulus (Figure 42D-I). Instead, the Or88a axons occupy one part of the now enlarged VA1v glomerulus (Figure 42G-J). Or88a specific *DIP-η* knock down, however, did not cause any noticeable phenotypes (Figure 42K, L).

The invasion of the VA1d glomerulus by Or47b ORN axons could occur due to conversion of Or88a neurons to Or47b neurons, as was previously observed in *alhambra* mutants (114). To test this hypothesis, we labeled Or47b neuron cell bodies with RFP

(Figure 42M, N). Comparison of Or47b ORN numbers in the antennae showed no significant difference between wildtype (56.7) and *DIP-η* knock down antennae (57.8, p=0.64, Figure 42O), suggesting that the expansion of VA1v glomerulus in *DIP-η* knock down flies is not due to an increase in neurons with Or47b ORN identity. We therefore conclude that DIP-η is required cell-autonomously, after the onset of olfactory receptor expression, to segregate Or47b ORN axons from Or88a ORN axons to form two distinct glomeruli.

Lack of wiring defects in single *DIP*/*dpr* knock downs might be due to the combinatorial and functionally redundant nature of DIP/Dpr family members. One approach to circumvent this problem is to knockdown *DIPs* and *dprs* in different combinations. To investigate this, we next analyzed double knockdown of *DIP-η* and *DIP-δ*. Knock down of *DIP-η* alone produces no observable defects when driven in all ORNs (Figure 41B, C). *DIP-δ* is not expressed in Or47b or Or88a ORNs, but is expressed in Or19a/b, Ir84a, and Or83c ORNs which innervate neighboring glomeruli. In addition, the DIP-δ ligand Dpr12 is expressed in all ORNs. No RNAi line currently exists for DIP-δ, so we instead used the deGradFP system to eliminate GFP tagged DIP-δ protein in ORNs. The deGradFP construct can be driven using the GAL4-UAS system and specifically targets GFP tagged proteins for degradation by the proteasome (145). We combined the *peb-GAL4* mediated RNAi knockdown of *DIP-η* expression with *UAS-deGradFP* expression to reduce DIP-δ protein levels in all ORNs. Analysis of Or47b,

Or47a, and Gr21a axon terminals using promoter fusion constructs showed very specific and localized defects in the VA1v glomerulus (Figure 43A, B). Most noticeably, Or47b ORN axon terminals extended radially towards the DC1/3 and VL2a glomeruli, targeted by Or19a/Or83c and Ir84a ORNs, respectively, splitting the glomerulus in two (Figure 43B). 50% of individuals displayed defects in one or both antennal lobes (n=10, Figure 43D). In this circumstance, disruption of intra-class attraction among Or47b ORN axons, and Ir84a, Or83c, and Or19a/b ORN axons due to loss of *DIP-η* and *DIP-δ*, respectively, is accompanied by the decrease in the complexity of DIP/Dpr code. This likely causes both classes of axons to become attracted to each other, and splits the VA1v glomerulus. We therefore conclude that DIP-η and DIP-δ are required for the sorting of Or47b axons in a combinatorial, context-dependent, and non-cell autonomous fashion.

4.2.5 Overexpression of DIP proteins causes local axon sorting defects

So far, we have shown that DIPs and Dprs help sort Or47b, Or88a, Or83c, Ir84a, and Or19a/b ORN axon terminals into 5 glomerular units in combinatorial, and context-dependent fashion. Because loss of DIPs/Dprs can lead to sorting defects, we hypothesized that addition of new factors to the code would also disrupt the wiring of these glomeruli. In particular, we expected that overexpression should cause ORN axons from different classes to converge because their code of expression has become more similar or compatible. To test this hypothesis, we overexpressed DIP-γ and DIP-δ with *OR-GAL4* drivers (Figure 44A-C).

When DIP-δ is overexpressed only in Or47b neurons, the VA1v glomerulus became deformed (Figure 44B). We observed a large group of axons closer to the VL2a glomerulus than normal, with a smaller but connected group on the opposite side of the VA1d glomerulus near the DC3 glomerulus (Figure 44B). 80% of individuals had a disrupted VA1v glomerulus in one or both antennal lobes (n=14, Figure 45A). Both Or83c and Ir84a ORNs express DIP-δ, but Or88a ORNs do not (Figure 39C). Therefore, Or47b ORN axons must have become more similar to Or83c and Ir84a axons in this condition, and appear to be attracted towards these glomeruli thereby disrupting the wildtype glomerular position and morphology (Figure 44K). Similar to knock down of *DIP-η*, overexpression of DIP-γ caused Or47b ORN axons to invade the VA1d glomerulus, although this invasion was partial (Figure 44C) seen only in 50% of individuals (n=8, Figure 45B). This result was unexpected because only Or83c ORNs in this cluster express *DIP-γ*. We therefore expected Or47b ORN axons to invade the DC3 glomerulus, not VA1d. DIP-γ appears to be expressed in very few or no ORNs (Figure 37T), which suggests that the expression we observed in the antennal lobe could come from interneurons as opposed to ORNs. DIP-γ binding partners in interneurons or projection neurons may contribute to segregation of the VA1v and VA1d glomeruli. These results suggest that alteration of DIP/Dpr profiles via addition of new factors disrupts normal sorting of ORN axons and glomerular formation.

When we drove expression of DIP-δ and DIP-γ in all ORNs with the *peb-GAL4* we did not observe any changes in the wiring patterns in the antennal lobe (Figure 44D-F). This was similar to what we observed with knock down of single *DIP* and *dpr* genes using *peb-GAL4*. This leads us to conclude that context-dependent DIP/Dpr interactions regulate ORN axon sorting.

4.2.6 Overexpression of Dpr1 causes non-cell autonomous splitting of ORN axons of the same class

Unlike DIP-γ and DIP-δ, Dpr1 is not expressed in the olfactory system in either ORNs or projection neurons (Figure 36A, 38A). Dpr1 interacts with DIP-η and DIP-θ (139,141), both of which are expressed in all or nearly all ORN classes, respectively (Figure 36H, 37L). We therefore predicted that expressing Dpr1 in particular classes of ORNs should disrupt axon sorting through interactions with neighboring axons that express DIP-η or DIP-θ. Using *OR-GAL4* drivers, we overexpressed Dpr1 in four classes of ORNs (Or47a, Or47b, Gr21a, and Or23a, Figure 44G, H). We did not observe any change in the wiring patterns of either Or47a or Or23a ORN axons. In contrast, both the V and VA1v glomeruli, targeted by Gr21a and Or47b ORNs, respectively, exhibited splitting phenotypes (Figure 44H, 45G, H). 20% of individuals showed a split V glomerulus, and ectopic innervation of Gr21a ORN axons to a dorsal glomerulus into the antennal lobe (n=10, Figure 45E). The Gr21a ORN class is notably the only class of ORNs that does not express *DIP-η* (Figure 36H). It is possible that these mistargeting axons are attracted to neighboring axons that do express *DIP-η* and therefore move dorsally

towards them in the presence of Dpr1. The low penetrance and severity of the phenotype may be explained by the timing of expression of the *Gr21a-GAL4* driver. *Gr21a* expression begins relatively late in development as compared with other ORs and therefore only a few axons may express Dpr1 early enough to be affected.

Overexpression of Dpr1 in Or47b ORNs also produced a similar but more dramatic phenotype (Figure 44H). Or47b ORNs express both *DIP-η* and *DIP-θ* (Figure 39C). We observed a splitting of the VA1v glomerulus, where some of the split Or47b ORN axons moved radially to form a second glomerulus on the other side of the VA1d glomerulus (Figure 44H, K). This phenotype was observed in 40% of individuals (n=10, Figure 45C). These data suggest that the introduction of Dpr1 interferes with axon-axon interactions among ORNs that express its receptors. Surprisingly, when we drove overexpression of Dpr1 with only the *Or47b-GAL4,* the phenotype was largely suppressed (Figure 44I, J). Similarly, expression of Dpr1 in Or88a ORNs did not result in any wiring defects (Figure 44L, M). These data suggest that the effects of Dpr1 overexpression on Or47b ORN wiring is not due to a cell autonomous function. This phenotype is dependent on the cell non-autonomous influence from surrounding axons also expressing *dpr1*, which may interact with the receptors DIP-η and/or DIP-θ on Or47b ORN axons.

Because the expression of Dpr1 in multiple classes of ORNs enhanced VA1v glomerular splitting, we used the *peb-GAL4* driver to express Dpr1 in all ORNs to

determine if further defects would arise. When we visualized Or47b, Or47a, and Gr21a ORN axons, we again observed that the VA1v glomerulus split, consistent with our previous conclusion that over expression of *dpr1* in multiple classes of ORNs amplifies the Or47b ORN wiring phenotype (Figure 44N-Q, 45C). 75% of individuals displayed a splitting of the VA1v glomerulus (n=8, Figure 45C). We also found a small and reproducible cluster of axon terminals in between the DA1 and VA1d glomeruli (Figure 44N, O). Labeling each ORN class individually revealed that this cluster was derived from Or47a ORN axons and was present in 50% of individuals (n=14, Figure 44R, S, 45D). These axons may mistarget along Or47a ORN axon tracks to their target DM3 glomerulus due to attraction to other ORN axons that now express Dpr1. These data suggest that DIP-Dpr interactions mediate ORN axon-axon adhesion.

4.2.7 Dpr10 controls glomerular targeting

So far, we have shown that DIPs and Dprs act primarily as adhesive molecules that regulate local ORN axon sorting. We suspected that DIPs and Dprs may regulate other aspects of ORN wiring, such as ORN-PN matching or targeting. We began with Dpr10 because it is expressed broadly in the antennal lobe, but labels the V glomerulus (Gr21a/Gr63a) most strongly, and is absent from the VA1v glomerulus (Or47b). We therefore tested whether Dpr10 controls the wiring of these two classes of ORNs as well as three other classes of ORNs that are weakly labeled by *dpr10* (Or47a, Or10a, and Or88a ORNs). We used the $dpr10^{MI03557}$ allele which contains a MIMIC insertion,

containing three premature stop codons, to analyze the loss of Dpr10 protein (142). *dpr10*^{MI03557} homozygous flies die prior to eclosion, around 90hrs APF. We therefore dissected both mutant and wildtype flies at 80-90hrs APF when the antennal lobe is fully formed but prior to the death of *dpr10* mutant flies. In homozygous mutant flies, both the DM3 (Or47a) and V glomeruli were dramatically disrupted (Figure 46A-D). These defects were associated with expansion of non-converged glomeruli to neighboring glomeruli, and defects in axon guidance to ectopic sites within the antennal lobe (Figure 46A-D, 47C, D). Specifically, we observed three phenotypes for Or47a ORN axons: splitting of the DM3 glomerulus, mistargeting of a subset of Or47a ORN axons, and mistargeting to ventromedial zones in the antennal lobe (Figure 46B, 47D). Or47a ORN mistargeting phenotypes were very penetrant with >70% (n=11) of individuals showing a split or mistargeting event in one or both antennal lobes (Figure 47C). The most common phenotype observed for Gr21a ORN axons (~39%, n=18) was a dorsal expansion of the V glomerulus (Figure 46D, 47C). In addition, we observed aberrant axons, as well as a complete splitting of the V glomerulus in a few rare cases (Figure 47C). We also analyzed Or10a axons, which are housed in the same sensillum as Gr21a neurons and target the DL1 glomerulus. Like Or47a axons, the Or10a glomerulus also exhibited splitting and dramatic mistargeting, with the most severe cases targeting to ventral positions on the opposite side of the antennal lobe (Figure 46L, M, 47E). Several individuals displayed Or10a axons that could not form a glomerulus at all, instead, the

axons formed a fascicle in between other glomeruli, mistargeting as well as losing their ability to converge (Figure 46M, 47E). These data suggest that Dpr10 not only regulates sorting of ORN axons, but also axon guidance of many ORN classes in the antennal lobe.

None of the major wiring phenotypes found in Gr21a, Or47a and, Or10a ORN classes were present in the Or47b ORNs. Rather the VA1v glomerulus showed only minor disruptions of its normal shape and position (Figure 46E, F), which likely results from secondary effects of the general disorganization of the antennal lobe glomeruli in *dpr10* mutants. To confirm this hypothesis, we visualized Or88a ORN axons in *dpr10* mutants because they express *dpr10*, and their target VA1d glomerulus is one of the closest to the VA1v glomerulus targeted by Or47b ORNs (Figure 39C, 46N, O). The stereotypical morphology of the Or88a glomerulus was disrupted in *dpr10* mutants (Figure 46O). We therefore conclude that Dpr10 is required for the proper wiring of Or47a, Gr21a, Or10a, and Or88a axons but not Or47b axons.

Changes in the number of ORNs of a given class tends to change the size of that glomerulus (42). Thus we next wanted to confirm that the wiring phenotypes of Or47a and Gr21a ORNs were not due to a change in the number of ORNs in either class (42,113,114). We visualized Gr21a and Or47a ORNs in the antenna using *UAS-mCD8GFP* reporters in wildtype and *dpr10* mutants (Figure 46G-J). We observed a statistically significant reduction in the number Or47a neurons in *dpr10* mutants (14.4 vs 6.8, $p<0.001$, Figure 46G, H, K). This reduction may explain the reduced size of the DM3

glomerulus we observed in the antennal lobe, but is insufficient to explain the splitting and mistargeting events. A slight reduction of Gr21a neurons was detected (30.8 vs 26.1) although it was not statistically significant ($p>0.05$, Figure 46I-K). Given that we observed an expansion of the Gr21a glomerulus, any reduction in the number of Gr21a neurons likely does not cause the phenotypes observed in the antennal lobe. These data suggest that *dpr10* mutation may partially affect the generation or survival of ORNs, in addition to its role in wiring of ORN axons.

We next wanted to determine whether *dpr10* is required specifically in ORNs. We first drove *dpr10 RNAi* using the *peb-GAL4*. We did not observe any wiring defects in this condition (Figure 41J). We next drove *dpr10 RNAi* in Or47a, Or47b, and Gr21a neurons using *OR-GAL4s*. As expected, the wiring of Or47b axons remained unchanged in the *dpr10* knockdown flies (Figure 47A, B). Or47a axons also did not exhibit any significant phenotypes (Figure 46P, Q). The Gr21a glomerulus did show some partial expansion, though not nearly as dramatic as in the genetic mutants and with a very low penetrance (~20% of individuals, Figure 46R, S). We have previously reported that the onset of OR expression is variable between ORN classes, and while Or47b is one of the earliest ORs to be expressed, Or47a and Gr21a turn on later, possibly after the function of Dpr10 is required (137). Differences in the expressivity and penetrance of the wiring defects in whole animal *dpr10* mutants versus ORN specific RNAi knockdowns suggests

the possible role of DIP/Dprs in components of the circuitry, other than ORNs, such as interneurons, and projection neurons.

4.3 Discussion

Despite advances in our understanding of neuronal wiring, how the diverse nervous system establishes repeatable and specific wiring patterns from a limited genetic repertoire of cell surface molecules remains poorly understood. In the *Drosophila* olfactory system, 50 classes of ORNs, on the antennae and maxillary palps, project their axons into the antennal lobe of the brain where they connect to their partner projection neurons in 50 class-specific glomeruli (18,24,25). Here we show that the Dpr family of Ig-domain transmembrane proteins and their heterophilic binding partners DIPs are expressed in subsets of ORN classes, creating a combinatorial code such that each ORN class is defined by a unique combination of DIPs and Dprs. Mathematical analysis of ORN classes based upon DIP/Dpr expression patterns uncovers clusters of ORN classes, which mimic the positional clustering of their target glomeruli, suggesting that DIP/Dpr expression patterns correlate with glomerular positioning. DIP/Dpr combinations are necessary for proper local sorting among ORN axon terminals in the antennal lobe, as loss of a single gene in a specific ORN class, or multiple genes in all ORNs, causes local invasions of neighboring glomeruli. Mis-expression of *DIPs* or *dprs* causes similar phenotypes, disrupting normal axon-axon interactions. Some Dprs, Dpr10 specifically, also control additional processes during wiring, such as correct guidance of ORNs to

appropriate glomerular regions, as seen in *dpr10* mutants. Together, our data reveals that DIPs and Dprs are critical players in sorting and formation of 50 ORN class-specific glomeruli.

Although this study provides a significant advance in understanding how a system is able to segregate axon terminals for 50 ORN classes into independent glomeruli, it is incomplete. First and foremost, we do not have expression data for several other DIP and Dpr family members (Dprs 4, 7, 14, 17, 18, 19, 20, 21, and DIP-α and DIP-ι). Second, we focused our analysis on five glomeruli targeted by Or47b, Or88a, Or83c, Ir84a, and Or19a ORNs, showing only a few examples of manipulations in other ORN classes. More sophisticated systems level genetic analyses of all DIP and Dpr manipulations, in addition to identification of CSM expression profiles in each ORN class and its target projection neuron will help refine our model, in the future.

4.3.1 Local Axon Sorting

One key feature of ORN wiring is the sorting of approximately 1500 ORN axon terminals into 50, uniquely positioned, and ORN class-specific glomerular units in the antennal lobe (18,24). One way to achieve this organization is through axon-axon interactions among ORNs. This type of interaction among ORN axons during development can utilize a logic that attracts ORN axons and terminals of the same class, simultaneously sorting from the axon terminals of other ORN classes, which themselves must self-adhere. The molecular mechanisms driving these different processes during

glomerular formation are not known. Examples of homophilic cell adhesion proteins, such as N-Cadherin, were previously shown to regulate glomerular formation by interfering with axon-axon interactions among the same class of ORNs (71,72). The effect of *Ncad* mutants however, are seen in all glomeruli, which does not explain selective adhesion that occurs among each class (71,72). Sema-1a signaling also contributes to repulsion of neighboring ORN axons of different classes, but again, effects are relatively general, causing sorting defect of many ORN classes (73). Here we show that both knock down and mis-expression of DIPs and Dprs produced reproducible and ORN-class specific wiring defects associated with local invasions of neighboring glomeruli. Given the previously reported adhesive function of DIP/Dpr interactions this then suggests that differential adhesion that emerges from ORN- specific DIP/Dpr profiles is a mechanism of class-specific sorting of ORN axon terminals.

Our results suggest that loss or addition of DIPs or Dprs generally do not cause random mistargeting events like those observed in *robo* and *dscam* mutants (68,69), but rather act locally in a class-specific manner during the last stages of glomerular targeting. In many instances, phenotypes can be generated by knocking down or overexpressing *DIP* and *dpr* genes using *OR-GAL4* drivers, after the onset of olfactory receptor expression. This result is interesting for how we view ORN wiring. For many years, the consensus has been that olfactory receptor genes are turned on after glomerular formation is complete. Our results suggest that, at least for olfactory

receptors that are turned on early in development, wiring is not complete. The finding that class-specific knockdown and overexpression experiments using *Or47b-GAL4* drivers in many instances and for many *DIP* genes leads to dramatic defects in the target VA1v glomerulus, indicates ongoing wiring decisions that require DIPs and Dprs after the onset of expression of *Or47b*.

When a specific *DIP*/*dpr* gene, or gene combination, is lost or ectopically expressed in ORNs, axons invade the glomerulus targeted by a class of ORNs with the most compatible DIP/Dpr code, or/and which also now has new adhesive properties due to the genetic state. This role is akin to Dscam, a fellow Ig superfamily protein, famously involved in controlling dendritic self-avoidance, where combinatorial expression of Dscam isoforms regulates recognition of self vs non-self-processes to produce distinct dendritic zones for each neuron (70). In the case of DIPs and Dprs in the olfactory system, combinatorial expression of DIP/Dprs regulates sorting of ORN axon terminals that belong to the same class (self) from axon terminals of other ORN classes (non-self) which target neighboring glomeruli in the antennal lobe.

4.3.2 Adhesive DIP-Dpr Interactions

The sorting defects observed in this study could, in theory, arise due to either defects in intra-class attraction or inter-class repulsion. Taken together, our data argue for a third option that merges the two, where differential adhesive interactions among axons sort out glomeruli of different classes. In many cases ligand-receptor DIP-Dpr

pairs are expressed in the same ORN class. Yet, some ORN classes, especially ones with more complex combinatorial codes, additionally express only specific Dpr ligands, without their DIP receptors. In these cases, we find the receptors can rather be expressed in ORN classes that target neighboring glomeruli. It is therefore possible that axon-axon interactions during development can help position axons from different ORN classes based on its DIP/Dpr profile. Indeed, our results with Dpr1 overexpression supports these early developmental interactions. When expressed in only Or47b neurons, Dpr1 does not produce any significant changes to the VA1v glomerulus. Yet when it is expressed either in three other ORN classes or all ORNs, the VA1v glomerulus splits dramatically. This suggests that the Dpr1 in either Or47b neurons, or other ORN classes is able to interact with the Dpr1 receptors, DIP-η and DIP-θ, during development, to generate forces that pull out Or47b axons to form two distinct glomeruli. Such interactions are consistent with previously reported roles for DIPs and Dprs in the *Drosophila* eye, where they control layer specific matching of photoreceptor cells with their targets in the medulla (139). Mutations in *DIPs* and *dprs* cause photoreceptors to overshoot their targets because they lack adhesion with their postsynaptic partners (139). A model of differential adhesion could provide an efficient solution to the separation of 50 class-specific glomeruli, where at each stage of wiring, axons interact with their neighbors based on their DIP/Dpr profiles with the highest adhesion occurring among the axons of the same ORN class, and perhaps determine the relative

glomerular position of other ORN classes nearby. Superimposed onto other earlier regulators of wiring, such as Semaphorin-1a and N-Cadherin, glomeruli can be sorted out from one another in a repeatable fashion (71,73).

4.3.3 Regulation of DIP/Dpr Expression

How do the class specific patterns of DIP/Dpr expression arise? It seems likely that similar mechanisms that lead to the singular expression of a particular olfactory receptor in each neuron would also control the expression of DIPs and Dprs. There are three major modes of regulation of OR selection: 1-prepatterning of the antennal disc by transcription factor networks that determine sensilla precursor identity, 2-regulation of neuronal fates by Notch-Delta signaling during asymmetric precursor cell divisions, and 3-terminal selector transcription factors regulating olfactory receptor gene expression and possibly other ORN identifiers (8,52,113). Each mode of regulation clearly controls ORN wiring as prepatterning network mutants change ORN connectivity to converted fates (42,113), Notch pathway mutants behave similarly (8,46), and factors like Pdm3 regulate glomerular shape as well OR expression (54). It is likely that each mode of regulation, layered on top of each other, work in concert to control DIP/Dpr expression. Indeed, none of the ORN classes clustered based on its Notch state or sensilla subtype identity in our MDS analysis (data not shown). This suggests class-specific differences in their DIP/Dpr profiles are generated during precursor divisions by the developmental programs mediating terminal differentiation of each ORN class. This would predict an

increase in the DIP/Dpr code for each ORN class, as ORN fates are diversified from precursors during development. There might be some DIP/Dprs, like *DIP-η* and *dpr12*, that are expressed earlier and more abundantly in all future ORNs, perhaps starting at precursor stages to coarsely sort early axons. Some DIPs/Dprs are indeed expressed in our RNA-seq analysis at 8 hrs APF although at much lower levels when compared to 40 hrs APF and adult antennae. DIP/Dprs expressed in only a few classes of ORNs, might be superimposed onto existing DIP/Dpr profiles in later stages of development, as individual ORN identities are defined by the onset of OR expression. Deeper understanding of exactly which transcription factors control DIP/Dpr expression and how they relate to larger programs of neuronal specification is needed.

4.3.4 Convergent molecular logic for glomerular organization

The mammalian olfactory bulb is organizationally very similar to the *Drosophila* antennal lobe. In both organisms, the ORNs that express the same receptor converge their axons onto a single class-specific glomerulus (18,146). Mammalian olfactory receptors are G-protein coupled receptors and differentially regulate the expression of adhesive and repulsive CSMs to position and sort ORN-specific glomeruli using both ligand-dependent and -independent signaling (64,140). Differential, ligand-independent cAMP signaling from each mammalian olfactory receptor gene regulates graded expression of Semaphorin and Neuropilin in different ORN classes, and controls the positioning of each glomerulus (64,140). In addition, olfactory receptor neuron activity

refines glomerular convergence through differential expression of homophilic adhesion Ig-domain proteins Kirrel2/3, and repulsive transmembrane signaling proteins EphA and ephrinA, which regulate intra-class attraction and inter-class repulsion respectively (64,140).

In contrast to mammalian olfactory receptors, Drosophila olfactory receptors are ligand-gated cation channels, and do not contribute to ORN wiring (147). Interestingly, DIPs and Dprs share homology with Kirrels and seem to operate with a similar logic. Differential and graded expression of adhesion proteins, Kirrels in mammals and a combination of DIPs/Dprs in flies, mediates class-specific glomerular convergence. They do this by regulating adhesion among the axons from the same ORN class, by creating differential adhesion forces locally in the olfactory bulb based on ORN-specific cell surface receptor profiles. Indeed, many interacting DIPs and Dprs are Kirrel-like (Figure 48). Thus, even though olfactory receptors in mammals and Drosophila are functionally and structurally diverse, our results reveal evolutionarily convergent downstream molecular strategies that sort ORN axon terminals into distinct glomeruli in a class-specific manner.

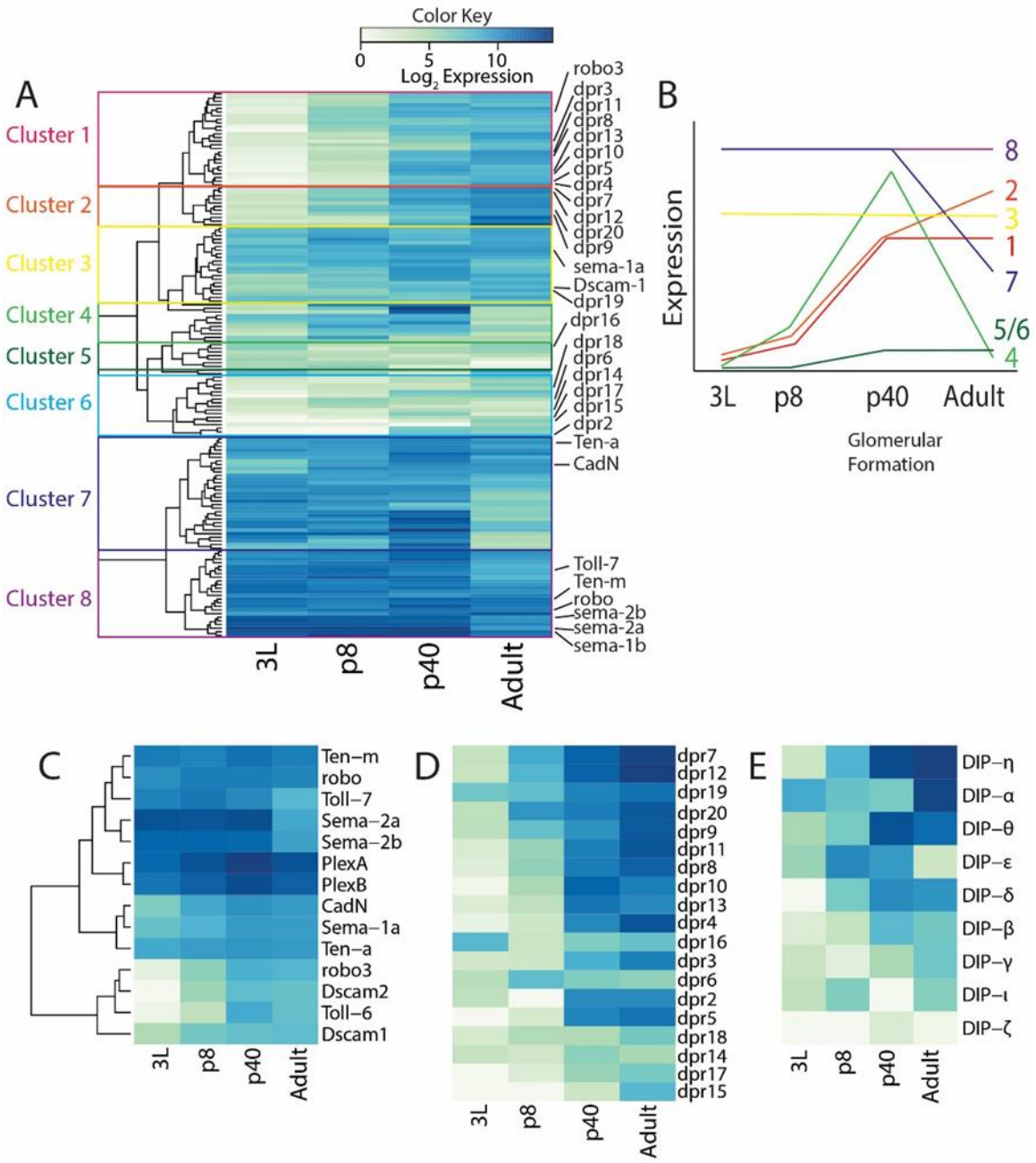

Figure 35: Transcriptional profiles of CSM genes in the developing Drosophila olfactory system. Heatmaps representing normalized $\log_2$ expression values for CSMs. Highly expressed genes are represented in darker colors, and genes with lower expression levels are represented with lighter colors. A) Hierarchical clustering of the developmental expression patterns of CSMs in the olfactory system groups genes into clusters. Known regulators of ORN wiring and members of the Dpr family are

highlighted. B) Schematic showing expression profile of genes in each cluster at the 4 developmental stages. C) Hierarchical clustering of the developmental expression patterns of known regulators of ORN wiring reveals two major expression patterns: high expression at all stages, and low expression at early stages followed by high expression at later stages. Expression patterns of Dpr (D) and DIP (E) genes ordered from highest expression across all stages to lowest. The majority of *DIP* and *dpr* genes are expressed primarily at later developmental stages (p40 and Adult).

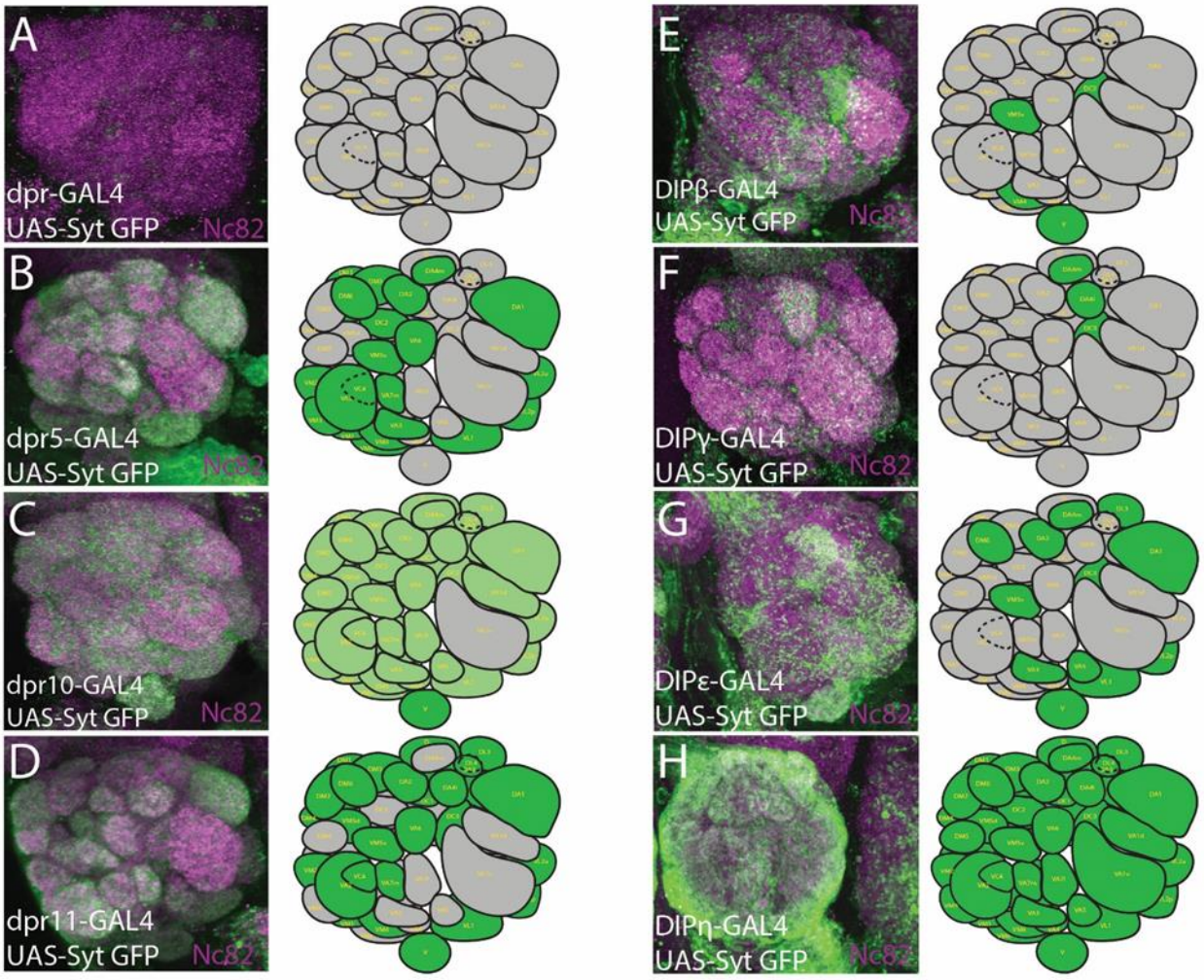

Figure 36: ORN class-specific expression patterns of *DIP* and *dpr* genes. *DIP* and *dpr-GAL4s* were used to drive *UAS-SynaptotagminGFP* (green, A-H) to visualize ORN axons terminals with staining for the neuropil (magenta). Each gene is expressed in a unique set of glomeruli and ORN classes. A map of the expression pattern of each

gene in the antennal lobe is provided in the right panel (A-H). Results for all genes are summarized in Figure 37.

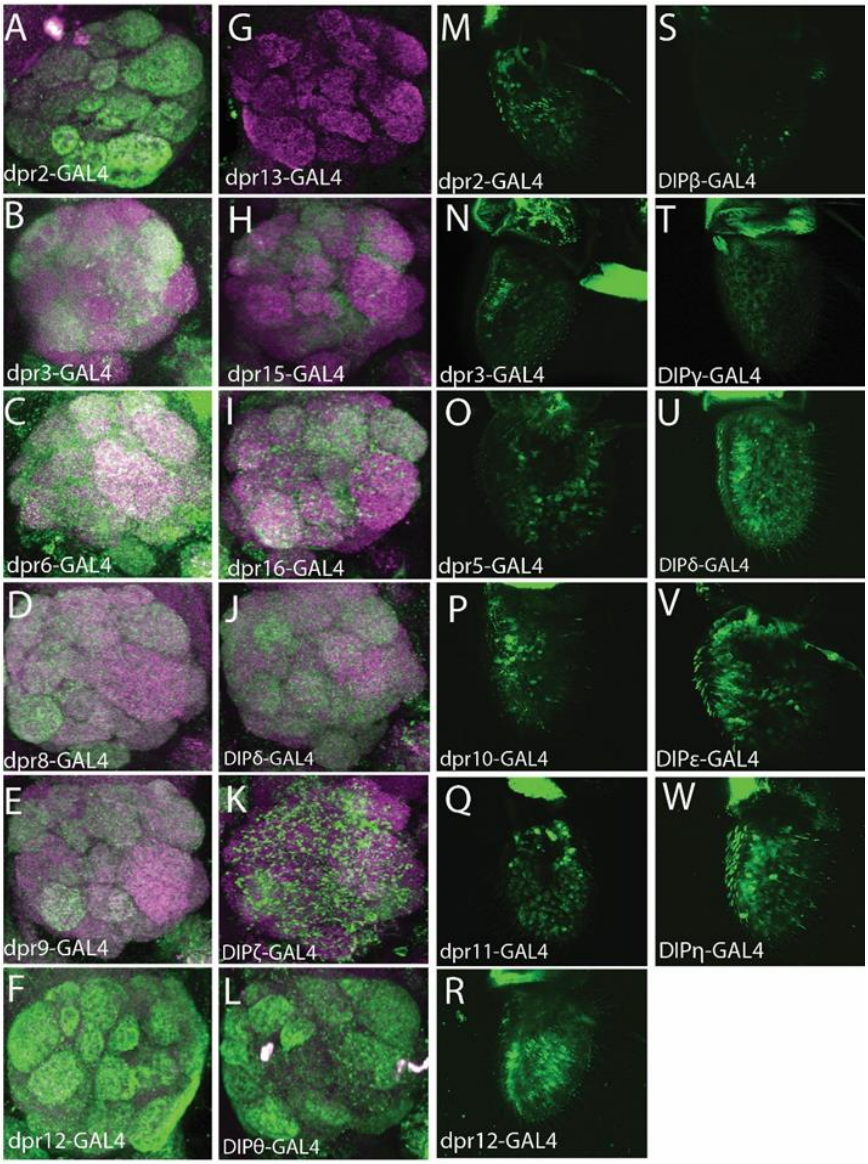

Figure 37: Expression of *DIPs* and *dprs* in the olfactory system. *DIP* and *dpr-GAL4* reporters driving *UAS-Synaptotagmin-GFP* (green) not shown in Figure 36 (A-L). DIP and *dpr-GAL4s* driving *UAS-CD8GFP* to visualize ORNs in the antenna (M-W). Most *DIPs* and *dprs* are expressed exclusively in ORNs although some are not expressed in the antenna at all.

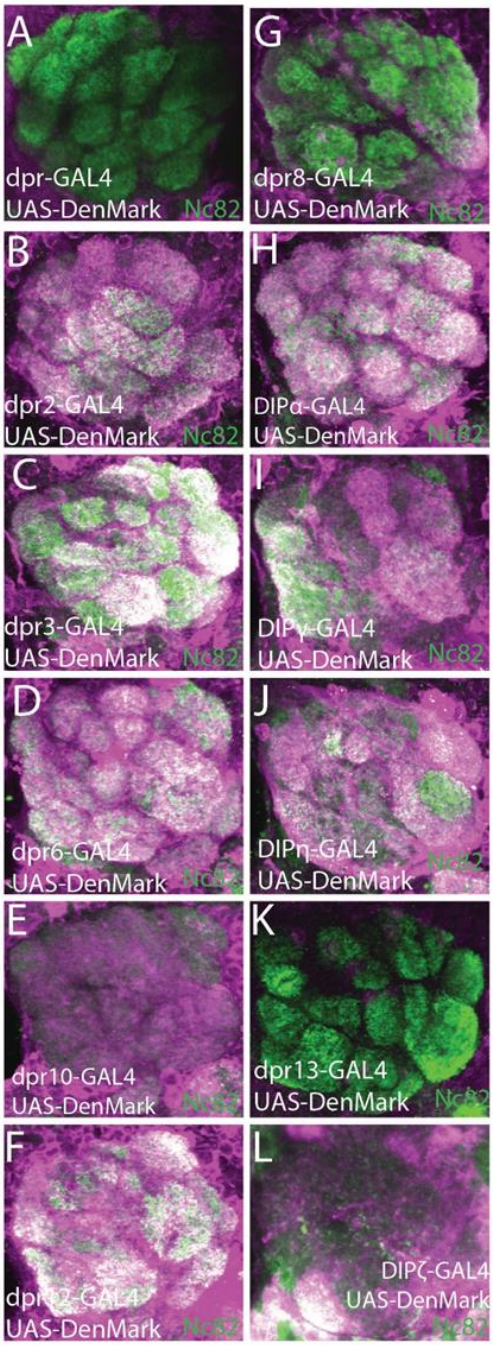

Figure 38: Expression of *DIPs* and *dprs* in Projection Neurons. *DIP* and *dpr-GAL4s* were used to drive *UAS-DenMark-RFP* (magenta) with staining for neuropil in green (A-L). *DIPs* and *dprs* are expressed in subsets of projection neurons, all PNs or none. Binding partners make no discernible matching pattern between ORNs and PNs.

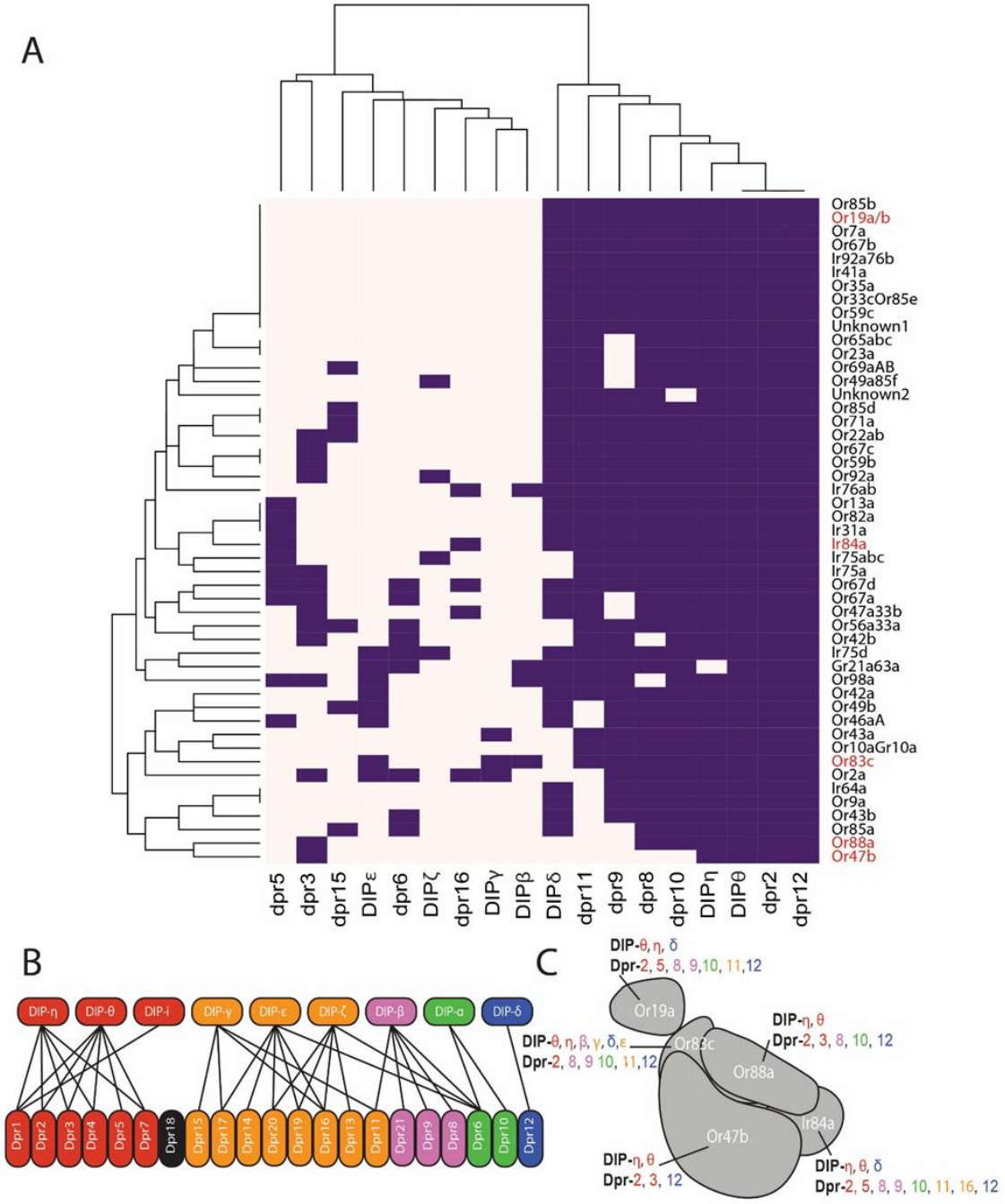

Figure 39: Combinatorial expression of DIPs and Dprs in the Drosophila olfactory system. (A) Hierarchical bi-clustering of DIP/Dpr expression patterns by ORN class reveals that each class of neurons expresses a unique combination of DIPs/Dprs. (B) Model of DIP-Dpr physical interactions (139,141)**. DIPs and Dprs heterophilically interact in a combinatorial network where one DIP typically interacts with multiple**

Dprs and Dprs interact with one or more DIPs. (C) Schematic of five glomeruli (Or47b, Or88a, Or83c, Ir84a, and Or19a) that will be analyzed in subsequent figures. The expression code for each glomerulus is highlighted with each receptor-ligand pair displayed in matching colors as in B.

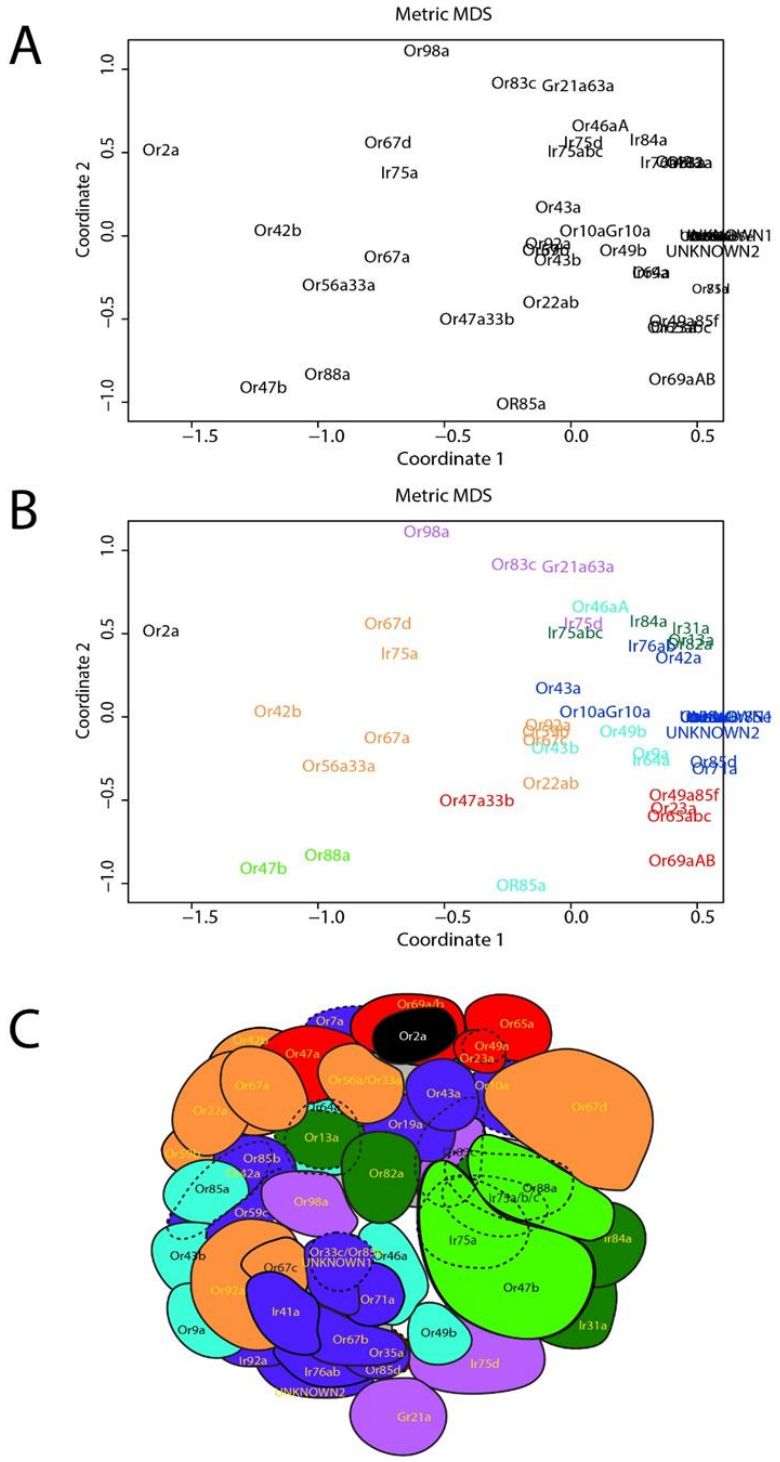

Figure 40: Multidimensional scaling clusters ORN classes by DIP/Dpr expression pattern, which mimics glomerular clusters in the antennal lobe. (A) Multidimensional

scaling analysis clusters ORN classes based upon DIP/Dpr expression and glomerular distances. (B) K-means clustering was used to determine which ORN classes shared the most similar DIP/Dpr expression profiles in the MDS analysis. Classes that were clustered together were assigned the same color. (C) The clustering observed in B mimics glomerular positioning in the antennal lobe. Coloring of glomeruli matches clusters in B.

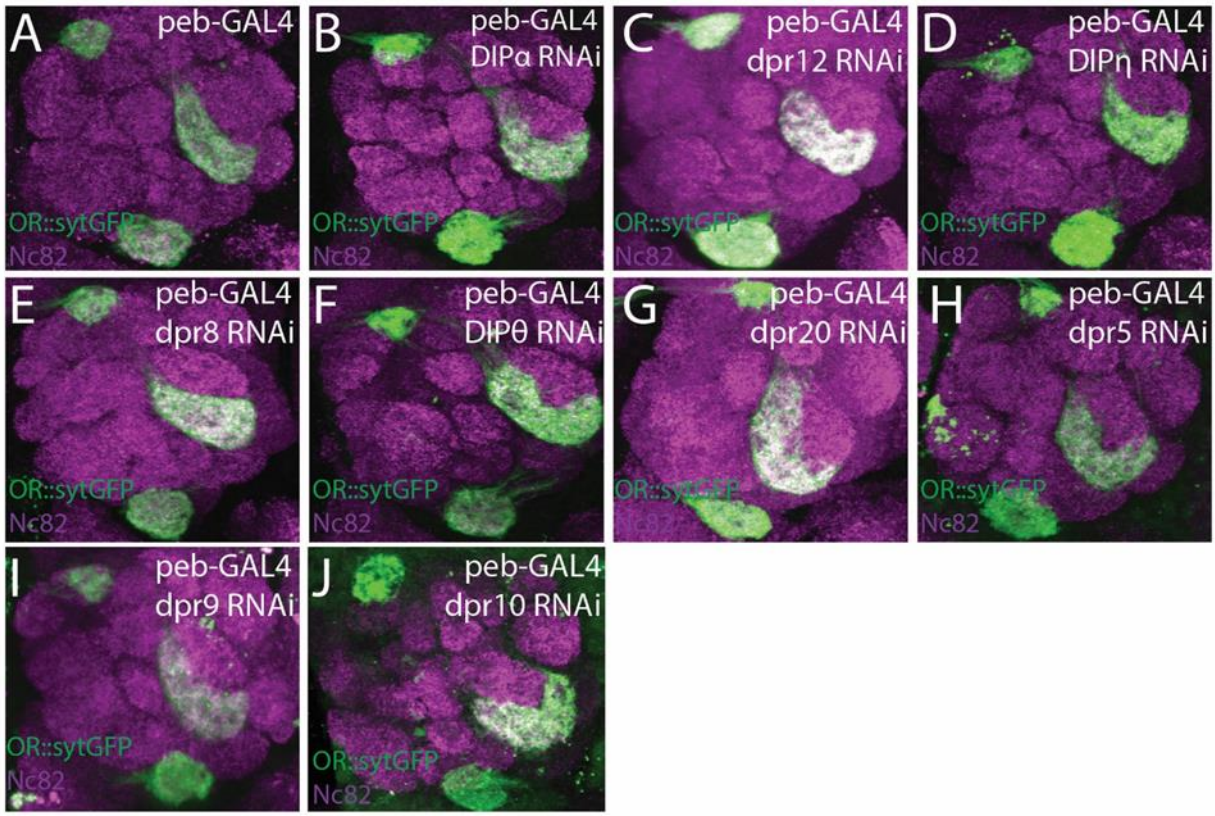

Figure 41: Single knockdown of DIPs/Dprs with pan-ORN driver does not disrupt ORN wiring. RNAi against single DIPs and Dprs were driven in all ORNs with peb-GAL4 and axon terminals of Or47b, Or47a, and Gr21a were visualized using direct fusion reporters driving Synaptotagmin-GFP (A-J). No defects were detected in any of the conditions.

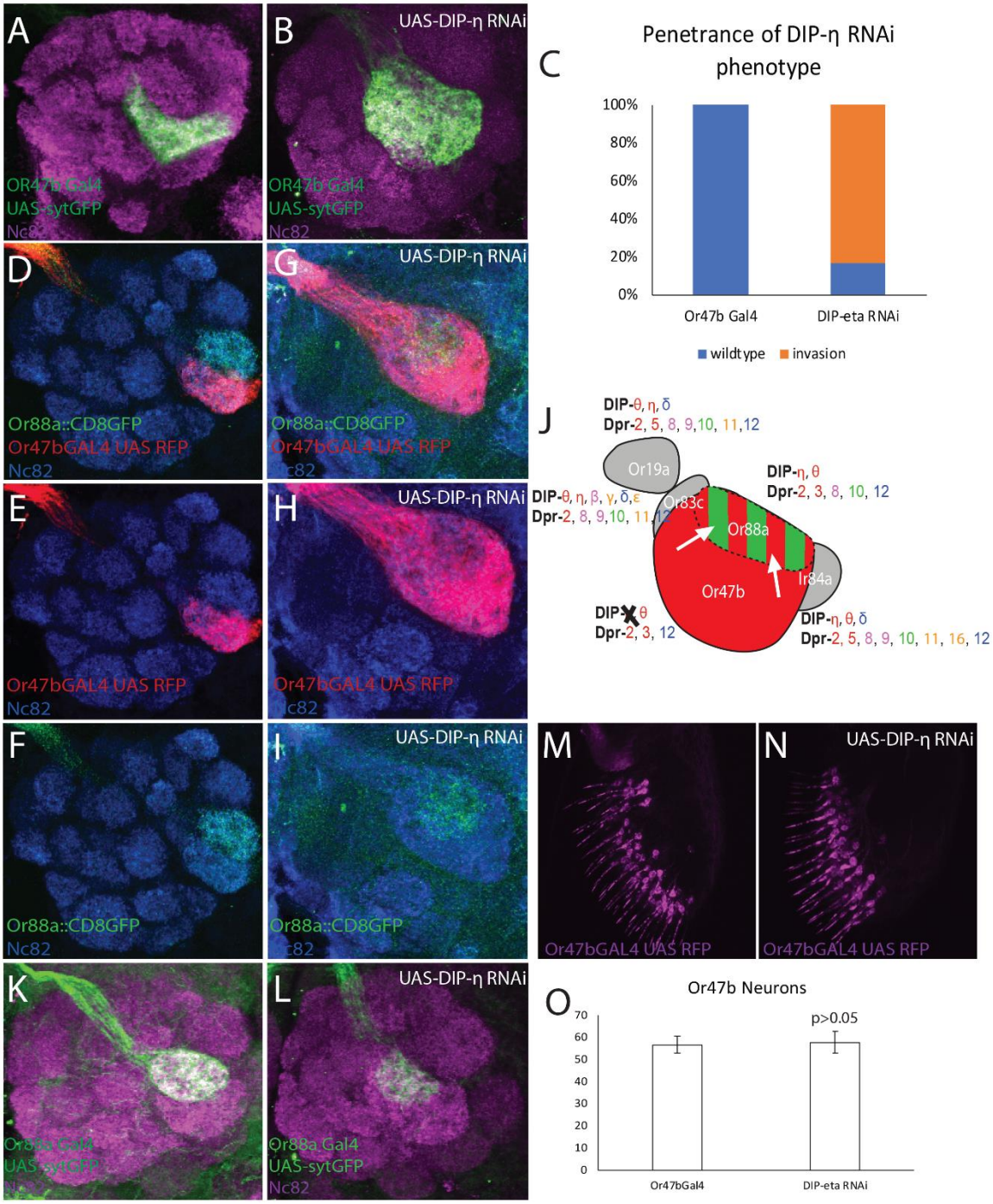

Figure 42: Cell-autonomous knockdown of DIP-η in Or47b ORNs disrupts sorting of Or47b axons from Or88a glomerulus. (A, B) Knockdown of *DIP-η* with the *Or47b-GAL4* driver, also used to drive *UAS-Synaptotagmin-GFP* (green), causes Or47b axons to expand and invade a neighboring glomerulus. (C) The expansion of the Or47b

glomerulus is highly penetrant in *DIP-η* knockdown, with 85% of individuals displaying invasion in one or both antennal lobes. (D-I) Simultaneous labeling of Or47b (red) and Or88a (green) axons reveals that knockdown of *DIP-η* causes Or47b ORN axons to invade the Or88a ORN target glomerulus, while Or88a ORN axons retain their ability to coalesce into a glomerulus despite intermingling with Or47b axons. (J) Schematic of axon sorting phenotypes in *DIP-η* knockdown. When *DIP-η* is specifically ablated from Or47b ORNs (black X), Or47b ORN axons (red) invade the Or88a ORN target glomerulus (white arrows) and intermingle with Or88a ORN axons (red/green striping). (K, L) Knockdown of *DIP-η* in Or88a ORNs using the *Or88a-GAL4* driver does not disrupt the Or88a ORN target glomerulus. (M-O) The number of Or47b ORNs does not change with knock down of *DIP-η* (p>0.05), suggesting that loss of *DIP-η* affects axon sorting and not OR expression.

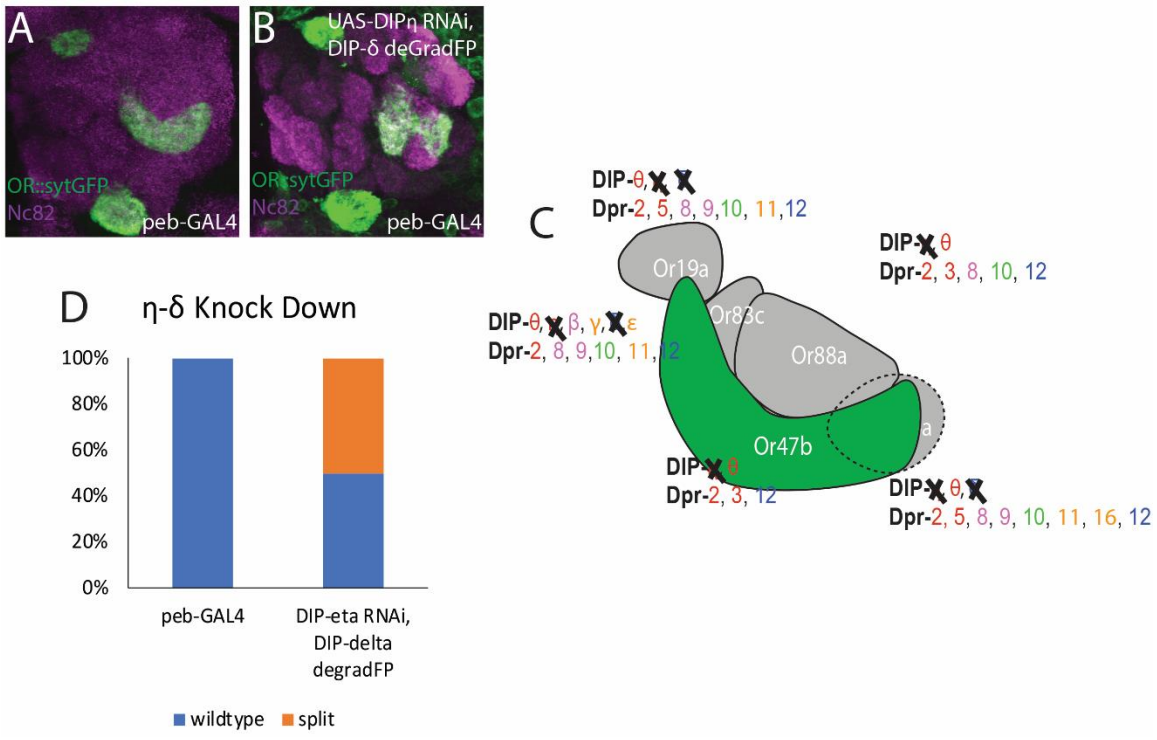

Figure 43: Pan-ORN knockdown of *DIP-η* and *DIP-δ* splits VA1v glomerulus. (A, B) Knock down of neither *DIP- δ* nor *DIP-η* alone disrupted the Or47b ORN target glomerulus (Figure 41). Knockdown of both genes simultaneously disrupted the shape and cohesion of the Or47b ORN target glomerulus. (C) Model of knock down of *DIP-δ*/*DIP-η* with the *peb-GAL4* driver. (D) Penetrance of VA1v glomerulus

splitting in *DIP-δ/DIP-η* knock down. 50% of brains showed splitting of the VA1v glomerulus in one or both antennal lobes.

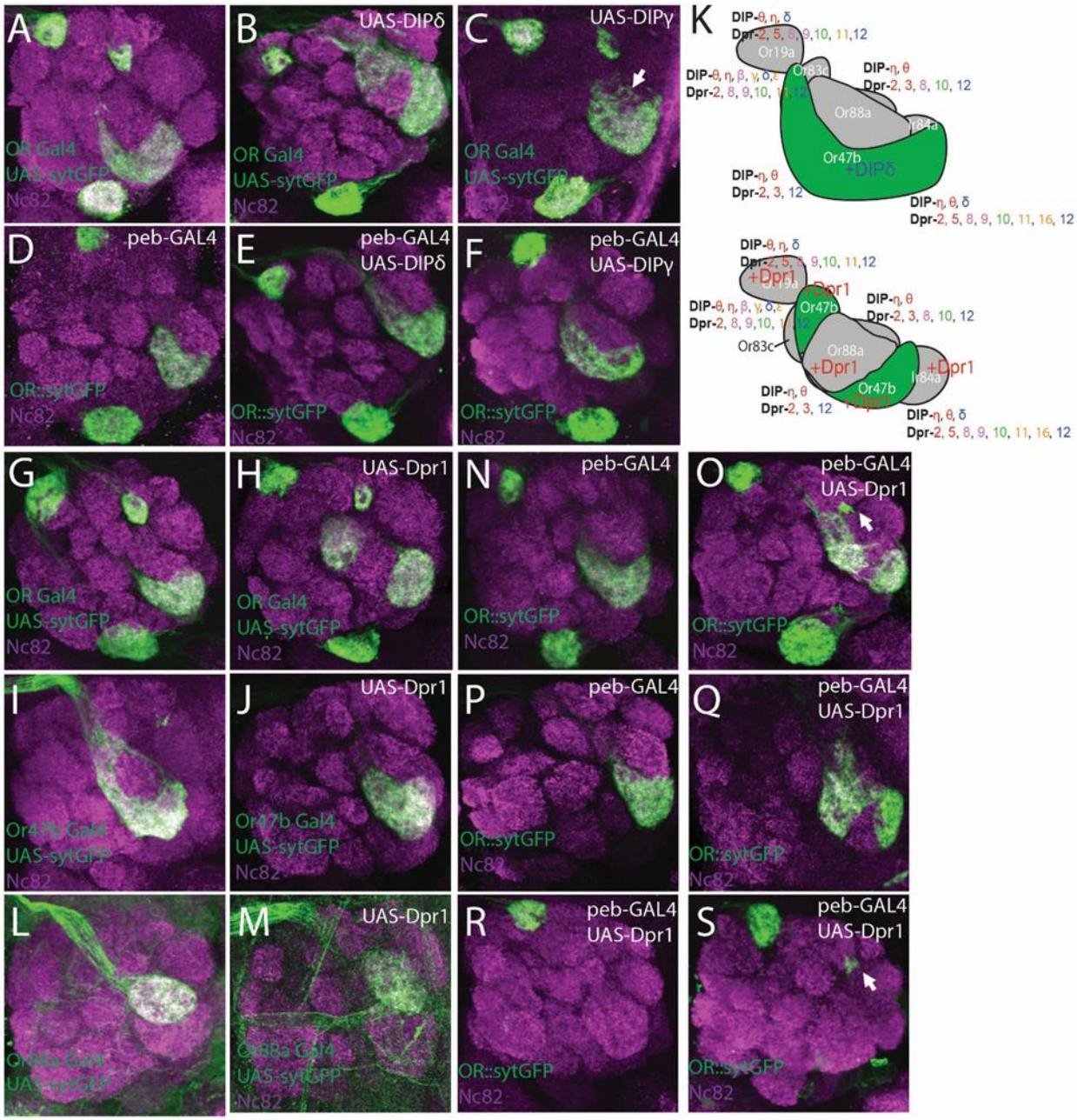

Figure 44: Overexpression of *DIPs/dprs* causes localized axon sorting defects. *OR-GAL4*s were used to drive expression of *UAS-DIP-δ* (B), *UAS-DIP-γ* (C) and *UAS-synaptotagmin-GFP* (green, A-C). Mis-expression of *DIP-δ* in Or47b ORNs caused the

target glomerulus to deform and split, with some axons moving towards the target glomerulus for Ir84a ORNs, and others towards the target glomerulus of Or83c ORNs (B), while other ORNs mis-expressing *DIP-δ* were unaffected. Over expression of *DIP-γ* in Or47b ORNs caused their axons to partially invade the Or88a target glomerulus (C), similar to knockdown of *DIP-η* (Figure 42). In contrast, other glomeruli that overexpressed *DIP-γ* were unaffected. (D-F) When *DIP-δ* and *DIP-γ* were overexpressed in all ORNs with the *peb-GAL4* driver, no disruptions were observed in the target glomeruli for Or47b, Or47a or Gr21a ORNs (green). (G, H) Over expression of *dpr1* in four classes of ORNs with *Or-GAL4* drivers caused a split Or47b glomerulus. (I, J) When *dpr1* was expressed only in Or47b ORNs, the glomerulus was unaffected. (K) Model of phenotypes of *DIP-δ* and *dpr1* over expression. Each gene is added to specifically Or47b ORNs or all neurons. Each DIP and Dpr is color coded to match its binding partners. (L, M) Expression of *dpr1* in Or88a ORNs did not affect either the Or88a or Or47b ORN targeting. (N-Q) Overexpression of *dpr1* with the *peb-GAL4* caused a split Or47b glomerulus phenotype as in H. Overexpression of *dpr1* with this driver also caused mistargeting/splitting of some Or47a ORN axons (N-O, R-S), creating a highly reproducible, ectopic glomerulus.

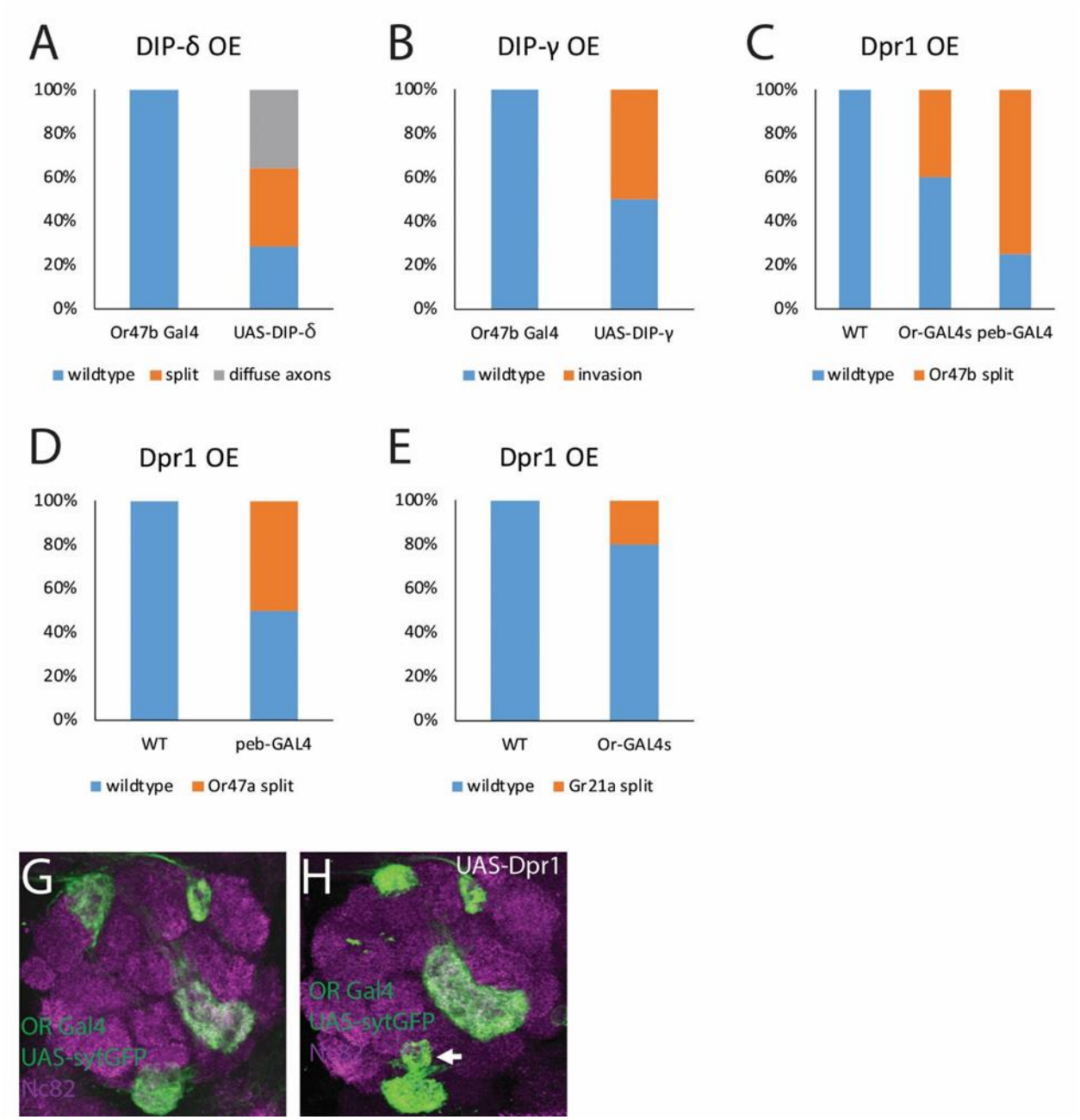

Figure 45: Summary and penetrance of DIP/Dpr overexpression phenotypes. (A) 71% of individuals displayed either a split of the Or47b glomerulus or diffuse axons within the Or47b glomerulus during DIP-δ overexpression. (B) 50% of individuals showed at least partial invasion of the Or88a glomerulus by Or47b axons when DIP-γ was expressed in Or47b neurons. (C) 40% and 80% of individuals displayed splitting of the Or47b glomerulus when Dpr1 was expressed in four ORN classes or all ORNs

respectively. (D) Splitting of the Or47a glomerulus accompanied by the formation of an ectopic glomerulus was present in 50% of individuals when *dpr1* was expressed in all ORNs. (E) Splitting of the Gr21a glomerulus was present in only 20% of individuals when Dpr1 was expressed in four ORN classes. (G-H) Representative images of Gr21a splitting with *dpr1* overexpression.

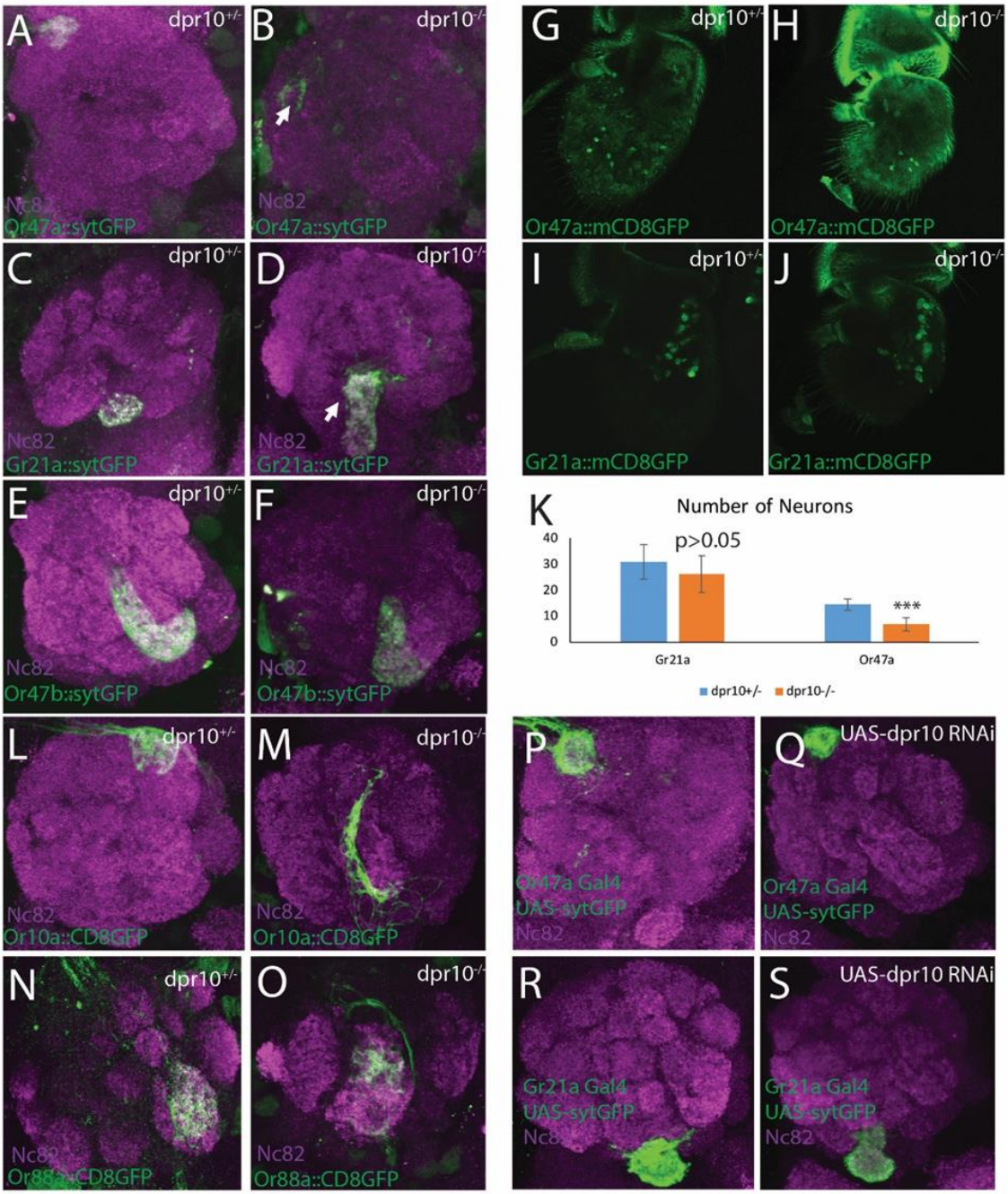

Figure 46: Dpr10 controls ORN wiring in the antennal lobe. Mutation of *dpr10* causes disruption of DM3 (A, B) and V (C, D) glomeruli but not the VA1v (E, F) glomerulus as visualized with OR reporters diving *synaptotagmin-GFP* (green). Disruptions to these glomeruli included splitting of the glomerulus (B, D), mistargeting (B, arrow) and expansion (D, arrow). Penetrance and full summary of these phenotypes are

described in Figure 47. (G-J) ORN cell bodies were visualized in heterozygous and mutant flies for both Gr21a and Or47a ORNs using *Or-GAL4* driven *UAS-CD8GFP*. A statistically significant decrease was observed for Or47a ORNs ($p<0.001$, K) but not for Gr21a ORNs ($p>0.05$, K). *dpr10* mutation also disrupts the wiring of both Or10a (L, M) and Or88a (N, O) ORNs. Or10a ORN axons lack proper glomerular convergence and mistarget (M) in *dpr10* mutants. The Or88a glomerulus is disrupted in both its shape and positioning (O). RNAi against *dpr10* was driven by either the *Or47a* (P, Q) or *Gr21a-GAL4s* (R, S). No mistargeting events were observed when *dpr10 RNAi* was driven in individual ORN classes (Q). When *dpr10 RNAi* was driven in Gr21a neurons a modest expansion phenotype was observed (S), but this effect was much less dramatic than in the *dpr10* homozygous whole animal mutant (D).

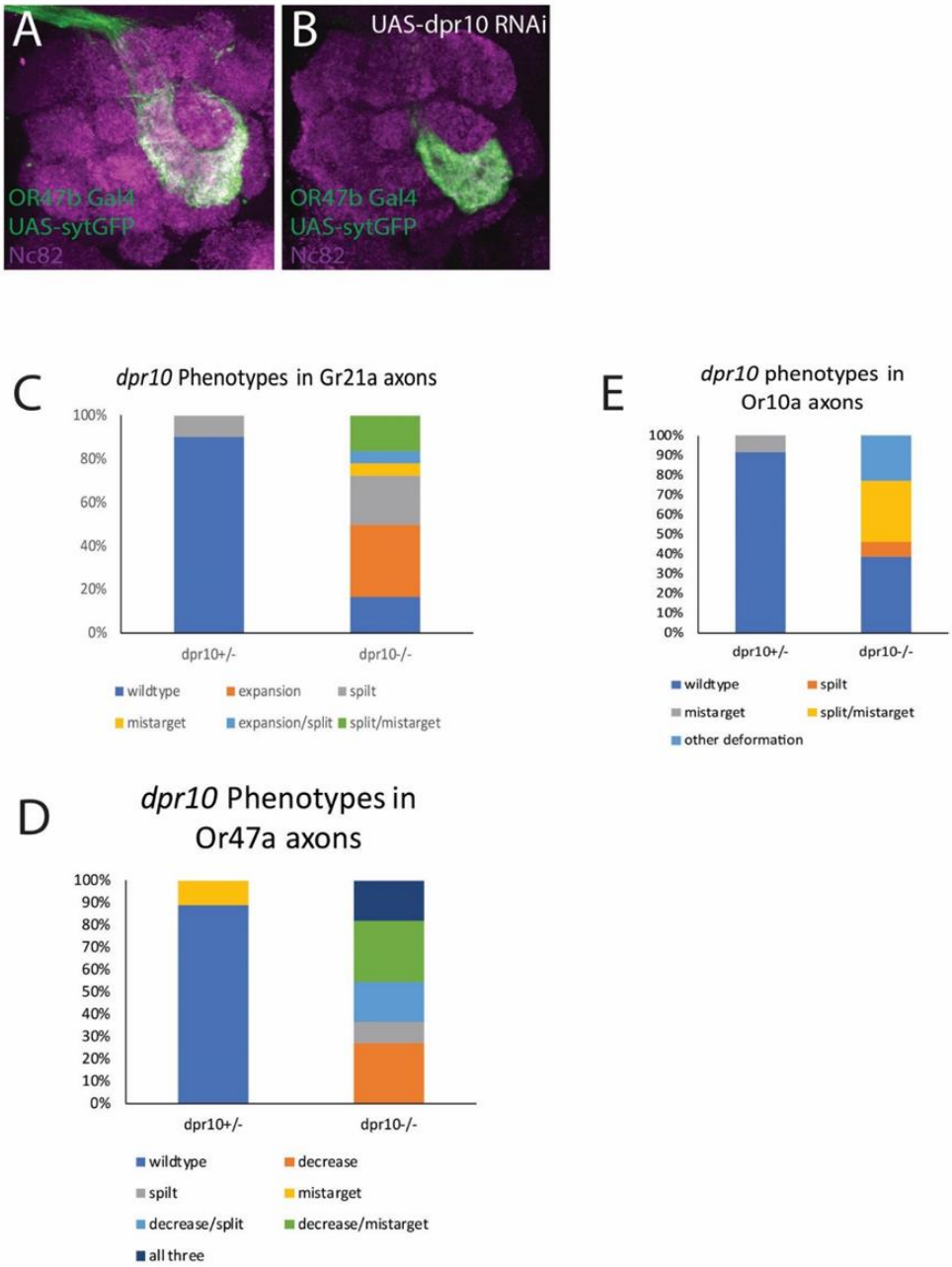

Figure 47: Summary and penetrance of *dpr10* mutant phenotypes. (A, B) Expression of *dpr10 RNAi* in Or47b neurons does not disrupt the shape of the Or47b glomerulus (green). (C-E) Summary of penetrance and phenotypes observed in each class of neurons labeled. In each class, greater than 60% of individuals displayed a mutant phenotype in one or both antennal lobes. A minimum of 10 brains were imaged for each class of neurons.

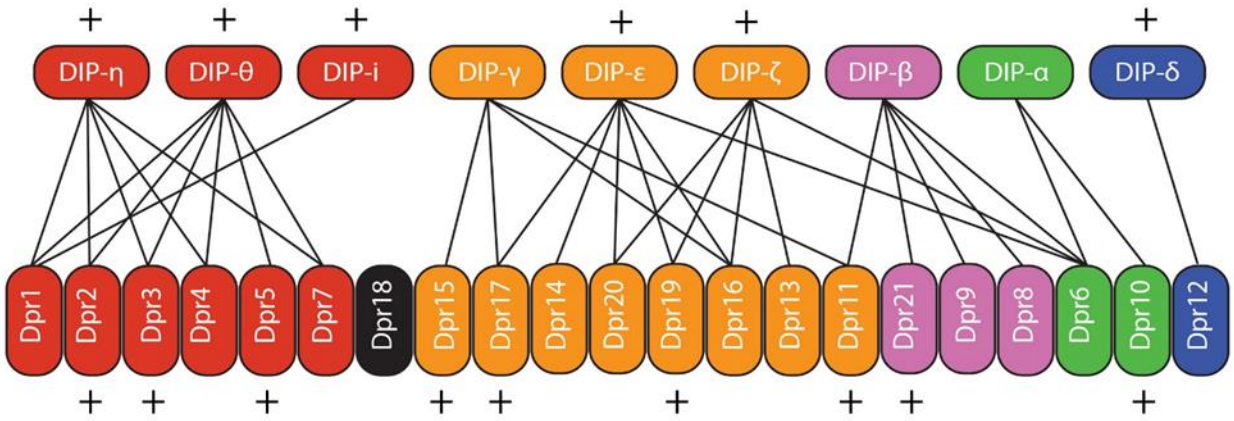

Figure 48: Some DIPs and Dprs share homology with Kirrels. Approximately of half of DIP/Dpr proteins are homologous to mammalian Kirrels (+), which control glomerular formation in the mouse olfactory system. Homology is based upon FlyBase DIOPT scores.

4.4 Materials and Methods

4.4.1 Fly Genetics

OR-CD8 GFP, OR-Syt GFP, OR-GAL4, IR-GAL4, GR-GAL4 lines were from Leslie Vosshall, Barry Dickson, Richard Benton and John Carlson, respectively. Dpr-GAL4 and DIP-GAL4 lines were from Larry Zipursky. *UAS-CD8 GFP*, *UAS-Syt GFP*, *ey-FLP*, *UAS-dpr1*, *UAS-DIPγ*, *UAS-DIPδ*, *dpr10*^{MI03557} and UAS-RNAi lines were all from Bloomington Stock Center.

4.4.1.1 Fly Genotypes

Figure 35A, C, D, E. *w*^{1118}

Figure 36A. *dpr-GAL4/UAS-sytGFP*

Figure 36B. *UAS-sytGFP/+; dpr5-GAL4/+*

Figure 36C. *UAS-sytGFP/+; dpr10-GAL4/+*

Figure 36D. *UAS-sytGFP/+; dpr11-GAL4/+*

Figure 36E. *DIP-β-GAL4/+; UAS-sytGFP/+*

Figure 36F. *UAS-sytGFP/+; DIP-γ-GAL4/+*

Figure 36G. *DIP-ε-GAL4/UAS-sytGFP*

Figure 36H. *DIP-η-GAL4/UAS-sytGFP*

Figure 37A. *dpr2-GAL4/UAS-sytGFP*

Figure 37B. *dpr3-GAL4/UAS-sytGFP*

Figure 37C. *UAS-sytGFP/+; dpr6-GAL4/+*

Figure 37D. *dpr8-GAL4/+; UAS-sytGFP/+*

Figure 37E. *UAS-sytGFP/+; dpr9-GAL4/+*

Figure 37F. *dpr12-GAL4/UAS-sytGFP*

Figure 37G. *dpr13-GAL4/UAS-sytGFP*

Figure 37H. *UAS-sytGFP/+; dpr15-GAL4/+*

Figure 37I. *UAS-sytGFP/+; dpr16-GAL4/+*

Figure 37J. *UAS-sytGFP/+; DIP-δ-GAL4/+*

Figure 37K. *DIP-ζ-GAL4/UAS-sytGFP*

Figure 37L. *DIP-θ-GAL4/UAS-sytGFP*

Figure 37M. *dpr2-GAL4/UAS-CD8GFP*

Figure 37N. *dpr3-GAL4/UAS-CD8GFP*

Figure 37O. *UAS-CD8GFP/+; dpr5-GAL4/+*

Figure 37P. *UAS-CD8GFP/+; dpr10-GAL4/+*

Figure 37Q. *UAS-CD8GFP/+; dpr11-GAL4/+*

Figure 37R. *dpr12-GAL4/UAS-CD8GFP*

Figure 37S. *DIP-β-GAL4/+; UAS-CD8GFP/+*

Figure 37T. *UAS-CD8GFP/+; DIP-γ-GAL4/+*

Figure 37U. *UAS-CD8GFP/+; DIP-δ-GAL4/+*

Figure 37V. *DIP-ε-GAL4/UAS-CD8GFP*

Figure 37W. *DIP-η-GAL4/UAS-CD8GFP*

Figure 38A. *dpr-GAL4/UAS-DenMark*

Figure 38B. *dpr2-GAL4/UAS-DenMark*

Figure 38C. *dpr3-GAL4/UAS-DenMark*

Figure 38D. *UAS-DenMark/+; dpr6-GAL4/+*

Figure 38E. *UAS-DenMark/+; dpr10-GAL4/+*

Figure 38F. *dpr12-GAL4/UAS-DenMark*

Figure 38G. *dpr8-GAL4/+; UAS-DenMark/+*

Figure 38H. *DIP-α-GAL4/+; UAS-DenMark/+*

Figure 38I. *UAS-DenMark/+; DIP-γ-GAL4/+*

Figure 38J. *DIP-η-GAL4/UAS-DenMark*

Figure 38K. *dpr13-GAL4/UAS-DenMark*

Figure 38L. *DIP-ζ-GAL4/UAS-DenMark*

Figure 41A. *peb-GAL4/+; Or47b-sytGFP, Or47a-sytGFP, Gr21a-sytGFP/+*

Figure 41B. *peb-GAL4/+; Or47b-sytGFP, Or47a-sytGFP, Gr21a-sytGFP/UAS-DIP-α RNAi*

Figure 41C. *peb-GAL4/+; Or47b-sytGFP, Or47a-sytGFP, Gr21a-sytGFP/+; UAS-dpr12RNAi/+*

Figure 41D. *peb-GAL4/+; Or47b-sytGFP, Or47a-sytGFP, Gr21a-sytGFP/UAS-DIP-η RNAi*

Figure 41E. *peb-GAL4/+; Or47b-sytGFP, Or47a-sytGFP, Gr21a-sytGFP/+; UAS-dpr8 RNAi/+*

Figure 41F. *peb-GAL4/+; Or47b-sytGFP, Or47a-sytGFP, Gr21a-sytGFP/+; UAS-DIP-θ RNAi/+*

Figure 41G. *peb-GAL4/+; Or47b-sytGFP, Or47a-sytGFP, Gr21a-sytGFP/+; UAS-dpr20 RNAi/+*

Figure 41H. *peb-GAL4/+; Or47b-sytGFP, Or47a-sytGFP, Gr21a-sytGFP/+; UAS-dpr5 RNAi/+*

Figure 41I. *peb-GAL4/+; Or47b-sytGFP, Or47a-sytGFP, Gr21a-sytGFP/+; UAS-dpr9 RNAi/+*

Figure 41J. *peb-GAL4/+; Or47b-sytGFP, Or47a-sytGFP, Gr21a-sytGFP/+; UAS-dpr10 RNAi/+*

Figure 42A. *Or47b-GAL4 UAS-sytGFP*/CyO

Figure 42B. *Or47b-GAL4 UAS-sytGFP/UAS-DIP-η RNAi*

Figure 42D-F. *Or47b-GAL4 UAS-RFP*/CyO; *Or88a-mCD8GFP/+*

Figure 42G-I. *Or47b-GAL4 UAS-RFP/UAS-DIP-η RNAi; Or88a-mCD8GFP/+*

Figure 42K. *Or88a-GAL4 UAS-CD8GFP*/CyO

Figure 42L. *Or88a-GAL4 UAS-CD8GFP/UAS-DIP-η RNAi*

Figure 42M. *Or47b-GAL4 UAS-RFP*/CyO

Figure 42N. *Or47b-GAL4 UAS-RFP/UAS-DIP-η RNAi*

Figure 43A. *peb-GAL4/+; Or47b-sytGFP/CyO; +/TM6B*

Figure 43B. *peb-GAL4/+; Or47b-sytGFP/UAS-DIP-η RNAi; DIP-δ-GFP/UAS-DeGradFP*

Figure 44A, G. *Or47b-GAL4 Or47a-GAL4 Or23a-GAL4 Gr21a-GAL4 UAS-sytGFP*/CyO; TM2/TM6B

Figure 44B. *Or47b-GAL4 Or47a-GAL4 Or23a-GAL4 Gr21a-GAL4 UAS-sytGFP/+; UAS-DIP-δ*/TM6B

Figure 44C. *Or47b-GAL4 Or47a-GAL4 Or23a-GAL4 Gr21a-GAL4 UAS-sytGFP/+; UAS-DIP-γ*/TM6B

Figure 44D, N. *peb-GAL4/+; Or47b-sytGFP, Or47a-sytGFP, Gr21a-sytGFP/+*

Figure 44E. *peb-GAL4/+; Or47b-sytGFP, Or47a-sytGFP, Gr21a-sytGFP/+; UAS-DIP-δ/+*

Figure 44F. *peb-GAL4/+; Or47b-sytGFP, Or47a-sytGFP, Gr21a-sytGFP/+; UAS-DIP-γ/+*

Figure 44H. *Or47b-GAL4 Or47a-GAL4 Or23a-GAL4 Gr21a-GAL4 UAS-sytGFP/UAS-dpr1*

Figure 44I. *Or47b-GAL4 UAS-sytGFP*/CyO

Figure 44J. *Or47b-GAL4 UAS-sytGFP/UAS-dpr1*

Figure 44L. *Or88a-GAL4 UAS-CD8GFP*

Figure 44M. *Or88a-GAL4 UASCD8GFP/UAS-dpr1*

Figure 44O. *peb-GAL4/+; Or47b-sytGFP, Or47a-sytGFP, Gr21a-sytGFP/UAS-dpr1*

Figure 44P. *peb-GAL4/+; Or47b-sytGFP*/CyO

Figure 44Q. *peb-GAL4/+; Or47b-sytGFP/UAS-dpr1*

Figure 44R. *peb-GAL4/+; Or47a-sytGFP*/CyO

Figure 44S. *peb-GAL4/+; Or47a-sytGFP/UAS-dpr1*

Figure 45G: *Or47b-GAL4 Or47a-GAL4 Or23a-GAL4 Gr21a-GAL4 UAS-sytGFP*/CyO

Figure 45H: *Or47b-GAL4 Or47a-GAL4 Or23a-GAL4 Gr21a-GAL4 UAS-sytGFP/UAS dpr1*

Figure 46A. *Or47a-sytGFP*; *dpr10*^{MI03557}/TM6B

Figure 46B. *Or47a-sytGFP*; *dpr10*^{MI03557}

Figure 46C. *Gr21a-GAL4 UAS-sytGFP*; *dpr10*^{MI03557}/TM6B

Figure 46D. *Gr21a-GAL4 UAS-sytGFP*; *dpr10*^{MI03557}

Figure 46E. *Or47b-sytGFP*; *dpr10*^{MI03557}/TM6B

Figure 46F. *Or47b-sytGFP*; *dpr10*^{MI03557}

Figure 46G. *Or47a-GAL4 UAS-sytGFP/UASCD8GFP*; *dpr10*^{MI03557}/TM6B

Figure 46H. *Or47a-GAL4 UAS-sytGFP/UASCD8GFP*; *dpr10*^{MI03557}

Figure 46I. *Gr21a-GAL4 UAS-CD8GFP*; *dpr10*^{MI03557}/TM6B

Figure 46J. *Gr21a-GAL4 UAS-CD8GFP*; *dpr10*^{MI03557}

Figure 46L. *Or10a-GAL4 UAS-CD8GFP*; *dpr10*^{MI03557}/TM6B

Figure 46M. *Or10a-GAL4 UAS-CD8GFP*; *dpr10*^{MI03557}

Figure 46N. *Or88a-GAL4 UAS-CD8GFP*; *dpr10*^{MI03557}/TM6B

Figure 46O. *Or88a-GAL4 UAS-CD8GFP*; *dpr10*^{MI03557}

Figure 46P. *Or47a-GAL4 UAS-sytGFP/+*

Figure 46Q. *Or47a-GAL4 UAS-sytGFP/+; UAS-dpr10 RNAi/+*

Figure 46R. *Gr21a-GAL4 UAS-sytGFP/+*

Figure 46S. *Gr21a-GAL4 UAS-sytGFP/+; UAS-dpr10 RNAi/+*

Figure 47A. *Or47b-GAL4 UAS-sytGFP/+*

Figure 47B. *Or47b-GAL4 UAS-sytGFP/+; UAS-dpr10 RNAi/+*

4.4.2 RNA-seq

RNAseq was performed as described before. Wandering third instar larval antennal discs (~70 for each genotype), 8hr APF pupal antennae (~50 for each genotype), 40hr APF pupal antennae (~50 for each genotype), and adult antennae (150 males and 150 females) from *w1118* flies were dissected. We extracted RNA only from the antennal portion of the larval eye-antennal discs in order to remove contamination by transcripts from the developing eye. RNA sequencing libraries were prepared with TruSeq Stranded mRNA Sample Prep Kit (Illumina) following the manufacturer's instructions. For the RNA fragmentation step, 94°C, 2min was used with the intention to obtain a median size ~185bp. PCR amplification was done with 15 cycles. A total of 24 multiplexed libraries (barcoded) were accessed for quality and mixed together before separating to two identical pooled libraries, which are subject to cluster generation followed by Illumina 50bp paired-end sequencing by UNC High-Throughput Sequencing Facility (HTSF), as described in Li and Barish et al 2016.

4.4.3 Analysis of RNAseq data

Following Li et al., the *Drosophila melanogaster* transcriptome (r5.57) was downloaded from Flybase and bwa indexed was created with bwa-0.7.8. Each sequencing file was aligned to the transcriptome, and .sam files for each sample were generated by putting two alignments from both reads together. At least 80% of the total reads were able to align to the reference sequence. Count tables were then made for each sample with a customized python script, and further consolidated into a matrix containing transcript ID and read counts from all genotypes for each stage with a Ruby script. These matrices were used as inputs for differential expression analysis using customized DESeq2 R script.

4.4.4 Immunohistochemistry

Samples were fixed with 4% paraformaldehyde, washed with phosphate buffer with 0.2% Triton X-100, and staining as previously described. Primary antibodies were used in the following dilutions: rabbit α-GFP 1:1000 (Invitrogen), rat α-Ncad 1:20 (Developmental Studies Hybridoma Bank), mouse α-Bruchpilot 1:20 (Developmental Studies Hybridoma Bank), mouse α-CD2 1:1000 (Serotec). The following secondary antibodies were used: Alexa 488 goat α-rabbit 1:1000, goat α-mouse-Cy3 1:100, Alexa 568 goat α-mouse IgG highly cross-adsorbed 1:300, Alexa 647 goat α-rat 1:200. Confocal images were taken by an Olympus Fluoview FV1000 or Zeiss LSM 510 (Light Microscopy Core Facility).

4.4.5 Statistical analysis of ORN class specific DIP/Dpr profiles

Biclustering analysis was performed using existing "biclust" package in R to hierarchically cluster both DIP/Dpr expression profile in each ORN class, and the ORNs that express each *DIP* or *dpr* gene.

Multidimensional scaling (MDS) was performed in R on a matrix for each ORN class and their DIP/Dpr profiles in a binary fashion (0, 1), where value 1 represents presence of a given DIP or Dpr in a given ORN class. The results were plotted in two dimensions.

k-means clustering in R was used to identify the 10 clusters below, which were later used to color code each cluster on the MDS plot. Same color coding was used on the antennal lobe scheme to highlight actual glomerular positions for each ORN class. Clusters are:

1- Or23a, Or65abc, Or47a, Or69a, Or49a

2- Or47b, Or88a

3- Or2a,

4- Or85a, Or49b, Or9a, Or43b, Or46a, Ir64a,

5- Or82a, Ir84a, Ir31a, Or13a, Ir75abc,

6- Or19a, Or43a, Or10a, Or85b, Or7a, Or67b, Ir92a, Ir41a, Or35a, Ir76ab, Or71a, Or42a, Or33c, Or85d, Or59c, UNKNOWN1, UNKNOWN2

7- Or67d, Or56a, Or22a, Or59b, Or42b, Or92a, Or67c, Or67a, Ir75a,

8- Or83c, Gr21a63a, Or98a, Ir75d

5. Conclusions and Future Directions

5.1 Conclusions

The work described in previous chapters provides new insights into the mechanisms that control two key aspects of neuronal identity: class-specific gene expression and connectivity. First, I described how a cross-regulatory network of transcription factors patterns ORN precursors to diversify an initially homogeneous field of cells (Chapter 2). The transcription factors of this network are expressed in overlapping concentric circles, thereby creating seven distinct rings within the antennal disc. Each ring is defined by the expression of a unique combination of transcription factors and gives rise to distinct subsets of ORNs and sensilla subtypes. Perturbations to this network alters the sensilla subtypes that are generated in the adult. This network also functions to pattern other Drosophila appendages, controlling both morphology and neuronal class specification. A similar logic also undergirds neuronal specification in mammals, where some of the same genes control the generation of neuronal fates.

Based upon our data, we propose a step-wise model of specification of ORN fates: 1) prepatterning of the antennal disc, 2) selection of neural precursors by proneural genes, and 3) asymmetric cell divisions, mediated by Notch signaling, select from restricted potentials to give rise to all of the neurons of olfactory system. This model, combining the work shown here and that of other labs provides clearer insight in ORN

specification and is able to explain a much larger amount of the diversity of the olfactory system.

We next presented a more thorough analysis of a developmental time course transcriptome data set. We found that antennal transcripts are highly dynamic across developmental stages with the greatest changes coming at the transition to adult antennae. When we profiled the expression of olfactory and ionotropic receptors, we found that approximately half are expressed at 40 hrs APF suggesting a temporal sequence to the onset of olfactory receptor expression that is confirmed by OR reporter expression. Analysis of transcription factor expression patterns revealed several distinct patterns of expression that may be predictive of their function within the olfactory system. Consistent with this hypothesis, we identified the transcription factor *distal antenna (dan)* as a prepatterning factor that regulates a subset of ORN fates.

Finally, we analyzed how the olfactory system is able to coordinately wire 50 classes of ORN axons into 50 class-specific glomeruli. We demonstrated that DIP and Dpr family proteins are expressed at the times of olfactory system development that correlate with glomerular formation and that they are expressed in subsets of ORN classes, creating a combinatorial code where each glomerulus is labeled by a unique combination of DIP/Dpr genes. Disruption to DIP/Dpr expression causes local axon sorting defects, where affected axons invade neighboring glomeruli based upon the similarity of their DIP/Dpr expression profiles. Based upon these data, we propose that

these proteins mediate adhesive interactions between axons, where differential adhesion forces separate each class of axons into their appropriate glomerulus. We also see that mammalian genes share homology with DIPs/Dprs and underlie a similar logic of axon sorting in the mouse olfactory system, suggesting convergent mechanisms of glomerular formation across taxa.

5.2 Future Directions

5.2.1 Completion of combinatorial maps

The results described here highlight the necessity of combinatorial coding in controlling both the specification of ORN fates and the sorting of ORN axons into 50 class-specific glomeruli. In both cases, we created a map of gene expression where each sensilla subtype fate or ORN class is defined by a unique combination of transcription factors or DIPs/Dprs respectively. Our maps explain a greater amount of the diversity of the olfactory system than previous models were able to, and yet are still incomplete, with several fates and ORN classes expressing identical combinations of transcription factors or DIPs/Dprs. Both maps therefore require refinement and completion in order to be able to create a full model of each process.

5.2.1.1 Completing the PD-network

Our model of sensilla subtype specification can be refined in a number of ways. First, seven fates were mapped to the R(7), the center of the antennal disc, but all other rings contain at most three fates. Second, some fates, such as ab3, expressed a

combination of transcription factors that we did not observe in the antennal disc, namely Dac and Bab only. Finally, nearly all rings contain multiple sensilla subtypes fates, and while we provide evidence to suggest that the levels of Bab expression within each ring separate these fates, other factors are likely at play.

The seven fates of R(7) were mapped to that ring because of how they behaved during overexpression of *Bar* and *ap*, or their expression of *ap* and *bab* or *bab* only. It is likely that further members of the PD-network may separate out R(7) into smaller rings, or that dorsal/ventral patterning controlled by Wingless (Wg) and Decapentaplegic (Dpp) signaling may control separation of fates within R(7). There are several candidate genes that could be involved in this process. *clawless* and *lim1* are both expressed in the center of the leg disc and control the development of the claw (83,87). Characterization of the expression domains of both of these genes within the antennal disc along with mutational analysis is necessary to understand whether these genes play a role in ORN specification. Downstream targets of both Wg and Dpp signaling are also good candidates to study as both genes are expressed in wedge shaped patterns through most rings and may separate fates within rings (37,82,148). The expression patterns of several other genes, such as Dichaete, have been characterized and also warrant study. Each of these genes, particularly those under the control of Wg and Dpp may also contribute to separation of fates within rings outside of R(7). As we have already mapped particular sensilla subtype fates to unique regions of the antennal disc, hypotheses about which

fates will be under the control of any gene should be informed by its expression pattern in relation to other transcription factors in the network.

Finally, to resolve potentially misplaced or unresolved fates, two major strategies should be employed: lineage tracing and single cell RNA-seq. The expression data used to map fates was based on GAL4s for each gene. However, the most appropriate analysis would be lineage tracing. Several technical challenges prevented our completion of these experiments. New reagents will need to be generated to complete these experiments as currently the Bar and Ap GAL4s in particular do not reflect expression observed with antibody staining (data not shown). RNA-sequencing at both the cell-type specific and single cell level can help to further define each ring and resolve expression differences. For example, the ab3 fate expresses both Dac and Bab but not Rn. Such a combination of expression was not observed in our analysis although it is possible that Dac-positive Rn-negative cells do express Bab but at levels below the detection threshold for the methods we employed. RNA-seq would resolve such questions and would also open avenues for identification of novel transcription factors in each ring, as well as allow for modeling ORN specification.

5.2.1.2 ORN CSM profiles

Our model of DIP/Dpr expression greatly increased the knowledge of what CSMs control glomerular formation but is clearly incomplete. Primarily, we lack expression data for several DIP/Dpr genes, as was previously discussed. These genes

currently lack GAL4 lines and therefore require the generation of new reagents. It is also likely that other CSMs, beyond DIPs and Dprs, are involved in ORN axon sorting. Beats and Sidesteps are attractive candidates because they have similar structure to DIPs/Dprs and interact in a similar network (149). Cadherins and proto-cadherins are also an interesting family of genes to study as they are often highly spliced which allows for efficient use of genomic space while creating diversity (11). Indeed, preliminary data not presented here suggests that at least one beat and one cadherin are involved in ORN axon sorting, as knockdown of both genes produces similar phenotypes as those observed in DIP/Dpr knockdowns.

RNA-seq of all ORN classes would provide a significant advancement in this field. First, it would provide confirmation of the expression patterns presented here, which is still lacking. Second, it would allow for a more comprehensive profiling of the expression patterns of a wide array of CSMs because it takes an unbiased approach. This would allow for the identification of novel regulators of ORN wiring in a class-specific manner. This analysis would ideally be able to generate a complete model of ORN wiring and create strategies for combinatorial manipulation of CSMs to uncover their roles at each stage of development.

5.2.2 Molecular mechanisms of ORN specification

It is well established that all of the neurons in a sensillum are generated from a single sensory organ precursor (SOP) that undergoes several asymmetric cell divisions

(8). In Chapter 2, we demonstrated that the SOPs of the antennal disc are patterned by a cross-regulatory network of transcription factors, which restrict the potential of each SOP, thereby limiting the possible neurons each cell can produce (113). It is still unclear however, what the molecular mechanisms are that drive this restriction of potential and how these changes are maintained across multiple cell divisions.

One attractive possibility is that changes to chromatin structure and architecture and/or epigenetic modifications to histones control fate restriction because such modifications can be retained across cell divisions and have been shown to play a role in neural differentiation (108,150,151). Such changes should occur at or around OR genes and their promoters because these genes are the ultimate determinants of ORN fate. Assaying global chromatin architecture, through methods like ATAC-seq, and specific epigenetic marks, through ChIP-seq, across developmental stages would provide key insights into how organization of the nucleus changes over time, leading to restriction of precursor potential and culminating in the expression of typically a singular OR gene. This analysis could also yield information about the differences created by Hox genes, because the same transcription factor network is employed by both the antennae and legs, but under distinct Hox gene control, to generate olfactory and gustatory receptor neurons respectively.

Considering that OR reporters can fully and specifically recapitulate OR expression outside their endogenous loci, it has been theorized that all of the

information needed for specific OR expression is contained with the promoter region (14,152,153). This observation would favor direct transcriptional control of OR genes over the function of broader nuclear organizational proteins like insulators, but does not eliminate the possibility that other chromatin modifiers may recognize specific motifs around OR genes. Nonetheless, uncovering the transcriptional cascades that are activated by prepatterning and proneural transcription factors will be critical to understanding how the restriction of potential is achieved during development. Transcription factors could be partitioned within cell types and across divisions and accumulate at OR promoters to regulate the expression of each OR gene. In order to uncover exactly what these transcriptional programs might be, whole transcriptome sequencing from specific cell types across multiple developmental stages will be necessary. Unbiased approaches will be more informative in this scenario because little is known about the downstream targets of any of the genes in the PD-network (85,87,154–157). In concert with cell type specific assays of chromatin architecture and epigenetic modifications transcriptional profiling can provide a comprehensive model of the molecular mechanisms that drive ORN specification.

5.2.3 Connecting specification and wiring

ORN specification and wiring specificity are intimately connected processes, as evidenced by the fact that all of the neurons that express the same receptor connect to the same glomerulus (18). In addition, mutations that affect prepatterning transcription

factors or Notch-Delta signaling are associated with conversions of one neuronal class to another and correspondingly convert their connectivity pattern as well (8,42). While the connection between these two programs is obvious, it is also clear that these programs diverge at some point during development. The data presented on Chapter 3 and work from others demonstrates that perturbation of wiring programs do not affect ORN specification (68,71,73,76,158). Conversely, disruptions to some terminal selector transcription factors causes misexpression of ORs but does not change the overall shape and position of glomeruli (52). Other late acting transcription factors, such as Acj6 and Pdm3, do cause generalized disruptions to glomerular shape and positioning unlike the more ordered conversions seen in *rn* mutants (54,123). Most interesting though is *alhambra*. Mutations in *alhambra* convert neurons to a default class within the same sensillum, yet the converted neurons continue to project to their original glomeruli (114). This is a clear decoupling of ORN specification as opposed to maintenance of OR expression as may be the case in the loss of some terminal selector transcription factors.

This begs the question, when during development do these programs decouple and at what point in the transcriptional cascade do they diverge? Not only are targets for prepatterning factors largely unknown, the same holds true for terminal selector transcription factors outside of their OR target genes. Unbiased transcriptional profiling in various mutant conditions across development will also be critical here to identify putative target genes. Genes that control the expression of *alhambra* will be particularly

interesting as they may be the first steps in the divergence of these two interconnected pathways. It is worth noting that Alhambra is only known to function in a limited set of sensilla subtypes, and whether it acts more broadly or whether other similar proteins operate in other sensilla subtypes is an open question as well (114).

5.2.4 Developmental expression and function of DIPs/Dprs

In Chapter 4 we present the temporal expression profiles of the DIP/Dpr family of proteins as well as the ORN class-specific expression for each gene. This class-specific expression data however was only derived from adult flies, therefore providing no information about whether *DIPs* and *dprs* are expressed in a class-specific manner earlier in development. Considering that ORN axon sorting and establishment of ORN wiring patterns are inherently temporal processes and that glomerular formation begins around 40 hrs after puparium formation (APF), analysis of developmental expression patterns will be key to understanding DIP/Dpr function. We found that nearly every *DIP* and *dpr* gene was expressed at 40 hrs APF in our RNA-seq data, making this an excellent time point to begin investigation. Preliminary data suggest that some genes, like *DIP-η*, are expressed in different patterns at 40-50 hrs APF than in the adult.

A few genes were also observed to be expressed at 8 hrs APF, long before ORN axon sorting would begin. It is possible DIPs and Dprs have multiple roles in ORN wiring beyond axon sorting, or that this temporally dynamic expression may also contribute to axon sorting. In such a model, *DIP* and *dpr* expression at early stages could

begin to sort early arriving axons in the antennal lobe and the onset of expression of each subsequent gene further separates each class as it reaches the brain. In this model, not only is the final code of *DIP*/*dpr* expression in each class of neurons critical but so it the code at each developmental stage particularly in relation to neighboring classes of axons. This hypothesis is consistent with the observation that glomerular separation occurs in a sequential manner.

A precise temporal map of the expression of all *DIPs* and *dprs* from 8 hrs APF to adult will likely provide insights not only into DIP and Dpr function but also the regulation of *DIP*/*dpr* expression.

5.2.5 Role of olfactory receptors in controlling ORN wiring

It has long been thought that ORs do not play any role in controlling ORN wiring in Drosophila (19,138). This is distinct from the mammalian olfactory system where G-protein signaling from ORs controls the expression of CSMs to direct both glomerular positioning and axon sorting (64,140). ORs in Drosophila are, however, inverted seven transmembrane domain proteins and instead act primarily as cation channels and therefore do not act primarily through GPCR signaling pathways (20,147,159). Further, *OR* mutants or mutations in the olfactory co-receptor, *orco*, do not visibly disrupt the organization of the antennal lobe (160). Finally, the onset of OR expression has been thought to occur too late to affect wiring decisions (19). The data presented in Chapter 3 argue that some of these conclusions may be incomplete. Namely, we found that

knockdown or overexpression of *DIPs* and *dprs* using *Or-GAL4s* were able to produce cell-autonomous phenotypes, which is the first demonstration that disruptions to ORN wiring can occur with the onset of *OR* expression. We also found that the most consistent phenotypes produced by *Or-GAL4s* were from ORs whose expression begins earliest in development, with later expressing ORs producing phenotypes with low penetrance or no observable phenotypes. Taken together this suggests that wiring decisions, particularly axon sorting, do not terminate prior to the onset of the earliest OR expression.

This still leaves the question of whether ORs or downstream signaling from ORs directly affect the expression of *DIPs* and *dprs*. There may be some sets of *DIPs* and *dprs* that are under the control of ORs and some that are not, particularly because the expression of many *DIPs* and *dprs* begins before *OR* expression. Investigations of whether ORs regulate wiring will likely require more complex genetic contexts than simple *OR* mutants. In combination with *DIP* or *dpr* knockdown *OR* mutations may uncover wiring defects not previously seen in *OR* mutants alone. With developmental expression data for each *DIP* and *dpr* such investigations could provide significant insights into how temporal and class-specific information is coordinated to achieve the wiring patterns observed in the antennal lobe.

5.2.6 Modeling ORN specification and wiring

In order to test the completeness creating models of olfactory system development will be necessary. These models should be able to recapitulate several key factors of the adult olfactory system. First, models of ORN specification should be able to reproduce all of the ORN fates, properly grouped into the correct sensilla subtypes and ideally predict the number correct of neurons for each class as well. Models of ORN wiring should recapitulate the positional relationships of glomeruli in the antennal lobe, thereby creating an accurate map of neighboring glomeruli. Second, they should be able to accurately represent mutant conditions during loss of an input factor.

As previously discussed, existing models, including those presented here are obviously incomplete as they do not meet either of these conditions. Not only is the identification of as yet unknown regulators of each process necessary to complete each model, but also modeling the modes of interactions between these proteins and the consequences of those interactions will be critical. It is also likely that analysis of a single developmental stage will be insufficient to accurately model both processes, and temporal information from all developmental stages will need to be incorporated in the model, adding further complexity. Generating such models can do more than provide important theories of olfactory system development and the mechanisms that underlie it, they can also point towards specific gaps in knowledge based upon the specific ways in which they do not meet the above conditions. Computational modeling along with

conventional biological approaches will be a critical method to advance our understanding of the logic and mechanisms that control olfactory system development going forward.

Appendix A: Supporting Text for Chapter 2

Explanation for the model in Fig 13B:

First, we wanted to use our model to explain the *rn* mutant phenotype. In the *rn* mutant imaginal disc, *Bar* is de-repressed and expression expands outside of the central fold, but this expansion respects the boundary between R(3) and R(4) (Fig 7E). Consequently, the new proximal limit of Bar is abutted by the distal limit of Dac. Another prominent phenotype is the reduction of Bab expression due to the lack of Rn activation, resulting in a shallower concentration gradient (Fig 7F, G). The combined effects, along with the loss of Rn, alter the combinatorial code of transcription factor expression for each ring. In particular, R(2) and the proximal part of R(3) become Dac only, converting the precursor potentials to R(1) potentials. We found that this conversion in precursor fates can explain the loss of ai1, ab7 and ab10 subtypes and the expansion of ab1 and ab9 observed in *rn* mutants (42). Although we do not have markers to show the origins of sensilla subtype conversions, we suspect that ab7 and ab10 may be converted to ab9 within the small basiconic sub-lineage, and ai1 might be converted to ab1. The precursors in the distal part of R(3) may die because of an invalid code.

Further, the code in R(5) is changed to the same one as in R(6), particularly because the decrease in Bab brings its level in R(5) closer to the level in R(6), while R(6) itself is Rn-independent and thus unaffected. This change leads to the loss of R(5) and

expansion of R(6). Meanwhile, the ectopic Bar in R(4) changes its code to Bab and Bar. We could not, however, detect expansion of Ap in R(4) (Fig 14A). It is possible that in this context Ap is not required because Rn is not present to repress *Bar*. Therefore, Bab and Bar expression in R(4) in *rn* mutants is equal to the code in R(6), and is sufficient to specify R(6) fates. Consistent with this argument, Ap function is not required for the specification of ac2 or at4 sensilla subtypes (Fig 20B), which are generated from R(6) according to our model. Based on this reasoning, it would appear that the major function of Ap is to protect Bar from being repressed by Rn in the quadruple positive zone R(5) consistent with previous reports (84,87,156). This function does not occur at the transcriptional level, but is perhaps mediated by formation of a complex with Bar and/or Rn to counteract Rn's repressive function. Consistently, Ap has been shown to interact with Bar in a protein complex (84,156). Therefore, our model can explain the loss of at1, at3, ab5, ac4 and ac1 sensilla subtypes from R(4) and R(5), and the expansion of ac2 and at4 normally specified in R(6). Again, we speculate that the conversions occur within sensilla type lineages: at1 and at3 are converted to at4; ac1 and ac4 are converted to ac2; ab5 might be lost due to an incompatible Bab level. Taken together, our model provides an explanation for lineage-specific conversions in sensilla subtypes found in *rn* mutants by changes in the network code.

Explanation for the model in Fig 14A:

We next wanted to use our model to explain the changes in sensilla subtype composition in *Bar*-overexpressing flies. As *ap* is not activated in ectopic domains in response to *Bar* overexpression (Fig 19B), precursors in R(4) acquire the new code of Rn, Bab, and Bar. Despite the absence of *ap*, this code could be sufficient to confer the fates normally specified in R(5), leading to sensilla subtype conversions from at1, at3 and ab5 to ac4 and ac1. The overexpression of *Bar* in R(5) may inhibit *rn* expression in this ring similar to the context-dependent repression of *rn* by Ap in this ring. It is unclear whether this repression occurs due to the disappearance of the central fold (Fig 14C). Nevertheless, it would appear that the precursors in R(5) are converted to R(6), causing the endogenous ac4 and ac1 to be converted to ac2 and at4. Accordingly, we saw increases in the transcription of receptors in ac2 and expansion of ORNs in at4 subtypes (Fig 14D, 12). Due to the large numbers of at1, at3 and ab5 being converted to ac4 and ac1, the overall numbers of ac4 and ac1 may still be increased despite the conversion of the endogenous population. Indeed, we found that receptors expressed by these two sensilla are up-regulated in *Bar* overexpression (Fig 14D). We also found that a number of sensilla subtypes from R(7) are increased (Fig 14D). Although we do not have a satisfying explanation for it at the moment, we suspect that the ectopic sensilla may originate from the Bab-positive R(3), in which this new code somehow is competent to induce the fates normally specified in the center of the disc. Lastly, ab10 from R(2) may

be lost due to the toxicity of the new code in this ring, which is consistent with the down-regulation of the tested receptor in ab10.

Explanation for the model in Fig 15A:

When we used *rn*^{89GAL4} to drive *UAS-ap*, we found *rn* expression in R(5) is lost (Fig 20A-C). Due to the code change, R(6) is expanded into R(5), leading to sensilla subtype conversions from ac4 and ac1 to ac2 and at4. In addition, we found *Bar* is expanded close to the R(3) and R(4) boundary (Fig 15C, 20D). As a result, the cells in the proximal portion of R(4) express *rn*, *bab* and *ap* (Fig 20B, D). We think that this subpopulation of cells may be converted to fates in R(7) in this line, because: 1) qPCR results showed that some sensilla subtypes from R(7) are increased; 2) all sensilla subtypes from R(4) are significantly reduced; 3) the new code is similar to that in R(7), except that it contains Rn (Fig 15A). One explanation for why the presence of Rn does not interfere with the rest of the factors specifying R(7) fates is that Ap may interact with Rn to counteract its function (84,156). On the other hand, the cells in the distal half of R(4) become quadruple positive for factors normally found in R(5), resulting in sensilla subtype conversions from at1, at3 and ab5 to ac4 and ac1. We noticed that ac4 and ac1 are changed in opposite directions (Fig 15D). This is likely caused by endogenous cells in R(5) being further converted to the fates in R(6) as mentioned earlier. The differences in cell numbers that are converted during this relay may account for the different

phenotypes for these two sensilla subtypes. Furthermore, sensilla subtypes from R(6) are increased and the corresponding glomeruli appear bigger in the overexpression line (Fig 19D, data not shown).

We have shown that *dac* levels are reduced in R(2) and R(3), and we deduced that *bab* expression should be elevated, despite our inability to detect changes in Bab expression. Based on our findings about the function of *bab* concentration gradients (see a later section in the main text), we think that this hypothetical de-repression of Bab may cause ai1, which requires lower levels of *bab*, to be converted to ab7, requiring higher levels of Bab, in R(3). However, it is unclear why the overexpression of *ap* in this domain does not affect ab7 specification. Finally, ab10 sensilla are dramatically reduced in *ap* overexpression (Fig 15D). This may be due to some toxic effect of this non-existing code, such as the blocking of Rn function by Ap leaving only low levels of *dac*, which is insufficient to specify any fate. Taken together, the proposed model can by and large explain the ORN phenotypes seen in *ap* overexpression flies.

An interesting phenomenon is that, even though *Bar* expansion is a critical contributor to the *rn* mutant phenotype, and indeed many sensilla subtypes in the *ap*/*Bar* overexpression lines show similar changes to those in *rn* mutants, the causes are very different in these situations based on our model. Because of the intercalated patterns of these transcription factors, changes to one factor often lead to a domino effect involving

many neighboring domains. In this sense, the similar phenotypes described above are essentially incidental and occur through distinct mechanisms.

Appendix B: Supplemental Tables for Chapter 3

Table 4: Transcripts with the top 50 scores for PC1 from PCA. Red line demarcates those transcripts with an absolute value greater 0.1 and those reported in the text.

Transcript Contribution to PC1		
Transcript	Gene	PC1 Coefficient
mt:CoI-RA	*mt:CoI*	0.362670056
Obp19d-RB	*Obp19d*	0.290916706
Obp19d-RA	*Obp19d*	0.290763774
mt:CoIII-RA	*mt:CoIII*	0.242858693
CG6409-RB	*CG6409*	0.194723886
CG6409-RA	*CG6409*	0.194508731
Osi3-RB	*Osi3*	-0.184806678
FBtr0100884		0.169408851
CG13023-RB	*CG13023*	-0.164344623
Osi3-RA	*Osi3*	-0.163685827
CG13023-RA	*CG13023*	-0.1626694
Jhedup-RA	*Jhedup*	0.1146772
a10-RA	*a10*	0.114238908
Os-C-RC	*Os-C*	0.111286772
Os-C-RB	*Os-C*	0.107051301
Os-C-RD	*Os-C*	0.104405402
Osi7-RA	*Osi7*	-0.101164687
Obp83a-RA	*Obp83a*	0.095235435
Msr-110-RB	*Msr-110*	0.09172122
Msr-110-RA	*Msr-110*	0.091157394
Msr-110-RD	*Msr-110*	0.090056284
Obp83a-RC	*Obp83a*	0.089699698
CG4702-RA	*CG4702*	-0.085953975
CG4702-RB	*CG4702*	-0.082721823
Ef1alpha48D-RA	*Ef1alpha48D*	-0.081407585
CG4702-RD	*CG4702*	-0.079550973

CG4702-RC	*CG4702*	-0.078226925
Drsl5-RA	*Drsl5*	0.07820147
Osi9-RA	*Osi9*	-0.076527259
Obp83b-RA	*Obp83b*	0.076335692
CG9497-RB	*CG9497*	0.075958907
mt:CoII-RA	*mt:CoII*	0.074265724
CG9497-RA	*CG9497*	0.073591802
Obp83a-RB	*Obp83a*	0.073051222
Ef1alpha48D-RC	*Ef1alpha48D*	-0.072398883
Ef1alpha48D-RE	*Ef1alpha48D*	-0.072303156
Ef1alpha48D-RD	*Ef1alpha48D*	-0.072288726
Msr-110-RC	*Msr-110*	0.072159813
OS9-RB	*OS9*	0.06144339
FBtr0100867		0.058082834
CG14661-RB	*CG14661*	0.056730698
CG14661-RA	*CG14661*	0.056418271
Osi22-RA	*Osi22*	-0.055800039
Gasp-RA	*Gasp*	-0.045662543
antdh-RA	*antdh*	0.044873458
Lcp65Ad-RB	*Lcp65Ad*	-0.042965772
Lcp65Ad-RA	*Lcp65Ad*	-0.042021211
Cpr65Ec-RA	*Cpr65Ec*	-0.041758977
CG42331-RC	*CG42331*	-0.040486946
CG42331-RD	*CG42331*	-0.040414238

Table 5: Transcripts with the top 50 scores for PC2 from PCA. Red line demarcates those transcripts with an absolute value greater 0.1 and those reported in the text.

Transcript Contribution to PC2		
Transcript	Gene	PC2 Coefficient
CG1150-RB	*Osi3*	0.300360561
CG1150-RA	*Osi3*	0.266068578
CG13023-RB	*CG13023*	0.265983528
CG13023-RA	*CG13023*	0.263304093
CG10287-RA	*Gasp*	-0.171572661
CG6955-RB	*Lcp65Ad*	-0.165844012
CG1153-RA	*Osi7*	0.164135197
CG6955-RA	*Lcp65Ad*	-0.161994879
CG8634-RA	*Cpr65Ec*	-0.160341131
CG7673-RA	*Edg78E*	-0.150760316
CG7673-RB	*Edg78E*	-0.146614156
CG4702-RA	*CG4702*	0.139333068
CG4702-RB	*CG4702*	0.134086191
CG12164-RB	*CG12164*	-0.131547015
CG12164-RA	*CG12164*	-0.130703699
CG10112-RA	*Cpr51A*	-0.12954384
CG4702-RD	*CG4702*	0.128964073
CG4702-RC	*CG4702*	0.126808953

CG15592-RA	*Osi9*	0.124413984
CG5812-RA	*TwdlT*	-0.123109307
CG34067-RA	*mt:CoI*	0.102257407
CG2150-RA	*CG2150*	-0.0982558
CG8280-RA	*Ef1alpha48D*	-0.095278329
CG8644-RA	*Osi22*	0.090779726
CG8280-RC	*Ef1alpha48D*	-0.083950134
CG8280-RE	*Ef1alpha48D*	-0.083682708
CG8280-RD	*Ef1alpha48D*	-0.083648894
CG8756-RG	*verm*	-0.080279082
CG10534-RA	*Lcp65Ag2*	-0.079826053
CG1668-RB	*Obp19d*	0.078885591
CG1668-RA	*Obp19d*	0.078858445
CG17052-RA	*obst-A*	-0.074158544
CG8756-RH	*verm*	-0.072654798
CG8756-RI	*verm*	-0.070451329
CG10287-RB	*Gasp*	-0.070404551
CG42331-RC	*CG42331*	0.065969717
CG42331-RD	*CG42331*	0.065835873
CG42331-RB	*CG42331*	0.065337439
CG32209-RB	*serp*	-0.06523533
CG34074-RA	*mt:CoIII*	0.062134786

CG32209-RC	*serp*	-0.060155371
CG16884-RA	*CG16884*	-0.059541065
CG17131-RB	*tyn*	0.058556912
CG17131-RC	*tyn*	0.057196056
CG14534-RA	*TwdlE*	-0.055993993
CG17052-RB	*obst-A*	-0.055960598
CG12045-RA	*Cpr100A*	-0.055927268
CG16885-RA	*CG16885*	-0.05474795
CG13731-RB	*CG13731*	-0.054295003
CG32356-RA	*ImpE1*	0.053757324

Table 6: Significantly differentially expressed genes between 3L and p8 stages. Table of significantly differentially expressed genes ($p>10^{-6}$) between 3L and p8, represented by red dots in Fig 25B.

Differentially Expressed Genes (3L vs p8)						
Gene	baseMean	log2FoldChange	lfcSE	stat	pvalue	padj
CG16884	8557	-9.892	0.394	-25.1	7.48E-139	5.84E-135
Edg84A	7927	-10.34	0.417	-24.8	1.18E-135	4.59E-132
TwdlT	16938	-8.271	0.368	-22.5	1.23E-111	3.19E-108
Cpr72Eb	4621	-9.981	0.45	-22.2	5.18E-109	1.01E-105
Cpr100A	8775	-10	0.454	-22	1.57E-107	2.46E-104
CG2150	13212	-9.787	0.458	-21.4	2.06E-101	2.68E-98
CG15212	5648	-10.25	0.49	-20.9	2.88E-97	3.21E-94

CG13722	1750	-8.058	0.39	-20.7	8.24E-95	8.04E-92
Cpr51A	18300	-6.709	0.326	-20.5	7.73E-94	6.70E-91
CG16885	7258	-9.489	0.467	-20.3	1.05E-91	8.22E-89
CG16820	924.9	-7.807	0.444	-17.6	3.57E-69	2.53E-66
Lcp65Ag2	9547	-9.668	0.601	-16.1	3.21E-58	2.09E-55
bnb	717.8	6.2912	0.398	15.81	2.46E-56	1.47E-53
ImpE2	3662	7.4644	0.48	15.54	1.90E-54	1.06E-51
Cpr97Ea	872.7	-9.244	0.607	-15.2	2.19E-52	1.14E-49
CG10657	538.7	-5.961	0.393	-15.2	5.44E-52	2.65E-49
CG32645	393.2	-6.548	0.433	-15.1	9.48E-52	4.35E-49
Cpr47Ec	629.1	-6.609	0.445	-14.8	8.08E-50	3.50E-47
Cpr97Eb	432.3	-8.696	0.59	-14.7	4.13E-49	1.69E-46
Lcp65Ag1	2040	-9.324	0.635	-14.7	9.54E-49	3.72E-46
CG2781	1048	-4.696	0.321	-14.6	2.38E-48	8.85E-46
Gasp	18790	-5.276	0.364	-14.5	1.29E-47	4.57E-45
CG17278	425.2	8.2567	0.6	13.76	4.41E-43	1.50E-40
Lcp65Ag3	1388	-9.164	0.675	-13.6	5.20E-42	1.69E-39
CG31871	691	-8.064	0.597	-13.5	1.39E-41	4.34E-39
CG5873	1499	-5.688	0.423	-13.4	3.54E-41	1.06E-38
Edg78E	621.5	-9.882	0.741	-13.3	1.29E-40	3.73E-38
CG1850	3835	-8.626	0.648	-13.3	2.11E-40	5.89E-38
CG1124	1550	-7.749	0.585	-13.2	4.92E-40	1.32E-37

Hsp67Bc	789.4	-5.449	0.42 2	-12.9	4.41E-38	1.15E-35
obst-A	4474	-5.418	0.42 3	-12.8	1.67E-37	4.20E-35
Lcp65Ad	681.3	-11.06	0.87 2	-12.7	8.05E-37	1.96E-34
CG13731	4559	-8.035	0.63 7	-12.6	1.97E-36	4.65E-34
CG9737	199.2	-6.433	0.52 4	-12.3	1.23E-34	2.82E-32
CG6142	375.1	-5.591	0.45 6	-12.3	1.28E-34	2.85E-32
CG32241	606	-8.486	0.69 2	-12.3	1.41E-34	3.06E-32
Npc2b	339.3	-5.436	0.44 6	-12.2	4.14E-34	8.73E-32
scrt	619.9	-5.654	0.46 5	-12.2	4.82E-34	9.89E-32
CG8736	612.4	-9.987	0.83	-12	2.39E-33	4.79E-31
CG6426	212	-5.856	0.48 8	-12	3.32E-33	6.49E-31
pgant8	208.9	-5.367	0.45	-11.9	8.30E-33	1.58E-30
yellow-h	957.2	-6.62	0.56 3	-11.8	6.83E-32	1.27E-29
ru	217.2	-5.073	0.43 3	-11.7	1.07E-31	1.95E-29
CG8646	241.3	-7.335	0.63 1	-11.6	3.36E-31	5.96E-29
CG30101	1868	-8.48	0.73	-11.6	3.53E-31	6.13E-29
NimC4	473	-9.557	0.83 3	-11.5	1.73E-30	2.93E-28
Cht7	4867	-4.549	0.39 9	-11.4	4.63E-30	7.68E-28
reb	171.6	-6.437	0.57	-11.3	1.35E-29	2.20E-27
CG30197	533.7	-4.462	0.39 8	-11.2	3.10E-29	4.94E-27
CG9134	607.7	-3.871	0.34 6	-11.2	5.26E-29	8.21E-27
CG13928	1456	-3.806	0.34 2	-11.1	7.90E-29	1.21E-26

Cpr78Cc	663	-10.71	0.963	-11.1	9.38E-29	1.41E-26
Cpr65Ec	17019	-9.176	0.833	-11	2.99E-28	4.41E-26
Zip89B	318	-4.413	0.402	-11	4.74E-28	6.85E-26
Ance	187.5	7.9454	0.724	10.97	5.43E-28	7.70E-26
TwdlE	1938	-8.055	0.737	-10.9	8.25E-28	1.15E-25
CG9514	344.6	-6.642	0.609	-10.9	9.83E-28	1.35E-25
Syt4	1258	-4.936	0.457	-10.8	3.54E-27	4.76E-25
nerfin-1	139.9	-5.974	0.555	-10.8	4.68E-27	6.19E-25
Inos	445	5.1187	0.483	10.61	2.78E-26	3.61E-24
CG17211	1551	3.759	0.355	10.59	3.47E-26	4.43E-24
CG11275	469.4	4.3083	0.407	10.58	3.65E-26	4.59E-24
CG43386	240.3	-9.178	0.869	-10.6	4.71E-26	5.83E-24
pgant2	182.7	-5.314	0.504	-10.5	5.72E-26	6.98E-24
CG1273	1549	4.963	0.474	10.47	1.13E-25	1.36E-23
Traf4	177.1	-4.08	0.396	-10.3	6.75E-25	7.98E-23
Con	313.8	-7.228	0.702	-10.3	7.13E-25	8.30E-23
CG16798	1136	-4.817	0.468	-10.3	7.64E-25	8.77E-23
CG31176	269.4	-4.147	0.404	-10.3	9.93E-25	1.12E-22
Lcp65Ae	150.9	-8.515	0.833	-10.2	1.65E-24	1.84E-22
ckd	185.2	-4.314	0.436	-9.89	4.46E-23	4.90E-21
CG6836	363.4	-6.076	0.616	-9.87	5.80E-23	6.29E-21
Tsf3	413.2	-4.178	0.424	-9.86	6.27E-23	6.70E-21

CG14397	259.1	-9.886	1.008	-9.81	1.05E-22	1.11E-20
CG6024	229.2	-6.033	0.624	-9.67	3.92E-22	4.08E-20
CG2556	788.2	-3.463	0.359	-9.64	5.66E-22	5.81E-20
Dfd	91.82	5.6827	0.593	9.587	9.05E-22	9.16E-20
mamo	876.7	-4.111	0.429	-9.59	9.16E-22	9.16E-20
rdx	778.6	-2.822	0.296	-9.54	1.36E-21	1.34E-19
CG14107	322.3	-8.291	0.87	-9.53	1.50E-21	1.46E-19
serp	732.2	-6.446	0.676	-9.53	1.58E-21	1.52E-19
CG15628	220.7	-4.204	0.441	-9.52	1.68E-21	1.60E-19
CG17386	138.7	-8.723	0.917	-9.51	1.90E-21	1.78E-19
CG17646	160.3	-5.194	0.554	-9.37	6.99E-21	6.49E-19
boss	410.2	-6.377	0.681	-9.37	7.36E-21	6.76E-19
Cda5	97.96	-5.035	0.54	-9.32	1.13E-20	1.02E-18
amos	142.7	-7.964	0.856	-9.31	1.31E-20	1.17E-18
tld	104.5	4.8462	0.522	9.289	1.56E-20	1.38E-18
CG7966	272.1	-3.778	0.415	-9.11	7.97E-20	6.98E-18
CG8568	263.6	-6.316	0.694	-9.11	8.50E-20	7.37E-18
SP2353	973.2	-5.068	0.557	-9.09	9.65E-20	8.28E-18
Cad88C	165.1	-4.582	0.506	-9.05	1.42E-19	1.20E-17
Gfat1	279.6	-3.432	0.38	-9.03	1.73E-19	1.45E-17
CG3831	68.35	-5.147	0.575	-8.95	3.47E-19	2.88E-17
dati	117.6	-7.914	0.885	-8.95	3.71E-19	3.05E-17

Kr-h1	161.6	7.7812	0.871	8.937	3.98E-19	3.24E-17
futsch	215.5	-5.253	0.59	-8.91	5.16E-19	4.15E-17
klg	327.8	-4.699	0.53	-8.86	7.87E-19	6.27E-17
Actbeta	455.3	-4.654	0.529	-8.79	1.44E-18	1.13E-16
mmy	184.3	-9.427	1.075	-8.77	1.77E-18	1.38E-16
Cralbp	139.1	-4.051	0.463	-8.74	2.31E-18	1.79E-16
CG43333	421.8	-3.891	0.447	-8.71	2.96E-18	2.26E-16
CG31728	555.3	6.1632	0.715	8.625	6.43E-18	4.87E-16
CG7402	321	-6.436	0.748	-8.61	7.62E-18	5.72E-16
CG1368	5105	-6.394	0.744	-8.59	8.46E-18	6.29E-16
pog	271.5	-6.403	0.749	-8.55	1.27E-17	9.34E-16
CR44024	524.9	-4.468	0.523	-8.54	1.31E-17	9.53E-16
CG32006	582.4	-4.78	0.56	-8.53	1.41E-17	1.02E-15
CG4928	2143	-3.434	0.404	-8.5	1.96E-17	1.40E-15
CG14692	1981	-4.964	0.585	-8.49	2.01E-17	1.43E-15
CG14688	95.19	-4.396	0.518	-8.48	2.29E-17	1.61E-15
CG10264	86.07	-7.591	0.898	-8.46	2.76E-17	1.92E-15
CR45952	105.8	-9.088	1.075	-8.45	2.81E-17	1.94E-15
Ugt86Da	446.6	3.0646	0.364	8.43	3.45E-17	2.36E-15
CG9876	99.64	-8.236	0.977	-8.43	3.53E-17	2.40E-15
gogo	213.7	-3.784	0.453	-8.36	6.23E-17	4.19E-15
sens	206.1	-3.303	0.397	-8.33	8.20E-17	5.47E-15

dpr20	194.4	-4.687	0.569	-8.24	1.66E-16	1.10E-14
CG12164	160.3	-10.74	1.307	-8.22	2.04E-16	1.34E-14
CG17786	1131	-3.502	0.427	-8.21	2.22E-16	1.44E-14
CG31522	60.23	-4.925	0.601	-8.19	2.64E-16	1.70E-14
Cow	539.3	-4.611	0.564	-8.17	3.05E-16	1.95E-14
CG10936	1735	-2.63	0.322	-8.16	3.27E-16	2.08E-14
CG10237	176.9	-4.88	0.604	-8.08	6.33E-16	3.98E-14
mthl4	91.06	3.6074	0.449	8.035	9.35E-16	5.84E-14
Mlc2	694.4	5.5134	0.686	8.032	9.56E-16	5.92E-14
HnRNP-K	576.1	-2.838	0.354	-8.01	1.16E-15	7.10E-14
dnd	281	-4.22	0.527	-8.01	1.18E-15	7.19E-14
CG30380	86.39	-5.65	0.713	-7.92	2.38E-15	1.44E-13
y	55.92	-5.625	0.713	-7.89	3.05E-15	1.83E-13
CG30069	6838	-2.544	0.328	-7.76	8.47E-15	5.05E-13
fd3F	73.25	-4.238	0.552	-7.68	1.61E-14	9.53E-13
Apoltp	170.1	-5.014	0.655	-7.66	1.93E-14	1.13E-12
brk	262.3	2.5265	0.331	7.632	2.30E-14	1.34E-12
peb	221.1	-4.335	0.57	-7.61	2.72E-14	1.57E-12
rk	109.2	-3.298	0.437	-7.55	4.40E-14	2.52E-12
ths	541.1	-3.178	0.422	-7.52	5.27E-14	3.00E-12
opa	84.45	3.726	0.497	7.501	6.35E-14	3.59E-12
kek2	221.6	-4.78	0.639	-7.48	7.53E-14	4.23E-12

CG30377	44.33	-5.919	0.792	-7.47	7.97E-14	4.44E-12
CG4525	199.6	-6.182	0.828	-7.47	8.07E-14	4.46E-12
ect	4742	-3.209	0.43	-7.46	8.47E-14	4.65E-12
wmd	277.7	-3.125	0.419	-7.45	9.04E-14	4.93E-12
Spn100A	5851	3.4019	0.457	7.444	9.76E-14	5.29E-12
CG15615	71.76	-8.454	1.141	-7.41	1.24E-13	6.68E-12
CG12947	74.1	-3.957	0.535	-7.4	1.36E-13	7.26E-12
sog	143.7	3.7749	0.51	7.395	1.42E-13	7.53E-12
PPO1	109	8.4531	1.144	7.389	1.48E-13	7.80E-12
caup	49.43	4.1432	0.562	7.376	1.63E-13	8.55E-12
CG13856	171.6	-4.447	0.603	-7.37	1.72E-13	8.96E-12
CG14752	2353	-9.167	1.247	-7.35	1.93E-13	9.99E-12
ase	98.71	-3.8	0.518	-7.33	2.31E-13	1.18E-11
lectin-28C	34.53	-5.183	0.714	-7.26	3.87E-13	1.97E-11
CG12507	1599	-4.428	0.615	-7.19	6.26E-13	3.17E-11
RapGAP1	484.2	-3.01	0.419	-7.18	6.78E-13	3.41E-11
dyl	1196	-5.675	0.79	-7.18	6.89E-13	3.45E-11
Pvf2	292	-3.097	0.432	-7.16	7.80E-13	3.85E-11
CG13436	96.04	-3.569	0.498	-7.16	7.80E-13	3.85E-11
Blimp-1	436.7	4.5009	0.629	7.157	8.24E-13	4.04E-11
Snmp2	41.31	-7.089	0.991	-7.15	8.60E-13	4.19E-11
sca	620.9	-3.166	0.443	-7.14	9.40E-13	4.56E-11

gsb	41.41	5.9144	0.831	7.12	1.08E-12	5.20E-11
CG3769	121.7	-5.47	0.77	-7.1	1.24E-12	5.95E-11
CG15213	85.91	-9.927	1.406	-7.06	1.65E-12	7.86E-11
msi	464	-2.93	0.416	-7.05	1.84E-12	8.71E-11
CG3556	912.3	-3.49	0.497	-7.02	2.22E-12	1.04E-10
Timp	467.7	-2.287	0.327	-7	2.60E-12	1.21E-10
laccase2	719.6	-2.918	0.417	-7	2.64E-12	1.23E-10
CG30438	182.4	-4.164	0.598	-6.97	3.28E-12	1.51E-10
CG5326	569.5	-3.046	0.438	-6.96	3.52E-12	1.62E-10
Osm6	175.1	-4.426	0.638	-6.94	4.04E-12	1.84E-10
CG6980	57.26	-4.721	0.683	-6.91	4.77E-12	2.17E-10
CG43164	687.1	3.0987	0.448	6.91	4.85E-12	2.19E-10
Cda4	2585	-2.768	0.402	-6.89	5.67E-12	2.54E-10
gsb-n	47.54	4.5899	0.667	6.885	5.79E-12	2.58E-10
CG32694	116.4	-8.3	1.207	-6.88	6.10E-12	2.71E-10
Sgs7	71.88	7.9555	1.159	6.863	6.75E-12	2.97E-10
CG14234	141.6	-3.744	0.546	-6.86	6.79E-12	2.97E-10
SPH93	45.92	-4.621	0.673	-6.86	6.81E-12	2.97E-10
CG34227	52.27	7.7492	1.132	6.848	7.47E-12	3.24E-10
CG14301	388.2	-2.274	0.334	-6.81	9.46E-12	4.08E-10
GILT2	34.13	-5.21	0.766	-6.8	1.04E-11	4.47E-10
CG33939	50.02	4.2234	0.622	6.786	1.16E-11	4.93E-10

CG14905	83.96	-5.799	0.857	-6.77	1.31E-11	5.54E-10
Pkc53E	122.3	-5.84	0.866	-6.74	1.54E-11	6.51E-10
fru	398.3	2.7279	0.405	6.738	1.60E-11	6.71E-10
TbCMF46	65.98	-6.588	0.978	-6.74	1.61E-11	6.71E-10
CG13024	53.3	-4.122	0.614	-6.71	1.90E-11	7.90E-10
edl	466.9	-2.42	0.361	-6.7	2.10E-11	8.68E-10
wrapper	96.8	-3.174	0.474	-6.69	2.26E-11	9.27E-10
qua	51.03	-6.16	0.922	-6.68	2.39E-11	9.77E-10
lh	99.72	-5.997	0.898	-6.68	2.40E-11	9.77E-10
Neurochondrin	113.1	4.9919	0.749	6.663	2.69E-11	1.09E-09
Cyp4e1	246.5	-2.973	0.447	-6.66	2.81E-11	1.13E-09
Ccp84Ab	149.7	-6.667	1.002	-6.65	2.92E-11	1.17E-09
CG8483	537.6	-2.387	0.36	-6.63	3.45E-11	1.37E-09
Ace	513.2	-3.864	0.584	-6.62	3.60E-11	1.43E-09
kirre	243.4	-3.036	0.459	-6.62	3.68E-11	1.45E-09
Lcp65Ac	182.3	-6.205	0.939	-6.61	3.87E-11	1.52E-09
beat-IIIc	212.8	-3.01	0.455	-6.61	3.91E-11	1.53E-09
CG10527	396.1	3.3124	0.502	6.603	4.03E-11	1.57E-09
CG13082	1356	4.4095	0.668	6.599	4.13E-11	1.60E-09
mab-21	604.3	2.0248	0.308	6.582	4.65E-11	1.79E-09
CG34409	76.48	-3.684	0.561	-6.57	5.11E-11	1.95E-09
CG15630	270.5	-2.812	0.428	-6.57	5.12E-11	1.95E-09

Eig71Ee	57.83	6.6583	1.017	6.549	5.81E-11	2.20E-09
Obp56a	5485	3.5392	0.544	6.5	8.01E-11	3.02E-09
Cad89D	2404	-3.185	0.492	-6.47	1.00E-10	3.75E-09
CG42327	890.3	-1.974	0.307	-6.44	1.21E-10	4.53E-09
nrm	156.8	-2.86	0.444	-6.44	1.22E-10	4.54E-09
tipE	149.4	-6.357	0.99	-6.42	1.37E-10	5.05E-09
GstZ2	171.5	-3.058	0.48	-6.38	1.82E-10	6.70E-09
Sgs3	71.11	7.6711	1.203	6.375	1.83E-10	6.70E-09
PPO2	150.4	4.7995	0.753	6.374	1.84E-10	6.73E-09
Ilp6	82.81	-2.996	0.471	-6.36	2.00E-10	7.26E-09
CG6405	95.94	-3.591	0.565	-6.36	2.04E-10	7.37E-09
CG14367	432.2	-3.417	0.538	-6.35	2.17E-10	7.80E-09
repo	181.6	-2.661	0.42	-6.34	2.27E-10	8.14E-09
St2	100	-2.831	0.447	-6.34	2.35E-10	8.37E-09
CG8180	87.55	-2.995	0.473	-6.33	2.47E-10	8.76E-09
CG31103	153.1	6.1912	0.983	6.295	3.07E-10	1.08E-08
Cpr65Eb	68.26	-6.734	1.07	-6.29	3.13E-10	1.10E-08
alphagamma-element:CR32865	269.5	-3.927	0.626	-6.27	3.50E-10	1.23E-08
Lim1	200.8	2.3896	0.382	6.257	3.93E-10	1.37E-08
CG31100	71.67	-6.378	1.019	-6.26	3.96E-10	1.37E-08
CrebA	179.9	2.3655	0.38	6.231	4.62E-10	1.58E-08
Rab3	635.7	-3.068	0.492	-6.23	4.64E-10	1.58E-08

CG3777	31.11	-4.945	0.794	-6.23	4.65E-10	1.58E-08
elav	830.8	-2.611	0.419	-6.23	4.65E-10	1.58E-08
Ror	165.8	-2.992	0.48	-6.23	4.73E-10	1.60E-08
Spec2	385	-2.042	0.328	-6.23	4.78E-10	1.62E-08
CG5888	57.24	-3.396	0.546	-6.22	4.95E-10	1.66E-08
CG13532	124.6	-3.897	0.627	-6.21	5.25E-10	1.76E-08
Btk29A	171.4	-2.733	0.441	-6.2	5.54E-10	1.85E-08
Dscam1	89.82	-3.602	0.581	-6.2	5.65E-10	1.88E-08
CenG1A	163	-2.41	0.389	-6.19	5.86E-10	1.94E-08
CG17150	111.2	-7.138	1.156	-6.18	6.52E-10	2.15E-08
Cpr92A	116.1	5.9631	0.966	6.171	6.80E-10	2.23E-08
CG9990	135.9	-2.537	0.412	-6.16	7.07E-10	2.31E-08
Rcd2	209.1	-2.857	0.465	-6.15	7.77E-10	2.53E-08
CG18675	45.65	-6.333	1.032	-6.14	8.33E-10	2.70E-08
Dif	338.7	-3.095	0.505	-6.13	8.60E-10	2.77E-08
Osi2	84.93	-5.656	0.927	-6.1	1.04E-09	3.35E-08
EbpIII	1061	-3.68	0.605	-6.08	1.20E-09	3.83E-08
CG2975	52.35	-3.174	0.522	-6.08	1.20E-09	3.83E-08
Lst	22.71	-5.331	0.88	-6.05	1.41E-09	4.46E-08
CG32447	49.44	3.5718	0.592	6.038	1.57E-09	4.94E-08
wb	49.41	-3.422	0.567	-6.03	1.64E-09	5.15E-08
Crg-1	68.69	-3.147	0.522	-6.03	1.67E-09	5.25E-08

CG15249	29.33	-8.317	1.383	-6.01	1.84E-09	5.73E-08
CG4580	31.47	-6.773	1.128	-6	1.92E-09	5.96E-08
btv	681.8	-2.581	0.431	-5.99	2.13E-09	6.60E-08
Cpr35B	43.18	-9.272	1.553	-5.97	2.38E-09	7.33E-08
CG14946	28.56	-3.954	0.664	-5.95	2.61E-09	8.02E-08
tsh	160.7	2.2901	0.385	5.941	2.83E-09	8.67E-08
CG13699	161	-3.423	0.576	-5.94	2.86E-09	8.71E-08
CycE	56.48	-3.152	0.531	-5.93	2.98E-09	9.03E-08
Osi7	22460	-2.228	0.376	-5.93	2.98E-09	9.03E-08
CG12998	28.06	-8.587	1.453	-5.91	3.46E-09	1.04E-07
spz3	229.6	-2.155	0.365	-5.9	3.64E-09	1.09E-07
Lmpt	54.73	-3.134	0.532	-5.89	3.84E-09	1.15E-07
CG16886	30.05	-8.436	1.433	-5.89	3.95E-09	1.18E-07
CG40006	1619	-2.82	0.479	-5.88	3.99E-09	1.18E-07
CG11409	68.12	-4.025	0.684	-5.88	4.02E-09	1.19E-07
CG18472	58.22	-3.942	0.672	-5.87	4.34E-09	1.27E-07
Ir75a	224.4	-7.049	1.201	-5.87	4.34E-09	1.27E-07
Eip93F	34.85	-7.315	1.246	-5.87	4.35E-09	1.27E-07
CR43436	20.22	-5.216	0.889	-5.87	4.44E-09	1.29E-07
jeb	322.3	-3.615	0.616	-5.87	4.47E-09	1.29E-07
CG10005	48.25	2.9793	0.508	5.866	4.47E-09	1.29E-07
dpr6	48.28	-3.573	0.61	-5.86	4.63E-09	1.33E-07

CG32428	279.8	-2.374	0.406	-5.84	5.12E-09	1.47E-07
E(spl)m6-BFM	34.06	-3.661	0.627	-5.84	5.26E-09	1.50E-07
CG2736	29.83	-4.687	0.803	-5.84	5.37E-09	1.53E-07
Fatp	84.78	-3.549	0.609	-5.83	5.69E-09	1.61E-07
cv-d	283.6	-2.29	0.393	-5.82	5.80E-09	1.64E-07
CG7294	33.38	7.9308	1.364	5.815	6.07E-09	1.71E-07
CG11041	140.2	-4.771	0.821	-5.81	6.22E-09	1.75E-07
Sgs4	38.97	8.1476	1.404	5.802	6.54E-09	1.83E-07
CG15161	131.1	-5.605	0.969	-5.78	7.31E-09	2.04E-07
hbs	263.2	-2.565	0.445	-5.77	8.07E-09	2.24E-07
alt	59.78	3.2382	0.562	5.764	8.21E-09	2.27E-07
CG5391	139.7	7.0653	1.226	5.762	8.29E-09	2.29E-07
CG42389	1095	-2.272	0.394	-5.76	8.32E-09	2.29E-07
tap	21	-6.911	1.203	-5.74	9.31E-09	2.55E-07
CG4374	156.6	-2.459	0.429	-5.73	9.79E-09	2.67E-07
CG13293	109.5	-3.204	0.56	-5.72	1.05E-08	2.86E-07
Cbp53E	218	-4.533	0.793	-5.71	1.10E-08	2.98E-07
CG34196	25.49	-8.791	1.544	-5.69	1.25E-08	3.38E-07
rha	57.35	-3.92	0.689	-5.69	1.27E-08	3.42E-07
Tie	1572	-1.911	0.336	-5.68	1.34E-08	3.59E-07
Poxm	24.28	-7.31	1.288	-5.68	1.37E-08	3.66E-07
CG42326	83.91	-3.624	0.639	-5.67	1.42E-08	3.79E-07

kni	38.31	4.6942	0.828	5.667	1.45E-08	3.85E-07
Cpr49Ah	334.5	3.8008	0.671	5.663	1.49E-08	3.92E-07
CG4500	26.06	-5.05	0.892	-5.66	1.49E-08	3.92E-07
Spn28Dc	719.7	-2.384	0.421	-5.66	1.50E-08	3.94E-07
Listericin	43.99	7.5782	1.341	5.652	1.58E-08	4.14E-07
fat-spondin	287.5	-2.775	0.491	-5.65	1.64E-08	4.28E-07
Hipk	1958	-2.239	0.397	-5.64	1.68E-08	4.38E-07
Lrch	107.8	-2.9	0.515	-5.63	1.76E-08	4.55E-07
Cpr72Ea	244.4	-4.019	0.714	-5.63	1.84E-08	4.75E-07
CG13067	33.13	-7.308	1.299	-5.63	1.85E-08	4.77E-07
Cpr65Ax2	24.11	-8.704	1.551	-5.61	1.98E-08	5.09E-07
CG17108	540.3	5.1666	0.926	5.578	2.43E-08	6.23E-07
lbk	596.6	1.668	0.299	5.572	2.52E-08	6.43E-07
Tsp5D	64.05	-5.562	0.999	-5.57	2.54E-08	6.46E-07
CG17075	296.2	-2.97	0.534	-5.56	2.71E-08	6.85E-07
CG14085	162.3	-4.785	0.862	-5.55	2.82E-08	7.11E-07
lobo	27.96	-4.574	0.824	-5.55	2.85E-08	7.17E-07
VAChT	805.9	-3.381	0.609	-5.55	2.86E-08	7.17E-07
CG9782	1886	-2.312	0.417	-5.54	3.05E-08	7.64E-07
Cpr64Ad	40.21	-6.779	1.225	-5.53	3.12E-08	7.77E-07
CG32369	168.3	-2.257	0.408	-5.53	3.16E-08	7.84E-07
aay	814.1	-2.143	0.389	-5.51	3.51E-08	8.68E-07

CG32793	22.7	4.5652	0.832	5.487	4.09E-08	1.01E-06
Ran	27.5	-3.92	0.718	-5.46	4.69E-08	1.15E-06
Cpr65Ea	322	-7.779	1.425	-5.46	4.80E-08	1.18E-06
CG30419	54.84	-5.529	1.015	-5.45	5.07E-08	1.24E-06
knrl	74.45	3.3838	0.622	5.443	5.24E-08	1.28E-06
Dhc16F	71.5	-4.755	0.874	-5.44	5.38E-08	1.31E-06
ken	587.8	-2.031	0.374	-5.44	5.44E-08	1.32E-06
CG13972	77.36	-4.087	0.752	-5.43	5.49E-08	1.33E-06
Cyp301a1	871.5	-2.163	0.398	-5.43	5.50E-08	1.33E-06
magu	61.03	2.4723	0.455	5.431	5.60E-08	1.34E-06
CG6329	442.4	-3.927	0.724	-5.42	5.84E-08	1.40E-06
obst-E	281.7	-4.481	0.828	-5.41	6.18E-08	1.47E-06
Edg91	40.28	-8.489	1.569	-5.41	6.34E-08	1.51E-06
CG14291	974.8	2.3116	0.428	5.403	6.55E-08	1.55E-06
CG17669	42.37	-4.169	0.772	-5.4	6.60E-08	1.56E-06
CG42711	43.25	-3.605	0.668	-5.4	6.71E-08	1.58E-06
spdo	90.81	-2.732	0.506	-5.4	6.75E-08	1.59E-06
CG9503	177.1	2.5127	0.467	5.384	7.28E-08	1.71E-06
Sox100B	23.22	-6.969	1.296	-5.38	7.63E-08	1.78E-06
CG15005	159.3	4.1279	0.769	5.367	8.01E-08	1.86E-06
mim	86.97	-2.967	0.553	-5.36	8.33E-08	1.93E-06
Sgs8	25.93	6.3801	1.191	5.359	8.37E-08	1.94E-06

CG12310	35.58	7.1359	1.334	5.351	8.74E-08	2.02E-06
sev	246.3	-3.531	0.66	-5.35	8.85E-08	2.04E-06
DIP-epsilon	40.11	-3.746	0.7	-5.35	8.90E-08	2.04E-06
CG17687	75.46	-6.345	1.187	-5.35	9.00E-08	2.06E-06
Tmhs	119.1	-2.175	0.408	-5.33	9.91E-08	2.26E-06
b6	40	-5.35	1.004	-5.33	9.95E-08	2.26E-06
CG17564	35.32	-6.788	1.276	-5.32	1.05E-07	2.37E-06
Idgf4	82.13	5.5573	1.046	5.312	1.09E-07	2.45E-06
htl	43.17	-3.316	0.625	-5.31	1.11E-07	2.51E-06
CG33993	157.8	-2.236	0.421	-5.31	1.11E-07	2.51E-06
tnc	103.9	3.0477	0.575	5.299	1.17E-07	2.62E-06
cv-c	31.22	-3.698	0.698	-5.3	1.18E-07	2.63E-06
Sox15	334	-3.8	0.718	-5.29	1.21E-07	2.70E-06
Rcd6	39.75	-2.811	0.532	-5.29	1.24E-07	2.75E-06
twit	304.4	-3.476	0.658	-5.28	1.26E-07	2.79E-06
CG10126	319.8	-2.324	0.44	-5.28	1.29E-07	2.85E-06
CG12880	2281	1.5968	0.303	5.262	1.42E-07	3.14E-06
CG10208	48.17	3.6295	0.691	5.254	1.49E-07	3.28E-06
CG12605	233.4	-5.044	0.963	-5.24	1.62E-07	3.55E-06
CG9650	37.34	-2.927	0.559	-5.24	1.63E-07	3.57E-06
CG5048	85.88	-6.189	1.185	-5.22	1.77E-07	3.86E-06
mthl1	95.46	-2.573	0.493	-5.21	1.84E-07	4.00E-06

CG2233	69.31	-2.308	0.444	-5.19	2.05E-07	4.45E-06
CR44922	279.2	-4.021	0.776	-5.18	2.17E-07	4.68E-06
CG3097	455.5	-1.977	0.382	-5.18	2.22E-07	4.79E-06
Mf	32.29	5.8947	1.141	5.165	2.40E-07	5.16E-06
SLC5A11	218.2	-2.246	0.435	-5.16	2.41E-07	5.16E-06
GNBP3	1088	1.6877	0.327	5.164	2.42E-07	5.17E-06
CR30009	20.41	-5.103	0.99	-5.15	2.55E-07	5.44E-06
CG4914	674.2	3.7368	0.725	5.151	2.59E-07	5.51E-06
CG14342	132	-5.994	1.164	-5.15	2.64E-07	5.60E-06
CG32365	87.6	-3.307	0.643	-5.15	2.66E-07	5.62E-06
CG7695	147.8	-6.367	1.241	-5.13	2.87E-07	6.05E-06
CG42458	83.38	-3.601	0.703	-5.12	3.00E-07	6.31E-06
CG34136	145.8	-3.818	0.745	-5.12	3.01E-07	6.31E-06
CG12885	46.4	-4.258	0.833	-5.11	3.16E-07	6.61E-06
CG13046	79.27	-2.472	0.484	-5.11	3.23E-07	6.73E-06
CG13737	225.6	-2.503	0.491	-5.1	3.33E-07	6.94E-06
hdc	3106	-2.096	0.411	-5.1	3.44E-07	7.15E-06
sNPF	569.6	-2.64	0.518	-5.1	3.48E-07	7.21E-06
fw	118.1	-2.655	0.522	-5.09	3.58E-07	7.40E-06
CG34115	43.75	-5.128	1.009	-5.08	3.74E-07	7.69E-06
CG43324	80.52	-6.053	1.191	-5.08	3.75E-07	7.69E-06
Che-13	88.97	-4.467	0.881	-5.07	3.93E-07	8.04E-06

CG14947	25.89	-6.458	1.273	-5.07	3.94E-07	8.04E-06
CG6495	200.5	-3.663	0.724	-5.06	4.17E-07	8.50E-06
CR45421	22.46	-3.826	0.756	-5.06	4.18E-07	8.50E-06
CG9850	36.3	-3.1	0.613	-5.06	4.26E-07	8.63E-06
RSG7	395.3	-4.442	0.879	-5.05	4.32E-07	8.73E-06
X11Lbeta	40.16	-5.259	1.041	-5.05	4.41E-07	8.90E-06
Hr4	244.8	2.7203	0.539	5.044	4.55E-07	9.15E-06
CG1698	16.47	-4.912	0.976	-5.03	4.89E-07	9.80E-06
inaC	13.33	-7.021	1.398	-5.02	5.12E-07	1.03E-05
AdamTS-A	44.24	2.6677	0.532	5.017	5.24E-07	1.05E-05
Lsp1alpha	39.27	4.1491	0.827	5.016	5.27E-07	1.05E-05
phyl	167.5	-2.239	0.447	-5.01	5.35E-07	1.06E-05
CG9372	452.9	-2.03	0.406	-5	5.75E-07	1.14E-05
dpn	194.2	-2.164	0.434	-4.99	5.99E-07	1.18E-05
mthl2	40.82	-2.777	0.557	-4.99	6.09E-07	1.20E-05
Eps-15	96.81	-3.47	0.696	-4.99	6.18E-07	1.21E-05
CG31121	160.9	2.0619	0.414	4.977	6.45E-07	1.26E-05
Mp20	18.43	4.8378	0.972	4.975	6.54E-07	1.28E-05
eater	40.83	2.9931	0.602	4.974	6.57E-07	1.28E-05
CG32676	80.25	-5.903	1.187	-4.97	6.58E-07	1.28E-05
CG30259	27.02	-5.316	1.07	-4.97	6.79E-07	1.32E-05
CG1444	171.7	-2.506	0.506	-4.95	7.25E-07	1.40E-05

onecut	56.56	-5.008	1.011	-4.95	7.25E-07	1.40E-05
CG4766	151.4	1.9251	0.389	4.949	7.47E-07	1.44E-05
Ugt35a	193	3.5538	0.718	4.948	7.50E-07	1.44E-05
CG5375	178.1	-2.406	0.487	-4.94	7.94E-07	1.52E-05
CG45263	109.6	-2.885	0.585	-4.93	8.07E-07	1.54E-05
CG10211	29.31	-3.115	0.632	-4.93	8.37E-07	1.60E-05
Sema-5c	149.6	-2.035	0.413	-4.93	8.41E-07	1.60E-05
CG14526	184.9	-3.017	0.613	-4.92	8.68E-07	1.65E-05
Nrk	70.48	-2.137	0.434	-4.92	8.72E-07	1.65E-05
Osi14	25.36	-6.714	1.366	-4.91	8.92E-07	1.68E-05
CG18547	77.91	3.1735	0.646	4.913	8.97E-07	1.69E-05
CG14853	154.4	-4.83	0.984	-4.91	9.13E-07	1.72E-05

Table 7: Significantly differentially expressed genes between p8 and p40 stages. Table of significantly differentially expressed genes ($p>10^{-6}$) between p8 and p40, represented by red dots in Fig 25C.

Differentially Expressed Genes (p8 vs p40)						
Gene	baseMean	log2FoldChange	lfcSE	stat	pvalue	padj
m	6041.94	-9.99663	0.407447	-24.5348	6.29E-133	5.30E-129
Cpr51A	18300.1	7.854489	0.330054	23.79761	3.54E-125	1.49E-121
Osi22	12411.92	-10.7058	0.474712	-22.5521	1.28E-112	3.60E-109
Edg84A	7926.701	8.673675	0.389434	22.2725	6.83E-110	1.44E-106
CG15888	5660.568	-10.468	0.470562	-22.2458	1.24E-109	2.09E-106

Osi12	5979.015	-9.70212	0.440126	-22.044	1.09E-107	1.53E-104
Osi7	22459.85	-7.88605	0.360275	-21.889	3.31E-106	3.99E-103
Cpr100A	8774.925	9.497286	0.450767	21.06917	1.53E-98	1.61E-95
Osi3	5746.283	-8.65129	0.412757	-20.9598	1.53E-97	1.43E-94
CG18735	3420.868	-10.7509	0.514921	-20.8787	8.36E-97	7.05E-94
Cpr72Eb	4620.952	8.881758	0.426911	20.80469	3.93E-96	3.01E-93
Spn100A	5850.659	-9.22425	0.454597	-20.291	1.54E-91	1.08E-88
Osi1	2859.681	-9.96093	0.495149	-20.117	5.23E-90	3.40E-87
CG32354	7035.807	-7.52098	0.377966	-19.8985	4.19E-88	2.52E-85
Obp56a	5485.198	-10.6223	0.539306	-19.6962	2.32E-86	1.31E-83
dsx-c73A	6308.554	-10.2541	0.521522	-19.6619	4.57E-86	2.41E-83
Osi8	3091.045	-10.0293	0.512785	-19.5585	3.49E-85	1.73E-82
CG15212	5648.481	9.156547	0.468963	19.5251	6.72E-85	3.15E-82
CG17211	1550.979	-6.82537	0.353449	-19.3107	4.36E-83	1.94E-80
CG4386	2390.303	-9.17385	0.475859	-19.2785	8.14E-83	3.43E-80
dy	4486.985	-8.2432	0.428677	-19.2294	2.10E-82	8.43E-80
CG13631	1419.25	-7.8785	0.409797	-19.2254	2.27E-82	8.71E-80
Osi11	1432.993	-8.01646	0.418972	-19.1336	1.33E-81	4.86E-79
ect	4741.583	-6.86176	0.365545	-18.7713	1.30E-78	4.56E-76
CG1273	1549.075	-8.78011	0.471704	-18.6136	2.49E-77	8.41E-75
Osi9	16995.34	-9.64159	0.529829	-18.1976	5.40E-74	1.75E-71
CG2150	13211.68	8.137766	0.44765	18.17887	7.59E-74	2.37E-71

Osi13	1170.392	-7.5752	0.425543	-17.8012	6.91E-71	2.08E-68
TwdlT	16937.64	6.488197	0.364749	17.7881	8.74E-71	2.54E-68
C901	911.6753	-7.71016	0.448954	-17.1736	4.18E-66	1.18E-63
CG10898	1133.164	-5.685	0.333353	-17.054	3.27E-65	8.89E-63
Obp28a	4915.252	-7.7602	0.463635	-16.7377	6.96E-63	1.83E-60
CG13722	1750.024	5.925238	0.356819	16.60573	6.33E-62	1.62E-59
Osi23	3575.429	-10.8062	0.658143	-16.4193	1.39E-60	3.45E-58
CG7173	925.1052	-6.00964	0.367709	-16.3434	4.84E-60	1.17E-57
Cad89D	2403.661	-6.56879	0.402378	-16.3249	6.56E-60	1.54E-57
CG15239	1241.468	-8.57721	0.528401	-16.2324	2.98E-59	6.78E-57
CG31808	1543.388	-5.63949	0.352297	-16.0078	1.13E-57	2.50E-55
CG43366	2550.509	-5.14233	0.322209	-15.9596	2.44E-57	5.28E-55
spz4	586.122	-7.06894	0.444341	-15.9088	5.50E-57	1.16E-54
CG13082	1356.35	-10.382	0.660617	-15.7157	1.18E-55	2.43E-53
CG3108	886.4119	-8.79472	0.565174	-15.5611	1.34E-54	2.69E-52
pncr002:3R	2096.25	7.921603	0.513478	15.42735	1.07E-53	2.10E-51
Osi24	1428.577	-6.10945	0.400207	-15.2657	1.29E-52	2.48E-50
CG17672	2505.221	-4.5424	0.298292	-15.228	2.30E-52	4.32E-50
CG6026	2345.451	-8.38489	0.552032	-15.1891	4.17E-52	7.65E-50
CG8483	537.6219	7.840001	0.516726	15.17245	5.38E-52	9.66E-50
CG10657	538.7475	6.215349	0.409729	15.16943	5.64E-52	9.90E-50
CG12507	1599.493	-6.16043	0.410839	-14.9948	7.94E-51	1.37E-48

CG8420	3978.891	-7.42307	0.498954	-14.8773	4.63E-50	7.81E-48
Lcp65Ag2	9547.246	8.835195	0.596262	14.81764	1.13E-49	1.86E-47
Osi21	952.3854	-10.1673	0.69018	-14.7314	4.05E-49	6.57E-47
Lcp65Ad	681.2512	9.299956	0.631675	14.72268	4.61E-49	7.34E-47
CG32645	393.1879	7.526129	0.515166	14.60914	2.46E-48	3.84E-46
Gasp	18790.29	5.273854	0.36413	14.48342	1.54E-47	2.37E-45
CG31559	387.5105	-7.52245	0.525508	-14.3146	1.77E-46	2.67E-44
RnrL	626.7656	5.661033	0.395645	14.30837	1.94E-46	2.87E-44
Pen	1751.696	5.690595	0.397851	14.30332	2.09E-46	3.03E-44
CG8945	507.8905	-8.86074	0.624131	-14.1969	9.57E-46	1.37E-43
CG16884	8556.606	5.11488	0.361841	14.13571	2.29E-45	3.22E-43
CG15506	599.421	-6.56064	0.469566	-13.9717	2.32E-44	3.21E-42
Lcp65Ag1	2040.393	8.756747	0.627179	13.96211	2.65E-44	3.61E-42
Klp61F	624.1311	7.396624	0.529932	13.95768	2.82E-44	3.78E-42
Ect3	1245.529	-7.97592	0.576713	-13.83	1.68E-43	2.22E-41
AOX2	497.5116	-7.60294	0.552236	-13.7676	3.99E-43	5.18E-41
spz6	2286.913	-7.16627	0.521415	-13.7439	5.54E-43	7.08E-41
asp	437.4321	6.904916	0.506579	13.63047	2.64E-42	3.32E-40
CG43164	687.1419	-6.07328	0.445697	-13.6265	2.79E-42	3.46E-40
CG13251	478.8419	-7.95325	0.584157	-13.6149	3.26E-42	3.99E-40
CG5326	569.4506	8.765241	0.646885	13.54991	7.93E-42	9.56E-40
bnb	717.8255	-5.35882	0.398748	-13.4391	3.57E-41	4.24E-39

Cda4	2585.243	5.464834	0.408012	13.39382	6.57E-41	7.70E-39
CG31728	555.2596	-9.50016	0.711982	-13.3433	1.30E-40	1.50E-38
CG6142	375.0692	6.936698	0.520989	13.31448	1.91E-40	2.17E-38
CG13578	554.5388	-8.39178	0.630925	-13.3008	2.29E-40	2.58E-38
CG13728	507.285	-8.37261	0.63108	-13.2671	3.59E-40	3.99E-38
Lcp65Ag3	1388.228	8.927793	0.679534	13.13811	1.99E-39	2.18E-37
dyl	1196.324	-5.63453	0.429531	-13.1179	2.60E-39	2.81E-37
CG15629	379.3308	-6.3675	0.488418	-13.037	7.54E-39	8.05E-37
CG13731	4559.442	8.371937	0.643438	13.01125	1.06E-38	1.11E-36
CG3339	1126.383	-8.51717	0.654627	-13.0107	1.06E-38	1.11E-36
Edg78E	621.4734	9.561744	0.743694	12.85709	7.85E-38	8.07E-36
CG13133	1213.399	-7.90489	0.618418	-12.7825	2.05E-37	2.09E-35
CG12880	2280.802	-3.84683	0.302711	-12.7079	5.35E-37	5.37E-35
CG43902	719.6837	-6.15237	0.48441	-12.7008	5.86E-37	5.81E-35
CG16885	7257.924	5.635148	0.444324	12.68252	7.39E-37	7.25E-35
BubR1	454.891	7.011025	0.554522	12.64336	1.22E-36	1.17E-34
jumu	1149.312	4.265496	0.337381	12.64295	1.22E-36	1.17E-34
pav	583.6355	6.909999	0.548049	12.60837	1.90E-36	1.80E-34
Rbp9	367.5616	-7.30569	0.582876	-12.5339	4.87E-36	4.57E-34
fru	398.2964	-5.02148	0.401498	-12.5069	6.85E-36	6.35E-34
br	584.2092	6.903618	0.552527	12.49463	7.99E-36	7.32E-34
Tsf3	413.1923	5.616179	0.454008	12.37022	3.79E-35	3.44E-33

tyn	237.1064	-6.06271	0.491661	-12.3311	6.16E-35	5.53E-33
ChLD3	315.4496	-7.24147	0.587935	-12.3168	7.36E-35	6.53E-33
CG14291	974.7623	-5.24088	0.425825	-12.3076	8.24E-35	7.24E-33
Hr4	244.7858	-6.49196	0.527555	-12.3058	8.43E-35	7.33E-33
Cpr49Ah	334.4881	-8.13883	0.661442	-12.3047	8.55E-35	7.36E-33
Tie	1572.184	-3.81538	0.312689	-12.2018	3.04E-34	2.59E-32
rod	465.6748	5.14043	0.422937	12.15414	5.45E-34	4.60E-32
Cpr97Eb	432.3261	4.669363	0.389099	12.00046	3.53E-33	2.95E-31
CG30197	533.7161	6.381323	0.53263	11.98078	4.48E-33	3.71E-31
Cyp301a1	871.4794	-4.36033	0.365717	-11.9227	9.01E-33	7.38E-31
Myo10A	568.0208	-4.86434	0.408395	-11.9109	1.04E-32	8.43E-31
CG31344	688.2573	-4.18724	0.351734	-11.9046	1.12E-32	9.00E-31
CG32241	606.041	8.818205	0.74344	11.86136	1.88E-32	1.49E-30
Np	276.349	-7.44215	0.627468	-11.8606	1.90E-32	1.49E-30
Cpr97Ea	872.7126	5.665115	0.479979	11.80284	3.77E-32	2.95E-30
Sox15	333.9537	-4.6786	0.397432	-11.7721	5.44E-32	4.21E-30
Cpr47Ec	629.1268	4.934127	0.420205	11.74219	7.75E-32	5.94E-30
CG42331	443.3607	-9.74657	0.830624	-11.734	8.53E-32	6.48E-30
CG1850	3835.197	7.51343	0.640611	11.72855	9.10E-32	6.85E-30
rt	587.3567	-4.30623	0.367948	-11.7034	1.22E-31	9.14E-30
DNApol-alpha180	289.346	6.117974	0.523012	11.69758	1.31E-31	9.70E-30
Skeletor	197.8208	-6.65218	0.570962	-11.6508	2.27E-31	1.67E-29

Eip78C	244.5706	-5.64431	0.484914	-11.6398	2.59E-31	1.88E-29
Cyp310a1	334.1171	6.499162	0.562394	11.55625	6.86E-31	4.95E-29
CG14625	263.1887	-8.66335	0.750177	-11.5484	7.52E-31	5.37E-29
Cyp18a1	283.5267	-5.28579	0.458107	-11.5383	8.45E-31	5.99E-29
Mcm5	346.3145	6.871309	0.595678	11.53528	8.76E-31	6.16E-29
RnrS	480.1911	5.631096	0.489279	11.50897	1.19E-30	8.29E-29
sprt	576.8842	-3.67544	0.319488	-11.5042	1.26E-30	8.69E-29
CG8301	213.4297	-6.06653	0.529708	-11.4526	2.28E-30	1.57E-28
Spindly	219.7406	5.285219	0.463315	11.4074	3.84E-30	2.61E-28
Cam	880.3549	-4.67354	0.41052	-11.3844	5.00E-30	3.37E-28
Blimp-1	436.7098	-7.11471	0.625878	-11.3676	6.07E-30	4.06E-28
tum	337.2551	6.789366	0.598528	11.34344	7.99E-30	5.31E-28
CG13023	403.8811	-6.35079	0.565917	-11.2221	3.18E-29	2.09E-27
CG34417	212.4997	-4.52554	0.404319	-11.193	4.41E-29	2.89E-27
CG13563	140.4833	-5.13376	0.459937	-11.1619	6.27E-29	4.07E-27
SMC2	517.8049	4.15182	0.372932	11.13293	8.67E-29	5.58E-27
CG8736	612.3568	7.0725	0.635418	11.13046	8.92E-29	5.70E-27
Cpr73D	199.5123	-7.59836	0.683727	-11.1131	1.08E-28	6.87E-27
Tis11	1013.424	4.330716	0.389778	11.11073	1.11E-28	7.00E-27
dpn	194.1697	6.051211	0.545328	11.09646	1.31E-28	8.15E-27
CG17786	1131.245	-4.14174	0.373443	-11.0907	1.39E-28	8.63E-27
E(spl)malpha-BFM	327.7585	5.56659	0.502867	11.0697	1.76E-28	1.08E-26

glu	551.0128	3.831245	0.348482	10.9941	4.08E-28	2.49E-26
ImpE2	3662.019	-5.26108	0.480747	-10.9436	7.13E-28	4.33E-26
yellow-e	193.7255	-7.43621	0.682534	-10.895	1.22E-27	7.34E-26
CG9737	199.2067	8.233556	0.759427	10.8418	2.18E-27	1.30E-25
CG5639	1370.399	-7.04784	0.651873	-10.8117	3.03E-27	1.80E-25
bdl	1017.259	-5.08201	0.470862	-10.793	3.71E-27	2.19E-25
para	1156.375	-5.49453	0.509463	-10.7849	4.05E-27	2.37E-25
sens	206.1367	8.423607	0.782853	10.76014	5.31E-27	3.07E-25
CG9336	1063.408	-4.74385	0.440874	-10.7601	5.31E-27	3.07E-25
serp	732.2018	7.628389	0.711943	10.71489	8.67E-27	4.97E-25
E(spl)m4-BFM	282.8163	8.450221	0.791008	10.68286	1.22E-26	6.98E-25
CG17843	284.1888	6.453706	0.605623	10.65631	1.63E-26	9.22E-25
Cks30A	351.1669	8.306815	0.781635	10.62748	2.22E-26	1.25E-24
Mink	406.8715	4.27129	0.402271	10.61793	2.46E-26	1.37E-24
CG4546	249.632	-5.01563	0.473447	-10.5939	3.18E-26	1.77E-24
Cap-D2	354.3254	3.934781	0.372413	10.56564	4.30E-26	2.37E-24
CG9689	929.4199	-4.42167	0.419478	-10.5409	5.60E-26	3.07E-24
AOX4	919.2392	-5.99817	0.569672	-10.5292	6.34E-26	3.45E-24
Pvf2	291.9695	4.801708	0.458258	10.47818	1.09E-25	5.88E-24
CG34155	154.8518	-6.02621	0.577893	-10.4279	1.85E-25	9.93E-24
Mcm2	345.7686	5.104509	0.48956	10.42673	1.87E-25	9.99E-24
Cpr65Ec	17019.08	8.657234	0.83196	10.40583	2.33E-25	1.24E-23

reb	171.5863	5.567122	0.538666	10.33502	4.89E-25	2.58E-23
CG16798	1136.362	-3.81478	0.369676	-10.3193	5.77E-25	3.02E-23
Cpr72Ea	244.4312	-4.48449	0.435074	-10.3074	6.52E-25	3.40E-23
CG1368	5104.517	7.719358	0.749417	10.30048	7.01E-25	3.63E-23
CG1275	170.6681	-5.66197	0.549884	-10.2967	7.29E-25	3.75E-23
CG6867	274.0115	-4.24139	0.415922	-10.1975	2.03E-24	1.04E-22
Spc25	256.7297	4.586806	0.450447	10.18279	2.37E-24	1.20E-22
CG9990	135.8621	6.626097	0.651087	10.17698	2.51E-24	1.27E-22
Dat	187.2887	-4.64951	0.457086	-10.1721	2.64E-24	1.33E-22
bru-3	191.9705	-4.62728	0.455053	-10.1687	2.74E-24	1.37E-22
Mlc2	694.3824	-6.97252	0.685817	-10.1667	2.79E-24	1.38E-22
CG15005	159.3394	-7.70358	0.759001	-10.1496	3.33E-24	1.64E-22
CG5065	165.7571	-4.4352	0.437003	-10.1491	3.34E-24	1.64E-22
obst-A	4474.33	4.282807	0.422143	10.1454	3.47E-24	1.69E-22
Cpr78Cc	662.9797	6.975493	0.688289	10.13454	3.88E-24	1.88E-22
CG33288	323.4889	-5.5532	0.550419	-10.089	6.18E-24	2.98E-22
E(spl)mgamma-HLH	118.6579	5.764295	0.571849	10.0801	6.77E-24	3.23E-22
Lcp65Ae	150.939	7.858238	0.779595	10.0799	6.78E-24	3.23E-22
CG10527	396.1313	-5.01353	0.498458	-10.0581	8.46E-24	4.01E-22
GstE6	698.6214	-5.78941	0.577728	-10.021	1.23E-23	5.81E-22
CG30069	6837.911	3.283756	0.328358	10.00053	1.52E-23	7.10E-22
CG12164	160.3138	8.353624	0.837524	9.974196	1.98E-23	9.21E-22

CG17386	138.6717	7.155924	0.720735	9.928645	3.12E-23	1.45E-21
Fancd2	179.0663	5.110079	0.516712	9.889607	4.62E-23	2.13E-21
CG15628	220.743	4.505948	0.456305	9.874859	5.35E-23	2.45E-21
bol	241.5104	-5.76103	0.584343	-9.85899	6.27E-23	2.86E-21
amd	283.6801	-4.94188	0.504614	-9.79339	1.20E-22	5.45E-21
FANCI	208.2945	6.710736	0.685887	9.784023	1.32E-22	5.95E-21
CG4089	364.7174	-3.23419	0.330658	-9.78107	1.36E-22	6.09E-21
Mcm10	168.7762	6.458801	0.663145	9.739649	2.04E-22	9.11E-21
Teh2	770.1252	-4.30907	0.443092	-9.72499	2.36E-22	1.05E-20
spz3	229.5629	3.806306	0.391748	9.716208	2.57E-22	1.14E-20
f	102.1848	-6.58743	0.679031	-9.70122	2.98E-22	1.31E-20
Ccn	298.7272	-5.24835	0.541042	-9.70046	3.00E-22	1.31E-20
CG14608	122.6274	-4.94876	0.511791	-9.6695	4.06E-22	1.77E-20
tnc	103.9322	-5.47007	0.566084	-9.66301	4.33E-22	1.87E-20
CG17450	93.96433	-5.70597	0.59062	-9.66098	4.42E-22	1.90E-20
Cpr49Ae	284.7513	-9.7713	1.012208	-9.65345	4.75E-22	2.03E-20
Faa	115.4006	-6.59741	0.683497	-9.65243	4.80E-22	2.04E-20
CG31871	691.0064	5.125526	0.532157	9.631603	5.88E-22	2.49E-20
CG10019	106.984	-7.18834	0.74641	-9.63054	5.94E-22	2.51E-20
Hsc70-3	760.195	-3.48794	0.362331	-9.62641	6.19E-22	2.60E-20
CG14960	251.1114	-6.38838	0.665491	-9.5995	8.03E-22	3.35E-20
fzy	313.0944	6.756893	0.704995	9.584318	9.31E-22	3.87E-20

CG13744	147.7361	-8.53646	0.892425	-9.56546	1.12E-21	4.62E-20
CG9752	178.2534	5.7431	0.601124	9.553928	1.25E-21	5.14E-20
CG8173	238.9854	3.839938	0.402018	9.551646	1.28E-21	5.23E-20
tau	184.6945	-7.5075	0.789509	-9.50908	1.92E-21	7.84E-20
Msh6	186.3826	4.463121	0.470044	9.495115	2.20E-21	8.92E-20
DIP-theta	128.0019	-4.57606	0.48252	-9.48367	2.45E-21	9.91E-20
Cralbp	139.0655	4.656384	0.491028	9.482925	2.47E-21	9.93E-20
Mdr65	469.5028	-4.71272	0.500227	-9.42116	4.46E-21	1.78E-19
CG9503	177.1013	-4.35683	0.462528	-9.4196	4.53E-21	1.80E-19
Cyp12a4	189.8889	-6.54843	0.697126	-9.39346	5.81E-21	2.30E-19
rk	109.1546	4.580068	0.488015	9.385103	6.29E-21	2.48E-19
Neurochondrin	113.08	-6.98665	0.744812	-9.38042	6.57E-21	2.58E-19
mey	497.9432	-11.7251	1.253789	-9.35173	8.62E-21	3.37E-19
CG13842	149.1768	-4.81642	0.515565	-9.34202	9.45E-21	3.67E-19
msb1l	151.7414	6.245975	0.670383	9.317021	1.20E-20	4.63E-19
Spn42Dd	135.8037	-4.92631	0.528785	-9.31628	1.20E-20	4.64E-19
Rab23	820.8043	-2.95321	0.31709	-9.31348	1.24E-20	4.74E-19
CG5873	1498.542	3.856571	0.416774	9.253391	2.17E-20	8.30E-19
ana3	211.7191	3.949319	0.428321	9.220472	2.96E-20	1.12E-18
CG8306	2205.085	-2.89081	0.313765	-9.21332	3.16E-20	1.20E-18
E(spl)mdelta-HLH	199.224	3.558072	0.38666	9.202059	3.51E-20	1.32E-18
nerfin-1	139.9264	4.667794	0.507346	9.20042	3.57E-20	1.34E-18

s-cup	340.6861	-4.99154	0.543864	-9.17791	4.40E-20	1.64E-18
CG32032	495.4433	-3.90356	0.425662	-9.17056	4.71E-20	1.75E-18
CG9294	222.1808	-9.90229	1.080037	-9.16847	4.80E-20	1.77E-18
CG7214	125.2686	-7.79896	0.850637	-9.16838	4.80E-20	1.77E-18
Hr46	200.2707	-8.23534	0.898767	-9.16293	5.05E-20	1.85E-18
CG6055	852.5384	-6.43922	0.703901	-9.1479	5.81E-20	2.12E-18
CG9628	151.4179	-4.94229	0.543084	-9.10042	9.00E-20	3.27E-18
DNA-ligI	154.7628	4.182288	0.460496	9.08214	1.06E-19	3.85E-18
Eip75B	801.7606	-3.5121	0.386949	-9.07637	1.12E-19	4.05E-18
Zwilch	122.5602	5.763994	0.637142	9.046635	1.47E-19	5.29E-18
CG2781	1048.014	2.811546	0.310808	9.045924	1.48E-19	5.30E-18
CG32855	118.6218	-4.7797	0.528879	-9.03742	1.60E-19	5.71E-18
CG15473	84.25736	-4.95165	0.548134	-9.03365	1.66E-19	5.88E-18
CG31121	160.9406	-3.69933	0.409917	-9.02458	1.80E-19	6.37E-18
GstE3	438.8039	-4.50738	0.49971	-9.02	1.88E-19	6.61E-18
CG13042	78.32402	-5.74844	0.640709	-8.97199	2.91E-19	1.02E-17
Cas	977.0172	3.345404	0.373012	8.968627	3.00E-19	1.05E-17
amos	142.6569	7.413584	0.828661	8.946463	3.67E-19	1.27E-17
CG7126	121.8122	-7.10666	0.794363	-8.94636	3.67E-19	1.27E-17
Epac	180.7472	-4.11541	0.460079	-8.94501	3.72E-19	1.28E-17
Sh	802.2374	-3.89962	0.435992	-8.94425	3.74E-19	1.28E-17
CG14567	256.8176	-3.44746	0.387657	-8.89305	5.95E-19	2.03E-17

CG34309	477.1054	-5.38598	0.605749	-8.89144	6.03E-19	2.05E-17
CG9134	607.6722	3.052247	0.343643	8.882027	6.57E-19	2.22E-17
CG32668	180.2471	-4.10067	0.464054	-8.83663	9.86E-19	3.33E-17
BBS8	169.4224	-4.21938	0.478462	-8.81863	1.16E-18	3.89E-17
Rab3	635.7406	-3.09085	0.350549	-8.81718	1.17E-18	3.93E-17
GstE4	3186.528	-4.17161	0.474055	-8.79984	1.37E-18	4.57E-17
sog	143.6978	-4.48042	0.509171	-8.79943	1.38E-18	4.57E-17
Dhit	172.829	-4.38071	0.501401	-8.73694	2.40E-18	7.92E-17
CG8910	127.4333	-4.19463	0.480492	-8.72988	2.55E-18	8.40E-17
Gfat1	279.5503	3.336396	0.382652	8.719129	2.80E-18	9.20E-17
e	68.94541	-5.47479	0.628228	-8.71466	2.92E-18	9.53E-17
CG32428	279.8203	3.67846	0.422416	8.708138	3.09E-18	1.01E-16
CG9743	161.5577	-4.60629	0.531043	-8.67404	4.17E-18	1.35E-16
CG13046	79.27256	6.393392	0.73712	8.67347	4.19E-18	1.35E-16
CG14274	271.1278	-6.28453	0.725809	-8.65865	4.77E-18	1.54E-16
niki	203.6968	-5.1521	0.595296	-8.65469	4.94E-18	1.58E-16
Brd	128.7796	7.701951	0.890195	8.651981	5.06E-18	1.62E-16
CR45952	105.8203	8.155838	0.947321	8.60937	7.35E-18	2.34E-16
fng	887.0372	-2.78745	0.324459	-8.59107	8.62E-18	2.73E-16
wntD	138.8224	-9.23416	1.07555	-8.58552	9.04E-18	2.86E-16
CG14921	68.51553	-4.88236	0.569251	-8.57681	9.75E-18	3.07E-16
Obp99c	76.90887	-6.26889	0.731542	-8.56942	1.04E-17	3.26E-16

Mcm7	98.10688	5.471293	0.641177	8.533199	1.42E-17	4.45E-16
Hsc70-2	168.0508	-4.1161	0.482423	-8.53215	1.44E-17	4.47E-16
mad2	165.2404	4.279685	0.502539	8.516122	1.65E-17	5.12E-16
CG15080	900.7429	-6.06537	0.712978	-8.50709	1.78E-17	5.51E-16
CG6836	363.3921	7.319911	0.862725	8.484641	2.16E-17	6.66E-16
CG17839	562.3773	-4.49563	0.529971	-8.48277	2.20E-17	6.74E-16
CG12017	79.36082	-7.34796	0.866387	-8.48115	2.23E-17	6.81E-16
wmd	277.6997	3.622315	0.427137	8.480458	2.24E-17	6.83E-16
CG7236	128.9984	-5.87003	0.692586	-8.47552	2.34E-17	7.10E-16
mwh	108.025	-8.64993	1.023635	-8.45021	2.91E-17	8.79E-16
CG42492	73.07136	-4.81328	0.571101	-8.42807	3.51E-17	1.06E-15
Mcm6	396.2248	4.081026	0.484881	8.416557	3.88E-17	1.16E-15
CG11966	90.90283	-8.00485	0.952928	-8.40027	4.45E-17	1.33E-15
sc	121.7084	7.550503	0.905294	8.340387	7.40E-17	2.21E-15
pgant8	208.8821	3.434767	0.412199	8.332791	7.90E-17	2.34E-15
CG31323	122.6715	-4.42522	0.531681	-8.32307	8.57E-17	2.54E-15
CG13318	114.1673	-5.09307	0.612202	-8.31925	8.85E-17	2.61E-15
jeb	322.2764	-3.18503	0.38326	-8.31036	9.54E-17	2.80E-15
Naam	465.8471	-3.38028	0.406861	-8.3082	9.72E-17	2.85E-15
CG2016	145.176	-4.05482	0.488099	-8.30739	9.78E-17	2.86E-15
ase	98.71286	4.614762	0.556929	8.286086	1.17E-16	3.40E-15
CG15209	116.8546	-5.43491	0.657053	-8.27164	1.32E-16	3.83E-15

mus301	107.988	4.437883	0.538002	8.248819	1.60E-16	4.62E-15
CG11069	850.5085	-2.58927	0.314492	-8.23317	1.82E-16	5.25E-15
CG32085	128.9778	-4.14594	0.504887	-8.21163	2.18E-16	6.26E-15
CG12038	116.5655	-3.92898	0.479053	-8.20156	2.37E-16	6.78E-15
pon	254.3117	4.024275	0.490927	8.197294	2.46E-16	7.01E-15
dgt3	100.7029	4.842089	0.590776	8.196153	2.48E-16	7.05E-15
CG10362	135.9212	-3.85691	0.470598	-8.19576	2.49E-16	7.05E-15
RecQ4	101.9979	6.605502	0.806457	8.190771	2.60E-16	7.32E-15
CG8854	64.65371	-6.939	0.849715	-8.16627	3.18E-16	8.94E-15
CG17075	296.1996	-3.41118	0.419076	-8.13976	3.96E-16	1.11E-14
aurA	86.0838	4.868169	0.598303	8.136628	4.06E-16	1.14E-14
Ance-2	96.52152	-8.46795	1.041731	-8.12873	4.34E-16	1.21E-14
sel	346.3436	-2.72666	0.335718	-8.12188	4.59E-16	1.27E-14
nyo	187.5366	-10.65	1.311838	-8.1184	4.72E-16	1.31E-14
Set	1039.405	2.407954	0.296871	8.111119	5.02E-16	1.38E-14
Mhcl	241.3272	-2.76296	0.341781	-8.084	6.27E-16	1.72E-14
CG11658	158.6879	-3.67766	0.455421	-8.07529	6.73E-16	1.84E-14
Mrp4	120.7396	-4.2066	0.521239	-8.07039	7.01E-16	1.91E-14
CG15322	72.39921	-5.46324	0.677382	-8.06524	7.31E-16	1.99E-14
alpha-Man-Ia	165.938	-3.78956	0.470041	-8.06219	7.49E-16	2.03E-14
dpr4	146.1387	-5.60888	0.696803	-8.04946	8.32E-16	2.25E-14
CycA	155.4153	4.219982	0.524919	8.039293	9.04E-16	2.43E-14

Cad87A	1782.061	-2.3122	0.288091	-8.02595	1.01E-15	2.71E-14
Rtnl1	577.6484	-2.61022	0.325468	-8.0199	1.06E-15	2.83E-14
Sik2	216.822	-3.22095	0.402187	-8.00858	1.16E-15	3.10E-14
CG42339	129.592	-3.89306	0.486626	-8.0001	1.24E-15	3.31E-14
GstT4	253.9101	-3.22503	0.403372	-7.99517	1.29E-15	3.43E-14
CG8245	370.0896	-3.76564	0.472515	-7.96935	1.60E-15	4.22E-14
CG10264	86.06776	5.768264	0.724568	7.960973	1.71E-15	4.50E-14
polo	111.5944	7.302248	0.91877	7.947854	1.90E-15	4.99E-14
ac	81.55994	7.281665	0.916666	7.943639	1.96E-15	5.14E-14
CG14598	91.40611	5.270262	0.663546	7.942577	1.98E-15	5.17E-14
CG10268	245.6073	-2.99423	0.377711	-7.92731	2.24E-15	5.83E-14
CG32318	85.40194	6.516424	0.824335	7.905066	2.68E-15	6.95E-14
vret	84.18092	5.566918	0.704788	7.898717	2.82E-15	7.29E-14
DNApol-delta	202.488	2.94903	0.373867	7.887902	3.07E-15	7.93E-14
CG15666	361.4696	-3.74963	0.476458	-7.8698	3.55E-15	9.13E-14
Spn43Aa	933.8443	-5.46858	0.695753	-7.85995	3.84E-15	9.85E-14
CG9815	106.3849	-3.55243	0.452126	-7.85717	3.93E-15	1.00E-13
CG9360	300.0985	-3.93084	0.500592	-7.85238	4.08E-15	1.04E-13
CG17572	91.07307	-6.33079	0.806423	-7.85046	4.15E-15	1.05E-13
cDIP	320.637	-6.20227	0.790346	-7.84753	4.24E-15	1.07E-13
CG5909	84.6516	-6.02999	0.769825	-7.83294	4.77E-15	1.20E-13
CG7708	376.0249	-4.83071	0.616943	-7.83007	4.88E-15	1.23E-13

CG10348	80.37254	-8.19609	1.047677	-7.8231	5.15E-15	1.29E-13
CG5391	139.7481	-9.5684	1.223394	-7.82119	5.23E-15	1.31E-13
CG7402	320.9589	5.040954	0.644574	7.820595	5.26E-15	1.31E-13
dao	129.1227	-4.04558	0.517421	-7.81874	5.34E-15	1.33E-13
CG13634	84.47774	-8.52525	1.090435	-7.81821	5.36E-15	1.33E-13
Ssb-c31a	236.0799	3.339618	0.427953	7.803696	6.01E-15	1.49E-13
CG13748	87.65144	-8.66451	1.110765	-7.80049	6.17E-15	1.52E-13
CG14626	60.19652	-6.95848	0.892525	-7.7964	6.37E-15	1.57E-13
CG13893	205.1112	-4.3013	0.552292	-7.78809	6.80E-15	1.67E-13
CG42261	321.3623	-3.90914	0.502216	-7.78378	7.04E-15	1.72E-13
CG1673	232.3387	3.728884	0.479911	7.769952	7.85E-15	1.91E-13
Art1	632.2117	2.646677	0.341662	7.746487	9.45E-15	2.30E-13
Chd3	69.11184	6.842622	0.883684	7.743291	9.69E-15	2.35E-13
Gen	97.55805	4.09532	0.529167	7.73919	1.00E-14	2.42E-13
CG34136	145.8099	-3.4475	0.446264	-7.72525	1.12E-14	2.69E-13
CG13720	105.1407	-5.84506	0.757406	-7.71721	1.19E-14	2.86E-13
Cpr66Cb	81.49558	-5.25553	0.681848	-7.70777	1.28E-14	3.07E-13
rtet	482.652	-2.88771	0.375715	-7.68592	1.52E-14	3.63E-13
CG12481	161.9405	9.731278	1.266567	7.683189	1.55E-14	3.70E-13
CG9313	135.6081	-5.5755	0.725998	-7.67978	1.59E-14	3.79E-13
CG13386	128.644	-10.0424	1.308419	-7.67518	1.65E-14	3.91E-13
antdh	4943.395	-3.4616	0.451371	-7.66909	1.73E-14	4.09E-13

sca	620.8509	3.416725	0.445648	7.666876	1.76E-14	4.15E-13
CR45536	56.03625	-6.12287	0.800161	-7.65204	1.98E-14	4.65E-13
Cyp9b2	192.7669	-5.05574	0.662211	-7.63463	2.26E-14	5.31E-13
Sse	79.61377	6.443861	0.844266	7.632504	2.30E-14	5.38E-13
CG15143	111.2598	-5.70098	0.747309	-7.62869	2.37E-14	5.53E-13
CG6362	176.7175	-6.56775	0.861167	-7.62657	2.41E-14	5.60E-13
Rgk1	134.9131	-7.62643	1.000152	-7.62527	2.44E-14	5.64E-13
Det	87.4677	5.094318	0.66817	7.624283	2.45E-14	5.67E-13
spn-E	56.419	4.966901	0.651634	7.622229	2.49E-14	5.75E-13
Dop1R1	103.807	-7.81618	1.026331	-7.61565	2.62E-14	6.03E-13
DNApol-alpha50	76.03375	4.968346	0.65256	7.613623	2.67E-14	6.11E-13
RpA-70	756.3932	2.406301	0.316454	7.603953	2.87E-14	6.56E-13
CG32694	116.4425	5.008093	0.659905	7.589108	3.22E-14	7.34E-13
atk	47.21115	-6.22895	0.822552	-7.57271	3.66E-14	8.31E-13
CG42450	249.7605	-3.35205	0.442953	-7.5675	3.80E-14	8.63E-13
lds	411.318	2.473009	0.326905	7.564909	3.88E-14	8.78E-13
Klp64D	414.4149	-2.52073	0.333245	-7.56421	3.90E-14	8.80E-13
CG3430	117.6077	3.361032	0.444621	7.559325	4.05E-14	9.11E-13
CG11836	108.7706	-3.69773	0.490249	-7.54257	4.61E-14	1.03E-12
bchs	506.5906	-2.34951	0.311802	-7.53528	4.87E-14	1.09E-12
CG3104	162.7887	-3.4005	0.452028	-7.52276	5.36E-14	1.20E-12
CG13868	134.0172	-4.04992	0.538373	-7.52252	5.37E-14	1.20E-12

CG15213	85.90574	7.881034	1.048504	7.516453	5.63E-14	1.25E-12
CG14342	131.9907	-3.33441	0.443712	-7.51481	5.70E-14	1.26E-12
CG14688	95.18501	3.73183	0.499376	7.47299	7.84E-14	1.73E-12
CG3257	325.7003	-2.97755	0.398685	-7.46843	8.12E-14	1.78E-12
Cpr92A	116.146	-7.20509	0.96474	-7.46843	8.12E-14	1.78E-12
Lcp65Ac	182.2689	9.112574	1.221503	7.460133	8.64E-14	1.89E-12
CG12605	233.4165	-3.29972	0.442708	-7.45347	9.09E-14	1.99E-12
CG32369	168.3339	3.144971	0.423421	7.427532	1.11E-13	2.41E-12
Amph	95.70942	-3.5269	0.474911	-7.42646	1.12E-13	2.42E-12
Hexo2	652.0446	-4.79498	0.645867	-7.4241	1.14E-13	2.46E-12
knrl	74.4519	-4.57609	0.616408	-7.42379	1.14E-13	2.46E-12
trbd	638.1309	-2.27693	0.306861	-7.42005	1.17E-13	2.53E-12
CG30463	126.4577	-3.75602	0.507172	-7.40582	1.30E-13	2.80E-12
crc	500.0999	2.76347	0.373896	7.39102	1.46E-13	3.13E-12
CG6329	442.4492	-3.08733	0.418142	-7.38345	1.54E-13	3.30E-12
CG14406	75.25127	-8.59265	1.163994	-7.38204	1.56E-13	3.33E-12
CG15615	71.75971	6.200205	0.840132	7.380039	1.58E-13	3.37E-12
CycE	56.47694	4.454708	0.603813	7.377623	1.61E-13	3.42E-12
CG13599	59.30555	6.014843	0.815978	7.371328	1.69E-13	3.58E-12
mus308	139.6921	3.19352	0.433348	7.369408	1.71E-13	3.62E-12
CG13721	44.05161	-5.17349	0.703076	-7.35837	1.86E-13	3.93E-12
CG12817	46.96253	-6.18694	0.841425	-7.35292	1.94E-13	4.08E-12

Syt4	1258.447	-2.48741	0.338336	-7.35189	1.95E-13	4.10E-12
CG5597	182.4362	-3.12236	0.425381	-7.34014	2.13E-13	4.47E-12
CG13690	90.46545	6.704791	0.913838	7.336957	2.19E-13	4.56E-12
CR31451	141.747	-3.28506	0.448227	-7.32901	2.32E-13	4.83E-12
osp	42.42832	-6.19092	0.845407	-7.32301	2.42E-13	5.04E-12
CG7272	452.832	-2.75096	0.375676	-7.32269	2.43E-13	5.04E-12
CG8920	75.25143	-4.42038	0.604479	-7.31271	2.62E-13	5.41E-12
hdc	3106.152	3.011309	0.411817	7.312243	2.63E-13	5.42E-12
CG4329	86.64012	-3.95256	0.5407	-7.31007	2.67E-13	5.49E-12
Ndc80	83.19327	4.286686	0.586996	7.302756	2.82E-13	5.79E-12
CG15878	62.23768	-4.21497	0.580153	-7.26528	3.72E-13	7.62E-12
Tsp42Ej	198.4781	-3.12796	0.430597	-7.26426	3.75E-13	7.66E-12
CG5281	69.86284	-3.58875	0.49429	-7.26041	3.86E-13	7.86E-12
verm	907.1133	5.818331	0.802793	7.247607	4.24E-13	8.62E-12
RfC3	95.86964	3.563623	0.491878	7.244934	4.33E-13	8.77E-12
CG13855	129.2684	-3.4775	0.480086	-7.2435	4.37E-13	8.84E-12
CG7759	41.68707	-5.51227	0.761115	-7.24236	4.41E-13	8.90E-12
Osi16	50.32387	-7.21474	0.996353	-7.24115	4.45E-13	8.96E-12
MESK2	78.06728	-5.19674	0.717799	-7.23982	4.49E-13	9.02E-12
Tom	369.5699	2.692827	0.371967	7.239418	4.51E-13	9.03E-12
wus	61.94055	-4.07169	0.562726	-7.23566	4.63E-13	9.26E-12
kkv	82.33825	-4.08265	0.565096	-7.22471	5.02E-13	1.00E-11

CG11498	46.71829	-4.65825	0.645535	-7.21611	5.35E-13	1.06E-11
Nup133	315.3809	2.538728	0.352945	7.192989	6.34E-13	1.26E-11
Sln	141.6604	-3.39582	0.472213	-7.19128	6.42E-13	1.27E-11
SmE	284.9171	2.436382	0.340166	7.162325	7.93E-13	1.57E-11
CG7372	469.0137	2.419006	0.337869	7.159596	8.09E-13	1.59E-11
feo	363.8914	4.071235	0.568929	7.155964	8.31E-13	1.63E-11
dpr21	106.3559	-3.62204	0.506817	-7.14663	8.89E-13	1.74E-11
CG9509	41.35615	-6.40592	0.89702	-7.14133	9.24E-13	1.81E-11
Exn	114.614	-3.47223	0.487885	-7.1169	1.10E-12	2.15E-11
Orc6	56.00571	4.62174	0.649404	7.116899	1.10E-12	2.15E-11
tefu	553.9751	2.951856	0.415148	7.110366	1.16E-12	2.25E-11
CG10339	146.3827	-3.54668	0.499318	-7.10304	1.22E-12	2.37E-11
Cyp49a1	49.77213	-4.07462	0.574151	-7.09677	1.28E-12	2.47E-11
dpr1	53.81806	-5.15374	0.730275	-7.05726	1.70E-12	3.28E-11
CG12858	143.156	-5.28613	0.749108	-7.05656	1.71E-12	3.29E-11
timeout	85.37334	3.887788	0.553194	7.02789	2.10E-12	4.03E-11
Ccp84Ab	149.7029	7.789774	1.109855	7.018729	2.24E-12	4.29E-11
CG1632	39.04038	-6.28376	0.895621	-7.01609	2.28E-12	4.36E-11
CG34247	283.8842	-3.97678	0.566877	-7.01525	2.30E-12	4.38E-11
yellow-e2	59.13985	6.39486	0.911916	7.012552	2.34E-12	4.46E-11
CG6330	318.3628	-2.84684	0.406019	-7.01158	2.36E-12	4.48E-11
VAChT	805.9152	-3.40579	0.48589	-7.00938	2.39E-12	4.54E-11

Orc5	71.41252	4.409001	0.629086	7.008585	2.41E-12	4.55E-11
shep	121.3573	-3.49896	0.501127	-6.98217	2.91E-12	5.48E-11
Orc2	82.26493	7.176701	1.028732	6.976256	3.03E-12	5.71E-11
CG13737	225.6014	-3.03911	0.436079	-6.96918	3.19E-12	5.99E-11
CR43432	87.85298	4.218108	0.605847	6.962329	3.35E-12	6.27E-11
Cpr66D	1342.82	-4.06484	0.58575	-6.93955	3.93E-12	7.36E-11
Ggamma1	1228.516	-2.52127	0.364912	-6.90925	4.87E-12	9.09E-11
CG31918	200.0059	3.193289	0.46229	6.907537	4.93E-12	9.18E-11
sm	44.68061	-4.23327	0.612938	-6.90652	4.97E-12	9.23E-11
E(spl)m8-HLH	123.888	7.7285	1.119366	6.904354	5.04E-12	9.35E-11
CG7166	136.7402	-3.01348	0.436534	-6.90321	5.08E-12	9.40E-11
eg	35.47324	-5.20254	0.7546	-6.89443	5.41E-12	9.98E-11
CG33543	66.59843	-4.77674	0.694922	-6.87377	6.25E-12	1.15E-10
CG42232	1326.751	2.571097	0.374184	6.871206	6.37E-12	1.17E-10
Pms2	212.222	2.828763	0.411832	6.868726	6.48E-12	1.19E-10
TwdlE	1938.069	4.92808	0.718375	6.860038	6.88E-12	1.26E-10
Fbxl7	386.975	-2.98559	0.435298	-6.85873	6.95E-12	1.27E-10
fred	51.54253	-6.36812	0.929307	-6.85255	7.25E-12	1.32E-10
GstD8	350.8845	-6.72885	0.983374	-6.84261	7.78E-12	1.41E-10
CG15144	72.28228	-6.24378	0.912691	-6.84106	7.86E-12	1.43E-10
mus205	155.0815	2.670728	0.39074	6.83505	8.20E-12	1.48E-10
CG14627	36.06285	-5.83259	0.853862	-6.83083	8.44E-12	1.52E-10

bru-2	92.97077	-6.04672	0.885761	-6.82658	8.70E-12	1.57E-10
Eaat2	357.7332	-4.97888	0.730175	-6.81875	9.18E-12	1.65E-10
CG5783	59.84194	-4.68082	0.687226	-6.81118	9.68E-12	1.74E-10
eys	84.73966	-3.69545	0.542747	-6.8088	9.84E-12	1.76E-10
sNPF	569.5841	-2.72257	0.400151	-6.80385	1.02E-11	1.82E-10
Gfrl	106.4508	-6.12088	0.90167	-6.78837	1.13E-11	2.02E-10
Ace	513.1792	-2.48222	0.366405	-6.77452	1.25E-11	2.22E-10
CG18130	127.6904	-3.87499	0.571995	-6.77452	1.25E-11	2.22E-10
Cpr50Ca	49.46422	-4.94148	0.730363	-6.76579	1.33E-11	2.35E-10
Toll-6	41.07744	-5.2423	0.775386	-6.76089	1.37E-11	2.42E-10
rho-5	202.293	-3.39292	0.502562	-6.75126	1.47E-11	2.59E-10
CG15704	63.0129	8.637969	1.282287	6.736377	1.62E-11	2.86E-10
CG43078	78.5605	-4.78507	0.710855	-6.73143	1.68E-11	2.95E-10
cutlet	74.71013	3.822927	0.567929	6.731349	1.68E-11	2.95E-10
Ptp99A	111.6512	-2.77206	0.411833	-6.73103	1.68E-11	2.95E-10
Tsp42Ef	1652.618	-2.09352	0.311197	-6.72731	1.73E-11	3.02E-10
CG18190	355.3275	2.37099	0.352713	6.722142	1.79E-11	3.12E-10
Uba2	1090.949	2.141932	0.319034	6.71381	1.90E-11	3.30E-10
CG7337	38.14206	-5.45751	0.813417	-6.70935	1.95E-11	3.39E-10
CG4914	674.2387	-4.86175	0.725165	-6.70434	2.02E-11	3.50E-10
dgt6	138.3175	3.100453	0.462826	6.698965	2.10E-11	3.63E-10
Ote	273.5076	3.871631	0.578024	6.698045	2.11E-11	3.64E-10

Sdr	40.70757	4.375514	0.654829	6.681918	2.36E-11	4.06E-10
DNApol-epsilon255	181.815	2.578303	0.386026	6.679088	2.40E-11	4.13E-10
CG42337	98.12903	-3.38956	0.5075	-6.67893	2.41E-11	4.13E-10
Gld	199.4278	-2.74601	0.411566	-6.6721	2.52E-11	4.31E-10
CR45232	36.185	-4.45523	0.668041	-6.66909	2.57E-11	4.39E-10
GlyP	96.49354	3.40396	0.510606	6.666504	2.62E-11	4.46E-10
CG6431	36.57119	-6.7845	1.018211	-6.66316	2.68E-11	4.56E-10
Lsp1gamma	190.1612	3.750844	0.563235	6.659461	2.75E-11	4.66E-10
CG15803	93.82468	-4.76187	0.715408	-6.65616	2.81E-11	4.76E-10
CG17599	208.2814	-3.3961	0.510331	-6.6547	2.84E-11	4.80E-10
Cow	539.2635	-2.40658	0.361669	-6.65409	2.85E-11	4.81E-10
CG4962	109.1416	-3.43637	0.516788	-6.64949	2.94E-11	4.95E-10
CG42672	43.12601	-6.97332	1.048893	-6.64827	2.97E-11	4.98E-10
CG14752	2352.743	8.236581	1.239592	6.644591	3.04E-11	5.10E-10
CG15651	57.44012	-6.10469	0.92175	-6.62293	3.52E-11	5.89E-10
Dh44-R1	46.93164	-5.27985	0.797437	-6.62102	3.57E-11	5.96E-10
igl	141.0015	-4.67896	0.706745	-6.62044	3.58E-11	5.97E-10
Ir25a	93.68872	-4.7414	0.717441	-6.60877	3.88E-11	6.45E-10
CG7744	122.8315	2.924607	0.442879	6.603631	4.01E-11	6.66E-10
alt	59.78096	-3.69865	0.561077	-6.59206	4.34E-11	7.19E-10
CG34107	35.71809	-5.78861	0.878193	-6.5915	4.35E-11	7.20E-10
glec	1330.375	-2.03676	0.309102	-6.58929	4.42E-11	7.29E-10

how	185.2644	-2.67853	0.40657	-6.58812	4.45E-11	7.34E-10
CG7054	213.1313	2.576436	0.391199	6.586001	4.52E-11	7.43E-10
sip2	52.33897	6.245934	0.948858	6.582583	4.62E-11	7.59E-10
CG4596	97.85255	-3.20764	0.487943	-6.5738	4.90E-11	8.03E-10
CG34114	78.39676	-4.0219	0.612424	-6.56718	5.13E-11	8.38E-10
Snmp2	41.31204	7.440695	1.133598	6.563784	5.25E-11	8.56E-10
CG42322	85.45712	-5.38688	0.821785	-6.5551	5.56E-11	9.05E-10
hmw	67.67514	-3.96787	0.605509	-6.55295	5.64E-11	9.17E-10
RSG7	395.2745	-3.31276	0.505657	-6.5514	5.70E-11	9.25E-10
NetB	193.4549	-2.6197	0.400167	-6.54651	5.89E-11	9.53E-10
gukh	53.10246	3.819969	0.583996	6.541088	6.11E-11	9.87E-10
CG30101	1868.269	4.58947	0.702155	6.536266	6.31E-11	1.02E-09
CG9864	64.23904	-6.00755	0.919929	-6.53045	6.56E-11	1.06E-09
Grip71	134.9276	2.908454	0.445522	6.52819	6.66E-11	1.07E-09
4-Sep	56.08296	-3.40988	0.522484	-6.52628	6.74E-11	1.08E-09
CG13154	33.41902	-6.39682	0.982687	-6.50952	7.54E-11	1.21E-09
CG30274	228.3458	-4.82527	0.741502	-6.50743	7.64E-11	1.22E-09
psh	66.19682	-3.82346	0.587562	-6.50733	7.65E-11	1.22E-09
Cpr50Cb	52.90186	-8.9983	1.383034	-6.5062	7.71E-11	1.23E-09
CG43729	158.7571	-6.52557	1.004074	-6.49909	8.08E-11	1.28E-09
CG13685	90.01288	-6.59265	1.015315	-6.4932	8.40E-11	1.33E-09
CG32040	217.8667	-3.47756	0.535892	-6.4893	8.62E-11	1.36E-09

CG34354	47.93847	-5.9874	0.923311	-6.48471	8.89E-11	1.40E-09
lectin-28C	34.52874	4.256657	0.65725	6.47647	9.39E-11	1.48E-09
CG30089	156.5553	-2.43368	0.376041	-6.47187	9.68E-11	1.52E-09
Atpalpha	3235.856	-2.40932	0.372763	-6.4634	1.02E-10	1.61E-09
CG30001	84.67672	3.426727	0.530414	6.460482	1.04E-10	1.64E-09
CG9541	243.8447	-4.28457	0.663346	-6.45902	1.05E-10	1.65E-09
CG33144	255.9568	-3.10027	0.480037	-6.4584	1.06E-10	1.65E-09
Drl-2	79.62678	-4.11339	0.637141	-6.456	1.08E-10	1.68E-09
Caf1-105	104.0012	2.928888	0.455214	6.434087	1.24E-10	1.93E-09
Spt	123.892	2.693174	0.418582	6.434041	1.24E-10	1.93E-09
CG8745	49.02806	-4.45282	0.692623	-6.42892	1.29E-10	1.99E-09
CG6201	32.27269	-6.04267	0.940416	-6.42553	1.31E-10	2.03E-09
CAP	186.9526	-2.90004	0.451985	-6.41624	1.40E-10	2.16E-09
Dcp-1	231.2522	2.626984	0.410013	6.407073	1.48E-10	2.29E-09
CG10137	153.923	-3.22969	0.504246	-6.40499	1.50E-10	2.31E-09
CG8646	241.2804	3.20241	0.500121	6.403269	1.52E-10	2.34E-09
CG34261	43.0222	5.854551	0.914873	6.399308	1.56E-10	2.39E-09
CG32392	153.4876	-5.15604	0.805862	-6.39817	1.57E-10	2.41E-09
Fhos	81.0009	-3.40014	0.532224	-6.38854	1.67E-10	2.56E-09
CG17111	311.4938	-5.08436	0.797029	-6.37914	1.78E-10	2.72E-09
AnxB9	115.0596	-2.75459	0.432216	-6.37319	1.85E-10	2.82E-09
Scgbeta	48.83601	-4.46279	0.7004	-6.37177	1.87E-10	2.84E-09

CG13003	35.82448	-6.95961	1.092578	-6.36989	1.89E-10	2.87E-09
CG11319	93.95757	-3.75989	0.590778	-6.3643	1.96E-10	2.97E-09
CG10185	2436.122	-2.80196	0.441185	-6.35099	2.14E-10	3.23E-09
CG16820	924.8781	2.327222	0.366826	6.344213	2.24E-10	3.37E-09
Dic1	114.588	-2.73847	0.43169	-6.34361	2.24E-10	3.38E-09
CG6426	212.0096	2.60644	0.411064	6.340722	2.29E-10	3.44E-09
Manf	956.8816	-2.64962	0.417915	-6.34009	2.30E-10	3.45E-09
CG7786	47.87051	-6.76172	1.066675	-6.33906	2.31E-10	3.46E-09
CG1635	38.36645	-4.6301	0.730533	-6.33797	2.33E-10	3.48E-09
Fpps	426.6975	-1.97733	0.312146	-6.33463	2.38E-10	3.55E-09
CrebA	179.8961	-2.41076	0.380593	-6.33422	2.39E-10	3.55E-09
CycB3	37.2628	5.399472	0.85364	6.325236	2.53E-10	3.76E-09
CG9135	431.6035	2.80955	0.444199	6.324986	2.53E-10	3.76E-09
CG15630	270.4972	-2.32934	0.368719	-6.3174	2.66E-10	3.94E-09
Ptpmeg2	64.09257	-3.04007	0.481308	-6.31627	2.68E-10	3.96E-09
Fit2	320.2015	-2.15522	0.341652	-6.30822	2.82E-10	4.17E-09
CG32082	169.1708	-2.22367	0.352624	-6.30608	2.86E-10	4.22E-09
CG13950	280.2488	-5.05664	0.802953	-6.29755	3.02E-10	4.45E-09
CG13650	293.7062	-2.80957	0.446303	-6.2952	3.07E-10	4.51E-09
tos	68.27022	3.449496	0.548242	6.291928	3.14E-10	4.60E-09
amon	368.7443	-2.63872	0.419413	-6.29146	3.14E-10	4.60E-09
sosie	157.164	-7.84455	1.248019	-6.2856	3.27E-10	4.77E-09

AMPdeam	96.23853	-3.24661	0.51691	-6.28079	3.37E-10	4.92E-09
CG11638	108.2263	-3.10341	0.494651	-6.27394	3.52E-10	5.13E-09
CG13972	77.36339	-2.77926	0.443004	-6.27367	3.53E-10	5.13E-09
CG12592	262.7956	2.570818	0.409825	6.272966	3.54E-10	5.14E-09
CG6985	74.11454	3.308247	0.527856	6.267326	3.67E-10	5.32E-09
E(spl)m6-BFM	34.06476	4.355562	0.695015	6.266859	3.68E-10	5.33E-09
Nep1	78.77094	-3.60275	0.575015	-6.26549	3.72E-10	5.37E-09
dar1	64.5781	-3.16395	0.505014	-6.26509	3.73E-10	5.37E-09
GV1	162.2626	4.811536	0.76874	6.258993	3.87E-10	5.58E-09
IP3K1	100.313	-2.55231	0.408311	-6.2509	4.08E-10	5.86E-09
Nuf2	67.72753	3.172915	0.507851	6.247726	4.16E-10	5.97E-09
Nrg	251.0844	-2.97642	0.476764	-6.24296	4.29E-10	6.15E-09
CG15564	44.82509	-4.23692	0.680161	-6.22929	4.69E-10	6.70E-09
CG13928	1456.284	-1.91884	0.308219	-6.22559	4.80E-10	6.85E-09
Jheh3	228.07	-3.65097	0.586849	-6.22131	4.93E-10	7.02E-09
CG4570	28.9694	5.462433	0.879096	6.213694	5.18E-10	7.36E-09
stg	85.98334	3.354235	0.539979	6.211784	5.24E-10	7.44E-09
CG13437	79.57019	-5.15335	0.82998	-6.209	5.33E-10	7.56E-09
RfC4	260.7726	2.772049	0.446796	6.20428	5.49E-10	7.78E-09
Ero1L	332.8466	-2.07608	0.334654	-6.20367	5.52E-10	7.79E-09
cv-2	250.498	-2.05828	0.332248	-6.19502	5.83E-10	8.22E-09
CG4757	45.26238	-8.32116	1.343459	-6.19384	5.87E-10	8.27E-09

CG30285	566.4441	-3.58962	0.579602	-6.19324	5.89E-10	8.28E-09
Ndc1	162.3707	2.453445	0.396256	6.191569	5.96E-10	8.36E-09
kek2	221.6452	-2.39348	0.386603	-6.19107	5.98E-10	8.37E-09
Lim1	200.823	-2.36788	0.382917	-6.1838	6.26E-10	8.75E-09
E(spl)m7-HLH	251.0017	2.261798	0.366134	6.177516	6.51E-10	9.09E-09
CG6231	48.16749	-4.60621	0.745793	-6.17626	6.56E-10	9.15E-09
CG15117	31.38428	-4.0941	0.66298	-6.17529	6.60E-10	9.19E-09
CG33177	515.4248	-4.05557	0.657822	-6.16515	7.04E-10	9.78E-09
CG12998	28.05847	5.912615	0.959152	6.16442	7.07E-10	9.81E-09
CG13699	161.0092	-2.85029	0.462402	-6.1641	7.09E-10	9.82E-09
Cyp12b2	120.9796	-4.97588	0.808386	-6.15533	7.49E-10	1.04E-08
Tsp	38.36771	-3.64117	0.591755	-6.15316	7.60E-10	1.05E-08
dpr5	42.1491	-5.82531	0.946954	-6.15163	7.67E-10	1.06E-08
Fen1	141.2516	2.924474	0.475578	6.149309	7.78E-10	1.07E-08
CG9766	104.5021	-2.88695	0.469576	-6.14799	7.85E-10	1.08E-08
chrb	1131.467	-2.4409	0.398243	-6.12916	8.83E-10	1.21E-08
CG14507	31.28657	-7.08169	1.155454	-6.12892	8.85E-10	1.21E-08
CG6495	200.4927	-2.94493	0.481984	-6.11001	9.96E-10	1.36E-08
spdo	90.8085	3.169595	0.519824	6.09744	1.08E-09	1.47E-08
Diap1	119.1427	-2.32687	0.381723	-6.0957	1.09E-09	1.48E-08
BicD	100.3583	-2.87541	0.472088	-6.09082	1.12E-09	1.53E-08
Sec63	561.0421	-2.15568	0.354666	-6.07806	1.22E-09	1.65E-08

CG13375	38.94018	-4.36985	0.719284	-6.07528	1.24E-09	1.68E-08
Nlg4	31.88079	-5.31109	0.875603	-6.06564	1.31E-09	1.78E-08
CG3323	32.10733	4.210913	0.695308	6.056186	1.39E-09	1.88E-08
Gycalpha99B	107.6097	-6.23526	1.030031	-6.05347	1.42E-09	1.91E-08
CG9850	36.2953	4.332403	0.715749	6.052962	1.42E-09	1.92E-08
Gbeta5	95.65444	-3.04224	0.50302	-6.04794	1.47E-09	1.97E-08
Jupiter	55.52878	-3.37419	0.558415	-6.04244	1.52E-09	2.04E-08
alphaSnap	1259.623	-1.76344	0.292033	-6.03849	1.56E-09	2.09E-08
Traf4	177.1169	2.251977	0.373036	6.036884	1.57E-09	2.10E-08
CG1126	170.4402	-2.60686	0.43202	-6.03413	1.60E-09	2.14E-08
CG31100	71.66989	4.058419	0.673155	6.028948	1.65E-09	2.20E-08
BthD	58.75487	7.549095	1.25313	6.024192	1.70E-09	2.26E-08
CG12836	78.23308	-7.6599	1.272158	-6.02118	1.73E-09	2.30E-08
Cdk1	775.6321	2.270263	0.377435	6.014972	1.80E-09	2.39E-08
CG10864	44.26456	-5.60421	0.932162	-6.01205	1.83E-09	2.43E-08
FK506-bp1	1119.903	2.446867	0.407645	6.002446	1.94E-09	2.57E-08
net	38.43302	3.905495	0.65085	6.000609	1.97E-09	2.60E-08
mam	269.9637	-2.12646	0.354426	-5.99973	1.98E-09	2.61E-08
kek3	35.34289	-5.1912	0.865255	-5.99962	1.98E-09	2.61E-08
wbl	34.17268	-7.9168	1.319765	-5.99864	1.99E-09	2.62E-08
DOR	96.31154	-5.38253	0.897693	-5.99595	2.02E-09	2.66E-08
GILT2	34.12603	4.19021	0.69889	5.995517	2.03E-09	2.66E-08

Glut1	42.57031	-4.07767	0.681127	-5.98665	2.14E-09	2.81E-08
His2Av	105.4283	3.038162	0.507772	5.983316	2.19E-09	2.86E-08
CG2736	29.8342	6.112812	1.022416	5.978793	2.25E-09	2.93E-08
CG10311	31.19456	-6.53012	1.093147	-5.97369	2.32E-09	3.02E-08
CG2975	52.35292	3.186641	0.533806	5.969657	2.38E-09	3.09E-08
CG30154	26.38837	-5.50423	0.923279	-5.96161	2.50E-09	3.25E-08
CG42361	65.33402	-2.87982	0.483186	-5.96006	2.52E-09	3.27E-08
CG30105	76.7618	3.297398	0.553349	5.958979	2.54E-09	3.29E-08
Orc1	69.69368	4.322557	0.725468	5.958298	2.55E-09	3.30E-08
CG12420	23.37746	-5.51143	0.926874	-5.94626	2.74E-09	3.54E-08
CG33110	290.4729	-2.85809	0.481887	-5.93104	3.01E-09	3.88E-08
CG11367	89.18904	-2.61516	0.441375	-5.92503	3.12E-09	4.02E-08
CG30271	178.4632	-5.27016	0.890887	-5.91563	3.31E-09	4.25E-08
Cpr92F	52.81739	-5.48114	0.927635	-5.90873	3.45E-09	4.43E-08
Mid1	146.6095	-3.03287	0.513538	-5.90582	3.51E-09	4.50E-08
GNBP3	1087.528	-1.92932	0.32688	-5.90223	3.59E-09	4.59E-08
5-HT1A	90.28655	-7.24386	1.228769	-5.89522	3.74E-09	4.78E-08
CG14367	432.2102	-2.24791	0.381559	-5.89138	3.83E-09	4.89E-08
fz2	157.9149	-3.05384	0.519357	-5.88005	4.10E-09	5.23E-08
Apoltp	170.1229	-2.39625	0.408265	-5.86935	4.38E-09	5.57E-08
CG3669	30.91216	-8.27732	1.411522	-5.86411	4.52E-09	5.74E-08
PVRAP	81.55056	-3.54034	0.604537	-5.85628	4.73E-09	6.00E-08

CG5280	53.6549	-4.09581	0.699767	-5.8531	4.82E-09	6.11E-08
CG45186	150.001	-2.07115	0.354012	-5.8505	4.90E-09	6.20E-08
CR44922	279.1895	-2.41382	0.4126	-5.85026	4.91E-09	6.20E-08
msd1	61.1622	5.724438	0.979122	5.8465	5.02E-09	6.33E-08
CG17278	425.1785	-3.59859	0.615853	-5.84326	5.12E-09	6.44E-08
CG34362	35.6287	-3.91177	0.669536	-5.84251	5.14E-09	6.46E-08
gudu	38.20842	-7.74844	1.327981	-5.83476	5.39E-09	6.76E-08
IM23	113.3424	-4.48856	0.76963	-5.83211	5.47E-09	6.86E-08
Syt1	271.1496	-3.06121	0.525066	-5.83015	5.54E-09	6.92E-08
klg	327.8216	-2.04438	0.350663	-5.83004	5.54E-09	6.92E-08
CG34437	31.81395	-7.77549	1.335468	-5.82229	5.80E-09	7.24E-08
CG34456	31.3264	-6.49092	1.115079	-5.82104	5.85E-09	7.29E-08
nemy	157.9957	-3.66396	0.630217	-5.8138	6.11E-09	7.60E-08
Fas3	733.8889	-1.71633	0.295619	-5.80589	6.40E-09	7.95E-08
CG15120	71.84588	-7.40373	1.276027	-5.80217	6.55E-09	8.12E-08
CG3777	31.11047	4.597581	0.792828	5.798964	6.67E-09	8.26E-08
olf186-F	40.85539	-3.905	0.673694	-5.79641	6.77E-09	8.38E-08
CG32521	182.9503	-2.39084	0.412496	-5.79604	6.79E-09	8.38E-08
Cyp12d1-p	56.68221	-6.22281	1.074292	-5.79248	6.94E-09	8.55E-08
DNApol-alpha73	64.20369	4.786641	0.826403	5.792139	6.95E-09	8.56E-08
Gmap	137.188	-2.63468	0.4551	-5.78924	7.07E-09	8.69E-08
CG17121	545.6401	-3.00919	0.52002	-5.78668	7.18E-09	8.81E-08

Teh3	142.0171	-6.02619	1.042301	-5.78161	7.40E-09	9.07E-08
GstD2	168.8364	-3.49118	0.603971	-5.78037	7.45E-09	9.12E-08
Cyp4s3	110.5555	-3.67829	0.636353	-5.78027	7.46E-09	9.12E-08
pic	776.1427	1.890738	0.327174	5.779006	7.51E-09	9.17E-08
tef	156.4307	2.62608	0.45449	5.778087	7.56E-09	9.21E-08
tsh	160.6757	2.669362	0.462162	5.775815	7.66E-09	9.32E-08
jp	86.18	-5.89613	1.020916	-5.77533	7.68E-09	9.33E-08
Efhc1.2	39.81997	-3.578	0.619678	-5.77397	7.74E-09	9.40E-08
shu	39.55634	6.164851	1.067741	5.773733	7.75E-09	9.40E-08
CG42541	29.86897	-4.7759	0.828325	-5.76573	8.13E-09	9.84E-08
CG13436	96.03826	2.81357	0.488117	5.764129	8.21E-09	9.92E-08
CG5890	123.0287	-3.71381	0.644691	-5.76061	8.38E-09	1.01E-07
CG7565	236.6901	-2.1768	0.378036	-5.7582	8.50E-09	1.02E-07
CG14431	27.80613	-7.87339	1.368388	-5.75377	8.73E-09	1.05E-07
CG43373	65.67163	-5.29971	0.921195	-5.75308	8.76E-09	1.05E-07
Cpr35B	43.17992	9.067633	1.576698	5.751028	8.87E-09	1.06E-07
pip	35.64699	-3.56808	0.620648	-5.74896	8.98E-09	1.08E-07
CG16734	105.5243	3.265629	0.568284	5.746473	9.11E-09	1.09E-07
Oseg2	260.1805	-3.07318	0.535423	-5.73973	9.48E-09	1.13E-07
Pka-C3	286.2727	-2.25243	0.392647	-5.73654	9.66E-09	1.15E-07
CG34205	28.70936	-7.9585	1.387494	-5.73588	9.70E-09	1.16E-07
betaGlu	223.327	2.017956	0.352206	5.729483	1.01E-08	1.20E-07

stl	25.73743	-4.22984	0.738468	-5.72786	1.02E-08	1.21E-07
CG42458	83.37849	-2.49117	0.435385	-5.72177	1.05E-08	1.25E-07
E2f1	91.67205	2.758805	0.483048	5.711242	1.12E-08	1.33E-07
CG10208	48.17324	-3.94522	0.69094	-5.70993	1.13E-08	1.34E-07
CG44085	36.28654	-3.90248	0.683904	-5.70617	1.16E-08	1.36E-07
CG16965	23.19352	-5.01392	0.879587	-5.70032	1.20E-08	1.41E-07
Hsp67Ba	166.7894	2.138834	0.375323	5.698651	1.21E-08	1.42E-07
CG8239	32.84088	-3.66526	0.643416	-5.69656	1.22E-08	1.44E-07
SP1029	37.15868	-3.68295	0.647049	-5.69192	1.26E-08	1.48E-07
Trpgamma	25.21062	-6.54995	1.151363	-5.68887	1.28E-08	1.50E-07
CG7896	1482.708	-2.11784	0.373249	-5.67406	1.39E-08	1.63E-07
CG34398	84.68152	-2.49087	0.439178	-5.67166	1.41E-08	1.65E-07
CG9522	20.91166	-5.24021	0.923975	-5.67138	1.42E-08	1.65E-07
CG3328	50.24296	-3.44644	0.607698	-5.6713	1.42E-08	1.65E-07
rig	446.2139	1.779715	0.314032	5.66731	1.45E-08	1.69E-07
CG9194	25.45751	-7.81404	1.379626	-5.66388	1.48E-08	1.72E-07
CG31522	60.23311	2.886773	0.509683	5.663854	1.48E-08	1.72E-07
CG42741	153.9495	-2.26602	0.400149	-5.66293	1.49E-08	1.73E-07
CG10131	39.44288	5.87481	1.037663	5.661577	1.50E-08	1.74E-07
Caf1-180	244.8175	2.387007	0.42163	5.661372	1.50E-08	1.74E-07
orb2	122.7338	-2.44925	0.433017	-5.65624	1.55E-08	1.79E-07
iav	148.1853	-3.14165	0.556023	-5.65022	1.60E-08	1.85E-07

CG5337	115.4534	-2.50131	0.442713	-5.64997	1.60E-08	1.85E-07
CR45514	21.22953	-5.43224	0.961686	-5.64866	1.62E-08	1.86E-07
DNApol-eta	140.7421	2.156868	0.382538	5.638309	1.72E-08	1.97E-07
spri	32.05281	-3.94964	0.701297	-5.63191	1.78E-08	2.05E-07
beat-IV	32.0524	-5.42807	0.96569	-5.62093	1.90E-08	2.18E-07
Ccp84Aa	453.7133	7.748447	1.378772	5.619815	1.91E-08	2.19E-07
CG32238	65.86855	-3.12513	0.556254	-5.61818	1.93E-08	2.21E-07
Snap24	542.3302	-1.71516	0.305555	-5.61327	1.99E-08	2.27E-07
mmy	184.3262	3.760618	0.670657	5.607363	2.05E-08	2.34E-07
DNApol-epsilon58	62.97705	7.267956	1.296611	5.605348	2.08E-08	2.37E-07
SPoCk	1089.994	-1.91367	0.342297	-5.59068	2.26E-08	2.57E-07
CG42284	253.4094	-5.70903	1.021785	-5.58731	2.31E-08	2.62E-07
PsGEF	121.8635	-2.60528	0.466504	-5.58468	2.34E-08	2.65E-07
ACC	77.18695	-2.72289	0.487884	-5.58102	2.39E-08	2.71E-07
nord	115.629	2.594326	0.465151	5.577382	2.44E-08	2.76E-07
CG6425	37.74132	5.25929	0.943512	5.574164	2.49E-08	2.81E-07
CG13055	19.81439	-5.1953	0.933187	-5.56726	2.59E-08	2.92E-07
CR45421	22.46024	6.569037	1.180936	5.562571	2.66E-08	2.99E-07
CG15249	29.33283	4.094261	0.73687	5.556285	2.76E-08	3.10E-07
Cdc16	214.2801	2.054365	0.369741	5.556227	2.76E-08	3.10E-07
Tsp74F	27.9597	4.423963	0.797518	5.547167	2.90E-08	3.26E-07
CG8398	27.26427	-3.87699	0.699359	-5.54363	2.96E-08	3.32E-07

Nlg3	33.27249	-6.0869	1.098605	-5.54057	3.01E-08	3.37E-07
Pask	70.35159	-3.39513	0.61319	-5.53684	3.08E-08	3.44E-07
Cda5	97.96132	2.552253	0.461012	5.5362	3.09E-08	3.45E-07
mGluR	26.81872	-4.39116	0.793216	-5.53589	3.10E-08	3.45E-07
Rbf2	78.891	2.843107	0.514074	5.530544	3.19E-08	3.55E-07
E(spl)m5-HLH	30.00777	7.392333	1.340648	5.513999	3.51E-08	3.90E-07
mgl	490.292	-2.04535	0.371014	-5.51286	3.53E-08	3.92E-07
nmo	60.75514	-2.71345	0.492223	-5.51264	3.53E-08	3.92E-07
CG8213	21.18284	-6.74315	1.223888	-5.50962	3.60E-08	3.98E-07
CG17324	33.5148	-7.48408	1.358851	-5.50765	3.64E-08	4.02E-07
CG14770	73.58249	-4.3734	0.794142	-5.50707	3.65E-08	4.03E-07
CenB1A	206.3743	-2.08039	0.377786	-5.50681	3.65E-08	4.03E-07
LManII	70.28593	-2.4055	0.437059	-5.50384	3.72E-08	4.09E-07
CG32204	56.20543	-3.75633	0.683386	-5.49664	3.87E-08	4.26E-07
Rpi	47.14938	3.259841	0.593111	5.496174	3.88E-08	4.26E-07
CG13982	23.96966	-5.43385	0.989316	-5.49254	3.96E-08	4.35E-07
CG17122	58.98978	-4.10924	0.748726	-5.48831	4.06E-08	4.44E-07
cato	34.5298	6.644027	1.2107	5.487755	4.07E-08	4.45E-07
RhoGEF4	50.10364	7.310404	1.332395	5.486663	4.10E-08	4.47E-07
Ca-beta	105.2726	-3.2782	0.597836	-5.48344	4.17E-08	4.55E-07
hook	416.629	-1.75562	0.320346	-5.4804	4.24E-08	4.62E-07
CG13185	385.3119	1.965618	0.359142	5.473092	4.42E-08	4.81E-07

CG34196	25.49061	8.586866	1.56929	5.471815	4.45E-08	4.84E-07
CG43155	31.07924	-5.91084	1.080839	-5.46875	4.53E-08	4.92E-07
Actbeta	455.2824	-2.08735	0.38173	-5.46813	4.55E-08	4.93E-07
SP2353	973.2076	-2.35236	0.430393	-5.46561	4.61E-08	4.99E-07
Ih	99.71948	3.976394	0.727747	5.46398	4.66E-08	5.03E-07
polybromo	487.1567	1.661819	0.304275	5.461568	4.72E-08	5.10E-07
CG5867	2369.734	-3.00256	0.550024	-5.45896	4.79E-08	5.17E-07
Ino80	325.0593	1.828705	0.335472	5.451139	5.00E-08	5.39E-07
wdp	22.59148	5.963888	1.094313	5.449892	5.04E-08	5.42E-07
Cyp311a1	53.06367	-5.75685	1.056368	-5.44966	5.05E-08	5.42E-07
Shab	151.6289	-5.58418	1.025843	-5.4435	5.22E-08	5.61E-07
Mur2B	27.81368	-7.35667	1.352576	-5.43901	5.36E-08	5.74E-07
CG32006	582.4147	-2.25998	0.415908	-5.43386	5.51E-08	5.90E-07
ckd	185.2205	2.233283	0.411301	5.429807	5.64E-08	6.03E-07
CG8924	191.7093	2.109451	0.38891	5.424004	5.83E-08	6.22E-07
mthl9	256.4836	2.173039	0.40094	5.419859	5.96E-08	6.36E-07
CG1309	564.8076	-2.37086	0.437525	-5.41879	6.00E-08	6.39E-07
CG6761	30.73104	-5.93474	1.095375	-5.418	6.03E-08	6.41E-07
Eb1	127.232	-2.27997	0.420835	-5.41773	6.04E-08	6.41E-07
sgg	617.4916	-2.09086	0.386835	-5.40504	6.48E-08	6.87E-07
CG34203	29.95881	-7.60859	1.408143	-5.40328	6.54E-08	6.93E-07
vri	57.74308	-2.87845	0.533252	-5.39792	6.74E-08	7.13E-07

Cpr65Ax2	24.11183	8.501242	1.575275	5.396672	6.79E-08	7.18E-07
CG13675	25.40016	-3.90802	0.724212	-5.39623	6.81E-08	7.18E-07
dpr2	30.63837	-7.13312	1.322745	-5.39267	6.94E-08	7.32E-07
CG7888	153.1627	-6.84588	1.269874	-5.39099	7.01E-08	7.38E-07
CG7593	71.44142	3.051001	0.566142	5.389105	7.08E-08	7.45E-07
CG11426	98.32869	-2.34987	0.437313	-5.37344	7.72E-08	8.11E-07
CG13065	21.92437	-8.20995	1.528486	-5.37129	7.82E-08	8.20E-07
Sld5	41.07378	5.682743	1.058102	5.370696	7.84E-08	8.22E-07
brp	57.31509	-2.85879	0.532347	-5.37016	7.87E-08	8.23E-07
Hsl	61.67239	-2.85349	0.532199	-5.3617	8.24E-08	8.62E-07
btd	85.78934	-2.33071	0.435395	-5.3531	8.65E-08	9.02E-07
Cubn	174.159	-1.85397	0.346578	-5.34937	8.83E-08	9.20E-07
CG14965	70.82581	2.786439	0.52108	5.347431	8.92E-08	9.29E-07
DIP-eta	51.16233	-3.33937	0.624858	-5.34422	9.08E-08	9.44E-07
CG16886	30.04583	4.446507	0.832392	5.341846	9.20E-08	9.56E-07
CG41284	283.1258	-2.35602	0.441315	-5.33863	9.37E-08	9.72E-07
Cyp28a5	158.259	-4.06784	0.762172	-5.33717	9.44E-08	9.78E-07
tap	21.00291	7.830269	1.467398	5.336159	9.49E-08	9.82E-07
kni	38.30915	-4.44181	0.832648	-5.33456	9.58E-08	9.90E-07
CG30438	182.3619	-2.07222	0.388848	-5.32912	9.87E-08	1.02E-06
toc	153.3059	-2.96111	0.555734	-5.32828	9.91E-08	1.02E-06
dom	417.4763	1.803155	0.338858	5.321278	1.03E-07	1.06E-06

Ugt35a	193.0282	-3.82495	0.718885	-5.32067	1.03E-07	1.06E-06
CR44929	18.4597	6.187855	1.163632	5.31771	1.05E-07	1.08E-06
CG31675	20.63193	-7.369	1.386249	-5.31578	1.06E-07	1.09E-06
Past1	532.571	-1.70628	0.321139	-5.31322	1.08E-07	1.10E-06
Hsp70Bc	1863.161	-4.10063	0.772429	-5.30875	1.10E-07	1.13E-06
Cpsf73	187.7789	2.033955	0.383724	5.300572	1.15E-07	1.18E-06
CR44283	57.10168	-4.92742	0.930676	-5.29445	1.19E-07	1.22E-06
rdgA	116.5495	-2.56016	0.484175	-5.28767	1.24E-07	1.26E-06
CG12268	18.2165	6.17177	1.167264	5.287381	1.24E-07	1.26E-06
Hsp70Bb	2173.333	-4.023	0.760882	-5.28728	1.24E-07	1.26E-06
CR43436	20.21697	4.361371	0.82536	5.284206	1.26E-07	1.28E-06
Eip74EF	53.58626	-2.77006	0.524517	-5.28116	1.28E-07	1.30E-06
Grip75	271.8046	2.432295	0.46061	5.280593	1.29E-07	1.31E-06
CG15522	23.98505	-4.81016	0.911873	-5.27503	1.33E-07	1.34E-06
CG15563	30.65311	-3.33212	0.632341	-5.2695	1.37E-07	1.38E-06
wtrw	77.88638	-2.49542	0.473835	-5.26642	1.39E-07	1.41E-06
kermit	52.59009	-2.68966	0.510815	-5.26542	1.40E-07	1.41E-06
CG14853	154.4173	-2.42754	0.461279	-5.26263	1.42E-07	1.43E-06
Nup75	190.226	2.341168	0.445191	5.258795	1.45E-07	1.46E-06
twit	304.3988	4.714396	0.897797	5.251068	1.51E-07	1.52E-06
GstE5	275.948	-2.46894	0.470234	-5.25046	1.52E-07	1.52E-06
CG33284	19.57643	-8.05356	1.536734	-5.2407	1.60E-07	1.60E-06

CG34120	477.0647	2.634117	0.502872	5.238145	1.62E-07	1.62E-06
CG17272	791.1946	-1.76606	0.337177	-5.23778	1.63E-07	1.63E-06
Ran	27.50102	3.932393	0.75094	5.23663	1.64E-07	1.63E-06
Ir75a	224.3907	3.25187	0.621822	5.229586	1.70E-07	1.70E-06
Hsp70Bbb	2030.546	-4.11574	0.787152	-5.22865	1.71E-07	1.70E-06
CG5038	103.2217	-2.04891	0.391903	-5.22811	1.71E-07	1.71E-06
CG9698	18.65656	-7.4138	1.418206	-5.22759	1.72E-07	1.71E-06
CG13272	18.78865	-7.59503	1.453077	-5.22686	1.72E-07	1.71E-06
papi	83.03256	2.231593	0.426983	5.226416	1.73E-07	1.71E-06
SNF4Agamma	64.10336	-2.73683	0.523741	-5.22555	1.74E-07	1.72E-06
ome	20.23063	-5.17713	0.991278	-5.22268	1.76E-07	1.75E-06
Su(var)2-HP2	377.8819	2.14213	0.410175	5.22248	1.77E-07	1.75E-06
ppk25	17.90783	-5.30254	1.015376	-5.22225	1.77E-07	1.75E-06
CG32473	247.2894	-1.98256	0.379794	-5.22009	1.79E-07	1.76E-06
Hmu	1247.018	-1.94937	0.37393	-5.21321	1.86E-07	1.83E-06
CG6126	168.6861	-2.37151	0.455026	-5.21182	1.87E-07	1.84E-06
CG5282	82.02415	-2.67726	0.513693	-5.21179	1.87E-07	1.84E-06
CG14490	20.60141	-7.00168	1.344492	-5.20768	1.91E-07	1.88E-06
Hsp70Ba	1798.642	-3.99621	0.767555	-5.20641	1.93E-07	1.89E-06
Eip63F-1	55.84615	-6.62416	1.273191	-5.2028	1.96E-07	1.92E-06
dpr11	44.15176	-4.97907	0.957132	-5.20207	1.97E-07	1.93E-06
CG33158	201.1354	2.119727	0.40783	5.197573	2.02E-07	1.97E-06

CG14085	162.3359	-2.30025	0.442703	-5.19593	2.04E-07	1.99E-06
CHES-1-like	66.55494	-2.75476	0.530327	-5.19446	2.05E-07	2.00E-06
CG3655	66.28544	-2.37992	0.458223	-5.1938	2.06E-07	2.01E-06
26-29-p	1551.058	-1.75431	0.337785	-5.19356	2.06E-07	2.01E-06
CG2091	259.8075	2.112532	0.407084	5.189421	2.11E-07	2.05E-06
CG31345	78.74003	-4.40616	0.850123	-5.18297	2.18E-07	2.12E-06
nrv3	41.53441	-4.01119	0.774234	-5.18085	2.21E-07	2.14E-06
CG9095	16.14121	-6.16866	1.192411	-5.17327	2.30E-07	2.23E-06
CG3045	85.40387	2.480516	0.479663	5.171374	2.32E-07	2.25E-06
CG6216	49.01184	-2.93636	0.568422	-5.16581	2.39E-07	2.31E-06
Grip91	258.1378	2.123894	0.411685	5.159024	2.48E-07	2.39E-06
aft	343.4762	1.926107	0.373349	5.159002	2.48E-07	2.39E-06
CG17032	32.85164	5.055766	0.980136	5.158231	2.49E-07	2.40E-06
CG43386	240.3436	2.303341	0.44695	5.15346	2.56E-07	2.46E-06
CG1637	438.8707	-3.02319	0.587623	-5.14478	2.68E-07	2.57E-06
GstD11	137.3767	-3.42904	0.666558	-5.1444	2.68E-07	2.58E-06
CG5493	15.88173	-5.5208	1.07421	-5.13941	2.76E-07	2.64E-06
Prx2540-2	77.0886	4.508721	0.877695	5.136999	2.79E-07	2.67E-06
CG5955	104.4402	-3.56136	0.693415	-5.13598	2.81E-07	2.68E-06
CG13041	132.3582	7.651269	1.490834	5.132209	2.86E-07	2.74E-06
CR44334	20.60194	5.898161	1.149309	5.131918	2.87E-07	2.74E-06
Rcd2	209.1343	2.375355	0.463009	5.130251	2.89E-07	2.76E-06

trsn	309.8925	1.649974	0.321952	5.124903	2.98E-07	2.83E-06
Cyp28d1	81.47586	-3.63025	0.708453	-5.12419	2.99E-07	2.84E-06
eya	20.11235	5.223406	1.020335	5.119303	3.07E-07	2.91E-06
Vha68-1	47.0676	-3.09298	0.604443	-5.11708	3.10E-07	2.94E-06
GckIII	482.1558	-2.31917	0.453687	-5.11183	3.19E-07	3.02E-06
DNApol-alpha60	68.33023	3.657184	0.715565	5.110905	3.21E-07	3.03E-06
CG10262	43.81554	-3.01573	0.590174	-5.1099	3.22E-07	3.05E-06
DAAM	22.87073	-3.68144	0.720495	-5.1096	3.23E-07	3.05E-06
beat-VI	20.17796	-7.08914	1.38775	-5.10837	3.25E-07	3.07E-06
zye	19.5963	5.07341	0.994741	5.100234	3.39E-07	3.20E-06
EMC3	307.9549	-2.73325	0.536502	-5.09457	3.50E-07	3.29E-06
prc	19.16636	-7.31474	1.437057	-5.09008	3.58E-07	3.37E-06
neb	81.52077	3.650971	0.717624	5.087584	3.63E-07	3.41E-06
chas	60.18589	-5.24441	1.031476	-5.08438	3.69E-07	3.46E-06
CG12075	22.95697	-4.28995	0.843982	-5.08298	3.72E-07	3.48E-06
CG33275	119.1776	-1.87046	0.368228	-5.07962	3.78E-07	3.54E-06
Sas-4	114.5474	2.435932	0.480375	5.070896	3.96E-07	3.70E-06
Mat89Ba	225.6862	1.812698	0.357605	5.068988	4.00E-07	3.74E-06
CG4038	272.5909	1.797228	0.354746	5.066237	4.06E-07	3.79E-06
Nnf1a	90.51542	2.271796	0.44844	5.065998	4.06E-07	3.79E-06
CR43641	18.02852	-7.26573	1.434594	-5.06466	4.09E-07	3.81E-06
Syn2	33.25674	-4.93134	0.97445	-5.06064	4.18E-07	3.89E-06

mute	97.63485	2.083891	0.412224	5.055236	4.30E-07	3.99E-06
alpha-Man-IIb	102.5422	-2.56138	0.506901	-5.05301	4.35E-07	4.04E-06
Top3alpha	127.1804	2.422504	0.479722	5.049803	4.42E-07	4.10E-06
LPCAT	547.949	-1.62265	0.32145	-5.04789	4.47E-07	4.14E-06
CG15701	107.5237	-2.34797	0.466031	-5.03823	4.70E-07	4.35E-06
mei-218	28.9574	3.361121	0.667176	5.037832	4.71E-07	4.35E-06
NnaD	48.19543	-3.3169	0.658651	-5.03591	4.76E-07	4.39E-06
CG13532	124.5531	-2.1726	0.431543	-5.03449	4.79E-07	4.42E-06
Ibf2	106.4815	2.166222	0.430402	5.033023	4.83E-07	4.45E-06
CG13008	19.69372	-5.73996	1.142611	-5.02355	5.07E-07	4.67E-06
CG11655	142.6785	-2.23346	0.444898	-5.02017	5.16E-07	4.74E-06
CG4393	43.10789	-2.82835	0.563428	-5.01989	5.17E-07	4.74E-06
CG8460	268.2919	1.756827	0.350097	5.018115	5.22E-07	4.78E-06
sqd	4332.609	1.879148	0.374493	5.017843	5.23E-07	4.79E-06
CG4676	27.76675	-3.23214	0.644628	-5.01396	5.33E-07	4.88E-06
CG14868	87.11133	-2.47964	0.494691	-5.0125	5.37E-07	4.91E-06
bora	27.44841	4.37216	0.872328	5.012061	5.39E-07	4.92E-06
Act88F	27.0103	-6.08145	1.215506	-5.00323	5.64E-07	5.14E-06
alpha-Est10	83.54868	-2.63864	0.527543	-5.00175	5.68E-07	5.17E-06
Shawl	21.3698	-6.99948	1.399755	-5.0005	5.72E-07	5.20E-06
CG14110	23.00464	-3.80714	0.761459	-4.99979	5.74E-07	5.22E-06
CG3556	912.2558	-2.09818	0.420065	-4.99489	5.89E-07	5.34E-06

Mip	16.18326	-7.55622	1.512874	-4.99461	5.90E-07	5.35E-06
bip1	41.41635	2.875483	0.576166	4.990719	6.02E-07	5.44E-06
Atet	57.16939	-4.67043	0.935845	-4.99061	6.02E-07	5.44E-06
CG11851	189.802	2.140195	0.428854	4.990499	6.02E-07	5.44E-06
CG13727	16.22555	-7.9889	1.601499	-4.98839	6.09E-07	5.50E-06
betaTub97EF	32.34166	-3.52659	0.707149	-4.98705	6.13E-07	5.53E-06
mbo	215.5745	1.719963	0.344904	4.986785	6.14E-07	5.53E-06
CG10433	58.03047	-3.2868	0.659271	-4.98551	6.18E-07	5.56E-06
Edg91	40.28066	7.111725	1.426997	4.983699	6.24E-07	5.61E-06
dpr12	76.00363	-2.53085	0.508211	-4.97992	6.36E-07	5.71E-06
Galphao	369.3009	-2.07027	0.415813	-4.97885	6.40E-07	5.74E-06
CG5033	292.6138	1.694175	0.34068	4.972926	6.59E-07	5.91E-06
CG1648	217.4511	-2.21042	0.444983	-4.96742	6.78E-07	6.07E-06
Ald	249.4098	-2.10931	0.424841	-4.96494	6.87E-07	6.15E-06
CG6040	2831.659	-1.63396	0.329201	-4.9634	6.93E-07	6.19E-06
Pde9	56.48349	-2.78287	0.561001	-4.96055	7.03E-07	6.27E-06
ato	181.509	2.98841	0.602535	4.959727	7.06E-07	6.29E-06
CG17387	39.86419	-2.54057	0.512428	-4.9579	7.13E-07	6.35E-06
Nek2	127.5577	2.641044	0.532745	4.957424	7.14E-07	6.36E-06
CG14397	259.0722	2.386847	0.481563	4.956463	7.18E-07	6.38E-06
asl	190.4436	1.83973	0.371424	4.953177	7.30E-07	6.48E-06
B4	352.6496	-2.12826	0.429869	-4.95095	7.39E-07	6.55E-06

CG7695	147.8187	3.845573	0.776961	4.949505	7.44E-07	6.59E-06
CG8303	23.57058	-4.06951	0.822452	-4.94802	7.50E-07	6.63E-06
CG15597	15.73543	-6.17377	1.247926	-4.94723	7.53E-07	6.66E-06
IntS10	140.1091	2.008076	0.405934	4.946802	7.54E-07	6.66E-06
Rbp6	150.0768	-2.22888	0.451305	-4.93874	7.86E-07	6.94E-06
CG13157	14.6386	-7.44928	1.508798	-4.93723	7.92E-07	6.98E-06
Lsm11	40.73536	3.081933	0.624295	4.936661	7.95E-07	7.00E-06
laccase2	719.628	-1.98629	0.402408	-4.93602	7.97E-07	7.01E-06
CG42633	86.68568	-2.90224	0.588193	-4.93416	8.05E-07	7.07E-06
qtc	22.67377	-3.8661	0.783751	-4.93281	8.11E-07	7.11E-06
CG45122	52.42035	-3.12298	0.633459	-4.93004	8.22E-07	7.21E-06
CG14946	28.55835	3.084352	0.626101	4.926285	8.38E-07	7.34E-06
CG44837	15.1244	-7.15995	1.456521	-4.91579	8.84E-07	7.74E-06
Cpr56F	17.79989	-6.99332	1.425992	-4.90418	9.38E-07	8.20E-06
Ctf4	91.63547	3.550039	0.723899	4.904051	9.39E-07	8.20E-06
CG5953	59.50272	-2.49823	0.509533	-4.90297	9.44E-07	8.23E-06
CG13325	17.40688	-4.98667	1.017076	-4.90294	9.44E-07	8.23E-06
mspo	33.77366	-3.05809	0.623901	-4.90156	9.51E-07	8.28E-06
ASPP	30.84328	-4.42948	0.904057	-4.89955	9.61E-07	8.35E-06

Table 8: Significantly differentially expressed genes between p40 and Adult stages. Table of significantly differentially expressed genes ($p>10^{-6}$) between p40 and Adult, represented by red dots in Fig 25D.

Differentially Expressed Genes (p40 vs Adult)						
	baseMean	log2FoldChange	lfcSE	stat	pvalue	padj
a10	12521.82	-9.62663	0.343631	-28.0145	1.08E-172	9.82E-169
OS9	6614.245	-9.40086	0.386627	-24.315	1.36E-130	6.16E-127
Osi7	22459.85	8.757466	0.362523	24.15699	6.30E-129	1.91E-125
CG17672	2505.221	7.968473	0.334685	23.80887	2.70E-125	6.13E-122
CG43366	2550.509	8.960842	0.384664	23.29522	4.96E-120	8.99E-117
ect	4741.583	9.00272	0.39075	23.0396	1.87E-117	2.83E-114
m	6041.94	8.316592	0.361289	23.01922	2.99E-117	3.88E-114
Jhedup	12573.11	-9.4994	0.416504	-22.8075	3.87E-115	4.38E-112
CG18735	3420.868	9.62431	0.423919	22.7032	4.17E-114	4.20E-111
Obp19a	4021.103	-10.0856	0.44714	-22.5559	1.18E-112	1.07E-109
Osi3	5746.283	9.350048	0.421459	22.18494	4.80E-109	3.96E-106
a5	4018.832	-9.31076	0.420022	-22.1673	7.10E-109	5.36E-106
CG15888	5660.568	9.348576	0.421944	22.15599	9.13E-109	6.37E-106
CG11391	3843.06	-9.45911	0.428144	-22.0933	3.66E-108	2.37E-105
Obp83b	8401.708	-8.73748	0.397725	-21.9686	5.75E-107	3.47E-104
Obp69a	3079.633	-9.26979	0.424944	-21.8141	1.70E-105	9.65E-103
Drsl5	8592.676	-9.04506	0.415014	-21.7946	2.61E-105	1.39E-102
Osi12	5979.015	8.730716	0.413503	21.11404	5.91E-99	2.98E-96
CG17211	1550.979	8.846951	0.42439	20.84628	1.65E-96	7.86E-94

CG12880	2280.802	6.682682	0.320983	20.81943	2.89E-96	1.31E-93
Osi22	12411.92	9.013232	0.443572	20.31965	8.62E-92	3.72E-89
Osi1	2859.681	8.47803	0.420566	20.15864	2.26E-90	9.31E-88
dy	4486.985	8.708332	0.432239	20.14702	2.86E-90	1.13E-87
Cad89D	2403.661	9.216088	0.458209	20.11328	5.65E-90	2.13E-87
Spn100A	5850.659	8.863371	0.443232	19.99713	5.83E-89	2.12E-86
CG4386	2390.303	9.212339	0.466039	19.7673	5.69E-87	1.99E-84
Osi11	1432.993	7.895862	0.404908	19.50038	1.09E-84	3.66E-82
Cyp6a20	2568.408	-7.15035	0.368087	-19.4257	4.68E-84	1.51E-81
CG1273	1549.075	8.90446	0.4643	19.17824	5.62E-82	1.76E-79
CG10185	2436.122	-6.5493	0.344362	-19.0187	1.19E-80	3.61E-78
CG12507	1599.493	8.720672	0.46837	18.6192	2.25E-77	6.57E-75
dsx-c73A	6308.554	8.986154	0.485887	18.49434	2.29E-76	6.50E-74
Ugt35b	3006.816	-8.32662	0.451486	-18.4427	5.97E-76	1.64E-73
Cht7	4867.001	7.539221	0.409764	18.39894	1.34E-75	3.57E-73
CG16798	1136.362	8.01872	0.43667	18.36335	2.58E-75	6.69E-73
CG11407	1478.8	-9.35152	0.511565	-18.2802	1.19E-74	3.00E-72
antdh	4943.395	-6.73876	0.36872	-18.2761	1.28E-74	3.14E-72
Osi24	1428.577	7.826367	0.429767	18.21071	4.24E-74	1.01E-71
Osi13	1170.392	9.355882	0.516265	18.12223	2.13E-73	4.95E-71
CG32354	7035.807	6.731841	0.372786	18.0582	6.80E-73	1.54E-70
CG7173	925.1052	9.181917	0.514129	17.85917	2.45E-71	5.42E-69

CG8420	3978.891	9.337528	0.525014	17.78528	9.19E-71	1.98E-68
C901	911.6753	8.255218	0.464888	17.75743	1.51E-70	3.18E-68
Obp56a	5485.198	8.402624	0.47338	17.75028	1.71E-70	3.53E-68
CG13082	1356.35	8.843107	0.49899	17.72203	2.84E-70	5.71E-68
Cyp301a1	871.4794	8.840315	0.505732	17.48025	2.03E-68	3.99E-66
Osi9	16995.34	9.079025	0.524248	17.3182	3.43E-67	6.62E-65
Osi21	952.3854	8.446982	0.490324	17.22736	1.66E-66	3.13E-64
CG5867	2369.734	-7.1022	0.415315	-17.1007	1.47E-65	2.71E-63
Cyp313a1	1321.404	-9.00947	0.529901	-17.0022	7.91E-65	1.43E-62
Cpr67B	1169.718	-8.1798	0.481916	-16.9735	1.29E-64	2.29E-62
Amt	1114.586	-8.94984	0.530964	-16.8558	9.51E-64	1.66E-61
dyl	1196.324	9.539992	0.566131	16.85122	1.03E-63	1.76E-61
Cyp9f2	907.6461	-6.01657	0.359497	-16.7361	7.16E-63	1.20E-60
CG7409	1314.866	-9.16902	0.549239	-16.694	1.45E-62	2.39E-60
GstE4	3186.528	-5.93434	0.355594	-16.6885	1.59E-62	2.57E-60
CG15239	1241.468	8.66762	0.519844	16.67352	2.04E-62	3.25E-60
spz4	586.122	7.614283	0.460448	16.53669	2.00E-61	3.12E-59
IA-2	719.0087	-6.62555	0.402102	-16.4773	5.34E-61	8.21E-59
CG9689	929.4199	8.721235	0.535169	16.29623	1.05E-59	1.59E-57
Dtg	901.8267	7.526777	0.46317	16.25057	2.21E-59	3.29E-57
CG3108	886.4119	8.448721	0.522603	16.16662	8.67E-59	1.26E-56
spz6	2286.913	8.930157	0.552403	16.16601	8.76E-59	1.26E-56

Obp59a	1344.143	-9.49813	0.590517	-16.0844	3.28E-58	4.65E-56
CG11069	850.5085	5.391119	0.336291	16.03109	7.75E-58	1.08E-55
Orco	859.7252	-8.10742	0.505903	-16.0257	8.46E-58	1.16E-55
CG4576	521.0229	-6.4898	0.411193	-15.7829	4.08E-56	5.52E-54
CG6026	2345.451	8.742936	0.554815	15.75829	6.02E-56	8.03E-54
CG10898	1133.164	5.072639	0.323998	15.65641	3.00E-55	3.95E-53
CAH1	685.8572	-6.60196	0.422856	-15.6128	5.96E-55	7.71E-53
CG8945	507.8905	8.170859	0.52354	15.60694	6.53E-55	8.34E-53
Rab23	820.8043	5.137968	0.331965	15.47744	4.93E-54	6.20E-52
Osi23	3575.429	8.745425	0.566725	15.43151	1.00E-53	1.25E-51
Jheh1	582.6436	-6.23528	0.408359	-15.2691	1.23E-52	1.51E-50
CG43093	613.6737	-8.30573	0.544164	-15.2633	1.34E-52	1.62E-50
CG43164	687.1419	8.812465	0.580946	15.16917	5.66E-52	6.75E-50
CG10936	1734.583	5.099533	0.336961	15.13391	9.68E-52	1.14E-49
CG13833	465.414	-7.70207	0.509943	-15.1038	1.53E-51	1.78E-49
ft	1585.66	6.27275	0.421518	14.88135	4.36E-50	5.00E-48
CG2254	1165.732	-7.56824	0.513179	-14.7478	3.18E-49	3.60E-47
CG30197	533.7161	-7.82857	0.531361	-14.7331	3.95E-49	4.43E-47
CG34120	477.0647	-7.17984	0.488865	-14.6867	7.84E-49	8.67E-47
AOX1	701.6756	-9.10665	0.620159	-14.6844	8.12E-49	8.87E-47
CG14687	513.8629	-6.94303	0.473543	-14.6619	1.13E-48	1.22E-46
CG9372	452.9324	-5.82757	0.397887	-14.6463	1.42E-48	1.52E-46

CG31728	555.2596	9.26085	0.637678	14.52276	8.69E-48	9.16E-46
Myo10A	568.0208	6.14056	0.427325	14.36977	8.01E-47	8.35E-45
CG6040	2831.659	4.741901	0.333479	14.21948	6.94E-46	7.15E-44
CG9447	878.1464	-10.0775	0.714789	-14.0986	3.88E-45	3.95E-43
CG17189	728.8123	-9.57131	0.683061	-14.0124	1.31E-44	1.32E-42
Osi8	3091.045	5.783237	0.413306	13.99264	1.73E-44	1.72E-42
fj	747.295	7.587055	0.550581	13.78008	3.36E-43	3.31E-41
Syngr	345.9156	-6.75865	0.49282	-13.7142	8.34E-43	8.13E-41
CG15169	443.0213	-8.19259	0.597838	-13.7037	9.65E-43	9.31E-41
CG31559	387.5105	8.868278	0.647428	13.69771	1.05E-42	1.00E-40
Cyp308a1	493.1914	-8.64804	0.633684	-13.6473	2.10E-42	1.98E-40
CG13728	507.285	8.711355	0.63984	13.6149	3.27E-42	3.05E-40
CG10357	511.7123	-7.99152	0.589203	-13.5633	6.61E-42	6.12E-40
Hsp67Bc	789.3891	5.278724	0.389895	13.53884	9.22E-42	8.45E-40
Hf	409.5432	-7.95046	0.594354	-13.3766	8.28E-41	7.51E-39
d	561.0434	5.484537	0.411738	13.32044	1.76E-40	1.58E-38
CG14625	263.1887	7.461614	0.561384	13.29145	2.59E-40	2.31E-38
Obp57c	487.1031	-8.98568	0.679698	-13.2201	6.72E-40	5.91E-38
aay	814.0527	-4.82056	0.365496	-13.1891	1.01E-39	8.84E-38
CG42331	443.3607	9.128564	0.692606	13.18003	1.14E-39	9.87E-38
CG9782	1885.763	5.912458	0.449911	13.14138	1.91E-39	1.63E-37
Cyp6a8	478.9738	-8.28568	0.631169	-13.1275	2.29E-39	1.94E-37

Snmp1	293.8819	-7.17225	0.548088	-13.0859	3.96E-39	3.33E-37
ImpE2	3662.019	6.437861	0.495809	12.98456	1.50E-38	1.25E-36
Ect3	1245.529	7.110359	0.549319	12.94395	2.54E-38	2.10E-36
CG9449	463.8011	-8.9114	0.688946	-12.9348	2.86E-38	2.34E-36
CG6834	321.7744	-6.84279	0.529651	-12.9194	3.50E-38	2.83E-36
CG4302	337.2178	-6.61743	0.51267	-12.9078	4.07E-38	3.26E-36
Cyp4d20	243.4577	-6.41342	0.497703	-12.886	5.40E-38	4.29E-36
CG10345	675.1043	-8.98043	0.696996	-12.8845	5.50E-38	4.34E-36
CG42747	589.3157	6.557422	0.510367	12.84845	8.77E-38	6.86E-36
CG17786	1131.245	4.821084	0.375648	12.83403	1.06E-37	8.19E-36
rt	587.3567	4.726291	0.369856	12.77872	2.16E-37	1.66E-35
AOX2	497.5116	6.084964	0.476941	12.75832	2.80E-37	2.13E-35
CG43092	334.3069	-6.96035	0.546058	-12.7466	3.26E-37	2.46E-35
CG17265	606.3589	4.488853	0.352707	12.72687	4.19E-37	3.14E-35
ChLD3	315.4496	7.786813	0.612479	12.7136	4.97E-37	3.69E-35
Cpr49Ah	334.4881	8.37726	0.660316	12.68675	7.00E-37	5.16E-35
Cpr72Ea	244.4312	7.804154	0.616449	12.65984	9.87E-37	7.22E-35
CG18302	646.3923	-10.2843	0.813335	-12.6446	1.20E-36	8.69E-35
Tsp47F	382.2951	-8.91	0.705792	-12.6241	1.55E-36	1.12E-34
Cyp18a1	283.5267	8.398342	0.667122	12.58892	2.43E-36	1.73E-34
CG33177	515.4248	-4.96519	0.394624	-12.5821	2.65E-36	1.88E-34
CG10553	390.146	-8.63865	0.687246	-12.57	3.09E-36	2.17E-34

Or42b	244.5675	-6.61589	0.528328	-12.5223	5.64E-36	3.93E-34
Cyp6d5	326.5223	-8.42776	0.673153	-12.5198	5.82E-36	4.02E-34
CAH2	407.1547	-5.22287	0.418045	-12.4936	8.09E-36	5.56E-34
rtet	482.652	4.9069	0.393306	12.47605	1.01E-35	6.88E-34
CG14291	974.7623	5.287139	0.423823	12.47489	1.02E-35	6.92E-34
Eip78C	244.5706	7.715199	0.620378	12.43628	1.66E-35	1.12E-33
alpha-Est8	292.3833	-6.3207	0.508492	-12.4303	1.79E-35	1.19E-33
CG15629	379.3308	5.668023	0.456588	12.41388	2.20E-35	1.45E-33
Ugt86Dd	267.1148	-7.80874	0.629518	-12.4043	2.48E-35	1.63E-33
mey	497.9432	9.723213	0.788052	12.33828	5.63E-35	3.67E-33
tyn	237.1064	8.088226	0.656533	12.31961	7.10E-35	4.60E-33
Ir8a	217.0994	-6.079	0.493818	-12.3102	7.98E-35	5.13E-33
CG31028	461.4051	6.250261	0.507934	12.30526	8.49E-35	5.42E-33
CG14153	419.569	-9.30615	0.760157	-12.2424	1.84E-34	1.17E-32
CG32473	247.2894	5.468962	0.447817	12.2125	2.67E-34	1.68E-32
Cyp4d21	612.1274	-10.155	0.832246	-12.202	3.03E-34	1.90E-32
Cyp6a2	251.4211	-6.38341	0.524289	-12.1754	4.20E-34	2.61E-32
CG31200	264.7432	-5.61592	0.463418	-12.1185	8.43E-34	5.20E-32
CG13737	225.6014	7.523888	0.623146	12.07404	1.45E-33	8.87E-32
CG13300	501.3908	4.808384	0.400199	12.01498	2.96E-33	1.80E-31
CG9498	455.4957	-9.79438	0.815366	-12.0123	3.06E-33	1.85E-31
CG14567	256.8176	4.950659	0.412816	11.99242	3.89E-33	2.34E-31

Skeletor	197.8208	7.536145	0.63339	11.89811	1.21E-32	7.22E-31
CCKLR-17D1	282.8067	-5.95694	0.502667	-11.8507	2.13E-32	1.26E-30
CG6830	202.3459	-6.48901	0.548061	-11.8399	2.43E-32	1.43E-30
Or92a	315.7987	-8.61619	0.729464	-11.8117	3.40E-32	1.99E-30
CG13023	403.8811	9.39039	0.796387	11.79124	4.33E-32	2.52E-30
CG43333	421.8265	7.323402	0.622104	11.77198	5.44E-32	3.14E-30
Cyp6t3	380.3963	-9.50027	0.808212	-11.7547	6.68E-32	3.83E-30
twz	304.1029	5.174943	0.440805	11.73974	7.97E-32	4.55E-30
CG31121	160.9406	5.84213	0.501504	11.64923	2.32E-31	1.31E-29
CG43980	193.6423	6.267092	0.539066	11.62584	3.05E-31	1.72E-29
Inos	445.0061	-5.41541	0.466072	-11.6193	3.29E-31	1.84E-29
knk	375.3852	5.632815	0.486032	11.58938	4.66E-31	2.59E-29
CG6429	205.0869	-7.56638	0.653578	-11.5769	5.40E-31	2.98E-29
Cpr66D	1342.82	6.919246	0.601903	11.49562	1.39E-30	7.62E-29
obst-A	4474.33	5.451341	0.475546	11.46333	2.02E-30	1.10E-28
Cyp4p1	172.3865	-6.26932	0.546961	-11.4621	2.04E-30	1.11E-28
NAAT1	180.5279	-6.90342	0.604115	-11.4273	3.05E-30	1.65E-28
Spn43Aa	933.8443	8.842972	0.773997	11.42507	3.13E-30	1.68E-28
CG9497	260.7513	-8.66024	0.760795	-11.3831	5.07E-30	2.71E-28
CG4721	177.7759	-6.62426	0.582363	-11.3748	5.58E-30	2.96E-28
CG6055	852.5384	8.610739	0.758282	11.35559	6.96E-30	3.67E-28
Cyp6a9	163.7561	-5.79835	0.513278	-11.2967	1.36E-29	7.14E-28

CG9514	344.6371	7.43269	0.65896	11.27942	1.66E-29	8.64E-28
CG8216	187.0984	-7.42049	0.658669	-11.2659	1.93E-29	1.00E-27
Fas3	733.8889	3.384254	0.301877	11.21071	3.61E-29	1.86E-27
CG16884	8556.606	4.355869	0.388987	11.19798	4.17E-29	2.14E-27
Ir75a	224.3907	-6.82527	0.609782	-11.193	4.41E-29	2.25E-27
Np	276.349	9.104012	0.813741	11.18786	4.68E-29	2.37E-27
Ugt86Da	446.6133	-3.91371	0.349876	-11.186	4.78E-29	2.41E-27
CG42741	153.9495	5.369649	0.480205	11.18198	5.00E-29	2.50E-27
CG30285	566.4441	-4.70901	0.422004	-11.1587	6.50E-29	3.24E-27
CG40006	1619.231	-5.21403	0.46945	-11.1067	1.16E-28	5.77E-27
CG8568	263.5912	5.141093	0.462987	11.10419	1.20E-28	5.90E-27
CG9503	177.1013	7.322895	0.660822	11.0815	1.54E-28	7.56E-27
CG7402	320.9589	-7.09441	0.64184	-11.0532	2.11E-28	1.03E-26
alpha-Est1	630.4761	-4.96985	0.449738	-11.0505	2.18E-28	1.06E-26
CG34247	283.8842	8.002124	0.724727	11.04158	2.41E-28	1.16E-26
Ir76b	387.5432	-9.97759	0.90761	-10.9933	4.12E-28	1.98E-26
IM1	165.644	-6.66438	0.607393	-10.9721	5.20E-28	2.48E-26
CG10863	269.9048	-5.06502	0.461638	-10.9719	5.22E-28	2.48E-26
wntD	138.8224	7.292391	0.665627	10.95567	6.24E-28	2.95E-26
CG6836	363.3921	-9.42771	0.860957	-10.9503	6.63E-28	3.11E-26
CG9519	252.3172	-8.92028	0.823942	-10.8264	2.58E-27	1.21E-25
CG31199	172.9842	-5.00322	0.463427	-10.7961	3.59E-27	1.67E-25

Or59b	197.2446	-8.28391	0.767728	-10.7902	3.83E-27	1.77E-25
CG43066	395.0858	-3.94812	0.367622	-10.7396	6.63E-27	3.05E-25
Teh4	173.9483	-6.46313	0.602136	-10.7337	7.07E-27	3.24E-25
CG13744	147.7361	8.013049	0.747971	10.71305	8.84E-27	4.03E-25
CG15080	900.7429	7.962223	0.74351	10.70896	9.24E-27	4.19E-25
twit	304.3988	-9.46305	0.884957	-10.6932	1.09E-26	4.94E-25
hbs	263.2241	5.671767	0.530471	10.69194	1.11E-26	4.98E-25
CG3649	223.5487	5.88108	0.551572	10.6624	1.53E-26	6.82E-25
esg	432.9292	6.207184	0.582393	10.65808	1.60E-26	7.10E-25
CG14608	122.6274	6.120127	0.57526	10.63889	1.96E-26	8.69E-25
CG15005	159.3394	5.74216	0.540033	10.63298	2.09E-26	9.21E-25
CG14107	322.257	9.233159	0.870214	10.61022	2.67E-26	1.17E-24
CalpC	759.7585	3.891048	0.367207	10.59633	3.10E-26	1.35E-24
CG6421	127.5949	-6.41478	0.605487	-10.5944	3.16E-26	1.37E-24
mwh	108.025	5.643154	0.533454	10.57852	3.75E-26	1.62E-24
SerT	128.6969	-6.27494	0.593616	-10.5707	4.07E-26	1.75E-24
Fbxl7	386.975	4.761673	0.451882	10.53743	5.81E-26	2.48E-24
CG14259	226.1929	-4.89478	0.465188	-10.5222	6.83E-26	2.91E-24
CG16820	924.8781	4.257364	0.404706	10.51964	7.01E-26	2.97E-24
CG13386	128.644	6.673955	0.635948	10.49449	9.16E-26	3.86E-24
CR44960	138.9073	-5.54261	0.528202	-10.4934	9.27E-26	3.89E-24
CG14301	388.218	3.955371	0.37719	10.4864	9.98E-26	4.17E-24

CG32091	375.4872	-3.65903	0.349126	-10.4806	1.06E-25	4.41E-24
Spn43Ab	127.9098	-6.68323	0.637884	-10.4772	1.10E-25	4.55E-24
CG13699	161.0092	5.476186	0.523213	10.46645	1.23E-25	5.08E-24
Or22b	212.9626	-8.70452	0.833951	-10.4377	1.67E-25	6.84E-24
CG31288	155.8445	-7.2036	0.690206	-10.4369	1.68E-25	6.87E-24
CG5731	567.0205	4.752185	0.455533	10.43214	1.77E-25	7.19E-24
CG13631	1419.25	3.595683	0.345728	10.40033	2.47E-25	1.00E-23
CG5873	1498.542	5.588221	0.538852	10.37061	3.37E-25	1.36E-23
Sh	802.2374	-3.61212	0.348345	-10.3694	3.42E-25	1.37E-23
CG16700	327.7066	-4.00392	0.386367	-10.363	3.65E-25	1.46E-23
CG17108	540.3228	-6.30683	0.609181	-10.353	4.06E-25	1.61E-23
CG1695	258.3715	-4.14562	0.400435	-10.3528	4.07E-25	1.61E-23
CG16978	152.8422	-7.87928	0.76415	-10.3112	6.27E-25	2.47E-23
CG14960	251.1114	8.659939	0.840572	10.30243	6.87E-25	2.70E-23
lox2	123.6903	-6.39778	0.621102	-10.3007	7.00E-25	2.73E-23
Pdk	172.6257	-4.73319	0.459564	-10.2993	7.10E-25	2.76E-23
Nckx30C	153.8192	-4.77723	0.463966	-10.2965	7.31E-25	2.83E-23
Gr63a	125.0259	-6.85458	0.665743	-10.2961	7.33E-25	2.83E-23
CG9134	607.6722	5.54538	0.538733	10.29337	7.55E-25	2.90E-23
sn	144.3216	5.289693	0.516096	10.24945	1.19E-24	4.55E-23
GstE9	216.9176	-5.53112	0.540056	-10.2418	1.29E-24	4.91E-23
CG43094	271.7281	-9.59745	0.93769	-10.2352	1.38E-24	5.23E-23

Act42A	3292.141	4.15765	0.407956	10.19142	2.17E-24	8.18E-23
CG9294	222.1808	9.484987	0.930914	10.1889	2.22E-24	8.36E-23
CG7695	147.8187	-7.73035	0.7596	-10.1769	2.52E-24	9.42E-23
wg	297.474	5.112611	0.503011	10.16401	2.87E-24	1.07E-22
SPE	131.396	-5.12487	0.504949	-10.1493	3.34E-24	1.24E-22
f	102.1848	6.624814	0.654186	10.12681	4.20E-24	1.55E-22
CG12290	187.5415	-4.42807	0.437489	-10.1216	4.43E-24	1.63E-22
CG4914	674.2387	8.079993	0.798954	10.11322	4.83E-24	1.77E-22
CG42784	114.1771	-5.48581	0.542507	-10.112	4.89E-24	1.79E-22
CG4928	2143.422	-3.99829	0.395529	-10.1087	5.05E-24	1.84E-22
Hr4	244.7858	4.361796	0.432711	10.08016	6.76E-24	2.45E-22
sob	276.7114	6.596018	0.654376	10.07986	6.78E-24	2.45E-22
Tina-1	450.5835	-3.48473	0.346136	-10.0675	7.69E-24	2.77E-22
nyo	187.5366	9.229088	0.917967	10.05383	8.84E-24	3.17E-22
CG42284	253.4094	-4.14106	0.412071	-10.0494	9.24E-24	3.30E-22
Obp84a	150.4059	-8.15181	0.812028	-10.0388	1.03E-23	3.66E-22
kuk	370.8082	3.395242	0.33951	10.00041	1.52E-23	5.37E-22
CG4797	156.0243	-6.83843	0.684176	-9.99514	1.60E-23	5.65E-22
CG33993	157.7835	5.184206	0.51877	9.993268	1.63E-23	5.73E-22
CG13377	209.3286	5.16058	0.516925	9.983219	1.81E-23	6.32E-22
Eaat2	357.7332	-3.95	0.395995	-9.97489	1.96E-23	6.85E-22
AcCoAS	205.0769	-4.84292	0.4859	-9.96692	2.13E-23	7.39E-22

Or22a	113.7168	-6.73175	0.676249	-9.95455	2.41E-23	8.34E-22
CG43068	119.0119	-5.20046	0.523591	-9.93231	3.01E-23	1.04E-21
Btk29A	171.3828	4.800172	0.483327	9.931521	3.04E-23	1.04E-21
CG32855	118.6218	7.63198	0.769385	9.919584	3.42E-23	1.17E-21
OSCP1	188.6892	-4.90397	0.494986	-9.9073	3.87E-23	1.32E-21
CG5391	139.7481	6.067507	0.613075	9.896844	4.30E-23	1.46E-21
dap	882.1689	3.64796	0.371303	9.824756	8.81E-23	2.98E-21
Mtp	552.6154	3.557045	0.362309	9.817715	9.45E-23	3.18E-21
Cyp4d8	173.5382	-5.12235	0.521985	-9.81322	9.88E-23	3.32E-21
grp	354.9432	5.134073	0.523807	9.801467	1.11E-22	3.71E-21
Fili	153.4485	4.645588	0.474174	9.797214	1.16E-22	3.86E-21
CG43693	117.8552	-5.80145	0.59374	-9.77103	1.50E-22	4.98E-21
Obp83a	189.0079	-8.99581	0.92809	-9.69282	3.23E-22	1.07E-20
Fpps	426.6975	3.089376	0.318783	9.691159	3.29E-22	1.08E-20
Zasp52	231.0054	3.873028	0.399679	9.690337	3.31E-22	1.09E-20
tnc	103.9322	7.223312	0.745548	9.688599	3.37E-22	1.10E-20
Esp	113.146	-6.14474	0.634493	-9.68449	3.51E-22	1.14E-20
ed	1651.748	3.69786	0.382068	9.678534	3.72E-22	1.21E-20
CG17111	311.4938	-3.98688	0.412338	-9.66897	4.08E-22	1.32E-20
para	1156.375	-3.47027	0.360115	-9.63655	5.60E-22	1.81E-20
CG9452	181.9015	-9.00091	0.935614	-9.62033	6.56E-22	2.11E-20
Drsl4	115.0629	-7.53564	0.783919	-9.61278	7.06E-22	2.26E-20

drm	156.1502	6.343095	0.661669	9.586501	9.11E-22	2.91E-20
Cad96Ca	1024.051	3.064284	0.319708	9.584636	9.28E-22	2.95E-20
CG4000	317.2977	-10.3052	1.075851	-9.57867	9.83E-22	3.12E-20
GstE5	275.948	-3.62737	0.378711	-9.5782	9.88E-22	3.12E-20
sxe2	255.1474	-9.95024	1.039497	-9.57217	1.05E-21	3.30E-20
CG13634	84.47774	5.51305	0.576052	9.57041	1.06E-21	3.34E-20
Gagr	129.391	-7.99712	0.835678	-9.56962	1.07E-21	3.35E-20
Prx6005	244.1212	-5.33641	0.558042	-9.56274	1.15E-21	3.57E-20
CG15201	117.8982	-6.44695	0.674808	-9.55375	1.25E-21	3.88E-20
ihog	767.4792	3.652881	0.382586	9.54786	1.32E-21	4.10E-20
Or85b	94.20517	-6.32324	0.662444	-9.54532	1.36E-21	4.18E-20
CG42808	97.92098	-6.13395	0.644305	-9.52025	1.73E-21	5.31E-20
CG33110	290.4729	-3.58418	0.377366	-9.49789	2.14E-21	6.56E-20
CG6435	105.7662	-5.09695	0.536685	-9.49709	2.16E-21	6.59E-20
hh	208.59	6.614397	0.69739	9.484496	2.44E-21	7.41E-20
Ca-alpha1T	123.2143	-4.41019	0.465534	-9.47341	2.71E-21	8.21E-20
CG4962	109.1416	5.599846	0.591377	9.469157	2.82E-21	8.53E-20
Ir75b	87.97474	-6.19873	0.654694	-9.46813	2.85E-21	8.58E-20
Ir64a	142.5018	-8.20842	0.867274	-9.46462	2.95E-21	8.84E-20
wrapper	96.79639	5.520008	0.583274	9.463836	2.97E-21	8.88E-20
ec	217.0235	3.791279	0.401858	9.434374	3.93E-21	1.17E-19
kdn	521.4668	-3.082	0.326741	-9.43256	4.00E-21	1.19E-19

CG14860	116.9488	4.791287	0.508747	9.417825	4.61E-21	1.36E-19
CG10939	1886.877	-2.76638	0.29381	-9.41553	4.71E-21	1.39E-19
CG2016	145.176	4.68413	0.498704	9.392601	5.85E-21	1.72E-19
Spec2	385.0057	3.073674	0.32772	9.378973	6.66E-21	1.95E-19
CG10257	165.3374	-5.20788	0.557214	-9.34627	9.08E-21	2.66E-19
bgm	97.78331	-7.26144	0.778418	-9.32846	1.07E-20	3.13E-19
Ance-2	96.52152	7.66392	0.823474	9.306818	1.32E-20	3.83E-19
CG6891	568.0711	4.970852	0.534243	9.304479	1.35E-20	3.90E-19
Or43b	126.9884	-4.01681	0.431772	-9.30309	1.36E-20	3.94E-19
CG9400	157.0948	-8.76541	0.942585	-9.29933	1.41E-20	4.07E-19
CG7896	1482.708	3.485105	0.375182	9.289095	1.56E-20	4.46E-19
Jheh3	228.07	-3.58412	0.386412	-9.2754	1.77E-20	5.06E-19
Or47b	110.8209	-5.02624	0.542765	-9.26045	2.04E-20	5.80E-19
ChAT	162.4717	-4.01438	0.433633	-9.25754	2.09E-20	5.95E-19
GABA-B-R1	132.2124	-4.235	0.457713	-9.25253	2.19E-20	6.21E-19
CG42272	98.52446	5.637393	0.610018	9.241354	2.43E-20	6.87E-19
CG14196	97.6019	-6.90099	0.747973	-9.22626	2.80E-20	7.89E-19
alpha-Est7	133.8454	-5.43018	0.588833	-9.22194	2.92E-20	8.19E-19
DIP-alpha	92.10558	-4.91779	0.533412	-9.21949	2.99E-20	8.35E-19
Cyp6a21	137.1062	-8.56356	0.930167	-9.20648	3.37E-20	9.40E-19
CG7708	376.0249	-3.44213	0.374082	-9.20154	3.53E-20	9.81E-19
CG9541	243.8447	-3.63136	0.3948	-9.19796	3.65E-20	1.01E-18

Diap1	119.1427	3.787033	0.414604	9.134095	6.60E-20	1.82E-18
Tmhs	119.1211	7.019984	0.769034	9.128316	6.96E-20	1.92E-18
CG32271	132.7408	-8.5479	0.938321	-9.10978	8.25E-20	2.27E-18
CG5549	135.2426	-8.52894	0.936718	-9.10513	8.62E-20	2.36E-18
CG31103	153.0925	-4.17307	0.458572	-9.10013	9.02E-20	2.46E-18
CG32694	116.4425	-5.96937	0.656926	-9.08683	1.02E-19	2.78E-18
fw	118.1331	5.489247	0.60577	9.061601	1.29E-19	3.49E-18
GstD8	350.8845	-3.43599	0.379504	-9.05391	1.38E-19	3.73E-18
CG1103	185.2432	3.615689	0.399503	9.050478	1.42E-19	3.84E-18
Kif3C	202.1832	-4.47082	0.497367	-8.98898	2.50E-19	6.71E-18
Sfp84E	123.7831	-8.40727	0.93579	-8.98413	2.61E-19	6.99E-18
CG18190	355.3275	4.873847	0.543563	8.966479	3.06E-19	8.19E-18
Exn	114.614	4.605088	0.51456	8.949566	3.57E-19	9.51E-18
GstE6	698.6214	-3.13618	0.350438	-8.94931	3.58E-19	9.51E-18
CG13332	86.60937	-5.44877	0.609518	-8.93948	3.91E-19	1.04E-17
Octbeta1R	154.7989	-4.04094	0.452085	-8.93846	3.95E-19	1.04E-17
crok	436.1671	2.805244	0.314128	8.930267	4.25E-19	1.12E-17
caix	102.023	-7.74287	0.868353	-8.91673	4.80E-19	1.26E-17
LanA	1230.53	2.757158	0.309577	8.906222	5.28E-19	1.38E-17
mam	269.9637	3.217462	0.361657	8.896439	5.77E-19	1.51E-17
l(1)G0320	1151.888	3.123354	0.351733	8.87989	6.69E-19	1.74E-17
CG4455	1381.961	3.703713	0.417334	8.874691	7.01E-19	1.82E-17

NaPi-III	524.8554	-3.91246	0.440954	-8.87272	7.14E-19	1.85E-17
danr	276.0559	4.846236	0.546961	8.86029	7.98E-19	2.06E-17
Cdk1	775.6321	3.781354	0.426927	8.857151	8.21E-19	2.11E-17
CG10562	124.161	-8.42828	0.951589	-8.85706	8.22E-19	2.11E-17
LanB1	188.1182	3.387287	0.382517	8.85525	8.35E-19	2.14E-17
CG13950	280.2488	-3.82836	0.432514	-8.85142	8.64E-19	2.21E-17
Neurochondrin	113.08	4.282439	0.483966	8.848633	8.86E-19	2.26E-17
Ir40a	69.36377	-5.77206	0.653438	-8.83336	1.02E-18	2.58E-17
NimC4	473.0282	3.844257	0.435976	8.81758	1.17E-18	2.96E-17
GstE7	110.3325	-4.15575	0.471335	-8.81698	1.18E-18	2.97E-17
Ndae1	254.0276	-4.35552	0.494059	-8.8158	1.19E-18	2.99E-17
CG8854	64.65371	5.788514	0.656733	8.814112	1.21E-18	3.03E-17
fru	398.2964	3.277862	0.372334	8.803553	1.33E-18	3.32E-17
EbpIII	1060.988	-3.96708	0.45091	-8.79792	1.39E-18	3.48E-17
AOX4	919.2392	-3.19884	0.363745	-8.79418	1.44E-18	3.59E-17
CG32444	112.5983	-8.22448	0.936579	-8.7814	1.61E-18	4.01E-17
CG43861	144.6315	-4.16039	0.474038	-8.77648	1.69E-18	4.18E-17
slo	90.47877	-4.67225	0.532598	-8.77257	1.75E-18	4.31E-17
CG6356	470.5116	-4.53154	0.516942	-8.76605	1.85E-18	4.56E-17
Syt1	271.1496	-3.57461	0.407803	-8.76552	1.86E-18	4.57E-17
Cht3	243.3814	5.024619	0.573288	8.764564	1.88E-18	4.59E-17
Alp4	115.9255	-8.40499	0.962328	-8.73402	2.46E-18	6.01E-17

CG11550	1640.757	-3.32142	0.380357	-8.7324	2.49E-18	6.08E-17
18w	1121.522	2.562009	0.293985	8.714766	2.91E-18	7.08E-17
CG11966	90.90283	8.214709	0.945284	8.690202	3.62E-18	8.77E-17
CG10680	87.16196	-7.51966	0.868013	-8.66307	4.59E-18	1.11E-16
GNBP3	1087.528	2.841799	0.328813	8.642606	5.49E-18	1.32E-16
CG30274	228.3458	-3.47275	0.402491	-8.62815	6.24E-18	1.50E-16
Fit2	320.2015	2.981523	0.345799	8.622136	6.57E-18	1.58E-16
CG14275	80.571	-7.17087	0.83237	-8.615	6.99E-18	1.67E-16
CG9815	106.3849	3.918604	0.455328	8.606107	7.56E-18	1.80E-16
CG15096	63.53863	-5.38305	0.625492	-8.60609	7.56E-18	1.80E-16
CG14400	173.6721	-9.73966	1.132753	-8.59822	8.10E-18	1.92E-16
CG32225	131.7594	-3.82798	0.445922	-8.5844	9.13E-18	2.16E-16
Kr-h1	161.6383	-7.49679	0.873413	-8.58332	9.22E-18	2.18E-16
wus	61.94055	6.367695	0.744404	8.554086	1.19E-17	2.80E-16
CG4374	156.6396	5.290164	0.618948	8.547032	1.26E-17	2.97E-16
Mvl	115.6793	-4.06962	0.476705	-8.53697	1.38E-17	3.23E-16
Akap200	129.1274	4.898514	0.575813	8.50712	1.78E-17	4.17E-16
Jhl-26	77.34043	-4.41275	0.518999	-8.50242	1.86E-17	4.33E-16
Apoltp	170.1229	3.571424	0.420126	8.500849	1.88E-17	4.38E-16
CG17026	68.8144	-5.35345	0.630315	-8.49329	2.01E-17	4.66E-16
CG31100	71.66989	-5.6475	0.664961	-8.49298	2.01E-17	4.66E-16
CG18268	95.38596	-8.07527	0.954427	-8.46086	2.65E-17	6.12E-16

Tollo	1184.928	3.209807	0.379391	8.460419	2.66E-17	6.13E-16
CG11836	108.7706	4.199741	0.497502	8.441656	3.13E-17	7.18E-16
CG3168	67.33619	-4.79703	0.569124	-8.4288	3.49E-17	8.00E-16
fng	887.0372	2.724521	0.323351	8.425882	3.58E-17	8.18E-16
CG15506	599.421	3.540087	0.421089	8.406983	4.21E-17	9.58E-16
CG34342	66.97422	-4.91648	0.584987	-8.40442	4.30E-17	9.77E-16
to	98.61372	-8.16745	0.972317	-8.39999	4.47E-17	1.01E-15
CG13720	105.1407	7.142771	0.850631	8.397022	4.58E-17	1.04E-15
ImpE3	216.0317	4.911672	0.58526	8.392293	4.77E-17	1.08E-15
CG34417	212.4997	3.107284	0.37037	8.389671	4.88E-17	1.10E-15
shg	3017.838	2.370743	0.282619	8.38848	4.92E-17	1.11E-15
l(1)G0196	87.65566	-5.82263	0.694213	-8.38738	4.97E-17	1.11E-15
Or13a	63.58266	-6.39268	0.763634	-8.37139	5.69E-17	1.27E-15
CG13563	140.4833	3.191274	0.382961	8.333158	7.87E-17	1.75E-15
laccase2	719.628	3.377607	0.405535	8.328759	8.17E-17	1.82E-15
Cyp4ac2	244.3849	-10.9763	1.31966	-8.31754	8.98E-17	1.99E-15
Cyp28a5	158.259	-3.70248	0.44598	-8.3019	1.02E-16	2.27E-15
CG15021	70.79476	-7.10907	0.858236	-8.28335	1.20E-16	2.64E-15
foi	102.7098	-4.33809	0.525281	-8.25862	1.47E-16	3.24E-15
pk	145.4868	3.262026	0.394996	8.258386	1.48E-16	3.24E-15
CG12947	74.10021	5.580411	0.676574	8.248046	1.61E-16	3.53E-15
Idgf4	82.13007	-7.5165	0.913911	-8.22455	1.96E-16	4.28E-15

AsnS	75.68088	-5.50438	0.66955	-8.22102	2.02E-16	4.40E-15
CG17841	596.7441	-2.53366	0.308345	-8.21695	2.09E-16	4.54E-15
Cad99C	69.15392	5.213957	0.635451	8.205134	2.30E-16	5.00E-15
CG4607	78.10026	-7.13065	0.869402	-8.20178	2.37E-16	5.12E-15
CG12655	82.0281	-7.88693	0.961834	-8.19989	2.41E-16	5.19E-15
Sytalpha	55.86869	-5.358	0.653749	-8.1958	2.49E-16	5.36E-15
Ugt35a	193.0282	-3.81007	0.464915	-8.1952	2.50E-16	5.37E-15
Or67d	80.37328	-7.87217	0.960719	-8.19404	2.53E-16	5.41E-15
CG42261	321.3623	-3.01173	0.368227	-8.17899	2.86E-16	6.12E-15
CG15473	84.25736	3.974296	0.486857	8.163161	3.26E-16	6.96E-15
CG43386	240.3436	5.099283	0.625164	8.156706	3.44E-16	7.33E-15
Cyp313a4	114.1457	-9.00391	1.104951	-8.14869	3.68E-16	7.81E-15
CG30116	69.77745	-5.19467	0.637723	-8.14566	3.77E-16	7.99E-15
Ald	249.4098	-3.00631	0.369088	-8.14524	3.79E-16	8.00E-15
CG30271	178.4632	-3.42589	0.420746	-8.14241	3.87E-16	8.17E-15
VhaSFD	85.90077	-4.04928	0.499502	-8.10665	5.20E-16	1.09E-14
Or35a	67.3285	-7.11533	0.878226	-8.10193	5.41E-16	1.14E-14
CG11841	66.19711	-7.06495	0.873352	-8.08947	5.99E-16	1.25E-14
CG16885	7257.924	3.795322	0.469668	8.080858	6.43E-16	1.34E-14
Cpr50Cb	52.90186	5.700203	0.706424	8.069091	7.08E-16	1.48E-14
CG13748	87.65144	8.861061	1.098974	8.063032	7.44E-16	1.55E-14
Or65a	78.1664	-7.83158	0.971366	-8.06244	7.48E-16	1.55E-14

CG42598	277.1112	3.198533	0.396991	8.056932	7.82E-16	1.62E-14
CG13794	105.6259	-8.93812	1.11136	-8.0425	8.80E-16	1.82E-14
odd	114.3433	4.291099	0.533811	8.038605	9.09E-16	1.87E-14
kkv	82.33825	8.423133	1.05004	8.021728	1.04E-15	2.14E-14
GstD2	168.8364	-3.3024	0.411782	-8.01978	1.06E-15	2.17E-14
Toll-7	1135.732	2.623182	0.327324	8.014028	1.11E-15	2.27E-14
CG6484	70.06575	-7.59561	0.952292	-7.97614	1.51E-15	3.08E-14
CG10444	198.182	-2.82228	0.354096	-7.9704	1.58E-15	3.22E-14
CG31207	186.6699	-10.8012	1.355982	-7.96559	1.64E-15	3.34E-14
CG12017	79.36082	8.641053	1.086124	7.95586	1.78E-15	3.61E-14
Sema-5c	149.5686	4.194362	0.527788	7.947063	1.91E-15	3.86E-14
CG4462	71.07097	-6.16414	0.776665	-7.93668	2.08E-15	4.19E-14
CG31098	90.40079	-3.99478	0.503396	-7.93567	2.09E-15	4.22E-14
Shab	151.6289	-3.46573	0.43776	-7.91697	2.43E-15	4.89E-14
Cct2	115.8763	-3.72272	0.470643	-7.90986	2.58E-15	5.17E-14
Or65b	89.31085	-8.61948	1.089831	-7.909	2.59E-15	5.19E-14
cln3	70.67124	-7.69095	0.972632	-7.90736	2.63E-15	5.25E-14
CG10031	97.24161	-8.81882	1.116584	-7.89803	2.83E-15	5.65E-14
Gasp	18790.29	2.917444	0.369418	7.897395	2.85E-15	5.66E-14
Or47a	57.4746	-6.56898	0.832949	-7.88641	3.11E-15	6.17E-14
TwdlT	16937.64	2.984222	0.378441	7.885564	3.13E-15	6.20E-14
IM2	107.3478	-4.09213	0.52047	-7.86237	3.77E-15	7.44E-14

ckd	185.2205	5.712155	0.728338	7.842726	4.41E-15	8.69E-14
Zip89B	318.0303	3.27906	0.418258	7.839803	4.51E-15	8.87E-14
sca	620.8509	4.16488	0.532414	7.822636	5.17E-15	1.02E-13
Cyp9h1	52.77328	-5.82141	0.744364	-7.82064	5.26E-15	1.03E-13
CG14397	259.0722	6.468874	0.827462	7.817734	5.38E-15	1.05E-13
CG6145	211.2968	-3.3241	0.425235	-7.81708	5.41E-15	1.05E-13
CG18135	113.5899	-3.31557	0.424221	-7.81567	5.47E-15	1.06E-13
GstD11	137.3767	-3.4526	0.441903	-7.81304	5.58E-15	1.08E-13
Obp99c	76.90887	4.458259	0.571126	7.806088	5.90E-15	1.14E-13
DopEcR	55.87635	-5.11245	0.656783	-7.78408	7.02E-15	1.36E-13
esn	215.1042	3.69741	0.475076	7.782776	7.10E-15	1.37E-13
Or9a	61.63825	-6.92254	0.890399	-7.77465	7.57E-15	1.46E-13
CG13972	77.36339	3.555774	0.457665	7.769379	7.89E-15	1.51E-13
nemy	157.9957	5.11282	0.658138	7.768614	7.93E-15	1.52E-13
CG6465	89.61937	-4.46391	0.574728	-7.76699	8.04E-15	1.54E-13
csw	74.39172	-4.5578	0.587741	-7.75477	8.85E-15	1.69E-13
amon	368.7443	-2.86105	0.369954	-7.73351	1.05E-14	1.99E-13
CG9717	269.3595	-3.9218	0.50735	-7.72996	1.08E-14	2.04E-13
PyK	391.6758	-3.09084	0.400318	-7.72096	1.15E-14	2.19E-13
CG30463	126.4577	3.893655	0.504576	7.71669	1.19E-14	2.26E-13
Men-b	229.0926	-3.25451	0.421815	-7.71549	1.21E-14	2.28E-13
CG11409	68.12039	7.897824	1.026362	7.694967	1.42E-14	2.67E-13

kay	129.6659	-3.2526	0.423315	-7.68363	1.55E-14	2.91E-13
IM14	90.09235	-8.8402	1.154905	-7.65448	1.94E-14	3.64E-13
CG15312	53.31849	-4.79176	0.626133	-7.65295	1.96E-14	3.68E-13
Cpr	298.0046	-2.66596	0.348381	-7.65243	1.97E-14	3.69E-13
CG14757	119.9893	-3.34758	0.437515	-7.65136	1.99E-14	3.71E-13
ninaB	73.31483	-3.84598	0.503118	-7.64429	2.10E-14	3.91E-13
Cyp4e3	88.52651	-3.67998	0.481416	-7.64407	2.10E-14	3.91E-13
CG31176	269.446	2.68963	0.351989	7.64124	2.15E-14	3.98E-13
CG10050	123.0168	-3.57759	0.468195	-7.64124	2.15E-14	3.98E-13
CG34309	477.1054	-3.00072	0.392971	-7.636	2.24E-14	4.14E-13
ppk	47.45889	-6.16232	0.808096	-7.62573	2.43E-14	4.47E-13
CG17839	562.3773	-3.15297	0.414224	-7.61176	2.70E-14	4.97E-13
Sec61beta	1166.944	2.733683	0.359836	7.597029	3.03E-14	5.56E-13
Teh2	770.1252	-2.8223	0.37193	-7.58825	3.24E-14	5.94E-13
CG13721	44.05161	6.68258	0.880763	7.58726	3.27E-14	5.97E-13
CG14186	187.5131	-3.71055	0.489632	-7.57824	3.50E-14	6.39E-13
CG1275	170.6681	3.639926	0.481194	7.564358	3.90E-14	7.10E-13
Cyp12a5	53.86007	-7.11785	0.941565	-7.55959	4.04E-14	7.35E-13
Or82a	44.42025	-5.84184	0.77334	-7.55403	4.22E-14	7.65E-13
CG1358	71.38254	-4.30354	0.570114	-7.54856	4.40E-14	7.96E-13
CG11498	46.71829	7.108229	0.943783	7.531636	5.01E-14	9.05E-13
CG42235	61.18381	-4.42407	0.587859	-7.52573	5.24E-14	9.45E-13

CG31436	52.70289	-6.99585	0.929755	-7.5244	5.30E-14	9.53E-13
Hexo2	652.0446	4.847294	0.644597	7.519878	5.48E-14	9.84E-13
Timp	467.6618	2.399806	0.319404	7.513397	5.76E-14	1.03E-12
Dronc	394.6444	2.79097	0.37159	7.51089	5.87E-14	1.05E-12
CG4586	254.3662	5.466319	0.728409	7.504463	6.17E-14	1.10E-12
Ir75c	45.55116	-5.62923	0.750338	-7.50226	6.27E-14	1.12E-12
CG13995	105.0702	-3.57209	0.477022	-7.48831	6.98E-14	1.24E-12
Tsf2	1561.655	2.260225	0.301919	7.486199	7.09E-14	1.26E-12
cDIP	320.637	-2.85138	0.382052	-7.46335	8.44E-14	1.49E-12
CG34461	67.14671	4.630725	0.62053	7.462537	8.49E-14	1.50E-12
ckn	87.07125	3.441938	0.461453	7.458915	8.72E-14	1.54E-12
Kif19A	66.16228	-4.24428	0.570089	-7.44496	9.70E-14	1.71E-12
Fmo-2	91.40278	-3.34793	0.450464	-7.43218	1.07E-13	1.88E-12
obst-B	2136.9	5.739103	0.772742	7.426931	1.11E-13	1.95E-12
CG14626	60.19652	8.2932	1.117302	7.422522	1.15E-13	2.01E-12
GAPsec	241.7778	2.557958	0.344689	7.421061	1.16E-13	2.03E-12
CG43091	124.9341	-10.3702	1.398404	-7.41575	1.21E-13	2.11E-12
CG18107	54.77908	-7.34404	0.990846	-7.41189	1.25E-13	2.17E-12
Or67a	65.52375	-7.92126	1.069743	-7.40482	1.31E-13	2.28E-12
CG8785	67.97054	-8.0506	1.089615	-7.38848	1.49E-13	2.57E-12
E(spl)m7-HLH	251.0017	3.556453	0.483932	7.349073	2.00E-13	3.45E-12
CG14688	95.18501	-3.66402	0.498654	-7.34783	2.01E-13	3.48E-12

Cda4	2585.243	3.415412	0.464898	7.346589	2.03E-13	3.50E-12
5-HT2B	59.89357	-3.92069	0.5351	-7.32702	2.35E-13	4.05E-12
CG34180	69.25836	-8.39471	1.146256	-7.32359	2.41E-13	4.15E-12
CG7888	153.1627	-3.19891	0.437031	-7.31963	2.49E-13	4.26E-12
bbg	78.93848	5.193969	0.710162	7.31378	2.60E-13	4.44E-12
Xrp1	251.5218	-2.92062	0.399844	-7.30439	2.79E-13	4.76E-12
CG4089	364.7174	2.350829	0.32241	7.291429	3.07E-13	5.23E-12
Cpr65Eb	68.26345	5.961558	0.817786	7.289871	3.10E-13	5.28E-12
CR45536	56.03625	8.100475	1.112082	7.284065	3.24E-13	5.50E-12
Tom	369.5699	4.81342	0.660896	7.283174	3.26E-13	5.52E-12
Tret1-1	86.74006	-4.85619	0.666783	-7.28302	3.26E-13	5.52E-12
CG17272	791.1946	2.462716	0.338277	7.280167	3.33E-13	5.63E-12
Nhe2	106.7058	-3.2824	0.451121	-7.27608	3.44E-13	5.79E-12
Galphaf	50.31308	-5.67163	0.780002	-7.2713	3.56E-13	5.99E-12
Cpr66Cb	81.49558	9.371441	1.289311	7.268566	3.63E-13	6.10E-12
CG30440	1558.398	3.164052	0.435774	7.260759	3.85E-13	6.45E-12
CG1927	1620.665	-2.5903	0.356776	-7.2603	3.86E-13	6.46E-12
CG8369	72.59325	-3.57498	0.493738	-7.24065	4.47E-13	7.45E-12
CG9509	41.35615	7.083543	0.97832	7.240515	4.47E-13	7.45E-12
CG8738	53.56028	-4.21174	0.581741	-7.23989	4.49E-13	7.47E-12
CG5945	49.6195	-7.25253	1.001848	-7.23915	4.51E-13	7.50E-12
CG13042	78.32402	9.681671	1.339222	7.229324	4.85E-13	8.05E-12

Est-6	40.07875	-5.68797	0.787029	-7.22714	4.93E-13	8.16E-12
Prx2540-2	77.0886	-6.29481	0.871065	-7.22656	4.95E-13	8.18E-12
comm2	175.7328	2.755315	0.381431	7.223623	5.06E-13	8.33E-12
Cyp12e1	43.39589	-5.60644	0.776136	-7.22353	5.07E-13	8.33E-12
mthl9	256.4836	3.762907	0.521058	7.221668	5.14E-13	8.43E-12
Tis11	1013.424	-2.82047	0.390723	-7.2186	5.25E-13	8.61E-12
CR45232	36.185	6.200778	0.859454	7.214791	5.40E-13	8.84E-12
CG7214	125.2686	3.744961	0.51935	7.210857	5.56E-13	9.08E-12
CG10019	106.984	3.090397	0.429121	7.201685	5.95E-13	9.70E-12
CG2781	1048.014	-2.23831	0.311005	-7.19702	6.15E-13	1.00E-11
CG10126	319.759	-2.97864	0.414103	-7.19299	6.34E-13	1.03E-11
Cyp4ac1	45.99944	-6.0817	0.845772	-7.19071	6.45E-13	1.05E-11
lh	99.71948	-5.18495	0.723812	-7.16339	7.87E-13	1.27E-11
CG15322	72.39921	9.325502	1.302239	7.16113	8.00E-13	1.29E-11
atk	47.21115	7.912958	1.105721	7.156375	8.28E-13	1.34E-11
Obp57a	59.35799	-8.12666	1.136868	-7.14829	8.79E-13	1.41E-11
CG1544	92.90232	4.532754	0.634258	7.146546	8.90E-13	1.43E-11
CG31300	50.15834	-7.25023	1.014704	-7.14517	8.99E-13	1.44E-11
CG14837	58.96695	-3.98639	0.558269	-7.14063	9.29E-13	1.49E-11
Or7a	63.02395	-4.02777	0.565165	-7.12672	1.03E-12	1.64E-11
Ser7	47.34934	-7.13828	1.001809	-7.12539	1.04E-12	1.66E-11
kermit	52.59009	3.899422	0.54802	7.115474	1.12E-12	1.78E-11

alt	59.78096	4.028947	0.566447	7.112661	1.14E-12	1.81E-11
CG10268	245.6073	2.644729	0.372028	7.108956	1.17E-12	1.86E-11
CG5028	326.8182	-2.60247	0.367572	-7.08018	1.44E-12	2.28E-11
CG33181	53.68214	-4.36425	0.616886	-7.07465	1.50E-12	2.37E-11
Cyp6w1	61.84024	-8.30407	1.174425	-7.07076	1.54E-12	2.43E-11
CG44836	50.97268	-4.40107	0.622434	-7.07074	1.54E-12	2.43E-11
Hsp67Ba	166.7894	4.711554	0.667229	7.061371	1.65E-12	2.59E-11
CG12512	81.86805	-3.74012	0.531853	-7.03225	2.03E-12	3.19E-11
CG10514	56.38235	-8.03702	1.143026	-7.03135	2.05E-12	3.21E-11
egh	462.8687	-2.27746	0.324108	-7.02686	2.11E-12	3.31E-11
CR44922	279.1895	-2.56479	0.365203	-7.02292	2.17E-12	3.39E-11
GstE1	461.0621	-2.40801	0.342886	-7.02276	2.18E-12	3.39E-11
St2	100.0494	8.220333	1.170978	7.020055	2.22E-12	3.45E-11
CG12288	129.6768	3.780699	0.539255	7.010969	2.37E-12	3.68E-11
hoe1	38.94771	-5.37492	0.767473	-7.0034	2.50E-12	3.88E-11
Teh3	142.0171	-2.96498	0.423563	-7.00009	2.56E-12	3.96E-11
Treh	60.62066	-3.86651	0.552664	-6.99613	2.63E-12	4.07E-11
ND-ASHI	48.14321	-3.91801	0.561322	-6.97996	2.95E-12	4.56E-11
sNPF	569.5841	-2.58586	0.370615	-6.97723	3.01E-12	4.64E-11
Hex-A	518.1779	-2.32798	0.334454	-6.96054	3.39E-12	5.22E-11
cpx	92.59629	-3.43877	0.494429	-6.95503	3.52E-12	5.42E-11
Or49b	39.77792	-4.85444	0.698833	-6.9465	3.74E-12	5.74E-11

CG5071	50.91131	-7.8697	1.133395	-6.94348	3.83E-12	5.86E-11
CG14406	75.25127	9.998001	1.440464	6.940822	3.90E-12	5.96E-11
CG34384	142.2389	-2.88885	0.416606	-6.93425	4.08E-12	6.23E-11
CG14526	184.8825	-3.59704	0.519123	-6.92907	4.24E-12	6.45E-11
CG5404	78.94974	-9.63809	1.391391	-6.92695	4.30E-12	6.54E-11
CG32055	368.2473	3.773432	0.545219	6.920945	4.49E-12	6.81E-11
Hk	40.97117	-4.62164	0.667837	-6.9203	4.51E-12	6.83E-11
CG14627	36.06285	6.901581	0.998451	6.912289	4.77E-12	7.22E-11
CG6067	76.66014	-9.6125	1.391431	-6.90836	4.90E-12	7.41E-11
pHCl	38.33211	-4.77288	0.692158	-6.89565	5.36E-12	8.09E-11
Ace	513.1792	-2.345	0.340094	-6.89514	5.38E-12	8.10E-11
CG31712	304.2129	-2.29475	0.333029	-6.89056	5.56E-12	8.36E-11
CG44085	36.28654	5.605837	0.813866	6.887913	5.66E-12	8.50E-11
IscU	760.3859	-2.37708	0.34525	-6.88511	5.77E-12	8.65E-11
CG32392	153.4876	-2.84459	0.41407	-6.86984	6.43E-12	9.62E-11
Tsp42Ef	1652.618	-2.09289	0.304695	-6.86881	6.47E-12	9.67E-11
CG5639	1370.399	4.344837	0.632684	6.867315	6.54E-12	9.76E-11
MFS14	42.09911	-4.37715	0.637993	-6.86081	6.85E-12	1.02E-10
CG15387	262.9072	3.109314	0.453316	6.859044	6.93E-12	1.03E-10
CG13154	33.41902	6.179543	0.900946	6.858951	6.94E-12	1.03E-10
Dif	338.7225	-2.87786	0.419687	-6.85715	7.02E-12	1.04E-10
CG9990	135.8621	-4.50311	0.656703	-6.85715	7.02E-12	1.04E-10

CG1632	39.04038	7.572384	1.104561	6.85556	7.10E-12	1.05E-10
lectin-46Ca	33.86506	-5.42917	0.791994	-6.85507	7.13E-12	1.05E-10
Hnf4	133.6213	-3.06261	0.446827	-6.85413	7.17E-12	1.06E-10
CG11275	469.4459	-2.82566	0.412366	-6.85231	7.27E-12	1.07E-10
Mgstl	557.4242	-2.59876	0.379427	-6.84918	7.43E-12	1.09E-10
pog	271.5267	-3.24439	0.473722	-6.84873	7.45E-12	1.09E-10
CR44065	47.50706	-7.77085	1.13576	-6.84198	7.81E-12	1.14E-10
Cyp49a1	49.77213	3.702086	0.541758	6.833466	8.29E-12	1.21E-10
LManII	70.28593	3.053645	0.447036	6.830865	8.44E-12	1.23E-10
Or98a	53.23414	-8.08921	1.184764	-6.8277	8.63E-12	1.26E-10
glec	1330.375	2.106317	0.308835	6.820191	9.09E-12	1.32E-10
hdly	191.9949	2.887205	0.423916	6.810803	9.71E-12	1.41E-10
Tob	162.91	-2.95745	0.434334	-6.80916	9.82E-12	1.42E-10
qin	44.34119	-4.51996	0.664593	-6.80109	1.04E-11	1.50E-10
btv	681.7793	-2.75777	0.405966	-6.7931	1.10E-11	1.58E-10
Obp57b	39.83178	-6.39145	0.941011	-6.79212	1.10E-11	1.59E-10
Sk1	38.77872	-6.72912	0.990916	-6.79081	1.12E-11	1.60E-10
CG13650	293.7062	-2.63828	0.388524	-6.79052	1.12E-11	1.61E-10
Cyp4s3	110.5555	4.390026	0.646586	6.789549	1.12E-11	1.61E-10
CG14529	34.86485	-5.0576	0.745317	-6.78583	1.15E-11	1.65E-10
FoxP	100.1718	-3.02995	0.446555	-6.78518	1.16E-11	1.66E-10
CG31272	43.58362	-6.96013	1.027552	-6.77351	1.26E-11	1.79E-10

CG10348	80.37254	3.19385	0.472081	6.765464	1.33E-11	1.89E-10
CG6749	51.20683	4.219304	0.624388	6.757504	1.40E-11	2.00E-10
eg	35.47324	7.368476	1.091366	6.751607	1.46E-11	2.08E-10
CG7720	36.3913	-4.70285	0.696558	-6.75155	1.46E-11	2.08E-10
CG9649	49.3634	-7.99308	1.184405	-6.74861	1.49E-11	2.11E-10
s-cup	340.6861	-2.44877	0.362927	-6.74728	1.51E-11	2.13E-10
CG3402	347.7776	2.269904	0.336587	6.743888	1.54E-11	2.18E-10
Cpr47Ec	629.1268	4.182465	0.620349	6.742114	1.56E-11	2.20E-10
CG6310	123.5511	2.949871	0.437688	6.739659	1.59E-11	2.23E-10
CG14696	169.8608	-3.21042	0.476608	-6.73598	1.63E-11	2.29E-10
CG3262	250.5086	-2.84014	0.42201	-6.73003	1.70E-11	2.38E-10
brat	1025.863	2.770716	0.412768	6.712521	1.91E-11	2.68E-10
CG3669	30.91216	6.198374	0.923425	6.712374	1.91E-11	2.68E-10
CG9396	45.97496	-7.72613	1.151169	-6.71155	1.93E-11	2.69E-10
SLC5A11	218.2146	-2.78115	0.414457	-6.71036	1.94E-11	2.71E-10
GstD3	474.0269	2.480848	0.369711	6.710233	1.94E-11	2.71E-10
CG15666	361.4696	-2.62512	0.391309	-6.70855	1.97E-11	2.73E-10
pip	35.64699	6.186215	0.923022	6.702134	2.05E-11	2.85E-10
Cat	1749.611	-2.0822	0.311642	-6.68138	2.37E-11	3.28E-10
MFS9	32.87995	-5.96731	0.893297	-6.6801	2.39E-11	3.31E-10
CG14921	68.51553	3.16441	0.474144	6.673937	2.49E-11	3.44E-10
CG4404	170.7428	-2.6554	0.398195	-6.66859	2.58E-11	3.56E-10

pgant8	208.8821	4.615915	0.692994	6.660827	2.72E-11	3.75E-10
CG30456	31.35216	-4.99016	0.750405	-6.64995	2.93E-11	4.03E-10
SP1029	37.15868	4.915261	0.739732	6.644649	3.04E-11	4.18E-10
CG2556	788.2143	2.353316	0.354184	6.644337	3.05E-11	4.18E-10
Or69a	43.52376	-7.75036	1.16802	-6.63547	3.23E-11	4.43E-10
CG14892	49.98328	-6.15989	0.929328	-6.62832	3.40E-11	4.64E-10
CG7991	38.97736	3.943003	0.594895	6.628071	3.40E-11	4.64E-10
CG6431	36.57119	7.6718	1.158325	6.623186	3.52E-11	4.79E-10
CG8550	36.81807	-6.15722	0.930106	-6.61991	3.59E-11	4.89E-10
wbl	34.17268	4.717951	0.715288	6.595879	4.23E-11	5.75E-10
Or56a	62.76821	-9.50447	1.441289	-6.59442	4.27E-11	5.79E-10
Osi16	50.32387	9.264863	1.406737	6.586064	4.52E-11	6.12E-10
CG33159	66.02699	-9.63786	1.463907	-6.58366	4.59E-11	6.21E-10
Cad87A	1782.061	1.890206	0.287178	6.581992	4.64E-11	6.27E-10
Slob	44.65504	-3.79752	0.57697	-6.58182	4.65E-11	6.27E-10
ptc	628.2311	2.086458	0.317499	6.571533	4.98E-11	6.71E-10
Inx3	1017.925	2.862475	0.436015	6.565083	5.20E-11	7.00E-10
Obp19d	30.66775	-5.30778	0.808547	-6.56459	5.22E-11	7.01E-10
Rtnl1	577.6484	2.114727	0.322188	6.563649	5.25E-11	7.04E-10
Src64B	97.2617	3.044107	0.464595	6.55217	5.67E-11	7.59E-10
exp	46.03431	4.435172	0.677266	6.548645	5.81E-11	7.76E-10
CG31769	39.21505	-7.4997	1.145679	-6.54607	5.91E-11	7.89E-10

CG31189	38.05118	-4.27599	0.65449	-6.53331	6.43E-11	8.58E-10
CG13248	62.33885	-3.24941	0.497623	-6.52987	6.58E-11	8.76E-10
PGRP-LB	30.40819	-5.89787	0.904534	-6.52034	7.01E-11	9.33E-10
CG42821	61.88409	-9.56385	1.467094	-6.51891	7.08E-11	9.40E-10
CG7840	129.5724	2.534856	0.389125	6.514249	7.31E-11	9.68E-10
CG34398	84.68152	2.880312	0.442364	6.511181	7.46E-11	9.87E-10
CG31810	48.89206	-3.84532	0.590802	-6.50865	7.58E-11	1.00E-09
CG13907	94.28688	-3.18711	0.489854	-6.50624	7.71E-11	1.02E-09
Obp28a	4915.252	-2.40763	0.370584	-6.49686	8.20E-11	1.08E-09
Cpr50Ca	49.46422	9.071314	1.398578	6.486096	8.81E-11	1.16E-09
Naam	465.8471	-2.31324	0.357208	-6.47591	9.42E-11	1.24E-09
NaCP60E	173.3294	-2.69015	0.415425	-6.47566	9.44E-11	1.24E-09
CG10077	2130.631	-2.92268	0.45144	-6.47413	9.54E-11	1.25E-09
Hydr1	35.36312	-4.24856	0.65779	-6.45884	1.06E-10	1.38E-09
yellow-f2	67.62383	-3.2558	0.504459	-6.45405	1.09E-10	1.42E-09
CG13285	38.38567	-7.58279	1.175075	-6.45303	1.10E-10	1.43E-09
Gr64f	57.08524	-9.46013	1.467942	-6.44448	1.16E-10	1.51E-09
CG14507	31.28657	5.075235	0.787631	6.443669	1.17E-10	1.52E-09
CG32104	280.9929	-2.47685	0.384916	-6.4348	1.24E-10	1.61E-09
CG17271	270.0465	2.068332	0.322378	6.415858	1.40E-10	1.82E-09
CG31777	35.84051	4.121561	0.642892	6.410969	1.45E-10	1.87E-09
CG9360	300.0985	-2.52672	0.394895	-6.39845	1.57E-10	2.03E-09

Pvf1	31.40524	-4.62579	0.723138	-6.39683	1.59E-10	2.05E-09
Vha100-2	193.1843	-2.41212	0.377736	-6.38575	1.71E-10	2.20E-09
Ir92a	31.92945	-6.62023	1.036844	-6.38499	1.71E-10	2.21E-09
ppl	121.6088	-2.57662	0.403728	-6.38206	1.75E-10	2.25E-09
crc	500.0999	-2.3848	0.37405	-6.37562	1.82E-10	2.34E-09
Tpr2	311.7821	2.500655	0.393129	6.360902	2.01E-10	2.57E-09
Zip48C	171.0877	-2.22317	0.349554	-6.36	2.02E-10	2.58E-09
CG3257	325.7003	-2.20731	0.34784	-6.34576	2.21E-10	2.83E-09
CG13659	33.23546	-7.16915	1.135347	-6.3145	2.71E-10	3.46E-09
AdSS	849.1855	-2.85835	0.453462	-6.30339	2.91E-10	3.71E-09
pgant2	182.7243	2.685702	0.426283	6.300278	2.97E-10	3.78E-09
CG9194	25.45751	5.199836	0.825792	6.296788	3.04E-10	3.86E-09
lectin-46Cb	33.95532	-4.39168	0.699334	-6.2798	3.39E-10	4.30E-09
Men	60.98963	-3.2475	0.517914	-6.27034	3.60E-10	4.57E-09
Picot	41.60584	-3.76313	0.600222	-6.26957	3.62E-10	4.58E-09
CG43646	46.87285	-3.61981	0.577429	-6.26884	3.64E-10	4.60E-09
CG6280	151.7818	6.284248	1.00341	6.26289	3.78E-10	4.77E-09
CG6583	556.3668	1.951068	0.312001	6.253409	4.02E-10	5.06E-09
CG5037	249.7652	-2.18797	0.349951	-6.2522	4.05E-10	5.10E-09
CG43222	36.20882	-7.54764	1.207598	-6.25013	4.10E-10	5.16E-09
Calx	45.5767	-4.28805	0.688197	-6.23084	4.64E-10	5.83E-09
Tspo	103.8997	-2.69236	0.432985	-6.21814	5.03E-10	6.31E-09

CG14367	432.2102	-2.22214	0.357988	-6.20732	5.39E-10	6.75E-09
CG31075	184.1155	-2.59144	0.41782	-6.20229	5.56E-10	6.96E-09
GstE3	438.8039	-2.45291	0.395976	-6.19458	5.84E-10	7.30E-09
CG1299	41.76424	-5.83213	0.941983	-6.19134	5.97E-10	7.44E-09
CG1665	228.2359	2.351548	0.379891	6.190065	6.01E-10	7.49E-09
CG34115	43.74627	8.204568	1.325964	6.187625	6.11E-10	7.60E-09
insc	50.45749	-3.56398	0.576075	-6.18665	6.15E-10	7.63E-09
Cpr97Ea	872.7126	4.508553	0.729499	6.180339	6.40E-10	7.93E-09
ITP	364.9667	-2.16102	0.349883	-6.17642	6.56E-10	8.12E-09
CG11529	26.98676	-5.33513	0.865729	-6.16258	7.16E-10	8.85E-09
aralar1	31.08101	-7.20197	1.16886	-6.16154	7.20E-10	8.90E-09
dl	25.13559	-5.27497	0.856676	-6.15749	7.39E-10	9.12E-09
bond	39.39289	-8.41599	1.367894	-6.15251	7.63E-10	9.39E-09
corn	41.64805	3.411442	0.554602	6.151158	7.69E-10	9.46E-09
CG6412	313.6082	-2.08259	0.339135	-6.14088	8.21E-10	1.01E-08
Ir75d	28.00136	-6.43014	1.047434	-6.13894	8.31E-10	1.02E-08
pwn	34.34488	7.794276	1.270413	6.135228	8.50E-10	1.04E-08
CG5890	123.0287	-2.72924	0.445353	-6.12825	8.88E-10	1.09E-08
stl	25.73743	7.031198	1.147344	6.12824	8.89E-10	1.09E-08
Wnt5	42.21567	4.204383	0.686261	6.126512	8.98E-10	1.10E-08
Gclc	56.47772	-3.10361	0.507279	-6.11816	9.47E-10	1.15E-08
CG5079	36.59472	-8.48683	1.388698	-6.11135	9.88E-10	1.20E-08

ergic53	323.7321	2.579737	0.422318	6.108513	1.01E-09	1.22E-08
CG42675	51.92663	-3.23969	0.53064	-6.10525	1.03E-09	1.25E-08
CG4615	195.4219	-2.17311	0.356494	-6.09578	1.09E-09	1.32E-08
DAAM	22.87073	5.255075	0.86251	6.092767	1.11E-09	1.34E-08
Map205	425.6379	2.520725	0.413814	6.091445	1.12E-09	1.35E-08
Vmat	29.77855	-7.09433	1.165193	-6.08854	1.14E-09	1.38E-08
Lac	2702.311	1.735144	0.285101	6.086061	1.16E-09	1.40E-08
Cyp317a1	29.16901	-7.08047	1.164689	-6.07928	1.21E-09	1.45E-08
CHKov2	176.7739	-2.96968	0.489341	-6.06873	1.29E-09	1.55E-08
CG10933	334.6123	2.542577	0.418971	6.068625	1.29E-09	1.55E-08
Rab3	635.7406	-1.96079	0.323217	-6.06648	1.31E-09	1.57E-08
tkv	404.0014	2.096629	0.345642	6.065902	1.31E-09	1.57E-08
RnrS	480.1911	-3.00357	0.495683	-6.05946	1.37E-09	1.63E-08
igl	141.0015	-2.5431	0.419768	-6.05835	1.38E-09	1.64E-08
Or85a	43.67509	-9.27077	1.531567	-6.05313	1.42E-09	1.69E-08
mus205	155.0815	-2.36088	0.391022	-6.03772	1.56E-09	1.86E-08
noe	32.30571	-3.94487	0.653571	-6.03587	1.58E-09	1.88E-08
CG3880	114.5116	5.217388	0.864418	6.035726	1.58E-09	1.88E-08
vih	589.8412	1.839651	0.305149	6.028697	1.65E-09	1.96E-08
CG30118	104.9898	-2.63001	0.436627	-6.02347	1.71E-09	2.02E-08
CG30076	26.04862	6.783866	1.127103	6.018853	1.76E-09	2.08E-08
Mmp2	92.39639	2.969312	0.493422	6.017789	1.77E-09	2.09E-08

TwdlE	1938.069	4.715931	0.783875	6.016174	1.79E-09	2.11E-08
Ir84a	28.78743	-7.17495	1.192716	-6.01564	1.79E-09	2.11E-08
Or43a	42.14459	-9.22167	1.534265	-6.01048	1.85E-09	2.18E-08
ppk26	28.32887	-6.2303	1.037049	-6.00772	1.88E-09	2.21E-08
TwdlV	40.78073	6.581587	1.095954	6.005352	1.91E-09	2.24E-08
CG4115	188.9464	4.594295	0.765039	6.005309	1.91E-09	2.24E-08
CG17278	425.1785	-2.3015	0.383303	-6.0044	1.92E-09	2.25E-08
nwk	24.81403	-5.33857	0.890364	-5.99594	2.02E-09	2.37E-08
Myo61F	30.99078	6.275938	1.047035	5.99401	2.05E-09	2.39E-08
CG6329	442.4492	-2.27048	0.378918	-5.99202	2.07E-09	2.42E-08
osp	42.42832	3.202114	0.535846	5.975809	2.29E-09	2.67E-08
CG11425	26.27977	-6.27747	1.050777	-5.97413	2.31E-09	2.69E-08
sel	346.3436	1.963578	0.328909	5.969974	2.37E-09	2.76E-08
NetB	193.4549	2.354854	0.395005	5.961586	2.50E-09	2.90E-08
Mctp	54.39697	-3.11565	0.523015	-5.9571	2.57E-09	2.98E-08
CG7759	41.68707	3.382468	0.568127	5.953722	2.62E-09	3.03E-08
Pal1	90.11389	2.580517	0.433468	5.953187	2.63E-09	3.04E-08
Cht5	93.93981	3.320631	0.558215	5.948658	2.70E-09	3.12E-08
CG14223	97.09116	3.307395	0.556045	5.94807	2.71E-09	3.13E-08
CG8192	74.14489	3.592588	0.604402	5.944033	2.78E-09	3.20E-08
CG6398	61.18138	3.335786	0.56151	5.940741	2.84E-09	3.26E-08
CG10560	308.3326	-7.57062	1.274372	-5.94067	2.84E-09	3.26E-08

Desat1	429.5866	-3.42571	0.576751	-5.93966	2.86E-09	3.28E-08
CG43729	158.7571	-2.42609	0.408861	-5.93377	2.96E-09	3.39E-08
E(spl)mdelta-HLH	199.224	3.816773	0.644329	5.923638	3.15E-09	3.60E-08
CG43795	37.71565	-3.51954	0.594392	-5.92125	3.20E-09	3.65E-08
Or67b	26.6803	-4.60515	0.777912	-5.91988	3.22E-09	3.68E-08
CG9631	35.1962	-8.73471	1.475948	-5.91804	3.26E-09	3.72E-08
GstE2	23.46376	-5.59317	0.947874	-5.90075	3.62E-09	4.12E-08
CR44298	25.05042	-5.5867	0.946937	-5.89976	3.64E-09	4.14E-08
kek1	740.8153	2.5466	0.431769	5.898064	3.68E-09	4.18E-08
CG9522	20.91166	5.122869	0.869456	5.892036	3.81E-09	4.33E-08
CG7369	587.1512	1.809411	0.307243	5.889178	3.88E-09	4.40E-08
CG14110	23.00464	6.680358	1.135301	5.884217	4.00E-09	4.53E-08
FANCI	208.2945	-4.07643	0.693488	-5.87816	4.15E-09	4.69E-08
IM23	113.3424	-2.70246	0.460394	-5.8699	4.36E-09	4.92E-08
GlyP	96.49354	-2.99981	0.511345	-5.86651	4.45E-09	5.02E-08
Cyp28c1	36.6692	-9.04366	1.542094	-5.86453	4.50E-09	5.07E-08
CG9876	99.64386	2.794203	0.476505	5.863954	4.52E-09	5.08E-08
CG5886	264.0893	2.186548	0.372954	5.86278	4.55E-09	5.11E-08
Ptpmeg2	64.09257	2.716471	0.463741	5.857733	4.69E-09	5.26E-08
CG31469	28.55349	-4.95429	0.845873	-5.85702	4.71E-09	5.28E-08
CG7054	213.1313	-2.29071	0.391288	-5.85428	4.79E-09	5.36E-08
Traf4	177.1169	2.505927	0.428135	5.853119	4.82E-09	5.38E-08

CR44024	524.8551	-2.94775	0.503624	-5.85307	4.83E-09	5.38E-08
PMCA	68.42886	-2.6067	0.445361	-5.85299	4.83E-09	5.38E-08
CG41284	283.1258	2.581338	0.441156	5.851305	4.88E-09	5.43E-08
Cyp12b2	120.9796	-2.58293	0.441646	-5.84843	4.96E-09	5.52E-08
CR44029	242.8078	-2.40942	0.411985	-5.84833	4.97E-09	5.52E-08
CG9411	66.30574	5.186578	0.887231	5.845806	5.04E-09	5.59E-08
Sema-2a	143.4256	3.050444	0.521978	5.844005	5.10E-09	5.65E-08
Egfr	281.5642	1.973816	0.33781	5.842969	5.13E-09	5.68E-08
elm	34.69788	-3.67948	0.63028	-5.83784	5.29E-09	5.85E-08
Nep4	32.04507	-4.25769	0.729569	-5.8359	5.35E-09	5.91E-08
CG7601	141.0602	-2.30196	0.395451	-5.82111	5.85E-09	6.45E-08
Sema-2b	446.3034	2.554965	0.439997	5.806777	6.37E-09	7.02E-08
CG12420	23.37746	4.298108	0.740452	5.804706	6.45E-09	7.09E-08
CG32333	108.2959	-2.98722	0.514724	-5.80354	6.49E-09	7.14E-08
trol	68.14829	-3.09523	0.533536	-5.80136	6.58E-09	7.21E-08
CG13675	25.40016	8.070067	1.391072	5.801331	6.58E-09	7.21E-08
HIP	1597.153	1.714001	0.295456	5.8012	6.58E-09	7.21E-08
CG9336	1063.408	-2.26447	0.391065	-5.79054	7.02E-09	7.67E-08
CG14661	34.17077	-8.95292	1.546216	-5.79021	7.03E-09	7.68E-08
CG3625	235.7265	-3.08373	0.533436	-5.78089	7.43E-09	8.10E-08
Cyp9b2	192.7669	-2.33511	0.403946	-5.78074	7.44E-09	8.10E-08
CG11453	33.80495	-8.93522	1.547594	-5.77362	7.76E-09	8.44E-08

CG11854	23.99882	-5.83484	1.01126	-5.76987	7.93E-09	8.62E-08
Ir41a	27.75323	-4.57574	0.793254	-5.76832	8.01E-09	8.69E-08
CenB1A	206.3743	2.170846	0.376421	5.767062	8.07E-09	8.75E-08
Ugt86De	33.53256	-8.92489	1.548099	-5.76506	8.16E-09	8.84E-08
CG18549	258.5277	-1.88491	0.326976	-5.76468	8.18E-09	8.85E-08
CG1718	54.18509	-2.95765	0.513267	-5.7624	8.29E-09	8.96E-08
Cirl	77.88252	3.162184	0.548771	5.762301	8.30E-09	8.96E-08
CG31321	24.21342	-5.95532	1.033672	-5.76132	8.35E-09	9.00E-08
CG43658	223.7822	2.204165	0.382682	5.759776	8.42E-09	9.07E-08
Prestin	222.8378	-2.49417	0.433043	-5.75963	8.43E-09	9.07E-08
CG2767	1108.801	1.991753	0.345843	5.759122	8.46E-09	9.08E-08
CG5946	27.26643	-4.72418	0.820439	-5.75811	8.51E-09	9.13E-08
KCNQ	32.00173	-3.97453	0.690358	-5.7572	8.55E-09	9.16E-08
Gs2	28.47847	-8.25978	1.435086	-5.7556	8.63E-09	9.24E-08
CG42392	22.89442	-6.66841	1.159162	-5.75278	8.78E-09	9.39E-08
CG32036	34.86851	4.286576	0.745571	5.749383	8.96E-09	9.56E-08
Rm62	187.7262	-2.24461	0.390499	-5.74807	9.03E-09	9.63E-08
CG14105	25.14052	-4.3028	0.749185	-5.74331	9.28E-09	9.89E-08
CG34205	28.70936	4.310607	0.750766	5.741614	9.38E-09	9.98E-08
CG11368	32.14768	-8.02957	1.399035	-5.73937	9.50E-09	1.01E-07
CG11367	89.18904	2.48948	0.433805	5.738711	9.54E-09	1.01E-07
Rbp6	150.0768	-2.25078	0.392306	-5.73731	9.62E-09	1.02E-07

plx	37.64036	-3.31914	0.579236	-5.7302	1.00E-08	1.06E-07
CG17279	30.89382	-8.63565	1.507451	-5.72864	1.01E-08	1.07E-07
CG3556	912.2558	-2.34864	0.41044	-5.72226	1.05E-08	1.11E-07
Ets98B	174.056	2.461958	0.430567	5.717951	1.08E-08	1.14E-07
haf	21.79312	5.901772	1.034456	5.705193	1.16E-08	1.23E-07
CG8492	26.12739	-7.56831	1.326756	-5.70437	1.17E-08	1.23E-07
CG18507	113.2713	-2.22912	0.390847	-5.70332	1.17E-08	1.24E-07
Cad88C	165.0752	2.798779	0.490901	5.701313	1.19E-08	1.25E-07
rdx	778.5675	1.680342	0.29487	5.698589	1.21E-08	1.27E-07
Cont	4568.477	1.79376	0.314916	5.695993	1.23E-08	1.29E-07
Nedd4	95.8614	-2.67504	0.469788	-5.69415	1.24E-08	1.30E-07
hgo	28.48895	-8.3735	1.471894	-5.68893	1.28E-08	1.34E-07
CG17843	284.1888	-3.47829	0.612073	-5.68279	1.33E-08	1.38E-07
Tsp	38.36771	3.088814	0.543755	5.680525	1.34E-08	1.40E-07
Drice	517.2123	1.747541	0.307911	5.675465	1.38E-08	1.44E-07
sinu	1415.019	1.998867	0.352308	5.673636	1.40E-08	1.46E-07
Cbp53E	218.02	-2.99602	0.528202	-5.67212	1.41E-08	1.47E-07
CG14044	26.8631	-3.78184	0.667712	-5.66387	1.48E-08	1.54E-07
CG32170	43.93923	-2.95832	0.522433	-5.66258	1.49E-08	1.55E-07
Rcd6	39.74517	3.858735	0.681991	5.658041	1.53E-08	1.59E-07
Efr	64.0091	-2.77251	0.490031	-5.65781	1.53E-08	1.59E-07
pyd3	87.68177	-2.62623	0.464337	-5.65586	1.55E-08	1.60E-07

Mst36Fa	21.2707	-4.59629	0.813637	-5.64906	1.61E-08	1.67E-07
CG7149	35.37414	-3.46679	0.613936	-5.64683	1.63E-08	1.69E-07
Cyp305a1	24.35208	-4.26899	0.756148	-5.6457	1.65E-08	1.69E-07
Ho	183.7613	-2.22292	0.393888	-5.64355	1.67E-08	1.71E-07
fa2h	23.67935	-4.44462	0.787658	-5.64283	1.67E-08	1.72E-07
Obp49a	29.01104	-4.39333	0.778715	-5.64176	1.68E-08	1.73E-07
Os-C	29.72906	-8.77056	1.555138	-5.63973	1.70E-08	1.75E-07
CG33099	35.32824	3.961871	0.703621	5.630688	1.79E-08	1.84E-07
CG42450	249.7605	-2.08291	0.369925	-5.63061	1.80E-08	1.84E-07
CR45517	30.23638	-6.18977	1.099835	-5.62791	1.82E-08	1.86E-07
CG7772	152.3828	-2.10091	0.373464	-5.62545	1.85E-08	1.89E-07
trio	48.56445	-2.81001	0.499711	-5.62328	1.87E-08	1.91E-07
CG17121	545.6401	2.913227	0.518835	5.614944	1.97E-08	2.00E-07
CG42269	24.74808	-3.88062	0.691465	-5.61217	2.00E-08	2.03E-07
ST6Gal	27.13183	-8.47976	1.511023	-5.61193	2.00E-08	2.03E-07
CG30345	67.04304	-2.71907	0.484539	-5.61166	2.00E-08	2.03E-07
Cyp6g2	34.51887	-7.90963	1.409844	-5.61029	2.02E-08	2.05E-07
PPO2	150.396	-6.12015	1.091074	-5.60929	2.03E-08	2.06E-07
tmod	466.0531	1.790613	0.319661	5.601601	2.12E-08	2.15E-07
Dak1	323.4392	-2.12569	0.379494	-5.60138	2.13E-08	2.15E-07
opa	84.45313	4.570616	0.816884	5.595187	2.20E-08	2.22E-07
CG31370	32.37526	-7.46549	1.334462	-5.59439	2.21E-08	2.23E-07

CR45514	21.22953	7.871006	1.407545	5.592008	2.24E-08	2.26E-07
DIP-epsilon	40.11092	4.762983	0.85296	5.584061	2.35E-08	2.36E-07
CG31115	26.07631	-4.39498	0.788228	-5.57577	2.46E-08	2.48E-07
CG9698	18.65656	6.482256	1.1642	5.567992	2.58E-08	2.59E-07
CG16786	43.90592	3.082008	0.554616	5.557016	2.74E-08	2.75E-07
CG17754	117.1834	2.825209	0.508529	5.555653	2.77E-08	2.77E-07
CG17450	93.96433	2.375638	0.427996	5.55061	2.85E-08	2.85E-07
CR46041	21.31401	-4.75818	0.857288	-5.55027	2.85E-08	2.85E-07
mew	267.2951	2.487161	0.448212	5.54907	2.87E-08	2.87E-07
CG31326	22.08391	-6.68678	1.20573	-5.54583	2.93E-08	2.92E-07
CG12206	37.93327	6.847109	1.235256	5.543067	2.97E-08	2.96E-07
CG15117	31.38428	3.299887	0.59562	5.540255	3.02E-08	3.01E-07
CG15309	25.14622	3.997513	0.722168	5.53543	3.10E-08	3.09E-07
Listericin	43.98745	-6.27909	1.134372	-5.5353	3.11E-08	3.09E-07
CG8213	21.18284	8.156015	1.473973	5.533354	3.14E-08	3.12E-07
CG17564	35.31653	3.760398	0.679653	5.532818	3.15E-08	3.12E-07
CG13065	21.92437	8.359623	1.511328	5.531309	3.18E-08	3.15E-07
CG5973	35.93583	-4.33629	0.784352	-5.5285	3.23E-08	3.19E-07
CG13001	199.3574	2.015534	0.364658	5.527184	3.25E-08	3.21E-07
CG3823	157.9235	2.754431	0.498605	5.524274	3.31E-08	3.26E-07
CG30022	169.4175	-1.97821	0.358506	-5.51792	3.43E-08	3.38E-07
CG13875	32.42731	3.370556	0.610848	5.517833	3.43E-08	3.38E-07

CG3534	197.1239	1.855501	0.336633	5.511945	3.55E-08	3.49E-07
Sod3	51.97174	-2.9127	0.528546	-5.51078	3.57E-08	3.51E-07
CG14961	67.08635	-4.13474	0.750534	-5.50907	3.61E-08	3.54E-07
CG9416	41.1192	3.232196	0.586793	5.508243	3.62E-08	3.55E-07
CG9149	642.4561	3.507377	0.636803	5.507793	3.63E-08	3.56E-07
CG7737	17.48309	5.233004	0.95029	5.506746	3.66E-08	3.57E-07
CG14694	57.73089	-3.22445	0.585852	-5.50387	3.72E-08	3.63E-07
CG12926	24.29748	-3.84501	0.698814	-5.50218	3.75E-08	3.66E-07
CG31195	1703.578	1.630971	0.296886	5.493587	3.94E-08	3.84E-07
CG5038	103.2217	2.135708	0.389175	5.487786	4.07E-08	3.96E-07
Or19b	75.43638	-3.27591	0.599122	-5.46786	4.55E-08	4.43E-07
Tudor-SN	81.29619	2.582761	0.473426	5.455468	4.88E-08	4.75E-07
CG8311	390.074	2.380464	0.436756	5.450328	5.03E-08	4.88E-07
CG8172	32.87828	7.136447	1.310355	5.446193	5.15E-08	4.99E-07
SK	29.11608	-3.9543	0.726649	-5.44184	5.27E-08	5.11E-07
CG16836	20.40609	-6.60826	1.215066	-5.4386	5.37E-08	5.20E-07
Ef1alpha48D	3179.198	1.612767	0.296807	5.433719	5.52E-08	5.33E-07
l(1)G0156	495.4787	-2.29652	0.42291	-5.43029	5.63E-08	5.43E-07
Sp212	28.642	-4.73891	0.873174	-5.42722	5.72E-08	5.52E-07
ko	60.73903	2.66737	0.491492	5.427087	5.73E-08	5.52E-07
CG14274	271.1278	-2.05704	0.379156	-5.4253	5.79E-08	5.57E-07
CG9095	16.14121	5.691398	1.049902	5.420883	5.93E-08	5.70E-07

grk	57.33101	3.07947	0.569024	5.411847	6.24E-08	5.99E-07
Obp83ef	24.84962	7.577518	1.400331	5.411235	6.26E-08	6.00E-07
CG42656	22.57953	-8.22644	1.522257	-5.40411	6.51E-08	6.24E-07
CG15071	47.89237	3.046849	0.564151	5.400769	6.64E-08	6.35E-07
CG13272	18.78865	7.756305	1.436382	5.399892	6.67E-08	6.38E-07
Eno	168.4244	-2.47313	0.45815	-5.39807	6.74E-08	6.44E-07
CG33284	19.57643	8.202113	1.519755	5.396997	6.78E-08	6.47E-07
ato	181.509	5.494493	1.018816	5.393016	6.93E-08	6.60E-07
CG31809	22.54976	-5.15297	0.956139	-5.38935	7.07E-08	6.73E-07
1-Sep	870.0414	1.688378	0.31335	5.388149	7.12E-08	6.77E-07
Cht2	115.9193	2.725565	0.50589	5.387659	7.14E-08	6.78E-07
CG17732	20.02567	-4.45163	0.827602	-5.37895	7.49E-08	7.11E-07
Cyp28d1	81.47586	-2.56299	0.476567	-5.37803	7.53E-08	7.14E-07
CG8503	24.03946	3.782065	0.703497	5.376092	7.61E-08	7.21E-07
CG42649	22.04055	-8.19303	1.525739	-5.36988	7.88E-08	7.45E-07
Mcr	3589.296	1.802398	0.335655	5.369797	7.88E-08	7.45E-07
pgant5	188.4767	2.999025	0.558969	5.365283	8.08E-08	7.63E-07
CG9555	21.74655	-8.17535	1.524751	-5.36176	8.24E-08	7.77E-07
CG17751	19.4282	-6.67311	1.247571	-5.34888	8.85E-08	8.34E-07
SPoCk	1089.994	-1.7951	0.335649	-5.34813	8.89E-08	8.37E-07
CG5745	270.1826	-2.04495	0.382489	-5.34642	8.97E-08	8.44E-07
Cubn	174.159	1.835616	0.343743	5.340082	9.29E-08	8.73E-07

CG8312	275.6108	-2.05671	0.38542	-5.33629	9.49E-08	8.90E-07
CG7747	159.1373	1.845317	0.345865	5.335369	9.54E-08	8.94E-07
CG14118	18.62199	4.239048	0.795856	5.326402	1.00E-07	9.38E-07
cry	245.5412	-2.92728	0.549678	-5.32544	1.01E-07	9.42E-07
boi	36.23266	6.012824	1.132451	5.309567	1.10E-07	1.03E-06
CG31337	32.98164	6.689324	1.260669	5.30617	1.12E-07	1.05E-06
CG44247	111.0321	-2.25622	0.425426	-5.30343	1.14E-07	1.06E-06
Mf	32.29302	-6.0521	1.142156	-5.29884	1.17E-07	1.09E-06
arr	740.1998	1.586419	0.299424	5.298242	1.17E-07	1.09E-06
CG13658	17.97523	-5.72535	1.080748	-5.29759	1.17E-07	1.09E-06
spz3	229.5629	-2.09544	0.396018	-5.29129	1.21E-07	1.13E-06
SsRbeta	1264.201	2.453459	0.463734	5.290665	1.22E-07	1.13E-06
CG15628	220.743	-2.43829	0.460876	-5.29055	1.22E-07	1.13E-06
Or65c	18.85641	-6.63565	1.254966	-5.28752	1.24E-07	1.15E-06
CG43647	19.27127	-4.77808	0.904169	-5.2845	1.26E-07	1.17E-06
CG2064	230.6852	-1.74717	0.33076	-5.2823	1.28E-07	1.18E-06
Pfk	97.1777	-2.25846	0.427621	-5.28146	1.28E-07	1.18E-06
Mst36Fb	18.0811	-5.45857	1.03377	-5.28025	1.29E-07	1.19E-06
CG3857	171.6329	-2.16269	0.409796	-5.27748	1.31E-07	1.21E-06
CG5335	26.64233	-3.4485	0.653887	-5.27385	1.34E-07	1.23E-06
CG5002	18.73312	-5.26676	0.998833	-5.27292	1.34E-07	1.23E-06
Ir62a	32.11413	-3.14119	0.59613	-5.2693	1.37E-07	1.26E-06

CG32365	87.60468	2.82891	0.537224	5.265798	1.40E-07	1.28E-06
Cpr49Ae	284.7513	2.184507	0.41521	5.261209	1.43E-07	1.31E-06
Ssb-c31a	236.0799	-2.26504	0.430751	-5.25836	1.45E-07	1.33E-06
Rab9	97.71295	-2.28967	0.435613	-5.25621	1.47E-07	1.35E-06
Obp18a	18.14116	-5.56656	1.059339	-5.25475	1.48E-07	1.35E-06
CG17974	18.99136	-6.6307	1.263567	-5.24761	1.54E-07	1.41E-06
vri	57.74308	2.74065	0.522362	5.246646	1.55E-07	1.41E-06
Or23a	17.53455	-5.74377	1.094974	-5.24558	1.56E-07	1.42E-06
CG13455	23.18613	-3.89575	0.74327	-5.24136	1.59E-07	1.45E-06
alphaTub84B	17609.59	2.302488	0.439393	5.240155	1.60E-07	1.46E-06
CAP	186.9526	-2.01778	0.385123	-5.23931	1.61E-07	1.46E-06
CG43095	19.64571	-4.37569	0.835325	-5.2383	1.62E-07	1.47E-06
CG5493	15.88173	7.602213	1.452493	5.233905	1.66E-07	1.50E-06
CG14431	27.80613	3.320104	0.634621	5.231636	1.68E-07	1.52E-06
CG15765	93.94825	-2.37405	0.454048	-5.22863	1.71E-07	1.55E-06
lobo	27.95724	4.743558	0.907765	5.225536	1.74E-07	1.57E-06
CG15515	24.85092	-4.58799	0.878099	-5.22491	1.74E-07	1.57E-06
CG14142	20.47339	-8.26685	1.583001	-5.22226	1.77E-07	1.59E-06
rut	16.79408	-6.29613	1.206073	-5.22036	1.79E-07	1.61E-06
Tgi	184.9604	2.478044	0.474924	5.217771	1.81E-07	1.63E-06
cold	178.8226	2.025937	0.388649	5.212772	1.86E-07	1.67E-06
Gpdh	20.3942	-4.01394	0.770221	-5.21142	1.87E-07	1.68E-06

CG8089	59.8963	2.95778	0.567683	5.210264	1.89E-07	1.69E-06
sls	120.5247	2.56034	0.49143	5.209978	1.89E-07	1.69E-06
Buffy	44.42438	-2.88104	0.553198	-5.20797	1.91E-07	1.71E-06
Sb	44.05954	4.186066	0.804046	5.206254	1.93E-07	1.72E-06
CG15546	21.60233	-4.23146	0.81372	-5.20014	1.99E-07	1.78E-06
CG31637	51.73667	2.574372	0.495931	5.190984	2.09E-07	1.87E-06
RpS27A	10704.38	1.45058	0.279615	5.187775	2.13E-07	1.90E-06
CG15822	18.91053	5.782623	1.116323	5.180063	2.22E-07	1.98E-06
beat-VII	91.68441	-2.36693	0.457032	-5.17893	2.23E-07	1.99E-06
CG4500	26.05738	4.38737	0.847471	5.177015	2.25E-07	2.01E-06
CG43220	28.27568	-3.71403	0.717658	-5.17521	2.28E-07	2.02E-06
CG9917	163.649	-2.33992	0.452272	-5.17371	2.29E-07	2.04E-06
CG31345	78.74003	-2.59495	0.50162	-5.17313	2.30E-07	2.04E-06
Cpr47Ee	17.21024	-5.90338	1.14309	-5.16441	2.41E-07	2.14E-06
CG3505	48.81507	-4.28046	0.829535	-5.16007	2.47E-07	2.19E-06
Hmt-1	318.135	-1.68275	0.326379	-5.15581	2.53E-07	2.23E-06
CG12858	143.156	-2.16822	0.420708	-5.15375	2.55E-07	2.26E-06
Mip	16.18326	7.709289	1.496524	5.151464	2.58E-07	2.28E-06
CG42329	17.88716	-7.6399	1.484371	-5.1469	2.65E-07	2.34E-06
CG15065	19.10899	-8.16802	1.589451	-5.13889	2.76E-07	2.43E-06
CG13727	16.22555	8.128274	1.584679	5.129286	2.91E-07	2.56E-06
Or83c	16.69707	-5.60655	1.093093	-5.12907	2.91E-07	2.56E-06

CG15597	15.73543	7.526466	1.468199	5.126325	2.95E-07	2.60E-06
CG14770	73.58249	3.974207	0.775385	5.125462	2.97E-07	2.60E-06
CG17364	27.69128	-3.29243	0.642425	-5.125	2.98E-07	2.61E-06
CR44938	25.97852	-3.65201	0.712684	-5.12431	2.99E-07	2.62E-06
in	151.061	2.438808	0.476236	5.121005	3.04E-07	2.66E-06
CG43110	32.47172	-3.42742	0.669574	-5.11881	3.07E-07	2.69E-06
Cyp4p3	17.35817	-7.77422	1.519777	-5.11537	3.13E-07	2.73E-06
CR44442	18.51825	-8.13057	1.590881	-5.11074	3.21E-07	2.80E-06
Gycalpha99B	107.6097	-2.19635	0.430139	-5.10615	3.29E-07	2.87E-06
CG11997	15.18928	7.573357	1.484053	5.103159	3.34E-07	2.91E-06
spri	32.05281	3.311777	0.648979	5.103055	3.34E-07	2.91E-06
CG13157	14.6386	7.602488	1.492266	5.094591	3.49E-07	3.04E-06
CG6696	16.64464	7.243966	1.422102	5.093846	3.51E-07	3.05E-06
Nrx-1	62.35951	-2.65776	0.521823	-5.09322	3.52E-07	3.05E-06
CG6287	817.6552	-1.79543	0.352605	-5.0919	3.54E-07	3.07E-06
CG2650	19.55858	-4.28313	0.842254	-5.08531	3.67E-07	3.18E-06
Or2a	15.57016	-6.05742	1.192301	-5.08044	3.77E-07	3.26E-06
CG9302	493.7071	1.613269	0.317612	5.079378	3.79E-07	3.27E-06
Cpr56F	17.79989	7.159305	1.409796	5.078256	3.81E-07	3.29E-06
CR43870	18.17002	-4.25229	0.837721	-5.07602	3.85E-07	3.32E-06
CG8066	15.93319	-4.89463	0.964876	-5.07281	3.92E-07	3.38E-06
daw	16.57163	-5.33894	1.053071	-5.06987	3.98E-07	3.43E-06

PK1-R	17.64919	-8.07348	1.593145	-5.06764	4.03E-07	3.46E-06
Or67c	32.7728	-3.04762	0.601561	-5.06619	4.06E-07	3.49E-06
Nox	14.56584	6.906071	1.364191	5.062394	4.14E-07	3.55E-06
CG10005	48.25402	3.547846	0.700839	5.062286	4.14E-07	3.55E-06
CG1371	718.4855	1.520853	0.300448	5.061949	4.15E-07	3.56E-06
Cad74A	18.81382	4.911567	0.970385	5.061464	4.16E-07	3.56E-06
CG18130	127.6904	-2.05348	0.406039	-5.05735	4.25E-07	3.64E-06
CG4752	16.95276	-7.27224	1.44053	-5.04831	4.46E-07	3.81E-06
Adk1	27.48264	-3.33624	0.660868	-5.04827	4.46E-07	3.81E-06
CR44807	16.16939	-5.78593	1.146651	-5.04594	4.51E-07	3.85E-06
mats	149.9024	2.187951	0.433998	5.041388	4.62E-07	3.94E-06
Blos3	97.97613	2.30185	0.45665	5.040734	4.64E-07	3.95E-06
CG42673	143.8067	2.161009	0.428825	5.039371	4.67E-07	3.97E-06
CR44320	24.70571	-3.39684	0.674347	-5.03722	4.72E-07	4.01E-06
CG3301	15.84627	-7.42884	1.475646	-5.0343	4.80E-07	4.07E-06
CG10483	40.15429	-2.82085	0.560508	-5.03266	4.84E-07	4.10E-06
CG8239	32.84088	2.990585	0.594786	5.028006	4.96E-07	4.20E-06
CG12483	17.77871	-8.03911	1.601598	-5.01943	5.18E-07	4.39E-06
Scp2	30.92047	-3.35991	0.670323	-5.01237	5.38E-07	4.55E-06
MFS3	293.8298	2.545928	0.50857	5.006048	5.56E-07	4.69E-06
Aldh-III	27.48094	-3.0663	0.612589	-5.00548	5.57E-07	4.70E-06
sosie	157.164	-2.02169	0.40396	-5.00467	5.60E-07	4.72E-06

nst	386.8678	2.856752	0.570945	5.00355	5.63E-07	4.74E-06
Efa6	131.2427	-2.15753	0.431243	-5.00305	5.64E-07	4.75E-06
sprt	576.8842	1.539667	0.3078	5.002161	5.67E-07	4.77E-06
CG10513	16.51565	-7.9891	1.597183	-5.00199	5.67E-07	4.77E-06
tos	68.27022	-2.75663	0.551463	-4.99876	5.77E-07	4.84E-06
CG9312	27.13063	-6.44822	1.290785	-4.99558	5.87E-07	4.92E-06
bsf	587.6455	-1.52528	0.305422	-4.99403	5.91E-07	4.95E-06
CG8449	185.1641	1.694666	0.33978	4.987546	6.12E-07	5.12E-06
CG14760	12.97159	7.255309	1.455052	4.986289	6.15E-07	5.15E-06
GNBP1	322.8347	1.639753	0.32941	4.977845	6.43E-07	5.37E-06
CG42369	61.56396	3.283475	0.660371	4.972166	6.62E-07	5.53E-06
26-29-p	1551.058	1.676881	0.337357	4.970637	6.67E-07	5.57E-06
CG14082	51.7761	-2.46012	0.494966	-4.97029	6.69E-07	5.57E-06
CG5835	213.7174	1.70167	0.342498	4.968409	6.75E-07	5.62E-06
CG32262	44.31514	-2.58222	0.519879	-4.96696	6.80E-07	5.65E-06
Cpr73D	199.5123	1.932291	0.389031	4.96694	6.80E-07	5.65E-06
CG5895	50.68214	-2.68276	0.540361	-4.96475	6.88E-07	5.71E-06
CG6424	71.85389	-2.32557	0.46865	-4.96226	6.97E-07	5.78E-06
CG8641	52.92028	-2.4073	0.485481	-4.95857	7.10E-07	5.88E-06
qua	51.03379	2.952456	0.595556	4.957475	7.14E-07	5.91E-06
CG43338	13.18735	6.019148	1.215016	4.953966	7.27E-07	6.01E-06
CG13893	205.1112	-2.03729	0.41195	-4.94547	7.60E-07	6.28E-06

rdgBbeta	107.1762	-1.90915	0.38611	-4.94458	7.63E-07	6.30E-06
CG7016	34.00212	-6.36946	1.289283	-4.94031	7.80E-07	6.43E-06
CG2604	15.41227	-5.15003	1.042666	-4.93929	7.84E-07	6.46E-06
CG5791	16.68608	-7.07744	1.433922	-4.93572	7.99E-07	6.58E-06
betaGlu	223.327	-1.73874	0.352304	-4.93534	8.00E-07	6.58E-06
mfrn	499.4342	-1.71605	0.347739	-4.93487	8.02E-07	6.59E-06
dmGlut	182.4005	-2.09714	0.425043	-4.93394	8.06E-07	6.62E-06
Trim9	30.90916	3.862366	0.782864	4.933634	8.07E-07	6.62E-06
CG4580	31.47394	6.662098	1.35127	4.930248	8.21E-07	6.73E-06
lambdaTry	12.94215	6.200386	1.257692	4.929971	8.22E-07	6.74E-06
CG11449	20.315	6.257507	1.269513	4.929059	8.26E-07	6.76E-06
Cerk	147.0787	-2.11898	0.430016	-4.92767	8.32E-07	6.80E-06
CG11619	25.78962	-3.61334	0.733703	-4.9248	8.44E-07	6.90E-06
SMSr	260.7242	1.569714	0.318811	4.923645	8.49E-07	6.93E-06
CG3740	111.3779	-1.93975	0.394124	-4.92167	8.58E-07	7.00E-06
CG30154	26.38837	3.422015	0.696585	4.912559	8.99E-07	7.32E-06
CG45186	150.001	1.70687	0.34748	4.912138	9.01E-07	7.33E-06
SdhD	557.3552	-2.60097	0.529647	-4.91075	9.07E-07	7.38E-06
CG11073	15.36189	-5.71169	1.163809	-4.90775	9.21E-07	7.48E-06
Atpalpha	3235.856	-1.81441	0.369937	-4.90465	9.36E-07	7.60E-06
CG33262	14.40311	5.377948	1.098449	4.895948	9.78E-07	7.93E-06
LPCAT	547.949	1.568206	0.320544	4.892331	9.96E-07	8.07E-06

Table 9: Key GO Terms in Fig 26. Translation of GO numbers into terms for Fig 26.

Key for GO terms in Fig 26 Top 500 Fold Change	
Bar Graph	
GO Number	GO Term
GO:0022609	multicellular organism adhesion to substrate
GO:0022608	multicellular organism adhesion
GO:0007594	puparial adhesion
GO:0022610	biological adhesion
GO:0007552	metamorphosis
GO:0009617	response to bacterium
GO:0042742	defense response to bacterium
GO:0040003	chitin-based cuticle development
GO:0042335	cuticle development
GO:0048856	anatomical structure development
GO:0044767	single-organism developmental process
GO:0032502	developmental process
GO:0044699	single-organism process
GO:0005576	extracellular region
GO:0030992	intraciliary transport particle B
GO:0005929	cilium
GO:0031012	extracellular matrix
GO:0044421	extracellular region part
GO:0001071	nucleic acid binding transcription factor activity
GO:0003700	transcription factor activity, sequence-specific DNA binding
GO:0005501	retinoid binding
GO:0005198	structural molecule activity
GO:0008010	structural constituent of chitin-based larval cuticle
GO:0005214	structural constituent of chitin-based cuticle
GO:0042302	structural constituent of cuticle
Bubble Chart	
GO:0040003	chitin−based cuticle development
GO:0042335	cuticle development
GO:0005214	structural constituent of chitin−based cuticle
GO:0042302	structural constituent of cuticle
GO:0008010	structural constituent of chitin−based larval cuticle
GO:0005198	structural molecule activity

GO:0031012 extracellular matrix
GO:0044421 extracellular region part
GO:0005576 extracellular region

Top 500 p-value

Bar Graph

GO:0022609 multicellular organism adhesion to substrate
GO:0022608 multicellular organism adhesion
GO:0007594 puparial adhesion
GO:0044707 single-multicellular organism process
GO:0022610 biological adhesion
GO:0009887 animal organ morphogenesis
GO:0007167 enzyme linked receptor protein signaling pathway
GO:0007166 cell surface receptor signaling pathway
GO:0007169 transmembrane receptor protein tyrosine kinase signaling pathway
GO:0048646 anatomical structure formation involved in morphogenesis
GO:0001754 eye photoreceptor cell differentiation
GO:0001751 compound eye photoreceptor cell differentiation
GO:0030182 neuron differentiation
GO:0048663 neuron fate commitment
GO:0046530 photoreceptor cell differentiation
GO:0045165 cell fate commitment
GO:0042384
GO:0044782 cilium organization
GO:0007422 peripheral nervous system development
GO:0006040 amino sugar metabolic process
GO:0006030 chitin metabolic process
GO:1901071 glucosamine-containing compound metabolic process
GO:0006022 aminoglycan metabolic process
GO:0048513 animal organ development
GO:0009653 anatomical structure morphogenesis
GO:0048731 system development
GO:0007165 signal transduction
GO:0040003 chitin-based cuticle development
GO:0042335 cuticle development
GO:0030030 cell projection organization
GO:0006928 movement of cell or subcellular component
GO:0048856 anatomical structure development
GO:0044767 single-organism developmental process
GO:0032502 developmental process
GO:0044699 single-organism process
GO:0005576 extracellular region

GO:0030992	intraciliary transport particle B
GO:0005929	cilium
GO:0031012	extracellular matrix
GO:0044421	extracellular region part
GO:0005887	integral component of plasma membrane
GO:0031226	intrinsic component of plasma membrane
GO:0044459	plasma membrane part
GO:0005886	plasma membrane
GO:0001012	RNA polymerase II regulatory region DNA binding
GO:0043565	sequence-specific DNA binding
GO:0001071	nucleic acid binding transcription factor activity
GO:0003700	transcription factor activity, sequence-specific DNA binding
GO:0004713	protein tyrosine kinase activity
GO:0005198	structural molecule activity
GO:0008010	structural constituent of chitin-based larval cuticle
GO:0005214	structural constituent of chitin-based cuticle
GO:0042302	structural constituent of cuticle
Bubble Chart	
GO:0048856	anatomical structure development
GO:0032502	developmental process
GO:0040003	chitin−based cuticle development
GO:0042335	cuticle development
GO:0044767	single−organism developmental process
GO:0044699	single−organism process
GO:0048731	system development
GO:0005214	structural constituent of chitin−based cuticle
GO:0042302	structural constituent of cuticle
GO:0008010	structural constituent of chitin−based larval cuticle
GO:0031012	extracellular matrix
GO:0044421	extracellular region part
GO:0005576	extracellular region

Table 10: Key GO Terms in Fig 27. Translation of GO numbers into terms for Fig 27.

Key for GO terms in Fig 27	
Top 500 Fold Change	
Bar Graph	
GO:0040003	chitin-based cuticle development
GO:0042335	cuticle development
GO:0048856	anatomical structure development
GO:0000280	nuclear division
GO:0007052	mitotic spindle organization
GO:0044767	single-organism developmental process
GO:0032502	developmental process
GO:0031012	extracellular matrix
GO:0044421	extracellular region part
GO:0005887	integral component of plasma membrane
GO:0031226	intrinsic component of plasma membrane
GO:0005214	structural constituent of chitin-based cuticle
GO:0042302	structural constituent of cuticle
GO:0008010	structural constituent of chitin-based larval cuticle
GO:0005198	structural molecule activity
Bubble Chart	
GO:0040003	chitin−based cuticle development
GO:0042335	cuticle development
GO:0005214	structural constituent of chitin−based cuticle
GO:0042302	structural constituent of cuticle
GO:0008010	structural constituent of chitin−based larval cuticle
GO:0031012	extracellular matrix
Top 500 p-value	
Bar Graph	
GO:0022402	cell cycle process
GO:0006259	DNA metabolic process
GO:1903047	mitotic cell cycle process
GO:0006260	DNA replication

GO:0007346	regulation of mitotic cell cycle
GO:0051726	regulation of cell cycle
GO:0051276	chromosome organization
GO:1901990	regulation of mitotic cell cycle phase transition
GO:1901987	regulation of cell cycle phase transition
GO:0010564	regulation of cell cycle process
GO:1903046	meiotic cell cycle process
GO:0007088	regulation of mitotic nuclear division
GO:0000280	nuclear division
GO:0048285	organelle fission
GO:0051783	regulation of nuclear division
GO:0098813	nuclear chromosome segregation
GO:0006270	DNA replication initiation
GO:1902099	regulation of metaphase/anaphase transition of cell cycle
GO:0030071	regulation of mitotic metaphase/anaphase transition
GO:0007052	mitotic spindle organization
GO:0006281	DNA repair
GO:0071897	DNA biosynthetic process
GO:0045839	negative regulation of mitotic nuclear division
GO:0051784	negative regulation of nuclear division
GO:0001709	cell fate determination
GO:2000816	negative regulation of mitotic sister chromatid separation
GO:0051985	negative regulation of chromosome segregation
GO:1902299	pre-replicative complex assembly involved in cell cycle DNA replication
GO:1902100	negative regulation of metaphase/anaphase transition of cell cycle
GO:0036388	pre-replicative complex assembly
GO:0006267	pre-replicative complex assembly involved in nuclear cell cycle DNA replication
GO:0045841	negative regulation of mitotic metaphase/anaphase transition
GO:2001251	negative regulation of chromosome organization
GO:0033048	negative regulation of mitotic sister chromatid segregation
GO:0033046	negative regulation of sister chromatid segregation
GO:0007096	regulation of exit from mitosis
GO:0033043	regulation of organelle organization
GO:0040003	chitin-based cuticle development
GO:0042335	cuticle development
GO:0048867	stem cell fate determination
GO:0048856	anatomical structure development
GO:0048523	negative regulation of cellular process
GO:0048731	system development
GO:0044767	single-organism developmental process

GO:0048519	negative regulation of biological process
GO:0032502	developmental process
GO:0010558	negative regulation of macromolecule biosynthetic process
GO:2000113	negative regulation of cellular macromolecule biosynthetic process
GO:0009890	negative regulation of biosynthetic process
GO:0031327	negative regulation of cellular biosynthetic process
GO:0010629	negative regulation of gene expression
GO:0044699	single-organism process
GO:0007552	metamorphosis
GO:0018958	phenol-containing compound metabolic process
GO:0000776	kinetochore
GO:0005876	spindle microtubule
GO:0051233	spindle midzone
GO:0005874	microtubule
GO:0036387	pre-replicative complex
GO:0005656	nuclear pre-replicative complex
GO:0042555	MCM complex
GO:0044430	cytoskeletal part
GO:0005819	spindle
GO:0031012	extracellular matrix
GO:0044421	extracellular region part
GO:0003677	DNA binding
GO:0034061	DNA polymerase activity
GO:0043138	3'-5' DNA helicase activity
GO:0003887	DNA-directed DNA polymerase activity
GO:0032559	adenyl ribonucleotide binding
GO:0030554	adenyl nucleotide binding
GO:0005524	ATP binding
GO:0008010	structural constituent of chitin-based larval cuticle
GO:0097367	carbohydrate derivative binding
GO:0005214	structural constituent of chitin-based cuticle
GO:0042302	structural constituent of cuticle
GO:0001882	nucleoside binding
GO:0032555	purine ribonucleotide binding
GO:0032550	purine ribonucleoside binding
GO:0035639	purine ribonucleoside triphosphate binding
GO:0017076	purine nucleotide binding
GO:0032553	ribonucleotide binding
GO:0032549	ribonucleoside binding
GO:0001883	purine nucleoside binding
GO:0036094	small molecule binding

GO:0016817	hydrolase activity, acting on acid anhydrides
GO:0016818	hydrolase activity, acting on acid anhydrides, in phosphorus-containing anhydrides
GO:0016462	pyrophosphatase activity
GO:0017111	nucleoside-triphosphatase activity
GO:1901265	nucleoside phosphate binding
GO:0000166	nucleotide binding
Bubble Chart	
GO:0032502	developmental process
GO:0044767	single−organism developmental process
GO:0040003	chitin−based cuticle development
GO:0042335	cuticle development
GO:0048856	anatomical structure development
GO:0022402	cell cycle process
GO:0005214	structural constituent of chitin−based cuticle
GO:0042302	structural constituent of cuticle
GO:0008010	structural constituent of chitin−based larval cuticle

Table 11: Key GO Terms in Fig 28. Translation of GO numbers into terms for Fig 28.

Key for GO terms in Fig 28 Top 500 Fold Change	
Bar Chart	
GO:0045455	ecdysteroid metabolic process
GO:0042445	hormone metabolic process
GO:0010817	regulation of hormone levels
GO:0019236	response to pheromone
GO:0019748	secondary metabolic process
GO:0055114	oxidation-reduction process
GO:0050911	detection of chemical stimulus involved in sensory perception of smell
GO:0007608	sensory perception of smell
GO:0050907	detection of chemical stimulus involved in sensory perception
GO:0009593	detection of chemical stimulus
GO:0051606	detection of stimulus
GO:0050906	detection of stimulus involved in sensory perception
GO:0007600	sensory perception
GO:0007606	sensory perception of chemical stimulus
GO:0050896	response to stimulus
GO:0050877	neurological system process
GO:0003008	system process

GO:0005887	integral component of plasma membrane
GO:0031226	intrinsic component of plasma membrane
GO:0005576	extracellular region
GO:0071683	sensory dendrite
GO:0044459	plasma membrane part
GO:0030425	dendrite
GO:0098590	plasma membrane region
GO:0044425	membrane part
GO:0032589	neuron projection membrane
GO:0032590	dendrite membrane
GO:0031256	leading edge membrane
GO:0031253	cell projection membrane
GO:0016021	integral component of membrane
GO:0031224	intrinsic component of membrane
GO:0044463	cell projection part
GO:0097458	neuron part
GO:0016020	membrane
GO:0004175	endopeptidase activity
GO:0004252	serine-type endopeptidase activity
GO:0008236	serine-type peptidase activity
GO:0017171	serine hydrolase activity
GO:0005550	pheromone binding
GO:0016491	oxidoreductase activity
GO:0009055	electron carrier activity
GO:0016705	oxidoreductase activity, acting on paired donors, with incorporation or reduction of molecular oxygen
GO:0022834	ligand-gated channel activity
GO:0015276	ligand-gated ion channel activity
GO:0005506	iron ion binding
GO:0020037	heme binding
GO:0046906	tetrapyrrole binding
GO:0015075	ion transmembrane transporter activity
GO:0022891	substrate-specific transmembrane transporter activity
GO:0022857	transmembrane transporter activity
GO:0004984	olfactory receptor activity
GO:0005549	odorant binding
GO:0004871	signal transducer activity
GO:0022892	substrate-specific transporter activity
GO:0038023	signaling receptor activity
GO:0005215	transporter activity
GO:0004872	receptor activity
GO:0060089	molecular transducer activity

GO:0004888	transmembrane signaling receptor activity
GO:0099600	transmembrane receptor activity
Bubble Chart	
GO:0007606	sensory perception of chemical stimulus
GO:0007608	sensory perception of smell
GO:0050911	detection of chemical stimulus involved in sensory perception
GO:0050907	detection of chemical stimulus involved in sensory perception
GO:0009593	detection of chemical stimulus
GO:0050906	detection of stimulus involved in sensory perception
GO:0051606	detection of stimulus
GO:0005549	odorant binding
GO:0004984	olfactory receptor activity
GO:0004872	receptor activity
GO:0060089	molecular transducer activity
GO:0099600	transmembrane receptor activity
GO:0004888	transmembrane signaling receptor activity
GO:0005506	iron ion binding
GO:0038023	signaling receptor activity
GO:0016705	oxidoreductase activity, acting on paired donors, with incorporation or reduction heme binding
GO:0020037	heme binding
GO:0046906	tetrapyrrole binding
GO:0009055	electron carrier activity
GO:0032589	neuron projection membrane
GO:0032590	dendrite membrane
GO:0031256	leading edge membrane
GO:0031253	cell projection membrane
GO:0016021	integral component of membrane
GO:0031224	intrinsic component of membrane
GO:0098590	plasma membrane region
GO:0097458	neuron part
GO:0044459	plasma membrane part
GO:0044425	membrane part
GO:0044463	cell projection part
GO:0016020	membrane
GO:0005576	extracellular region

Top 500 p-value

GO:0005886	plasma membrane
GO:0005887	integral component of plasma membrane
GO:0031226	intrinsic component of plasma membrane
GO:0005576	extracellular region

GO:0044459	plasma membrane part
GO:0098590	plasma membrane region
GO:0044425	membrane part
GO:0043005	neuron projection
GO:0016020	membrane
GO:0016021	integral component of membrane
GO:0031224	intrinsic component of membrane
GO:0097458	neuron part
GO:0031253	cell projection membrane
GO:0044463	cell projection part
GO:0032589	neuron projection membrane
GO:0032590	dendrite membrane
GO:0031256	leading edge membrane
GO:0005550	pheromone binding
GO:0005416	cation:amino acid symporter activity
GO:0016765	transferase activity, transferring alkyl or aryl (other than methyl) groups
GO:0015370	solute:sodium symporter activity
GO:0015294	solute:cation symporter activity
GO:0004364	glutathione transferase activity
GO:0016491	oxidoreductase activity
GO:0015293	symporter activity
GO:0020037	heme binding
GO:0046906	tetrapyrrole binding
GO:0009055	electron carrier activity
GO:0004871	signal transducer activity
GO:0015081	sodium ion transmembrane transporter activity
GO:0016705	oxidoreductase activity, acting on paired donors, with incorporation or reduction of molecular oxygen
GO:0038023	signaling receptor activity
GO:0004872	receptor activity
GO:0060089	molecular transducer activity
GO:0022804	active transmembrane transporter activity
GO:0015291	secondary active transmembrane transporter activity
GO:0005506	iron ion binding
GO:0015077	monovalent inorganic cation transmembrane transporter activity
GO:0004888	transmembrane signaling receptor activity
GO:0046873	metal ion transmembrane transporter activity
GO:0099600	transmembrane receptor activity
GO:0022890	inorganic cation transmembrane transporter activity
GO:0005549	odorant binding
GO:0008324	cation transmembrane transporter activity
GO:0004984	olfactory receptor activity

Bubble Chart	
GO:0005549	odorant binding
GO:0004984	olfactory receptor activity
GO:0031224	intrinsic component of membrane
GO:0016021	integral component of membrane
GO:0044459	plasma membrane part
GO:0016020	membrane
GO:0044425	membrane part
GO:0032589	neuron projection membrane
GO:0032590	dendrite membrane
GO:0098590	plasma membrane region
GO:0031256	leading edge membrane
GO:0031253	cell projection membrane
GO:0097458	neuron part

Table 12: Normalized $\log_2$ expression values of olfactory receptors used to create Figure 29. Values for the expression of all antennal ORs are listed including the olfactory co-receptor *orco*.

	OR Expression			
Gene Name	3L	p8	p40	Adult
Or67d	0	1.643799	1.553226	9.881348
Or23a	0	0	1.475883	7.683158
Or83c	0	0.950677	1.475883	7.549226
Or19a	5.06466	4.026933	5.710379	9.349583
Or19b	5.189711	3.993779	5.776857	9.388201
Or2a	2.66706	1.643799	0.475883	7.471314
Or43a	0	0	0	8.95443
Or47b	0	0	5.156894	10.31702
Or65a	1.368728	0	1.475883	9.863058
Or65b	1.574306	2.11002	0.626633	10.04417
Or65c	0	0	1.553226	8.551542
Or88a	0	0	0.626633	8.783599
Or10a	0.813492	0	5.495404	9.560056
Or42b	1.368728	1.643799	4.723151	11.46889
Or92a	2.221762	2.253501	2.860014	11.8263
Gr21a	0	1.643799	5.899715	9.110922
Gr63a	4.701908	3.573436	4.831775	9.892332

Or59b	1.574306	0.950677	2.553226	11.12932
Or85a	0	0	0	9.00854
Or22a	1.574306	1.950677	3.175359	10.43582
Or22b	0.75421	2.744412	2.590397	11.30303
Or85b	0	0	3.3925	10.07426
Or56a	0	1.643799	0.475883	9.49559
Or7a	1.574306	5.097885	5.066932	9.321279
Or47a	6.945334	3.410109	2.163075	9.258038
Or82a	0	2.643799	2.860014	8.903289
Or49b	0.368728	0.950677	3.890138	8.811268
Or67c	0.368728	0.253501	5.299722	9.014099
Or98a	0	0	0.626633	9.283976
Or43b	8.437211	8.285863	8.204278	10.60341
Or9a	2.75421	0.950677	2.553226	9.453537
Or67b	0	1.950677	3.748038	8.284568
Or69a	0.368728	0	0.626633	8.736106
Or49a	0	0	0	3.909596
Or67a	4.487192	3.895661	0	9.512562
Or85f	2.093944	3.157563	5.590758	8.106081
Or13a	0.368728	0	2.890138	9.614992
Ir31a	2.461524	3.032547	3.349783	11.27158
Ir92a	0	0.253501	1.475883	8.527065
Ir41a	4.993739	5.445797	3.860014	7.942521
Or35a	1.574306	0	2.211596	9.609254
Ir75c	0.368728	1.950677	3.163075	9.206283
Ir84a	0.368728	0	0.475883	8.36879
Ir76a	4.982369	5.351614	4.897863	8.9634
Ir75a	0	7.641205	4.360581	11.28852
Ir75b	2.574306	2.643799	4.212066	10.19208
Ir75d	7.156331	6.643799	6.750254	11.21658
Ir76b	2.75421	2.643799	1.553226	12.15121
Orco	28.29026	20.90774	137.3073	44362.67

Table 13: Notch State and Expression Status of ORs Across Development. Table displaying the Notch state (adapted from Endo et al., 2007) and expression status for each OR at all developmental stages.

Notch State and Expression Status of ORs Across Development

Sensilla subtype	OR	Notch State	3L	p8	p40	Adult	3L_pvalue	P8_pvalue	P40_pvalue
at1	*Or67d*	On	-	-	-	+	0.771582	0.110001	0.084378
at2	*Or23a*	On	-	-	-	+	0.771582	0.771588	0.79558
	Or83c	Off	-	-	-	+	0.771582	0.110001	0.79558
at3	*Or2a*	Off	+	-	-	+	0.026311	0.110001	0.79558
	Or19a	On	+	+	+	+	0.026311	0.006141	8.74E-05
	Or19b	On	+	+	+	+	0.026311	0.009596	5.68E-05
	Or43a	On	-	-	-	+	0.771582	0.771588	0.79558
at4	*Or47b*	Off	-	-	+	+	0.771582	0.771588	0.000669
	Or88a	On	-	-	-	+	0.771582	0.771588	0.084378
	Or65a/b/c	On	-	-	-	+	0.771582	0.771588	0.79558
ab1	*Or10a/Gr10a*	On	-	-	-	+	0.771582	0.771588	0.79558
	Or92a	Off	-	-	+	+	0.043714	0.771588	0.039687
	Gr21a/63a	On	-	-	-	+	0.771582	0.771588	0.79558
	Or42b	On	-	-	+	+	0.771582	0.110001	0.003083
ab2	*Or59b*	On	-	-	+	+	0.090905	0.110001	0.039687

	Or85a	Off	-	-	-	+	0.771582	0.771588	0.79558
ab3	*Or22a/b*	On	-	+	+	+	0.090905	0.02622	0.015325
	Or85b	Off	-	-	+	+	0.771582	0.771588	0.010558
ab4	*Or7a*	On	-	+	+	+	0.090905	0.006141	0.001805
	Or56a	Off	-	-	-	+	0.771582	0.110001	0.79558
ab5	*Or47a*	On	+	-	+	+	1.17E-05	0.110001	0.039687
	Or82a	Off	-	+	+	+	0.771582	0.048511	0.039687
ab6	*Or49b*	On	-	-	+	+	0.771582	0.110001	0.00753
ab7	*Or67c*	On	-	-	+	+	0.771582	0.771588	0.002349
	Or98a	Off	-	-	-	+	0.771582	0.771588	0.084378
ab8	*Or9a*	On	+	-	+	+	0.017429	0.110001	0.039687
	Or43b	Off	+	+	+	+	3.70E-06	1.30E-08	0.000135
ab9	*Or67b*	Off	-	-	+	+	0.771582	0.110001	0.010558
	Or69a	On	-	-	-	+	0.771582	0.771588	0.084378
ab10	*Or49a*	Off	-	-	-	-	0.771582	0.771588	0.79558
	Or85f	Off	-	+	+	+	0.090905	0.006141	0.000418
	Or67a	On	+	+	-	+	0.001388	0.015475	0.79558
ai1	*Or13a*	Off	-	-	+	+	0.771582	0.771588	0.023486
ac1	*Ir31a*	Off	-	-	-	+	0.771582	0.771588	0.79558
	Ir92a	On	-	-	-	+	0.771582	0.771588	0.79558
ac2	*Ir41a*	On	+	+	-	+	0.004908	0.002671	0.79558
ac3	*Ir75b*	Off	-	-	+	+	0.090905	0.110001	0.015325
	Ir75c	Off	-	-	+	+	0.771582	0.110001	0.015325

	Or35a	On	-	-	+	+	0.090905	0.771588	0.023486
ac4	*Ir84a*	Off	-	-	-	+	0.771582	0.771588	0.79558
	Ir76a	On	-	-	-	+	0.771582	0.771588	0.79558
Non-specific	*Ir75d*	On	-	-	-	+	0.771582	0.771588	0.79558
	Ir76b	On	+	+	-	+	0.017429	0.048511	0.084378
	Ir75a	Off	-	+	+	+	0.771582	2.86E-13	0.00753

Table 14: Normalized $\log_2$ expression values of transcription factors used to create Figure 31. Values for the expression of all transcription factors extracted from Flybase are listed.

Expression of Transcription Factors in the Olfactory System

Gene Symbol	3L	p8	p40	Adult
ac	8.23742	9.407121	1.553226	0.388447483
achi	8.728037	8.421705	7.762679	7.935738946
acj6	4.381661	5.860018	8.624151	10.24128093
Adf1	11.10238	10.60913	11.18767	9.717033977
Aef1	10.09221	10.31894	11.27992	10.67613167
al	10.24035	8.991906	9.134654	8.298553537
amon	4.744231	6.31539	8.835245	11.87270212
amos	2.75421	10.52862	3.163075	0.388447483
aop	10.68673	10.44003	10.6619	9.364957967
ap	8.143065	8.563013	6.563869	5.096692247
apt	7.803952	9.078673	7.335324	7.426365509
ara	8.690935	4.006818	4.731494	3.417062707
ase	6.405614	10.03405	5.212066	0
Atac3	9.239726	8.536735	8.640325	8.222565398
Atf3	8.794308	7.720299	7.384846	10.70277978
Atf6	11.1819	11.95591	11.23124	11.52881079
ato	9.867814	10.00208	7.012658	0.499652838
Awh	8.001226	0.950677	4.066932	0
az2	8.467704	8.127558	7.532895	7.081175993
bab1	7.842994	8.17003	8.13423	8.157248196
bab2	11.84321	11.98813	11.13848	11.53673091
bap	3.475176	0.253501	2.553226	0.499652838

Bap60	11.99698	10.69154	9.701626	9.699061747
bbx	8.771658	8.216664	7.90103	9.887783755
bcd	2.776433	2.643799	2.680695	4.840082817
B-H1	8.159268	7.803373	8.448385	9.440067393
B-H2	7.963803	7.055829	7.522621	9.076082477
bi	9.011359	9.70809	10.26549	9.582357248
bigmax	7.947953	6.864337	7.474626	8.705593435
bin	0	0	0	0.499652838
Blimp-1	9.718555	4.634411	11.62875	10.77849037
bowl	11.11179	10.02842	9.579179	8.098924142
brk	11.16486	8.33183	8.319737	8.651191212
bs	8.722246	8.375446	7.853667	8.332222236
bsh	0	3.29661	0.626633	0
btd	8.087263	6.643799	8.72291	8.013525647
btn	4.408776	1.950677	4.150685	0.499652838
Bug22	9.666372	10.09152	9.869296	9.775820748
byn	0.953691	0.838463	2.060845	1.388447483
C15	7.923726	7.246025	6.854144	5.132678718
cad	0	0	0.626633	0
can	0	2.338469	0	1.445121382
cas	0.368728	0.950677	0	2.244515069
cato	6.852466	8.012851	1.553226	0
caup	9.217289	4.627008	4.949125	4.030083883
cbt	8.896887	12.26635	9.139231	10.97103573
Cf2	7.537743	7.386116	7.872799	9.285717478
cg	11.32367	11.14403	11.06547	10.92486747
CG10431	7.879691	9.843468	9.888347	8.982342823
CG10576	13.94757	12.1504	11.65181	10.50371147
CG11085	0	0	0.475883	0
CG11294	0	0	0	0
CG11617	2.093944	2.272605	4.429271	5.866207069
CG11835	4.639049	7.542928	10.66089	4.494558963
CG11970	10.09482	9.869214	10.10072	9.415451144
CG13148	0	0.950677	0	0.388447483
CG15011	8.636184	7.029743	6.959817	7.352456209
CG15398	0	0	0	0.388447483
CG15696	0	0	0	0
CG1647	9.43355	9.663717	8.965802	8.865889352
CG17118	3.970908	3.643799	3.3925	3.291636529
CG1965	10.67478	9.982974	9.906852	10.90791983
CG2678	5.131293	5.579603	3.731494	4.864909392

CG32006	3.998473	8.879119	11.023	11.96785925
CG32105	1.368728	0	0.626633	0
CG32532	3.791659	4.122053	3.543782	2.066666238
CG32856	8.64581	8.487986	8.70721	8.02935418
CG3328	11.08315	9.33202	12.0843	11.9147444
CG33557	0.368728	1.253501	0	0
CG3711	10.963	10.32933	10.51785	10.8336629
CG3815	9.58668	8.466445	8.611426	8.032674874
CG3909	10.08363	9.028435	7.786056	8.387400769
CG4328	5.94581	4.660397	3.731494	4.048491009
CG6272	9.262597	9.204794	9.353477	9.914173596
CG7368	2.093944	3.390345	6.274025	8.913285869
CG7786	0.75421	0.950677	8.076788	7.887093375
CG7818	9.862884	9.394911	7.963945	7.86346792
CG7839	10.83108	9.85083	8.722146	8.829823685
CG7927	10.60744	9.827171	10.16039	9.90801267
CG9305	10.04968	8.846035	8.254085	8.367983933
CG9876	0	9.610352	8.171067	5.532584223
CHES-1-like	9.282945	8.653182	10.45333	11.64479738
chm	9.86608	9.352667	9.271467	8.739742131
chn	9.743086	10.58693	10.25176	10.31358243
ci	13.7322	13.59928	11.43807	10.18623256
CkIIalpha-i1	7.237697	7.193947	6.3139	6.530948733
Clk	2.633654	2.11002	2.163075	8.501639877
comr	0.368728	0	3.112865	0
crc	13.87484	13.39147	13.67366	13.74407567
CrebA	11.35224	8.450702	11.11902	10.30396196
Crg-1	7.943256	9.462733	8.300423	8.887349302
croc	6.756235	4.726851	0.475883	0.388447483
ct	11.17152	10.58618	12.1174	10.53525826
CTCF	10.44779	10.05856	9.399448	9.408574145
cyc	10.45461	9.871942	10.23791	9.903131345
CYLD	9.909391	10.48927	10.29394	10.6448844
D	13.10236	11.99232	12.62787	8.163848117
d4	10.90983	11.09513	10.0021	9.823624995
dac	7.928728	7.155878	8.117093	7.740803686
Dad	11.30743	10.61555	9.416591	10.34270822
dan	9.777654	10.22358	9.399435	1.973409984
danr	9.99346	10.20646	9.845042	5.06883049
Deaf1	9.482945	9.528228	10.02556	9.290800011
Dfd	10.24594	4.228761	2.112865	1.388447483

Dif	8.078505	11.0704	9.09612	12.29804573
dimm	3.159268	3.44042	1.475883	0
disco	10.85444	9.817312	9.49362	8.961264341
disco-r	12.09296	11.34117	10.9961	11.6007583
Dll	12.58545	12.84292	12.55308	13.04717207
dmrt11E	0.75421	0	0.626633	5.039316803
dmrt93B	2.221762	0	0	0
dmrt99B	0.368728	3.183543	0.626633	0
Doc1	9.022471	6.698365	4.524328	3.445121382
Doc2	8.64447	6.819948	5.026285	3.458948698
Doc3	8.254144	5.83758	3.829247	3.810838292
dp	8.238615	9.132387	9.088485	8.864902795
dpn	9.736225	11.19198	5.684659	2.011438864
Dr	7.408975	1.253501	1.060845	0.499652838
Dref	11.70122	11.10264	9.734802	9.667542295
dsx	10.0829	8.876155	6.980435	8.452362473
dve	8.666733	9.321926	6.598761	6.43599241
dwg	8.690569	7.446483	8.010878	8.140207413
E(spl)m3-HLH	10.30012	9.63092	10.6424	9.014532225
E(spl)m5-HLH	7.072657	7.740899	0	0.388447483
E(spl)m7-HLH	10.36222	10.44232	8.11593	4.621208224
E(spl)m8-HLH	9.753186	9.237595	0.475883	0
E(spl)mbeta-HLH	11.54493	9.693582	10.22511	8.529720897
E(spl)mdelta-HLH	9.409592	10.60643	6.929173	3.030083883
E(spl)mgamma-HLH	8.760828	9.988023	5.090081	3.030083883
e(y)1	9.033578	8.12595	8.091639	8.21888269
E2f1	10.93789	11.09048	9.635013	10.15175448
E2f2	9.913417	9.36825	8.51813	8.742733484
E5	10.01903	8.654396	9.903421	8.638640955
EcR	10.77955	11.37429	12.14454	10.36569664
eg	5.175615	4.37595	9.940483	2.472644744
Eip74EF	9.727493	11.15392	12.26793	8.661123617
Eip75B	10.88154	10.13672	12.71383	11.60626885
Eip78C	9.779488	7.758585	13.91972	7.805354327
Eip93F	4.76814	13.53121	11.99013	12.99544572
ems	10.70513	10.18569	10.65074	9.399590951
en	9.740107	8.560611	8.769885	8.417656462
ERR	8.56297	8.283805	9.223308	10.05241462
esg	11.0761	11.04363	9.909436	3.657636618
Ets21C	6.432483	7.26906	8.062262	8.874852134
Ets65A	2.776433	7.224582	7.158685	8.254578608

Ets96B	4.84752	4.164102	2.3925	7.59113767
Ets97D	9.425897	8.834634	8.283332	8.510687838
Ets98B	8.331722	8.930945	11.01309	8.824252782
eve	1.574306	0	0	0
ewg	6.59294	7.131847	6.746142	7.775527405
exd	13.13343	13.09298	12.57031	12.16483122
exex	3.339172	0	0	0
ey	7.229613	8.004444	6.298429	4.226522171
eyg	9.872404	10.54472	9.361991	9.94805563
fd102C	3.574306	0.950677	1.553226	0
fd19B	0	0	2.349783	1.445121382
fd59A	0.75421	1.643799	0.475883	0
fd64A	0	1.643799	0.475883	1.445121382
fd96Ca	8.747632	6.602133	8.600253	7.77774915
fd96Cb	11.51206	10.15313	9.394453	8.8349489
Fer1	2.857395	7.044235	11.16974	11.6343615
Fer2	2.461524	0.950677	1.797811	0.499652838
Fer3	0	0	0	4.020791494
fkh	1.953691	6.955065	8.382862	7.8859938
foxo	10.17866	10.73702	9.889953	10.99368055
fru	10.27296	7.456438	13.53662	10.01912133
ftz-f1	9.001178	13.70677	7.969757	11.01256482
fu2	8.833554	8.406263	7.063566	7.797091863
GATAd	10.55553	11.20123	10.60872	10.740004
GATAe	2.093944	0	0	0
gcm	3.66706	6.582574	2.553226	0.388447483
gcm2	0	3.060855	0	0
gem	11.80809	12.6744	12.35823	13.71213043
gl	2.475176	7.993221	2.163075	0
grau	8.883072	7.803682	8.723756	8.706846768
grn	8.397424	7.203437	7.286875	6.530130292
gsb	9.003223	2.253501	5.086577	0
gsb-n	9.173289	4.085647	5.387645	0.499652838
Gsc	0	0.253501	0	0
gt	4.415872	1.744412	4.046488	6.405114241
h	11.1442	10.78578	10.53759	10.74363069
H15	9.929649	9.205008	9.551619	10.82543059
H2.0	6.435782	0	0	1.973409984
ham	3.738582	7.932208	6.272596	6.685747656
Hand	4.475176	1.253501	0.626633	0
hb	0.75421	2.895661	2.978015	3.149829791

hbn	0	2.712932	2.748038	4.390325994
Hcf	11.02339	11.35011	10.12621	10.42083249
her	9.915947	10.0304	9.26641	9.452686442
Hey	0	3.253501	3.247861	3.904553001
HGTX	0.75421	0	0	0
HHEX	0.75421	0	0.626633	0.388447483
HLH3B	0	0	0.626633	0.499652838
HLH4C	0	0	0.475883	0
HLH54F	3.025521	0.253501	1.475883	0
Hmr	9.502732	9.216888	7.853189	8.105125652
Hnf4	8.548541	9.066359	8.601196	10.74784473
Hr38	4.398868	5.341356	6.076917	9.230935013
Hr46	9.026931	6.363333	12.18882	9.777376994
Hr51	0	0	0	0
Hr78	9.949524	9.326508	9.767292	9.027186435
Hr83	1.574306	0	2.211596	1.388447483
Hr96	8.417001	8.000832	8.271053	9.994385401
Hsf	11.00491	10.87809	11.48288	10.65267344
hth	14.06015	13.87406	13.54519	12.95645332
ind	0	0	0.475883	0.388447483
jim	11.48778	11.07657	11.58893	10.67678267
Jra	10.09781	9.440514	10.13867	10.66454536
jumu	12.11457	13.10382	8.748321	7.847644118
kay	9.114146	8.191753	8.717387	10.49896353
ken	9.806503	11.54277	10.89585	9.630271523
kn	1.574306	2.338469	2.349783	4.252476304
kni	9.12218	3.370306	8.635653	8.662326591
knrl	9.481021	5.652122	10.32305	9.832016747
Kr	3.591807	0.253501	1.626633	0
l(1)sc	0.368728	5.239848	0	0
l(3)mbt	10.29919	9.687977	9.738421	10.17159397
lab	7.699841	3.44042	2.553226	2.011438864
lbe	2.408776	1.253501	1.553226	2.445121382
lbl	9.991442	7.81198	8.417165	7.271659917
lilli	9.099949	9.527085	10.15329	10.04971321
Lim1	10.32992	7.522544	10.00544	8.81723865
Lim3	0.75421	3.401456	3.371299	2.417062707
lmd	3.093944	3.895661	6.188017	0.388447483
lms	7.717451	7.736045	7.491448	9.27721651
lola	10.81705	11.27105	11.88141	10.90903609
lolal	11.50551	11.78069	12.13449	10.75894073

luna	9.3409	10.5395	10.06955	8.572521619
lz	7.77815	8.355884	6.746304	4.1455611
Mad	10.88355	10.49304	10.6976	10.13723309
maf-S	9.813542	9.712422	9.91407	10.30381841
Max	10.18873	9.324832	9.092449	9.448477964
Med	10.44968	9.860612	10.6088	9.914060747
MED26	12.58373	13.22563	12.13512	12.20812719
Mef2	8.954632	10.46185	9.082603	11.13057201
Meics	9.086013	8.938027	8.96643	7.764797039
Met	8.750148	10.05765	10.10885	10.38198845
mia	8.205967	7.196966	5.638472	6.60653065
mirr	10.05298	7.700328	7.562116	7.234521769
Mnt	8.334324	9.223673	9.086893	9.494860806
mRpL55	8.281342	7.485853	7.451105	8.880378901
Mrtf	10.70337	10.27566	10.14589	9.837237081
MTA1-like	12.15026	11.83969	11.87541	10.70275801
MTF-1	7.912486	7.128755	7.953249	7.706484577
Myb	9.96513	9.816531	8.772647	8.388078466
nau	0	0	0.626633	0
NC2alpha	8.686787	7.828206	7.769865	7.444252759
NC2beta	8.920977	7.403789	8.445485	7.718015228
nerfin-1	4.701012	10.56966	5.731658	4.465812974
nerfin-2	2.093944	3.499196	7.499458	7.393245299
nesd	10.78507	10.20196	5.455087	5.954112132
net	9.227697	10.03973	5.787214	7.330812979
NFAT	9.114177	10.73378	10.20724	10.37473333
NfI	4.879514	6.520084	10.27732	12.0688113
Nf-YA	9.840892	9.200989	8.971113	9.114819876
Nf-YB	9.224643	9.388746	9.778943	8.447819251
Nf-YC	9.167873	8.20695	8.041761	8.384922354
nht	0	3.401456	0.475883	0
NK7.1	9.021519	9.216856	9.096226	10.55465228
nvy	8.175787	10.28268	10.52848	9.058412795
oc	8.439749	5.000313	6.898863	2.011438864
Octbeta2R	3.817482	3.775219	5.534275	7.705586068
odd	9.463394	8.332635	8.409908	4.149829791
OdsH	4.786193	1.253501	4.338903	5.340853907
Oli	1.574306	2.643799	5.785212	6.475163769
onecut	5.072657	9.36759	10.74065	12.09650825
opa	9.863424	5.727805	6.844561	2.011438864
Optix	7.911161	6.888847	4.194067	0.499652838

org-1	3.159268	2.11002	3.444976	3.995020888
otp	0	1.643799	0	0.499652838
ovo	10.73428	9.437973	9.93503	8.839329606
p53	8.604693	8.440428	7.740429	8.376195701
pb	3.621428	1.643799	0.626633	0
Pcl	11.03878	10.75946	9.575148	9.105125652
pdm2	3.354026	6.131373	8.237532	7.410674311
pdm3	10.46799	8.440718	12.52622	11.12769128
Pdp1	6.79612	7.705775	9.66588	12.23150614
peb	7.787827	11.10293	11.57478	11.46111082
PHDP	0	1.838463	4.150685	0
pho	12.27057	12.60847	11.47574	11.14185181
phtf	9.295326	9.747108	10.92431	10.40472587
pnr	8.577978	6.48165	5.768773	4.320247559
pnt	10.10209	11.5903	11.70278	10.21520867
Poxm	0.75421	7.575895	5.871384	5.269209575
Poxn	6.515447	2.11002	0.475883	0
Pph13	0	2.838463	0.475883	2.445121382
prd	1.368728	0	0	1.755891406
pros	4.867203	8.341541	10.2709	10.6881578
Ptx1	0.368728	0	0	0
Rbf2	9.193094	8.68807	5.890138	5.611955566
Rel	10.48112	10.48779	10.06898	11.36186113
repo	6.094802	8.214921	9.56008	9.93303567
retn	7.111647	7.501692	5.434793	2.445121382
rib	2.66706	3.711005	6.641796	5.991409246
rn	9.572247	10.47029	5.344353	5.806734142
ro	5.714818	6.362719	2.590397	3.011438864
run	5.885344	8.613107	9.447873	9.631901385
Rx	5.336272	2.744412	4.515073	5.494558963
sage	6.663427	3.828487	5.408608	5.873968715
salr	11.18706	10.80861	10.02302	8.510994757
sbb	12.11988	11.71482	12.08677	11.49810589
sc	9.351356	9.73485	1.626633	0
Scm	10.73104	10.51085	9.895249	10.74241395
Scr	7.757554	4.71895	2.590397	0
scro	3.627554	6.403922	1.797811	0.973409984
scrt	6.423906	11.74484	10.89154	12.02445976
sd	11.25088	11.4357	10.96432	9.31867917
sens	7.973585	11.01327	2.163075	3.458948698
shn	8.789897	8.443264	7.466428	8.627220965

sim	0	3.662393	0	0
Sin3A	10.47901	10.16249	9.901565	9.59408554
sisA	0	0.253501	0.626633	0
slbo	2.857395	4.889486	4.764713	3.236509658
slou	0.368728	0	0	0
slp1	8.887579	6.560636	8.570348	9.328931826
slp2	8.993048	7.576988	8.840114	9.452353692
Smox	11.7842	12.21302	11.18394	11.67351397
sna	3.281661	4.973193	2.553226	0.388447483
so	6.949482	7.186064	4.773139	4.487830422
sob	10.92699	9.432936	9.552072	2.800015058
Sox100B	0	7.191785	6.112614	5.1283589
Sox102F	8.900964	10.07948	10.03697	7.840399558
Sox14	9.264604	10.22795	9.21499	10.02566589
Sox15	2.475176	6.401456	11.07062	10.51745103
Sox21a	1.574306	0	0	0
Sox21b	8.621153	2.575429	3.852383	1.084615338
SoxN	5.559079	9.366695	9.082351	10.11873672
Sp1	11.06444	10.93085	12.88697	13.4743317
Spt3	8.055475	6.4603	7.883823	7.4113502
sqz	9.703489	8.652293	8.768852	7.620623854
srp	5.145349	6.421659	6.184983	4.804028242
Sry-delta	9.878194	8.201353	8.736289	8.380170585
ss	10.56132	11.06898	11.37837	13.03095625
Stat92E	9.222874	9.404781	9.400856	10.56744883
stc	10.77535	9.506741	9.943395	9.753369188
Su(H)	9.355743	9.317324	11.05257	11.70582345
sv	6.050167	9.606444	9.616621	10.14919289
svp	3.896234	7.334184	8.783801	8.248133006
Taf1	9.526695	8.687954	8.4145	8.332109622
Taf10	9.273933	8.342856	8.873307	9.078390838
Taf10b	9.303051	8.178249	8.525117	8.705397457
Taf11	9.191803	7.759751	8.340788	7.760783684
Taf12	9.506879	8.312905	9.816115	10.00820148
Taf13	9.20345	9.068663	7.717387	8.147430207
TAF1B	10.20294	9.628215	6.763697	8.101130188
Taf2	10.73327	9.999721	8.607659	8.482247397
Taf4	9.183226	8.82566	8.387819	8.839594147
Taf5	10.01819	9.583316	9.336665	8.633224244
Taf6	9.874087	8.621342	8.820013	9.00471494
Taf7	8.698509	8.482349	7.525764	7.74538042

tap	0	7.878944	0	2.800015058
Tbp	9.296847	8.513436	7.289647	8.129202808
TFAM	10.55993	9.003963	8.557701	8.748008201
tin	2.093944	0	0.626633	0.499652838
tio	9.326935	5.10323	6.026686	7.653267511
tj	0	3.11002	0	0.499652838
tll	0.75421	6.036116	0.475883	0
toe	8.957824	8.804969	9.064821	10.22530843
toy	11.20923	10.96566	8.564007	4.608858112
Trf	8.348321	7.156055	6.259447	5.653071934
Trl	10.35476	9.655066	9.970224	9.971510646
trx	10.79085	11.58303	11.08592	11.15811333
tsh	10.77457	8.204231	5.392914	4.615046384
ttk	11.25378	11.02367	11.73358	11.41025082
tup	9.696902	3.895661	4.005795	3.431160257
twi	7.1951	8.022416	6.096555	2.472644744
Ubx	1.953691	1.643799	1.553226	0.499652838
unc-4	10.2684	8.54431	9.462674	9.451766145
unpg	0	3.610019	6.838628	7.460632909
Usf	8.643232	9.530026	8.956367	9.8447243
ush	7.812264	6.414042	6.534275	5.534217862
usp	10.019	9.583394	10.42426	9.913436413
vg	6.181407	2.980621	2.163075	0
vis	7.09382	5.837138	5.965272	5.782911576
vri	9.321412	8.139503	13.68196	11.48095006
wek	8.930174	8.300346	7.801232	7.862492921
wor	3.765364	0.950677	0	0
Xbp1	12.25057	11.23839	13.22431	13.44785239
zen	0	0	0	0
zen2	0	1.53564	0	0.499652838
zf30C	12.04724	10.98566	10.24891	9.926457534
zfh1	8.738447	11.35135	10.01646	8.920929693

Table 15: Normalized log_2 expression values of commonly used housekeeping genes.

	Housekeeping Genes			
	3L	p8	p40	Adult
RpL19	39533.89	14775.95	19347.57	8828.812
Gapdh2	16353.69	8270.431	6514.645	14587.58
Act5C	43364.76	27250.53	33969.52	6180.419
betaTub56D	59647.18	18356	38582.75	13009.07

Table 16: Raw expression values for Figure 35A. DESeq2 normalized expression values used for hierarchical clustering in Figure 35A. Genes are ordered by their position in the heat map in Figure 35A and each cluster is labeled.

	Gene	3L	p8	p40	Adult
Cluster 1	*beat-IIIb*	5.086467951	50.69560586	286.9691671	544.2731
	CG42313	5.775573857	23.89768109	230.9765314	431.5151
	Lapsyn	3.139382781	39.76680748	149.4516214	350.5484
	Dscam3	5.148439351	38.29969113	635.50252	192.7438
	beat−IIIa	2.636191076	104.0833478	373.9854428	686.2021
	robo3	2.636191076	93.56659118	569.6191165	460.1149
	CG13532	7.533034574	107.5135515	460.1394395	382.8695
	2mit	7.533034574	84.47394298	151.1999044	276.2895
	CG12402	6.718130742	120.6815229	122.070072	181.2879
	CG4168	1.757460717	69.71191806	294.9364388	364.8679
	Dscam2	0	58.67213366	356.7411779	263.5645
	axo	7.345265247	15.94612338	214.5757256	884.1451
	beat−VII	4.896843498	23.86369206	103.1408764	681.8651
	dpr3	5.084612825	5.841408586	115.0601079	384.6287
	Unc−89	5.775573857	41.10489993	44.80301509	193.8485
	beat−Ia	3.139382781	13.59596434	34.39151348	293.7178
	dpr11	3.139382781	22.31957872	361.0623833	1034.171
	dpr8	2.636191076	26.65988193	393.8362942	856.239

	CG34113	1.695489317	24.99576362	260.3508926	740.7817
	beat−IV	2.00905657	14.77104386	505.1384752	703.8357
	Toll−6	1.757460717	17.85927055	711.7954373	274.0809
	dpr10	1.318095538	16.27214924	741.3638313	360.8583
	dpr13	2.887786928	9.092648203	523.1291829	304.1515
	CG33543	1.757460717	6.004421514	198.8372027	397.1887
	dpr5	0	4.460308169	316.3732166	499.7182
	dpr4	1.757460717	6.004421514	299.2279559	1044.361
Cluster 2	*dpr7*	8.036226279	129.715212	786.3252273	1750.445
	dpr12	7.345265247	98.67895106	806.827493	1888.774
	CG12950	13.56205941	93.73862305	591.0667629	989.8214
	CG7166	13.37243496	181.9029042	1085.114622	1376.824
	CG6867	7.784630426	43.00902816	759.1436742	1410.946
	sev	18.08150913	181.0566093	286.0138473	1583.029
	dpr20	8.914956638	216.453298	387.4420925	966.2161
	dpr9	8.914956638	67.79877089	230.8310068	968.2209
	CG15312	15.25754873	13.19294149	138.1986483	4336.477
	CG12484	6.404563489	10.79075554	286.7434581	2143.183
	CG17839	23.66745853	29.37005586	622.4992761	7146.351
Cluster 3	*wdp*	206.8615797	547.1765011	298.0281073	661.6151
	CG42709	209.2406095	605.0127735	237.2123521	675.4447
	Cad86C	401.1184978	731.1007798	319.4332089	556.8337
	htl	171.0778103	1444.840347	380.1856117	511.9105
	trol	185.2688593	884.8794445	161.4678692	692.9565
	Ptp99A	486.8188244	419.2246158	987.1275413	758.3324
	Sema−1a	245.8473571	525.0186821	1176.996663	998.3677
	Lar	269.208015	372.289413	675.6556407	781.6135
	Dscam4	390.3165723	410.0480384	513.4958004	498.5307
	stan	308.2024141	583.0941309	1006.010217	218.8058
	CG4950	141.3813269	441.7203998	613.1064467	129.6964
	NetB	310.3298481	193.0196856	1138.808552	278.4576
	Lrt	219.8603311	141.9800161	1096.044869	288.5642
	CG15630	36.159308	227.5520416	1021.934821	654.3317
	CG5597	56.87700821	107.4455734	882.3314227	326.7378
	Pvr	65.72813832	194.1156814	158.2603645	503.1954
	Dscam1	36.0353652	189.4334012	290.2400241	329.3533
	dpr19	51.60277093	73.34121043	351.2013039	559.8624
	kek6	87.63813613	84.24295199	162.8112546	294.1279
	Ptp4E	203.2245706	231.3353279	122.1670884	642.9578
	CG7800	249.8666715	154.9690234	155.6686223	160.9543
Cluster 4	*Con*	13.81180014	1610.647307	2519.848596	753.71

	Cad89D	20.96929606	176.084379	16511.1956	32.24017
	C901	9.793686996	29.45607179	6299.246346	24.3028
	grk	248.4921699	418.6447156	377.2691562	29.58055
	Trim9	219.3589945	260.9904884	461.4382923	43.16369
	Cad96Cb	85.51255727	344.878271	1401.616531	14.1153
	Cad88C	37.16940167	812.119549	350.3301441	61.86103
	beat−IIb	19.39960467	233.8575188	355.8660424	86.53242
	beat−IIa	12.11631082	155.3110004	133.5675738	18.32932
	rk	94.92699536	841.4222988	33.67873466	33.7128
	CG5096	105.9730962	105.0024662	33.43619366	23.81153
Cluster 5	*btl*	85.9482122	22.11355783	19.20341278	72.82632
	dpr16	89.84052741	6.896483147	39.28196098	65.70704
	CG14964	23.72942993	18.66531625	37.40299754	54.33314
	Lgr3	35.78562448	28.08399031	8.64638657	20.45678
	NetA	56.06210438	16.4691512	18.53914216	5.073305
	Toll−9	38.48193183	48.05340999	35.6378825	0
	chp	40.62049658	93.47155631	4.631074494	2.045678
	hig	238.7604543	17.36121283	34.03512407	1294.71
	CG32373	364.9350732	135.0946386	9.099792379	256.6108
Cluster 6	*CG7607*	11.67509051	5.11235988	22.53961005	153.5076
	CG31431	8.411764932	4.100293285	24.8066391	60.67492
	CG44153	5.713602457	13.95597922	13.73086687	111.8581
	dpr18	4.393651793	12.66089474	14.08725628	47.37772
	CG31814	2.260652423	11.88883807	160.5442256	194.5021
	beat−Ib	0	7.222509003	84.37602527	111.5309
	dpr6	10.73624388	74.98729086	38.92557157	25.69365
	Ptp52F	12.93306978	60.216247	33.15998864	8.182713
	CG18249	7.093669394	37.57966136	11.33514523	10.06483
	dpr14	7.784630426	5.481393702	28.25469696	17.02025
	frac	2.887786928	7.66853982	98.12372415	5.195976
	dpr17	0.439365179	3.002210757	22.63662645	46.31399
	dpr15	0	0	6.282341123	91.76899
	CG14141	4.01811314	3.328236612	0.906811619	47.4595
	CadN2	1.130326211	0.892061634	138.0362917	117.7492
	beat−VI	0.878730359	0.892061634	188.8791069	79.41373
	dpr2	9.356176943	0	276.9922514	285.8222
Cluster 7	*Ptp10D*	818.6137398	969.049573	1870.31528	920.6796
	Ten−a	693.4870694	1014.050832	1476.519542	1109.495
	sli	808.0745409	902.7296962	1700.118852	652.4075
	InR	1334.950554	776.5730398	1792.839346	1244.713
	dsd	713.9004779	721.0848397	4212.200172	1779.085

	CG14372	508.3495733	517.0274564	2669.942751	445.9172
	CG45263	112.5053128	868.2313293	2611.029684	887.7846
	CadN	137.6110994	781.9614853	1480.994224	1130.156
	nrm	209.8150482	1546.882938	1085.749204	840.1201
	beat−IIIc	115.890726	775.5020141	745.9315534	819.0911
	plum	885.4629287	697.3134238	900.8052246	422.8832
	CG15744	1315.88753	739.7397223	684.6960564	250.064
	slow	1218.386315	459.5262288	427.6942175	333.3235
	CG34371	1515.238337	1208.839362	1300.826844	336.8006
	babos	887.0474611	1336.906407	1350.258945	175.9292
	otk	1704.570585	1639.523408	973.9391454	85.8367
	CG7702	1621.9588	780.6948017	777.2779188	60.14305
	ihog	3733.237542	1247.067573	1250.211725	123.3137
	CG3408	1131.884071	1041.240674	151.7018184	141.3971
	shf	1274.382738	603.958371	340.776946	74.38073
	uif	1182.739474	1795.154846	6523.834639	99.01094
	hbs	816.3530874	2930.823013	4193.060112	113.8626
	pwn	1320.281182	827.5398152	9165.365242	53.06525
	Cad99C	2577.051458	1908.596494	6141.656216	209.9688
	Fili	2660.60951	913.5357308	3274.891869	247.3229
	rdo	602.5273465	1757.14033	16200.03158	291.9189
	ft	4603.347558	4914.993701	3016.238764	45.25084
	Ser	2287.478268	535.6546102	2827.725985	26.34847
	boi	1333.232803	171.3660231	1359.10334	31.7489
	NT1	267.5800624	332.03148	6807.417113	21.68436
	haf	141.636633	311.2518411	2659.683667	43.32754
Cluster 8	*caps*	1336.430447	2424.423972	4362.761519	1160.924
	Tl	1181.218016	1768.470065	4560.105836	1032.867
	CG7896	1895.750091	1644.781415	6746.060875	752.4012
	Cad96Ca	1184.24905	2610.602702	3462.774041	519.0298
	Tollo	2863.760978	3379.913727	2766.59241	373.2957
	Toll−7	2520.799729	3941.132895	2104.853717	429.2659
	Dl	2615.949741	3211.307075	1351.473638	492.3536
	Sema−5c	2867.065516	6657.986052	4128.390212	327.4456
	18w	3078.153737	1787.582084	3278.643832	699.5413
	CG6959	3629.964463	1948.444543	1964.181151	836.3149
	Egfr	3938.940969	2208.173193	3294.652597	1336.932
	sas	4454.213138	3724.460985	1404.745839	1048.537
	CG13506	1424.988878	1685.366117	912.0245336	1794.879
	Ten−m	3407.818611	2456.590217	4806.338855	2921.107
	CG16974	2693.051286	1941.970464	3235.513821	3121.794

Cad87A	2968.343979	1517.125068	6933.505414	2363.129
robo	2365.477226	3299.842701	3324.381885	1725.92
tutl	677.8576922	1179.113465	3173.730819	7035.538
Sema−2b	7138.406321	6858.938567	6390.695374	979.7818
N	8561.341523	6282.285591	4355.795158	1165.711
shg	7284.266188	7134.137357	7516.585156	1831.618
Sema−2a	8674.909625	7556.691022	8997.763474	565.9577
Sema−1b	7097.862024	8891.67198	11499.15337	3684.565
kug	6383.615102	14554.94326	10553.22029	2343.531

References

1. Azevedo FACC, Carvalho LRBB, Grinberg LT, Farfel JM, Ferretti RELL, Leite REPP, et al. Equal numbers of neuronal and nonneuronal cells make the human brain an isometrically scaled-up primate brain. J Comp Neurol [Internet]. 2009 Apr 10 [cited 2014 Jul 13];513(5):532–41. Available from: http://www.ncbi.nlm.nih.gov/pubmed/19226510

2. Molyneaux BJ, Arlotta P, Menezes JRL, Macklis JD. Neuronal subtype specification in the cerebral cortex. Nat Rev Neurosci. 2007;8:427–37.

3. Ihara S, Yoshikawa K, Touhara K. Chemosensory signals and their receptors in the olfactory neural system. Neuroscience [Internet]. IBRO; 2013;254:45–60. Available from: http://dx.doi.org/10.1016/j.neuroscience.2013.08.063

4. Allen NJ, Barres B a. Signaling between glia and neurons: Focus on synaptic plasticity. Curr Opin Neurobiol. 2005;15:542–8.

5. van Bokhoven H. Genetic and epigenetic networks in intellectual disabilities. Annu Rev Genet [Internet]. 2011 Jan [cited 2013 Oct 27];45:81–104. Available from: http://www.ncbi.nlm.nih.gov/pubmed/21910631

6. Cohen S, Greenberg ME. Communication Between the Synapse and the Nucleus in Neuronal Development, Plasticity, and Disease. Annu Rev Cell Dev Biol [Internet]. 2008 Nov [cited 2017 Aug 28];24(1):183–209. Available from: http://www.ncbi.nlm.nih.gov/pubmed/18616423

7. Sananbenesi F, Fischer A. The epigenetic bottleneck of neurodegenerative and psychiatric diseases. Biol Chem [Internet]. Walter de Gruyter; 2009 [cited 2017 Aug 28];390:1145–53. Available from: https://s3.amazonaws.com/academia.edu.documents/41880445/The_epigenetic_bottleneck_of_neurodegene20160202-507-hfi8rm.pdf?AWSAccessKeyId=AKIAIWOWYYGZ2Y53UL3A&Expires=1503957255&Signature=r5QTNcuo5ncY1gCigz0OgrSSdgo%3D&response-content-disposition=inline%3B filename%3DThe_epigenetic_bottleneck_of_neurodegene.pdf

8. Endo K, Aoki T, Yoda Y, Kimura K, Hama C. Notch signal organizes the Drosophila olfactory circuitry by diversifying the sensory neuronal lineages. Nat Neurosci [Internet]. 2007 Feb [cited 2013 Oct 27];10(2):153–60. Available from:

http://www.ncbi.nlm.nih.gov/pubmed/17220884

9. Tietjen I, Rihel JM, Cao Y, Koentges G, Zakhary L, Dulac C. Single-Cell Transcriptional Analysis of Neuronal Progenitors. Neuron [Internet]. 2003 Apr;38(2):161–75. Available from: http://www.sciencedirect.com/science/article/pii/S0896627303002290

10. Feldheim D a., Vanderhaeghen P, Hansen MJ, Frisén J, Lu Q, Barbacid M, et al. Topographic guidance labels in a sensory projection to the forebrain. Neuron [Internet]. 1998 Dec;21(6):1303–13. Available from: http://www.ncbi.nlm.nih.gov/pubmed/9883724

11. de Wit J, Ghosh A. Specification of synaptic connectivity by cell surface interactions. Nat Rev Neurosci [Internet]. 2015 Dec 10 [cited 2017 Aug 28];17(1):4–4. Available from: http://www.ncbi.nlm.nih.gov/pubmed/26656254

12. de Castro F, López-Mascaraque L, De Carlos J a. Cajal: lessons on brain development. Brain Res Rev [Internet]. 2007 Oct [cited 2013 Aug 8];55(2):481–9. Available from: http://www.ncbi.nlm.nih.gov/pubmed/17408567

13. Brochtrup A, Hummel T. Olfactory map formation in the Drosophila brain: Genetic specificity and neuronal variability. Curr Opin Neurobiol [Internet]. Elsevier Ltd; 2011;21(1):85–92. Available from: http://dx.doi.org/10.1016/j.conb.2010.11.001

14. Fuss SH, Ray A. Mechanisms of odorant receptor gene choice in Drosophila and vertebrates. Mol Cell Neurosci [Internet]. Elsevier Inc.; 2009 Jun [cited 2013 Oct 27];41(2):101–12. Available from: http://dx.doi.org/10.1016/j.mcn.2009.02.014

15. Takeuchi H, Sakano H. Neural map formation in the mouse olfactory system. Cell Mol Life Sci. 2014;71:3049–57.

16. Clyne PJ, Warr CG, Freeman MR, Lessing D, Kim J, Carlson JR. A novel family of divergent seven-transmembrane proteins: candidate odorant receptors in Drosophila. Neuron [Internet]. 1999/03/09. 1999;22(2):327–38. Available from: http://www.ncbi.nlm.nih.gov/pubmed/10069338

17. Vosshall LB, Amrein H, Morozov PS, Rzhetsky A, Axel R. A spatial map of olfactory receptor expression in the Drosophila antenna. Cell [Internet]. 1999 Mar 5;96(5):725–36. Available from: http://www.ncbi.nlm.nih.gov/pubmed/10089887

18. Couto A, Alenius M, Dickson BJ. Molecular, anatomical, and functional organization of the Drosophila olfactory system. Curr Biol [Internet]. 2005/09/06. 2005;15(17):1535–47. Available from: http://www.ncbi.nlm.nih.gov/pubmed/16139208

19. Rodrigues V, Hummel T. Development of the Drosophila olfactory system. Adv Exp Med Biol [Internet]. 2008/08/08. 2008;628:82–101. Available from: http://www.ncbi.nlm.nih.gov/pubmed/18683640

20. Benton R, Vannice KS, Gomez-Diaz C, Vosshall LB. Variant ionotropic glutamate receptors as chemosensory receptors in Drosophila. Cell [Internet]. 2009/01/13. 2009;136(1):149–62. Available from: http://www.ncbi.nlm.nih.gov/pubmed/19135896

21. Kwon JY, Dahanukar A, Weiss L a, Carlson JR. The molecular basis of CO2 reception in Drosophila. Proc Natl Acad Sci U S A. 2007;104:3574–8.

22. Yao CA, Carlson JR. Role of G-proteins in odor-sensing and CO2-sensing neurons in Drosophila. J Neurosci. 2010;30(13):4562–72.

23. Jones WD, Cayirlioglu P, Kadow IG, Vosshall LB. Two chemosensory receptors together mediate carbon dioxide detection in Drosophila. Nature. 2007;445(January):86–90.

24. Fishilevich E, Vosshall LB. Genetic and functional subdivision of the Drosophila antennal lobe. Curr Biol [Internet]. 2005/09/06. 2005;15(17):1548–53. Available from: http://www.ncbi.nlm.nih.gov/pubmed/16139209

25. Vosshall LB, Wong AM, Axel R. An olfactory sensory map in the fly brain. Cell [Internet]. 2000/08/16. 2000 Jul 21;102(2):147–59. Available from: http://www.ncbi.nlm.nih.gov/pubmed/10943836

26. Bhalerao S, Sen A, Stocker R, Rodrigues V. Olfactory neurons expressing identified receptor genes project to subsets of glomeruli within the antennal lobe of Drosophila melanogaster. J Neurobiol. 2003;54:577–92.

27. Clowney EJJ, LeGros MAA, Mosley CPP, Clowney FGG, Markenskoff-Papadimitriou ECC, Myllys M, et al. Nuclear Aggregation of Olfactory Receptor Genes Governs Their Monogenic Expression. Cell [Internet]. 2012/11/13. Elsevier Inc.; 2012 Nov [cited 2012 Nov 9];151(4):724–37. Available from:

http://www.ncbi.nlm.nih.gov/pubmed/23141535

28. Ressler KJ, Sullivan SL, Buck LB. A zonal organization of odorant receptor gene expression in the olfactory epithelium. Cell [Internet]. 1993/05/07. 1993 May [cited 2015 Apr 15];73(3):597–609. Available from: http://www.ncbi.nlm.nih.gov/pubmed/7683976

29. Aplin AC, Kaufman TC. Homeotic transformation of legs to mouthparts by proboscipedia expression in Drosophila imaginal discs. Mech Dev. 1997;62:51–60.

30. Morata G. How Drosophila appendages develop. Nat Rev Mol Cell Biol. 2001;2(2):89–97.

31. Yao LC, Liaw GJ, Pai CY, Sun YH. A common mechanism for antenna-to-Leg transformation in Drosophila: suppression of homothorax transcription by four HOM-C genes. Dev Biol. 1999;211:268–76.

32. Dong PD, Chu J, Panganiban G. Coexpression of the homeobox genes Distal-less and homothorax determines Drosophila antennal identity. Development. 2000;127:209–16.

33. Schneuwly S, Klemenz R, Gehring WJ. Redesigning the body plan of Drosophila by ectopic expression of the homoeotic gene Antennapedia. Vol. 325, Nature. p. 816–8.

34. Stocker RF. The organization of the chemosensory system in Drosophila melanogaster: A review. Cell Tissue Res. 1994;275:3–26.

35. Dahanukar A, Hallem E a., Carlson JR. Insect chemoreception. Curr Opin Neurobiol. 2005;15:423–30.

36. Ling F, Dahanukar A, Weiss L a, Kwon JY, Carlson JR. The molecular and cellular basis of taste coding in the legs of Drosophila. J Neurosci [Internet]. 2014;34(21):7148–64. Available from: http://www.ncbi.nlm.nih.gov/pubmed/24849350

37. Royet J, Finkelstein R. Establishing primordia in the Drosophila eye-antennal imaginal disc: the roles of decapentaplegic, wingless and hedgehog. Development. 1997;124:4793–800.

38. Goulding SE, zur Lage P, Jarman AP. amos, a proneural gene for Drosophila olfactory sense organs that is regulated by lozenge. Neuron [Internet]. 2000 Jan;25(1):69–78. Available from: http://www.ncbi.nlm.nih.gov/pubmed/10707973

39. zur Lage PI, Prentice DR a, Holohan EE, Jarman AP. The Drosophila proneural gene amos promotes olfactory sensillum formation and suppresses bristle formation. Development. 2003;130:4683–93.

40. Gupta BP, Rodrigues V. Atonal is a proneural gene for a subset of olfactory sense organs in Drosophila. Genes Cells [Internet]. 1997 Mar;2(Simpson 1990):225–33. Available from: http://www.ncbi.nlm.nih.gov/pubmed/9189759

41. Gupta BP, Flores G V, Banerjee U, Rodrigues V. Patterning an epidermal field: Drosophila lozenge, a member of the AML-1/Runt family of transcription factors, specifies olfactory sense organ type in a dose-dependent manner. Dev Biol [Internet]. 1998 Nov 15;203(2):400–11. Available from: http://www.ncbi.nlm.nih.gov/pubmed/9808789

42. Li Q, Ha TSS, Okuwa S, Wang Y, Wang Q, Millard SSS, et al. Combinatorial Rules of Precursor Specification Underlying Olfactory Neuron Diversity. Curr Biol [Internet]. Elsevier Ltd; 2013 Nov [cited 2013 Nov 25];1–10. Available from: http://linkinghub.elsevier.com/retrieve/pii/S0960982213013286

43. Song E, de Bivort B, Dan C, Kunes S. Determinants of the Drosophila Odorant Receptor Pattern. Dev Cell [Internet]. Elsevier Inc.; 2012;22(2):363–76. Available from: http://dx.doi.org/10.1016/j.devcel.2011.12.015

44. Blagburn JM. Engrailed expression in subsets of adult Drosophila sensory neurons: An enhancer-trap study. Invertebr Neurosci. 2008;8:133–46.

45. Sen A, Kuruvilla D, Pinto L, Sarin A, Rodrigues V. Programmed cell death and context dependent activation of the EGF pathway regulate gliogenesis in the Drosophila olfactory system. Mech Dev. 2004;121:65–78.

46. Endo K, Karim MR, Taniguchi H, Krejci A, Kinameri E, Siebert M, et al. Chromatin modification of Notch targets in olfactory receptor neuron diversification. Nat Neurosci [Internet]. 2011 [cited 2013 Oct 28];15(2):224–34. Available from: http://www.nature.com/neuro/journal/vaop/ncurrent/full/nn.2998.html

47. Alkhori L, Öst A, Alenius M. The corepressor Atrophin specifies odorant receptor expression in Drosophila. FASEB J. 2014;28:1355–64.

48. Sim CK, Perry S, Tharadra SK, Lipsick JS, Ray A. Epigenetic regulation of olfactory receptor gene expression by the Myb-MuvB/dREAM complex. Genes Dev [Internet]. 2012/10/30. 2012;26(22):2483–98. Available from: http://www.ncbi.nlm.nih.gov/pubmed/23105004

49. Hobert O. Neurogenesis in the nematode Caenorhabditis elegans. WormBook. 2010;1–24.

50. Ayer RK, Carlson J. Olfactory physiology in theDrosophila antenna and maxillary palp:acj6 Distinguishes two classes of odorant pathways. J Neurobiol [Internet]. Wiley Subscription Services, Inc., A Wiley Company; 1992 Oct 1 [cited 2017 Sep 3];23(8):965–82. Available from: http://doi.wiley.com/10.1002/neu.480230804

51. Clyne PJ, Certel SJ, de Bruyne M, Zaslavsky L, Johnson W a, Carlson JR. The odor specificities of a subset of olfactory receptor neurons are governed by Acj6, a POU-domain transcription factor. Neuron. 1999;22:339–47.

52. Jafari S, Alkhori L, Schleiffer A, Brochtrup A, Hummel T, Alenius M. Combinatorial activation and repression by seven transcription factors specify drosophila odorant receptor expression. PLoS Biol. 2012;10.

53. Bai L, Carlson JR. Distinct functions of acj6 splice forms in odor receptor gene choice. J Neurosci. 2010;30(14):5028–36.

54. Tichy AL, Ray A, Carlson JR. A new Drosophila POU gene, pdm3, acts in odor receptor expression and axon targeting of olfactory neurons. J Neurosci. 2008;28(28):7121–9.

55. Lee M-H, Salvaterra PM. Abnormal chemosensory jump 6 is a positive transcriptional regulator of the cholinergic gene locus in Drosophila olfactory neurons. J Neurosci [Internet]. 2002 Jul 1 [cited 2017 Sep 3];22(13):5291–9. Available from: http://www.ncbi.nlm.nih.gov/pubmed/12097480

56. Miller CJ, Carlson JR. Regulation of odor receptor genes in trichoid sensilla of the drosophila antenna. Genetics [Internet]. 2010 Sep [cited 2013 Oct 26];186(1):79–95. Available from: http://www.pubmedcentral.nih.gov/articlerender.fcgi?artid=2940313&tool=pmcen

trez&rendertype=abstract

57. Cayirlioglu P, Kadow IG, Zhan X, Okamura K, Suh GSB, Gunning D, et al. Hybrid neurons in a microRNA mutant are putative evolutionary intermediates in insect CO2 sensory systems. Science [Internet]. 2008 Feb 29;319(5867):1256–60. Available from: http://www.pubmedcentral.nih.gov/articlerender.fcgi?artid=2714168&tool=pmcentrez&rendertype=abstract

58. Hartl M, Loschek LF, Stephan D, Siju KP, Knappmeyer C, Kadow ICG. A New Prospero and microRNA-279 Pathway Restricts CO2 Receptor Neuron Formation. J Neurosci. 2011;31(44):15660–73.

59. Jhaveri D, Sen A, Reddy GV, Rodrigues V. Sense organ identity in the Drosophila antenna is specified by the expression of the proneural gene atonal. Mech Dev. 2000;99:101–11.

60. Jefferis GSXE, Hummel T. Wiring specificity in the olfactory system. Semin Cell Dev Biol. 2006;17:50–65.

61. Sweeney LB, Couto A, Chou YH, Berdnik D, Dickson BJ, Luo L, et al. Temporal Target Restriction of Olfactory Receptor Neurons by Semaphorin-1a/PlexinA-Mediated Axon-Axon Interactions. Neuron. 2007;53:185–200.

62. Feinstein P, Bozza T, Rodriguez I, Vassalli A, Mombaerts P. Axon guidance of mouse olfactory sensory neurons by odorant receptors and the beta2 adrenergic receptor. Cell. 2004;117:833–46.

63. Imai T, Suzuki M, Sakano H. Odorant receptor-derived cAMP signals direct axonal targeting. Science [Internet]. 2006 Oct 27 [cited 2013 Oct 3];314(5799):657–61. Available from: http://www.ncbi.nlm.nih.gov/pubmed/16990513

64. Nakashima A, Takeuchi H, Imai T, Saito H, Kiyonari H, Abe T, et al. XAgonist-independent GPCR activity regulates anterior-posterior targeting of olfactory sensory neurons. Cell [Internet]. Elsevier Inc.; 2013;154(6):1314–25. Available from: http://dx.doi.org/10.1016/j.cell.2013.08.033

65. Chou YH, Zheng X, Beachy P a., Luo L. Patterning Axon Targeting of Olfactory Receptor Neurons by Coupled Hedgehog Signaling at Two Distinct Steps. Cell [Internet]. Elsevier Ltd; 2010;142(6):954–66. Available from:

http://dx.doi.org/10.1016/j.cell.2010.08.015

66. Komiyama T, Carlson JR, Luo L. Olfactory receptor neuron axon targeting: intrinsic transcriptional control and hierarchical interactions. Nat Neurosci. 2004;7(8):819–25.

67. Joo WJW, Sweeney LBL, Liang L, Luo L. Linking Cell Fate, Trajectory Choice, and Target Selection: Genetic Analysis of Sema-2b in Olfactory Axon Targeting. Neuron [Internet]. Elsevier Inc.; 2013 May [cited 2013 May 22];78(4):673–86. Available from: http://dx.doi.org/10.1016/j.neuron.2013.03.022

68. Hummel T, Vasconcelos ML, Clemens JC, Fishilevich Y, Vosshall LB, Zipursky SL. Axonal targeting of olfactory receptor neurons in Drosophila is controlled by Dscam. Neuron. 2003;37:221–31.

69. Jhaveri D, Saharan S, Sen A, Rodrigues V. Positioning sensory terminals in the olfactory lobe of Drosophila by Robo signaling. Development. 2004;131:1903–12.

70. Hattori D, Demir E, Kim HW, Viragh E, Zipursky SL, Dickson BJ. Dscam diversity is essential for neuronal wiring and self-recognition. Nature. 2007;449(September):223–7.

71. Hummel T, Zipursky SL. Afferent induction of olfactory glomeruli requires N-cadherin. Neuron. 2004;42:77–88.

72. Zhu H, Luo L. Diverse functions of N-cadherin in dendritic and axonal terminal arborization of olfactory projection neurons. Neuron. 2004;42:63–75.

73. Lattemann M, Zierau A, Schulte C, Seidl S, Kuhlmann B, Hummel T. Semaphorin-1a Controls Receptor Neuron-Specific Axonal Convergence in the Primary Olfactory Center of Drosophila. Neuron. 2007;53:169–84.

74. Zhu H, Hummel T, Clemens JC, Berdnik D, Zipursky SL, Luo L. Dendritic patterning by Dscam and synaptic partner matching in the Drosophila antennal lobe. Nat Neurosci. 2006;9(3):349–55.

75. Hong W, Mosca TJ, Luo L. Teneurins instruct synaptic partner matching in an olfactory map. Nature [Internet]. 2012/03/20. Nature Publishing Group; 2012 Apr 12 [cited 2013 Oct 21];484(7393):201–7. Available from: http://www.pubmedcentral.nih.gov/articlerender.fcgi?artid=3345284&tool=pmcen

trez&rendertype=abstract

76. Ward A, Hong W, Favaloro V, Luo L. Toll Receptors Instruct Axon and Dendrite Targeting and Participate in Synaptic Partner Matching in a Drosophila Olfactory Circuit. Neuron [Internet]. 2015 Mar 4 [cited 2017 Aug 28];85(5):1013–28. Available from: http://www.ncbi.nlm.nih.gov/pubmed/25741726

77. Sen S, Hartmann B, Reichert H, Rodrigues V. Expression and function of the empty spiracles gene in olfactory sense organ development of Drosophila melanogaster. Development. 2010;137:3687–95.

78. Huang DW, Sherman BT, Lempicki RA. Bioinformatics enrichment tools: paths toward the comprehensive functional analysis of large gene lists. Nucleic Acids Res [Internet]. 2009 Jan;37(1):1–13. Available from: http://www.pubmedcentral.nih.gov/articlerender.fcgi?artid=2615629&tool=pmcentrez&rendertype=abstract

79. Huang DW, Sherman BT, Lempicki RA. Systematic and integrative analysis of large gene lists using DAVID bioinformatics resources. Nat Protoc [Internet]. 2009 Jan;4(1):44–57. Available from: http://www.ncbi.nlm.nih.gov/pubmed/19131956

80. Kojima T, Sato M, Saigo K. Formation and specification of distal leg segments in Drosophila by dual Bar homeobox genes, BarH1 and BarH2. Development. 2000;127:769–78.

81. Couderc J-L, Godt D, Zollman S, Chen J, Li M, Tiong S, et al. The bric à brac locus consists of two paralogous genes encoding BTB/POZ domain proteins and acts as a homeotic and morphogenetic regulator of imaginal development in Drosophila. Development. 2002;129:2419–33.

82. Estella C, Voutev R, Mann RS. A Dynamic Network of Morphogens and Transcription Factors Patterns the Fly Leg [Internet]. 1st ed. Vol. 98, Current Topics in Developmental Biology. Elsevier Inc.; 2012. 173-198 p. Available from: http://dx.doi.org/10.1016/B978-0-12-386499-4.00007-0

83. Kojima T. The mechanism of Drosophila leg development along the proximodistal axis. Dev Growth Differ. 2004;46(2):115–29.

84. Natori K, Tajiri R, Furukawa S, Kojima T. Progressive tarsal patterning in the Drosophila by temporally dynamic regulation of transcription factor genes. Dev

Biol [Internet]. Elsevier Inc.; 2012;361(2):450–62. Available from: http://dx.doi.org/10.1016/j.ydbio.2011.10.031

85. Baanannou A, Mojica-Vazquez LH, Darras G, Couderc JL, Cribbs DL, Boube M, et al. Drosophila Distal-less and Rotund Bind a Single Enhancer Ensuring Reliable and Robust bric-a-brac2 Expression in Distinct Limb Morphogenetic Fields. PLoS Genet. 2013;9(6).

86. Giorgianni MW, Mann RS. Establishment of Medial Fates along the Proximodistal Axis of the Drosophila Leg through Direct Activation of dachshund by Distalless. Dev Cell [Internet]. Elsevier Inc.; 2011;20(4):455–68. Available from: http://dx.doi.org/10.1016/j.devcel.2011.03.017

87. Pueyo JI, Galindo MI, Bishop S a, Couso JP. Proximal-distal leg development in Drosophila requires the apterous gene and the Lim1 homologue dlim1. Development. 2000;127:5391–402.

88. Casares F, Mann RS. The ground state of the ventral appendage in Drosophila. Science. 2001;293(2001):1477–80.

89. Li Q, Barish S, Okuwa S, Volkan PC. Examination of endogenous rotund expression and function in developing Drosophila olfactory system using CRISPR-Cas9 mediated protein tagging. G3 Genes|Genomes|Genetics [Internet]. 2015;5:2809–16. Available from: http://www.ncbi.nlm.nih.gov/pubmed/26497147

90. Godt D, Couderc JL, Cramton SE, Laski F a. Pattern formation in the limbs of Drosophila: bric à brac is expressed in both a gradient and a wave-like pattern and is required for specification and proper segmentation of the tarsus. Development. 1993;119:799–812.

91. Chu J, Dong PDS, Panganiban G. Limb type-specific regulation of bric a brac contributes to morphological diversity. Development. 2002;129:695–704.

92. Galindo MI, Bishop S a, Greig S, Couso JP. Leg patterning driven by proximal-distal interactions and EGFR signaling. Science. 2002;297(2002):256–9.

93. St Pierre SE, Galindo MI, Couso JP, Thor S. Control of Drosophila imaginal disc development by rotund and roughened eye: differentially expressed transcripts of the same gene encoding functionally distinct zinc finger proteins. Development. 2002;129(5):1273–81.

94. Jarman a. P, Grau Y, Jan LY, Yuh Nung Jan. atonal Is a proneural gene that directs chordotonal organ formation in the Drosophila peripheral nervous system. Cell. 1993;73:1307–21.

95. Bayraktar OA, Doe CQ. Combinatorial temporal patterning in progenitors expands neural diversity. Nature [Internet]. Nature Publishing Group, a division of Macmillan Publishers Limited. All Rights Reserved.; 2013 Jun 27 [cited 2015 Sep 10];498(7455):449–55. Available from: http://dx.doi.org/10.1038/nature12266

96. Jacob J, Maurange C, Gould AP. Temporal control of neuronal diversity: common regulatory principles in insects and vertebrates? Development. 2008;135:3481–9.

97. Hoppe R, Breer H, Strotmann J. Promoter motifs of olfactory receptor genes expressed in distinct topographic patterns. Genomics. 2006;87:711–23.

98. Hoppe R, Frank H, Breer H, Strotmann J. The Clustered Olfactory Receptor Gene Family 262 : Genomic Factors The Clustered Olfactory Receptor Gene Family 262 : Genomic Organization , Promotor Elements , and Interacting Transcription Factors. Genome Res. 2003;2674–85.

99. Kolterud A, Alenius M, Carlsson L, Bohm S. The Lim homeobox gene Lhx2 is required for olfactory sensory neuron identity. Development. 2004;131:5319–26.

100. Jessell TM. Neuronal specification in the spinal cord: inductive signals and transcriptional codes. Nat Rev Genet. 2000;1:20–9.

101. Ulloa F, Briscoe J. Morphogens and the control of cell proliferation and patterning in the spinal cord. Cell Cycle. 2007;6(February 2015):2640–9.

102. Franco SJ, Gil-Sanz C, Martinez-Garay I, Espinosa A, Harkins-Perry SR, Ramos C, et al. Fate-Restricted Neural Progenitors in the Mammalian Cerebral Cortex. Vol. 337, Science. 2012. p. 746–9.

103. Bayraktar OA, Fuentealba LC, Alvarez-buylla A, Rowitch DH. Astrocyte Development and Heterogeneity. 2015;

104. Greig LC, Woodworth MB, Galazo MJ, Padmanabhan H, Macklis JD. Molecular logic of neocortical projection neuron specification, development and diversity. Nat Rev Neurosci [Internet]. Nature Publishing Group; 2013;14(11):755–69. Available from: http://dx.doi.org/10.1038/nrn3586

105. Ray A, Van Der Goes Van Naters W, Carlson JR. A regulatory code for neuron-specific odor receptor expression. PLoS Biol. 2008;6(5):1069–83.

106. Magklara A, Yen A, Colquitt BM, Clowney EJ, Allen W, Markenscoff-Papadimitriou E, et al. An epigenetic signature for monoallelic olfactory receptor expression. Cell [Internet]. 2011/05/03. 2011;145(4):555–70. Available from: http://www.ncbi.nlm.nih.gov/pubmed/21529909

107. Lyons DB, Allen WE, Goh T, Tsai L, Barnea G, Lomvardas S. An epigenetic trap stabilizes singular olfactory receptor expression. Cell [Internet]. Elsevier Inc.; 2013;154(2):325–36. Available from: http://dx.doi.org/10.1016/j.cell.2013.06.039

108. Alexander JM, Lomvardas S. Nuclear architecture as an epigenetic regulator of neural development and function. Neuroscience [Internet]. IBRO; 2014;264:39–50. Available from: http://dx.doi.org/10.1016/j.neuroscience.2014.01.044

109. Akam M, Dawson I, Tear G. Homeotic genes and the control of segment diversity. Development [Internet]. 1988;133:123–33. Available from: http://dev.biologists.org/content/104/Supplement/123.short

110. Abzhanov A. Von Baer's law for the ages: Lost and found principles of developmental evolution. Trends Genet [Internet]. Elsevier Ltd; 2013;29(12):712–22. Available from: http://dx.doi.org/10.1016/j.tig.2013.09.004

111. Kurtovic A, Widmer A, Dickson BJ. A single class of olfactory neurons mediates behavioural responses to a Drosophila sex pheromone. Nature. 2007;446(March):542–6.

112. Jusiak B, Wang F, Karandikar UC, Kwak S, Wang H, Chen R, et al. Genome-wide DNA binding pattern of the homeodomain transcription factor Sine oculis (So) in the developing eye of Drosophila melanogaster. GDATA. Elsevier B.V.; 2014;

113. Li Q, Barish S, Okuwa S, Maciejewski A, Brandt AT, Reinhold D, et al. A Functionally Conserved Gene Regulatory Network Module Governing Olfactory Neuron Diversity. PLoS Genet [Internet]. 2016 Jan [cited 2016 Jun 15];12(1):e1005780. Available from: http://www.ncbi.nlm.nih.gov/pubmed/26765103

114. Hueston CE, Olsen D, Li Q, Okuwa S, Peng B, Wu J, et al. Chromatin Modulatory

Proteins and Olfactory Receptor Signaling in the Refinement and Maintenance of Fruitless Expression in Olfactory Receptor Neurons. Hassan BA, editor. PLOS Biol [Internet]. Public Library of Science; 2016 Apr 19 [cited 2016 Jun 27];14(4):e1002443. Available from: http://dx.plos.org/10.1371/journal.pbio.1002443

115. Kwon JY, Dahanukar A, Weiss L a., Carlson JR. A map of taste neuron projections in the Drosophila CNS. J Biosci. 2014;39(July):565–74.

116. Freeman EG, Dahanukar A. Molecular neurobiology of Drosophila taste. Curr Opin Neurobiol. 2015;34:140–8.

117. Thorne N, Amrein H. Atypical expression ofDrosophila gustatory receptor genes in sensory and central neurons. J Comp Neurol [Internet]. Wiley Subscription Services, Inc., A Wiley Company; 2008 Feb 1 [cited 2016 Nov 18];506(4):548–68. Available from: http://doi.wiley.com/10.1002/cne.21547

118. Weiss L a., Dahanukar A, Kwon JY, Banerjee D, Carlson JR. The molecular and cellular basis of bitter taste in Drosophila. Neuron [Internet]. Elsevier Inc.; 2011;69(2):258–72. Available from: http://dx.doi.org/10.1016/j.neuron.2011.01.001

119. Kreher SA, Kwon JY, Carlson JR. The Molecular Basis of Odor Coding in the Drosophila Larva. Neuron. 2005;46(3):445–56.

120. Ramaekers A, Magnenat E, Marin EC, Gendre N, Jefferis GSXE, Luo L, et al. Glomerular maps without cellular redundancy at successive levels of the Drosophila larval olfactory circuit. Curr Biol. 2005;15:982–92.

121. Guo S, Kim J. Molecular evolution of Drosophila odorant receptor genes. Mol Biol Evol. 2007;24:1198–207.

122. Abuin L, Bargeton B, Ulbrich MH, Isacoff EY, Kellenberger S, Benton R. Functional Architecture of Olfactory Ionotropic Glutamate Receptors. Neuron. 2011;69:44–60.

123. Bai L, Goldman AL, Carlson JR. Positive and negative regulation of odor receptor gene choice in Drosophila by acj6. J Neurosci. 2009;29(41):12940–7.

124. Song E, de Bivort B, Dan C, Kunes S. Determinants of the Drosophila Odorant Receptor Pattern (supp). Dev Cell. 2012;22:363–76.

125. Dong PD, Chu J, Panganiban G. Proximodistal domain specification and interactions in developing Drosophila appendages. Development. 2001;128:2365–72.

126. Emerald BS, Curtiss J, Mlodzik M, Cohen SM. Distal antenna and distal antenna related encode nuclear proteins containing pipsqueak motifs involved in antenna development in Drosophila. Development. 2003;130:1171–80.

127. Sen A, Reddy GVV, Rodrigues V. Combinatorial expression of Prospero, Seven-up, and Elav identifies progenitor cell types during sense-organ differentiation in the Drosophila antenna. Dev Biol [Internet]. 2003 Feb [cited 2013 Oct 27];254(1):79–92. Available from: http://linkinghub.elsevier.com/retrieve/pii/S0012160602000210

128. Singson A, Leviten MW, Bang AG, Hua XH, Posakony JW. Direct downstream targets of proneural activators in the imaginal disc include genes involved in lateral inhibitory signaling. Genes Dev [Internet]. 1994 Sep 1 [cited 2015 Jul 13];8(17):2058–71. Available from: http://genesdev.cshlp.org/content/8/17/2058.short

129. de Celis JF, de Celis J, Ligoxygakis P, Preiss A, Delidakis C, Bray S, et al. Functional relationships between Notch, Su(H) and the bHLH genes of the E(spl) complex: the E(spl) genes mediate only a subset of Notch activities during imaginal development. Development [Internet]. The Company of Biologists Ltd; 1996 Sep [cited 2016 Jun 20];122(9):2719–28. Available from: http://www.ncbi.nlm.nih.gov/pubmed/8787746

130. Ligoxygakis P, Yu SY, Delidakis C, Baker NE. A subset of notch functions during Drosophila eye development require Su(H) and the E(spl) gene complex. Development [Internet]. 1998 Aug [cited 2016 Jun 20];125(15):2893–900. Available from: http://www.ncbi.nlm.nih.gov/pubmed/9655811

131. Artavanis-Tsakonas S, Rand MD, Lake RJ. Notch signaling: cell fate control and signal integration in development. Science. 1999;284(April):770–6.

132. Nolo R, Nolo R, Abbott L a, Abbott L a, Bellen HJ, Bellen HJ. Senseless, a Zn finger transcription factor, is necessary and sufficient for sensory organ development in Drosophila. Cell [Internet]. 2000;102:349–62. Available from: http://www.ncbi.nlm.nih.gov/pubmed/10975525

133. Suzanne M, Estella C, Calleja M, Sánchez-Herrero E. The hernandez and fernandez genes of Drosophila specify eye and antenna. Dev Biol. 2003;260(2):465–83.

134. Eden E, Navon R, Steinfeld I, Lipson D, Yakhini Z, Ashburner M, et al. GOrilla: a tool for discovery and visualization of enriched GO terms in ranked gene lists. BMC Bioinformatics [Internet]. BioMed Central; 2009 [cited 2016 Jul 19];10(1):48. Available from: http://www.biomedcentral.com/1471-2105/10/48

135. Walter W, Sánchez-Cabo F, Ricote M. GOplot: an R package for visually combining expression data with functional analysis. Bioinformatics [Internet]. 2015 Sep 1 [cited 2016 Nov 21];31(17):2912–4. Available from: http://www.ncbi.nlm.nih.gov/pubmed/25964631

136. Alexa A, Rahnenführer J. Gene set enrichment analysis with topGO. 2016 [cited 2016 Nov 21]; Available from: http://www.mpi-sb.mpg.de/~alexa

137. Barish S, Li Q, Pan JW, Soeder C, Jones C, Volkan PC. Transcriptional profiling of olfactory system development identifies distal antenna as a regulator of subset of neuronal fates. Sci Rep [Internet]. 2017 Jan 19 [cited 2017 Mar 22];7:40873. Available from: http://www.ncbi.nlm.nih.gov/pubmed/28102318

138. Barish S, Volkan PC. Mechanisms of olfactory receptor neuron specification in Drosophila [Internet]. Vol. 4, Wiley Interdisciplinary Reviews: Developmental Biology. 2015 [cited 2016 Jun 15]. p. 609–21. Available from: http://www.ncbi.nlm.nih.gov/pubmed/26088441

139. Carrillo RA, Özkan E, Menon KP, Nagarkar-Jaiswal S, Lee P-T, Jeon M, et al. Control of Synaptic Connectivity by a Network of Drosophila IgSF Cell Surface Proteins. Cell [Internet]. 2015 Dec 17 [cited 2015 Dec 26];163(7):1770–82. Available from: http://www.sciencedirect.com/science/article/pii/S0092867415015020

140. Serizawa S, Miyamichi K, Takeuchi H, Yamagishi Y, Suzuki M, Sakano H. A Neuronal Identity Code for the Odorant Receptor-Specific and Activity-Dependent Axon Sorting. Cell [Internet]. 2006 [cited 2017 Aug 28];127(5):1057–69. Available from: http://www.sciencedirect.com/science/article/pii/S0092867406014048

141. Tan L, Zhang KX, Pecot MY, Nagarkar-Jaiswal S, Lee P-T, Takemura S, et al. Ig

Superfamily Ligand and Receptor Pairs Expressed in Synaptic Partners in Drosophila. Cell [Internet]. 2015 Dec [cited 2015 Dec 18];163(7):1756–69. Available from: http://www.sciencedirect.com/science/article/pii/S0092867415015019

142. Venken KJT, Schulze KL, Haelterman NA, Pan H, He Y, Evans-Holm M, et al. MiMIC: a highly versatile transposon insertion resource for engineering Drosophila melanogaster genes. Nat Methods [Internet]. NIH Public Access; 2011 Sep [cited 2017 Oct 4];8(9):737–43. Available from: http://www.ncbi.nlm.nih.gov/pubmed/21985007

143. Nicolaï LJJ, Ramaekers A, Raemaekers T, Drozdzecki A, Mauss AS, Yan J, et al. Genetically encoded dendritic marker sheds light on neuronal connectivity in Drosophila. Proc Natl Acad Sci U S A [Internet]. National Academy of Sciences; 2010 Nov 23 [cited 2017 Jul 21];107(47):20553–8. Available from: http://www.ncbi.nlm.nih.gov/pubmed/21059961

144. Li H, Horns F, Wu B, Xie Q, Li J, Li T, et al. Classifying Drosophila Olfactory Projection Neuron Subtypes by Single-cell RNA Sequencing. bioRxiv [Internet]. 2017 [cited 2017 Jun 9]; Available from: http://biorxiv.org/content/early/2017/06/03/145045

145. Caussinus E, Affolter M. deGradFP: A System to Knockdown GFP-Tagged Proteins. In Humana Press, New York, NY; 2016 [cited 2017 Oct 11]. p. 177–87. Available from: http://link.springer.com/10.1007/978-1-4939-6371-3_9

146. Ressler KJ, Sullivan SL, Buck LB. A zonal organization of odorant receptor gene expression in the olfactory epithelium. Cell [Internet]. 1993/05/07. 1993;73(3):597–609. Available from: http://www.ncbi.nlm.nih.gov/pubmed/7683976

147. Wicher D, Schäfer R, Bauernfeind R, Stensmyr MC, Heller R, Heinemann SH, et al. Drosophila odorant receptors are both ligand-gated and cyclic-nucleotide-activated cation channels. Nature. 2008;452(April):1007–11.

148. Abu-Shaar M, Mann RS. Generation of multiple antagonistic domains along the proximodistal axis during Drosophila leg development. Development. 1998;125:3821–30.

149. Li H, Watson A, Olechwier A, Anaya M, Sorooshyari SK, Harnett DP, et al. Deconstruction of the beaten Path-Sidestep interaction network provides insights into neuromuscular system development. Elife [Internet]. 2017 Aug 15 [cited 2017

Oct 23];6. Available from: https://elifesciences.org/articles/28111

150. Mohn F, Schübeler D. Genetics and epigenetics: stability and plasticity during cellular differentiation. Trends Genet [Internet]. 2009 Mar [cited 2013 Oct 20];25(3):129–36. Available from: http://www.ncbi.nlm.nih.gov/pubmed/19185382

151. Sanosaka T, Namihira M, Nakashima K. Epigenetic mechanisms in sequential differentiation of neural stem cells. Epigenetics [Internet]. 2009 Feb 16;4(2):89–92. Available from: http://www.ncbi.nlm.nih.gov/pubmed/19287212

152. Ray A, van Naters WVDG, Shiraiwa T, Carlson JR, van der Goes van Naters W, Shiraiwa T, et al. Mechanisms of Odor Receptor Gene Choice in Drosophila. Neuron [Internet]. 2007 Feb 1 [cited 2013 Oct 27];53(3):353–69. Available from: http://www.pubmedcentral.nih.gov/articlerender.fcgi?artid=1986798&tool=pmcentrez&rendertype=abstract

153. Ray A, Van Der Goes Van Naters W, Carlson JR, van Naters WVDG, Carlson JR, Van Der Goes Van Naters W, et al. A regulatory code for neuron-specific odor receptor expression. Eisen MB, editor. PLoS Biol [Internet]. 2008 [cited 2013 Oct 27];6(5):1069–83. Available from: http://biology.plosjournals.org/perlserv/?request=get-document&doi=10.1371%252Fjournal.pbio.0060125

154. Pointud JC, Larsson J, Dastugue B, Couderc JL. The BTB/POZ domain of the regulatory proteins Bric à brac 1 (BAB1) and Bric à brac 2 (BAB2) interacts with the novel Drosophila TAF(II) factor BIP2/dTAF(II)155. Dev Biol. 2001;237:368–80.

155. Kozu S, Tajiri R, Tsuji T, Michiue T, Saigo K, Kojima T. Temporal regulation of late expression of Bar homeobox genes during Drosophila leg development by Spineless, a homolog of the mammalian dioxin receptor. Dev Biol. 2006;294:497–508.

156. Pueyo JI, Couso JP. Chip-mediated partnerships of the homeodomain proteins Bar and Aristaless with the LIM-HOM proteins Apterous and Lim1 regulate distal leg development. Development. 2004;131:3107–20.

157. Prpic NM, Tautz D. The expression of the proximodistal axis patterning genes Distal-less and dachshund in the appendages of Glomeris marginata (Myriapoda: Diplopoda) suggests a special role of these genes in patterning the head appendages. Dev Biol. 2003;260:97–112.

158. Mosca TJ, Luo L. Synaptic organization of the Drosophila antennal lobe and its regulation by the Teneurins. Elife. 2014;1–29.

159. Sato K, Pellegrino M, Nakagawa T, Nakagawa T, Vosshall LB, Touhara K. Insect olfactory receptors are heteromeric ligand-gated ion channels. Nature. 2008;452(April):1002–6.

160. Jefferis GSXE. Developmental origin of wiring specificity in the olfactory system of Drosophila. Development [Internet]. 2004 [cited 2017 Sep 17];131(1):117–30. Available from: http://dev.biologists.org/content/131/1/117.long

Biography

Scott Barish was born in Silver Spring, MD on October 3, 1990. He began his scientific career with Dr. Alva Mitchell at the USDA through an internship program with Eleanor Roosevelt High School. He then attended Hampshire college beginning in 2008, where I received a BA in Molecular Biology. Scott next moved to Durham, NC to attend Duke University where I joined Dr. Pelin Volkan's lab. With Dr. Volkan he has co-authored several journal articles including: Mechanisms of olfactory receptor neuron specification in Drosophila in *WIRE's Developmental Biology*, Examination of Endogenous Rotund Expression and Function in Developing Drosophila Olfactory System Using CRISPR-Cas9–Mediated Protein Tagging in *Genes, Genomes, and Genetics*, A Functionally Conserved Gene Regulatory Network Module Governing Olfactory Neuron Diversity in *PLOS Genetics*, Transcriptional profiling of olfactory system development identifies *distal antenna* as a regulator of subset of neuronal fates in *Scientific Reports*, Patterns of transcriptional parallelism and variation in the developing olfactory system of Drosophila species in *Scientific Reports* and Combinations of DIPs and Dprs control olfactory receptor neuron axon sorting in *Drosophila* has been submitted to *Neuron*. He received the Graduate Summer Research Fellowship from Duke twice and the Biology One Semester Research Fellowship from the Biology Department at Duke.